NAVAL POSTGRADUATE SCHOOL
Monterey, California

THESIS

EFFECT OF VORTEX CIRCULATION ON INJECTANT FROM A SINGLE FILM-COOLING HOLE AND A ROW OF FILM-COOLING HOLES IN A TURBULENT BOUNDARY LAYER, PART 2: INJECTION BENEATH THE VORTEX UPWASH

by

Pisut Kaisuwan

December, 1989

Thesis Advisor: P. M. Ligrani
Co-Thesis Advisor: Chelakara S. Subramanian

Unclassified

security classification of this page

REPORT DOCUMENTATION PAGE

1a Report Security Classification Unclassified			1b Restrictive Markings
2a Security Classification Authority			3 Distribution/Availability of Report: Approved for public release; distribution is unlimited.
2b Declassification/Downgrading Schedule			
4 Performing Organization Report Number(s)			5 Monitoring Organization Report Number(s)
6a Name of Performing Organization: Naval Postgraduate School	6b Office Symbol (*if applicable*) 69		7a Name of Monitoring Organization: Naval Postgraduate School
6c Address (*city, state, and ZIP code*): Monterey, CA 93943-5000			7b Address (*city, state, and ZIP code*): Monterey, CA 93943-5000
8a Name of Funding/Sponsoring Organization: **Wright Aeronautical Laboratory**	8b Office Symbol (*if applicable*)		9 Procurement Instrument Identification Number: **MIPR FY 1455-88-N0608**
8c Address (*city, state, and ZIP code*): **Wright-Patterson Air Force Base Dayton, Ohio 45433**			10 Source of Funding Numbers: Program Element No / Project No / Task No / Work Unit Accession No

11 Title (*Include security classification*) EFFECT OF VORTEX CIRCULATION ON INJECTANT FROM A SINGLE FILM-COOLING HOLE AND A ROW OF FILM-COOLING HOLES IN A TURBULENT BOUNDARY LAYER, PART2 : INJECTION BENEATH VORTEX UPWASH

12 Personal Author(s) Pisut Kaisuwan

13a Type of Report	13b Time Covered	14 Date of Report (*year, month, day*)	15 Page Count
Master's Thesis	From To	December 1989	183

16 Supplementary Notation The views expressed in this thesis are those of the author and do not reflect the official policy or position of the Department of Defense or the U.S. Government.

17 Cosati Codes			18 Subject Terms (*continue on reverse if necessary and identify by block number*)
Field	Group	Subgroup	Embedded vortex, vortex circulation film-cooled turbulent

19 Abstract (*continue on reverse if necessary and identify by block number*)

Results are presented which illustrated the effects of single embedded longitudinal vortices on heat transfer and injectant downstream of a row of film-cooling holes and downstream of a single hole in a turbulent boundary layer. Attention is focussed on the changes resulting as circulation magnitudes of the vortices are varied from 0.0 to 0.144 m^2/s. Mean temperature results are presented which show how injectant is distorted and redistributed by vortices, along with heat transfer measurements and mean velocity surveys. Injection hole diameter is 0.952 cm to give a ratio of vortex core diameter to hole diameter of about 1.5-1.6. The freestream velocity is maintained at 10 m/s, and the blowing ratio is approximately 0.5. Film-cooling holes are oriented 30 degrees with respect to the test surface. Stanton numbers are measured on a contant heat flux surface with a nondimensional temperature parameter of about 1.5. The situation studied is one where the middle injection hole is beneath the vortex upwash. For all results, vortex centers pass within 2.9 vortex core diameters of the middle injection hole.

To quantity the influences of the vortices on the injectant, the parameter S is introduced, defined as the ratio of vortex circulation to injection hole diameter times mean injection velocity. The perturbation to film injectant and local heat transfer is determined by the magnetude of S. When S is greater than 1.0-1.5, injectant is swept into the vortex upwash and above the vortex core by secondary flows, and Stanton number data show evidence of injectant beneath the vortex core and downwash near the wall for x/d only up to about 17.5. For larger x/d, local hot spots are present, and the vortices cause local Stanton numbers to be augmented by as much as 25 percent in the film-cooled boundary layers. When S is less than 1.0, some injectant remains near the wall beneath the vortex core and downwash where it continue to provide some thermal protection. In some cases, the protection provided by film cooling is augmented because of vortex secondary flows which cause extra injectant to accumulate near upwash regions.

20 Distribution/Availability of Abstract	21 Abstract Security Classification	
☒ unclassified/unlimited ☐ same as report ☐ DTIC users	Unclassified	
22a Name of Responsible Individual: Phillip. M. Ligrani	22b Telephone (*include Area code*): (408) 646-3382	22c Office Symbol: 691.i

DD FORM 1473,84 MAR 83 APR edition may be used until exhausted. All other editions are obsolete

security classification of this page

Unclassified

Approved for public release; distribution is unlimited.

Effect of Vortex Circulation on Injectant from a Single Film-Cooling Hole and a Row of Film-Cooling Holes in a Turbulent Boundary Layer, Part 2 : Injection beneath the vortex upwash

by

Pisut Kaisuwan
Lieutenant Commander, Royal Thai Navy
B.S., Royal Thai Navy Academy, THAILAND, 1980

Submitted in partial fulfillment
of the requirements for the degree of

MASTER OF SCIENCE IN MECHANICAL ENGINEERING

from the

NAVAL POSTGRADUATE SCHOOL
December 1989

Author: Pisut Kaisuwan
Pisut Kaisuwan

Approved by: Phillip M. Ligrani
Phillip M. Ligrani, Thesis Advisor

Chelakara S. Subramanian
Chelakara S. Subramanian, Co-Thesis Advisvor

Anthony J. Healey
Anthony J. Healey, Chairman
Department of Mechanical Engineering

ABSTRACT

Results are presented which illustrated the effects of single embedded longitudinal vortices on heat transfer and injectant downstream of a row of film-cooling holes and downstream of a single hole in a turbulent boundary layer. Attention is focussed on the changes resulting as circulation magnitudes of the vortices are varied from 0.0 to 0.144 m^2/s, Mean temperature results are presented which show how injectant is distorted and redistributed by vortices, along with heat transfer measurements and mean velocity surveys. Injection hole diameter is 0.952 cm to give a ratio of vortex core diameter to hole diameter of about 1.5-1.6. The freestream velocity is maintained at 10 m/s, and the blowing ratio is approximately 0.5. Film-cooling holes are oriented 30 degrees with respect to the test surface. Stanton numbers are measured on a constant heat flux surface with a nondimensional temperature parameter of about 1.5. The situation studied is one where the middle injection hole is beneath the vortex upwash. For all results, vortex centers pass well within 2.9 vortex core diameters of the middle injection hole.

To quantify the influences of the vortices on the injectant, the parameter S is introduced, defined as the ratio of vortex circulation to injection hole diameter times mean injection velocity. The perturbation to film injectant and local heat transfer is determined by the magnitude of S. When S is greater than 1.0-1.5, injectant is swept into the vortex upwash and above the vortex core by secondary flows, and Stanton number data show little evidence of injectant beneath the vortex core and downwash

near the wall for x/d only up to about 17.5. For large x/d, local hot spots are present, and the vortices cause local Stanton numbers to be augmented by as much as 25 percent in the film-cooled boundary layers. When S is less than 1.0, some injectant remains near the wall beneath the vortex core and downwash where it continue to provide some thermal protection. In some cases, the protection provided by film cooling is augmented because of vortex secondary flows which cause extra injectant to accumulate near upwash regions.

Accession For	
NTIS GRA&I	X
DTIC TAB	☐
Unannounced	☐
Justification	
By	
Distribution/	
Availability Codes	
Dist	Avail and/or Special
A-1	

TABLE OF CONTENTS

LIST OF TABLES

LIST OF FIGURES

TABLE OF SYMBOLS

A	- area of injection hole
d	- injection hole diameter
U	- mean velocity
m	- blowing ratio, $\rho_c U_c/\rho_\infty U_\infty$
St	- Stanton number with vortex and film injection
Sto	- baseline Stanton number, no vortex, no film-cooling
Stf	- Stanton number, with film-cooling
X, x	- steamwise distance
Y	- distance normal to the surface
Z	- spanwise distance from test surface centerline
x/d	- dimension streamwise position : streamwise distance measured from the downstreram edges of the injection holes, divided by injection hole diameter
T	- static temperature
ρ	- density
θ	- non-dimensional injection temperature, $(Tr_c-Tr_\infty)/(Tw-Tr_\infty)$
Γ	- circulation of streamwise cirlation vorticity
S	- non-dimensional circulation, $\Gamma/U_c.d$
ω_x	- streamwise vorticity

ω_{xmax} - maximum streamwise vorticity, occuring at vortex core center

Zcore, Ycore, Z2core, Y2core - core radii in the Z and Y directions, symbols used in vorticity plots representing values derived from different vortex core models

Cr, Cr2 - vortex circulation, symbols used in vorticity plots representing circulation values derived from different vortex core models

2c/d - dimensionless core size parameter : twice the average core radius divided by the injection hole diameter

Zcen - spanwise location of vortex core center

Subscripts

c - injectant at exits of injection holes

w - wall

r - recovery condition

∞ - freesteam

ACKNOWLEDGEMENTS

This research was supported by Wright Aeronautical Laboratories, Wright-Patterson Air Force Base; Dr. Dick Rivir, program monitor.

The composition of this study was greatly influenced by Phillip M. Ligrani along with the work of S. L. Joseph, A. Ortiz, G. E. Schwartz and W. W. Williams.

Technical contributions were made by Dr. Chelakara Subramanian through his expert adaptation of computer software and his knowledgeable instruction in surface flow visualization techniques. Also, a special thanks for his assistants in the review of this thesis.

I wish to express my heartfelt thanks to my thesis advisor, Professor Phillip M. Ligrani, whose invaluable guidance, time, enthusiasm made this end result possible. I am deeply grateful for having had the good fortune of working with a man of his patience and understanding.

I. INTRODUCTION

A. BACKGROUND AND RELATED STUDIES

In order to devise improved film cooling schemes to protect surfaces of components in high temperature engines from thermal loading which results from exposure to hot gases, designers must be able to account for the detrimental effects resulting from the presence of embedded longitudinal vortices. This is because, firstly, embedded vortices are abundant in many such components. Secondly, embedded vortices cause significant perturbations to local wall heat transfer distributions (Eibeck and Eaton [Ref. 1]), as well as to the distributions of film coolant along with the accompanying thermal protection [Ref. 2; Ref. 3]. Of importance are the magnitude of perturbations to wall heat transfer and injectant distribution as well as the spatial extents of these perturbations on high temperature engine component surfaces. To determine such perturbations and extents, the designer must have knowledge of the effects of vortex strength, vortex size, and vortex location relative to a vast array of film cooling injection rates, hole sizes, geometries and configurations.

The size and strength of embedded longitudinal vortices are particularly varied in turbine blade passages of gas turbine engines. At the intersection of the blade leading edge and end wall, a horseshoe or leading edge vortex develops as a result of the intense local pressure gradient which forces fluid toward the end wall. The horseshoe vortex then splits into a suction side leg and a pressure side leg. As the pressure side leg further develops, it become the passage vortex and is influenced by

the cross-passage static pressure gradient. Depending on the amount of blade loading, the suction leg may reside at the intersection of the suction side and the endwall, or it may be pushed away from the endwall by the passage vortex from an adjacent blade. Corner vortices also develops at many locations, along with Taylor-Goertler vortices which from near concave surface of turbine blades as a result of centrifugal instabilities. Because of the complexity and variety of fluid/thermal interactions between film injectant and the different embedded vortices, numerical modelling and prediction of these flows are not presently practical and experiments are needed to clarify physical behavior.

However, in spite of this, experimental studies of the interactions of embedded vortices and film cooling are relatively scarce. One of the earliest is reported by Blair [Ref. 4], who measured heat transfer on an endwall film-cooled using a slot inclined at a 30 degree angle. The large vortex located in the corner between the endwall and the suction surface of their cascade was believed to cause significant variations of measured heat transfer and film cooling effectiveness. Goldstein and Chen [Ref. 5; Ref. 6] studied the influence of flows originating near the endwall on blade film cooling from one and two row of holes. A triangular region was found on the convex side of the blade where coolant was swept away from the surface by the passage vortex.

Ligrani, et al, [Ref. 2] examined the influences of embedded longitudinal vortices on film cooling from a single row of film cooling holes in turbulent boundary layers. Each hole was inclined at an angle of 30 degrees with respect to the test surface, and spaced 3 hole diameters from neighboring holes. Blowing ratios ranged from 0.47 to 0.98, and freestream velocities were 10 m/s and 15 m/s. Surface heat transfer

distributions, mean velocities, and mean temperatures show that film coolant is greatly disturbed and local Stanton numbers are altered significantly by the secondary flows within vortices. Because characteristics of these secondary flows change around the vortex, the spanwise position of the vortex with respect to film cooling holes is very important. Secondary heat transfer peaks are also present which are associated with region of high streamwise velocity. These peaks become higher in magnitude and persistent with downstream distance as the blowing ratio increases from 0.47 to 1.26, Ligrani, et al, [Ref. 19].

To further clarify the interactions between vortices and wall jets, Ligrani and Williams [Ref. 3] then examined the effects of an embedded vortex on injectant from a single film-cooling hole in a turbulent boundary layer. Attention was focussed on the effect of spanwise position of the vortices with respect to film injection holes. The ratio of vortex circulation to injection velocity times hole diameter was 3.16, and the ratio of the vortex core size to injection hole diameter was 1.58. The main conclusion of this study is that injection hole centerlines must be at least 2.9-3.4 vortex core diameters away from the vortex center in the lateral direction to avoid significant alterations to wall heat transfer and distributions of film injectant.

The present study is different from and an extension of results presented by Ligrani, et al [Ref. 2] and Ligrani and Williams [Ref. 3] by focussing on the changes which result as vortex circulation is altered. Heat transfer, mean velocity components, and injection distributions are measured downstream of a row of injection holes and downstream of a single film-cooling hole. All holes are inclined at 30 degrees with a blowing ratio of about 0.5. For all tests, the vortex upwash passes above the center line

of the middle injection hole such that the vortex center passes a distance equivalent to 0.87 vortex core diameters away in the positive spanwise direction. Vortices are generated using a half-delta wing placed on the wind tunnel test surface, and vortex circulation is varied by changing the angle of attack of the delta wing.

With these results, additional physical understanding of the convective heat transfer processes as a result of an extremely complex shear layer interaction are provided. Such design information will lead to improved film-cooling configurations which minimize the detrimental effects of vortex secondary flows on film cooling protection. These results will ultimately result in lower thermal stress distributions, giving higher turbine inlet temperatures, more efficient engines, and improved power to weight ratios.

B. THESIS OBJECTIVES

The present study is an extension of the work of References 2, 3, 10, 15, 17, 18 and 19. In those studies, attention was focussed on effects of blowing ratio and spanwise vortex position. The principal objective of the present study is to study the interactions between a single longitudinal embedded vortex and injectant from a single film cooling hole and a row of film cooling holes as vortex circulation is varied from 0 m^2/s to 0.144 m^2/s. Of particular interest are the changes imposed upon surface heat transfer and distributions of film injectant. The circulation of embedded vortices is altered by changing the angle of attack of the delta wing used to generate the vortices from 0 to 18 degrees. The single injection hole and the middle hole of the row of hole are always located beneath the vortex upwash as the vortex passes the injection location.

C. THESIS ORGANIZATION

The organization of this report is now discussed. In section 2 experimental apparatus and procedures are presented. This is followed by section 3 which gives experimental results. The results section consists of definitions of key parameters, velocity and streamwise vorticity surveys, mean temperature surveys, heat transfer measurements, and flow visualization results. Section 4 contains the summary and conclusions. This is followed by appendix A, which contains figures.

II. EXPERIMENTAL APPARATUS AND PROCEDURES

In order to isolate the interactions between film injectant and the vortices embedded in turbulent boundary layers, measurements are made on a flat plate in a zero pressure gradient. Wind tunnel speed is 10 m/s and temperature differences are maintained at levels less than 30 degrees Centigrade to maintain constant property conditions. With this approach, many of the other effects present in high-temperature engines are not present (curvature, high free-stream turbulence, variable properties, stator/blade wake interactions, shock waves, compressibility, rotation, etc.) since these may obscure and complicate the interaction of interest.

Detailed measurements are made in spanwise planes at different streamwise locations in order to elucidate the development and evolution of flow behavior. In order to match the conditions found in many practical applications, the boundary layer, embedded vortex, and wall jet are all turbulent.

A. WIND TUNNEL AND COORDINATE SYSTEM

The wind tunnel is the same one used in the experiments of Ligrani, et al [Ref. 2] and Ligrani and Williams [Ref. 3]. The facility is open-circuit, subsonic, and located in the laboratories of the Department of Mechanical Engineering of the Naval Postgraduate School. A centrifugal blower is located at the upstream end, followed by a diffuser, a header box containing a honeycomb and three screens, and then a 16 to 1 contraction ratio nozzle. The nozzle leads to the test section which is a rectangular

duct 3.05 m long and 0.61 m wide, with a top wall having adjustable height to permit changes in the streamwise pressure gradient.

A schematic showing the test section and coordinate system is presented in Figure 1. The vortex generator base plate is shown to be located 0.48 m downstream of the boundary layer trip. The left edge of this base plate (looking downstream) is the base edge referred to in Table 1 as a location reference. This is further clarified in Figures 2-5. The downstream edge of the row of 13 injection holes is then 0.60 m further downstream from this base plate. The surface used for heat transfer measurements is then located a short distance farther downstream. With this surface at elevated temperature, an unheated starting length of 1.10 m exists, and the direction of heat transfer is then from the wall to the gas. Thermocouple row locations along the test surface are labelled in Figure 2. In regard to the coordinate system, Z is the spanwise coordinate measured from the test section centerline, X is measured from the upstream edge of the boundary layer trip, and Y is measured normal to the test surface. x is measured from the downstream edge of the injection holes and generally presented as x/d.

B. INJECTION SYSTEM

The injection system is described by Ligrani, et al [Ref. 2] and Ligrani and Williams [Ref. 3]. Of the thirteen injection holes, the one referred to as the middle hole is located on the spanwise centerline (Z = 0.0 cm) of the test surface. Each hole has a diameter of 0.952 cm, is inclined at an angle of 30 degrees with respect to the test surface and is spaced 3 diameters from neighboring holes. Air for the injection system originates in a 1.5 horsepower DR513 Rotron Blower capable of producing 30

cfm at 2.5 psig. From the blower, air flows through a regulating value, a Fisher and Porter rotometer, a diffuser, and finally into the injection heat exchanger and plenum chamber. The exchanger provides means to heat the injectant above the ambient temperature. With this system and test plate heating, the non-dimensional injection temperature parameter θ was maintained at about 1.5 for all tests to maintain conditions similar to ones existing in gas turbine components. The plenum connects to thirteen plexiglass tubes, each 8 cm long with a length/diameter ratio of 8.4. With no vortex present, boundary layer displacement thickness at the injection location is 0.28d.

Injection system performance was checked by measuring discharge coefficients which compared favorably with earlier measurements. Procedures to measure discharge coefficients and blowing ratios are described by Ligrani, et al [Ref. 2].

C. GENERATION AND CONTROL OF VORTEX CHARACTERISTICS

The device used to generate the vortices is shown in Figure 3. The generator is a half delta wing with 3.2 cm height and 7.6 cm base. The wing is attached to a base plate and rotated about the pivot point to give different generator angle which, in turn, result in different vortex circulation magnitudes.

With half-delta wing generators, vortices are produced with secondary flow vectors such as the ones presented in chapter III. As vortex circulation becomes larger, secondary flow velocities between the vortex center and the wall increase, and amount of spanwise vortex drift increases as the vortices are convected downstream. Thus, if the pivot point is maintained at the same location, increasing angle A produces stronger vortices whose centers are located at more negative Z locations along the test surface.

In order to obtain systematic results as circulation is changed, the present study requires that the same portion of the vortex be located over the middle injection hole as the vortex passes. In other words, the distance between the centerline of the middle injection hole and vortex centers (located at local vorticity maxima) must be maintained constant. To accomplish this, spanwise starting locations of the vortices must be altered by changing positions of the generator mounting plate in the spanwise direction, as listed in Table 1.

The first step in determining the spanwise locations in Table 1 was to measure spanwise locations of the local vorticity maxima as the delta wing angle A was changed, while maintaining constant the location of the generator pivot point (Figure 3). The Z locations of these maxima at x/d = 0.0 gave amount of spanwise drift of the vortices at the streamwise location of the injection holes. The amount of required base plate adjustment was then determined from these Z locations. Positions in Table 1 are then the ones which maintain constant vortex center locations with respect to the middle injection hole centerline, as the vortices pass this injection hole. In the present study, the injection emerges beneath the vortex upwash and the vortex center is located at about +1.3 cm relative to Z = 0.0. This spanwise location corresponds to the centerline of the middle hole which is also the centerline of the test surface.

Vortices with different circulation magnitudes are labelled r, w, x, y, and z in Tables 1, 2, 3 and 4, where a particular label applies to a particular generator angle. The same vortex labels are then used whether of not injection is employed, which is important because vortex characteristics are often altered slightly by injectant. Table 2 gives characteristics of vortices r, w, x, y, and z with no injection. Table 3 gives

characteristics of embedded vortices for a single injection hole with m = 0.5. Table 4 gives characteristics of embedded vortices when m = 0.5 injection emerges from 13 holes. All of these data were obtained from measurements at x/d = 41.9. In these tables, c is the vortex core radius, determined as one half of the sum of average core radii in Y and Z directions (as measured from vortex centers). These radii are determined for the area which encompasses all vorticity values greater than or equal to 40 percent of peak vorticity (at the center) for a particular vortex. The choice of 40 percent was made to give a good match to core radii determined at the locations of maximum secondary flow vectors, Craig [Ref. 7]. The area enclosed by secondary flow maxima is important because, for ideal Rankine vortices, it corresponds to the area containing all vorticity. Secondary flow vector maxima are not used to determine core size because this leads to results which are less accurate than the 40 percent threshold approach. 2c/d then gives the ratio of the vortex core diameter to injection hole diameter. Core sizes are about the same even though peak vorticity varies, as indicated by 2c/d values ranging from 1.45 to 1.62 for vortices r, w, x, y, and z in Tables 2-4. Also contained in the latter two Tables is parameter S, which will be discussed in chapter III.

Table 1 Vortex Generator Spanwise positions for different vortex strengths

Vortex	Vortex Generator Angle (degrees)	Spanwise Z Locations of the Generator Base Edge
r	18	+3.80
w	15	+3.29
x	12	+2.27
y	8	+0.24
z	4	-0.27

Table 2 Characteristics of Embedded Vortices for No Film-Cooling

Vortex	Vortex Generator Angle (degrees)	Maximum Streamwise Vorticity (1/s)	Circulation (m^2/s)	2c/d
r	18	760.	0.150	1.62
w	15	626.	0.116	1.52
x	12	522.	0.085	1.49
y	8	278.	0.041	1.47
z	4	179.	0.019	1.51
no vortex	0	000.	0.000	----

Table 3 Characteristics of Embedded Vortices with Injection from a Single Hole

Vortex	Vortex Generator Angle (degrees)	Maximum Streamwise Vorticity (1/s)	Circulation (m^2/s)	S	2c/d
r	18	745.5	0.144	3.03	1.61
w	15	668.3	0.113	2.38	1.56
x	12	536.8	0.079	1.67	1.52
y	8	303.9	0.039	0.82	1.48
z	4	159.0	0.017	0.35	1.49
no vortex	0	000.0	0.000	0.00	----

Table 4 Characteristics of Embedded Vortices with Injection from 13 holes

Vortex	Vortex Generator Angle (degrees)	Maximum Streamwise Vorticity (1/s)	Circulation (m^2/s)	S	2c/d
r	18	763.	0.134	2.82	1.58
w	15	663.	0.108	2.28	1.53
x	12	593.	0.079	1.67	1.50
y	8	339.	0.430	0.91	1.45
z	4	155.	0.010	0.26	1.49
no vortex	0	000.	0.000	0.00	----

D. MEAN VELOCITY COMPONENTS

Mean velocity components were measured using a five-hole pressure probe with a conical tip manufactured by United Sensors Corporation. Celesco transducers and Carrier Demodulators were used to sense pressures when connected to probe output ports. Following Ligrani, et al [Ref. 8], corrections were made to account for spatial resolution and downwash velocity effects. An automated traverse used for injectant surveys was used to obtain surveys of secondary flow vectors, from which, mean streamwise vorticity contours were calculated (see section III A). These devices, measurement procedures employed, as well as data acquisition equipment and procedures used are further detailed by Ligrani, et al [Ref. 2; Ref. 9].

E. STANTON NUMBER MEASUREMENTS

Details on the measurement of local Stanton numbers are given by Craig [Ref.7], Ligrani, et al [Ref. 2], and Ligrani and Williams [Ref. 3]. A summary of these procedures is also repeated here.

The heat transfer surface is designed to provide a constant heat flux over its area. The surface next to the airstream is stainless steel foil painted flat black. Immediately beneath this is a liner containing 126 thermocouple, which is just above an Electrofilm Corp. etched foil heater rated at 120 volts and 1500 watts. Located below the heater are several layers of insulating materials including a several Lexan sheets, foam insulation, styrofoam and balsa wood. Surface temperature levels and convective heat transfer rates are controlled by adjusting power into the heater using a Standard Electric Co. variac, type 3000B. To determine the heat loss by conduction, an energy balance was performed. Radiation losses from the top of the test surface were estimated

analytically. The thermal contact resistance between thermocouples and the foil top surface was estimated on the basis of outputs of the thermocouples and measurements from calibrated liquid crystals on the surface of the foil. This difference was then correlated as a function of heat flux through the foil.

After the surface was completed, a variety of qualification tests were conducted to check its performance. These are described in detail by Ortiz [Ref. 10].

F. MEAN TEMPERATURE MEASUREMENTS

Copper-constantan thermocouples were used to measure temperature along the surface of the test plate, the freestream temperature, as well as temperature distributions which are correlated to injection distributions. For the distributions, a thermocouple was traversed over spanwise/normal planes (800 probe locations) using an automated two-dimensional traversing system which could be placed at difference streamwise locations. Ligrani, et al [Ref. 2] and Ligrani and Williams [Ref. 3] gives additional detail including procedures used for calibration.

G. EXPERIMENTAL UNCERTAINTIES

Uncertainty analysis details are given by Schwartz [Ref. 11]. Uncertainty estimates are based upon 95 percent confidence levels, and determined following procedures described by Kline and McClintock [Ref. 12], and by Moffat [Ref. 13]. Typical nominal values of freestream recovery temperature and wall temperature are 18.0 and 40.0 degrees Centigrade, with respective uncertainties of 0.13 and 0.21 degrees Centigrade. The freestream density, freestream velocity and specific heat uncertainties are 0.009 kg/m^3 (1.23 kg/m^3), 0.06 m/s (10.0m/s) and 1 J/kg K (1006 J/kg K), where

typical nominal values are given in parenthesis. For total convective heat transfer, heat transfer coefficient, and heat transfer area, 10.5 W (270 W), 1.03 W/m^2K (24.2 W/m^2K), and 0.0065 m^2 (0.558 m^2) are typical. Uncertainties of St, St/Sto, m and x/d are 0.000086 (0.00196), 0.058 (1.05), 0.025 (0.5), and 0.36 (41.9), respectively.

III. EXPERIMENTAL RESULTS

A. DEFINITIONS OF KEY PARAMETERS

Circulation over a region A in the Y-Z plane is given by :

$$\Gamma = \int_A \omega_x dA$$

where ω_x is the streamwise vorticity, given by :

$$\omega_x = \frac{\partial U_z}{\partial y} - \frac{\partial U_y}{\partial z}$$

Streamwise vorticity is approximated using a finite difference equation for each sample point :

$$\omega_x(y, z) = \frac{U_z(y + \Delta y, z) - U_z(y - \Delta y, z)}{2\Delta y} - \frac{U_y(y, z + \Delta z) - U_y(y, z - \Delta z)}{2\Delta z}$$

where Δy and Δz are the incremental probe positions in the y and z directions, respectively.

Circulation magnitudes are calculated assuming that all vorticity values less than threshold are equal to zero. The same numerical threshold of 76. (1/s) is used throughout this thesis. This value is equal to 10 percent of the maximum vorticity of vortex r with no injection, as measured at x/d = 41.9 (Table 2). Schwartz [Ref. 11]

utilizes a threshold vorticity of 100 s^{-1}. In order to provide continuity between Schwartz results and those of the present study, circulation is also estimated based a threshold vorticity of 100 s^{-1}.

To quantify the influences of the vortex circulation on injectant, the following dimensionless parameter S is used, defined as :

$$S \approx \Gamma/(U_c.d)$$

As such, S quantifies vortex strength relative to injection jet strength, U_c and d are the average injection velocity at the wall and the diameter of the injection hole, respectively. For all cases of the present study, U_c and d are not changed as the blowing ratio m is maintained constant and injection geometry is not altered. With no film cooling (m = 0, U_c = 0), S has no meaning and therefore is not used.

The dimensionless parameter used to compare vortex core size relative to injection hole size is defined by :

$$2c/d = \frac{2\,((Z_{core} + Y_{core})/2)}{d}$$

Here, c represents the average vortex core radius. Two separate schemes for calculating the average vortex core diameter are used. These are mentioned in chapter II. In the first, 2c is estimated for the area surrounded by maximum secondary flow velocity vectors. The magnitudes of these vectors are defined as $(U_y^2 + U_z^2)^{1/2}$. This method is accurate only within ±0.51 cm., since this is the spacing between sample points in the

Z and Y directions with the second scheme, the vortex core is consider to include the area containing all vorticity magnitudes greater than 40 % of the peak value.

Figures 6-17 show streamwise vorticity distributions. Circulation magnitudes determined based on a threshold vorticity of 100 s^{-1} are denoted on these figures as Cr, while of circulation based on the 76.03 s^{-1} vorticity threshold are annotated Cr2. Vortex core radii calculated from secondary velocity maxima and minima are denoted as Zcore and Ycore, while core radii calculated using the 0.4 ω_{xmax} approach are denoted as Z2core and Y2core.

B. FIVE HOLE PRESSURE PROBE SURVEY

Figures 6-53 show distributions of streamwise vorticity, streamwise mean velocity, secondary flow vectors and total pressure. These surveys are obtained using the five hole pressure probe. For each survey, the probe is positioned at 800 different locations in spanwise normal planes at x/d = 41.9. The surveys are conducted for a single injection hole and a row of 13 injection holes. All results are obtained with a blowing ratio m of 0.5. The freestream velocity U_∞ is maintained at about 10 m/s.

1. Streamwise Vorticity Contours

S is represented as Cr2/(Uc.d) and Cr/(Uc.d) in Figures 6-17. Values of ω_{xmax}, 2c/d, Zcore, Ycore, Z2core and Y2core are also given in these figures. Figure 17 shows the vorticity distribution with no vortex to provide a baseline check on measurement procedure. From these data, it is evident that sizes of vortices and magnitudes of vorticity both increase as the vortex generator angle increases from 0 to 18 degrees. Streamwise vorticity contours are presented in Figures 6 - 10 when a single injection hole is employed. At x/d = 41.9, spanwise locations of the vortex

center (Zcen) for each of these five vortices are within ± 0.51 cm of Z = 0.0 cm. Table 5 summarizes vortex parameter data for this experimental configuration.

Table 5 Streamwise Vorticity Parameter Data for a Single Injection Hole

Vortex	Vortex Generator Angle (degree)	ω_{max} (1/s)	Γ (m^2/s)	S	2c/d	Zcore cm.	Ycore cm.	Z2core cm.	Y2core cm.
r	18	745.5	.144	3.03	1.61	.76	.51	.76	.76
w	15	668.3	.113	2.38	1.56	.76	.76	.74	.74
x	12	536.8	.079	1.67	1.52	.51	.76	.72	.72
y	8	303.9	.039	0.82	1.48	.51	.76	.69	.72
z	4	159.0	.017	0.35	1.49	.76	.76	.68	.73

Figures 12-16 show streamwise vorticity contours when a row of 13 injection holes is employed. At x/d = 41.9, spanwise locations of vortex centers (Zcen) for each of these five vortices are again within ± 0.51 cm of Z = 0.0 cm. Vortex characteristics for this configuration are given in Table 6.

Table 6 Streamwise Vorticity Parameter Data for a row of 13 Injection Holes

Vortex	Vortex Generator Angle (degree)	ω_{max} (1/s)	Γ (m^2/s)	S	2c/d	Zcore cm.	Ycore cm.	Z2core cm.	Y2core cm.
r	18	736.6	.134	2.82	1.58	.51	.76	.75	.75
w	15	662.5	.108	2.28	1.53	.76	.76	.72	.73
x	12	593.1	.079	1.67	1.50	.51	.51	.71	.72
y	8	338.9	.043	0.91	1.45	.76	.25	.68	.71
z	4	154.8	.013	0.26	1.49	.76	.76	.71	.71

2. Secondary Flow Vectors Field, Streamwise Velocity Distributions, and Total Pressure Distributions

Secondary flow vectors, streamwise velocity distributions and total pressure distributions are presented in figures 18-53. Figures 18-35 show results for the single injection hole experiments. Figures 36-53 show results when the row of 13 injection holes was employed.

For a single injection hole film cooling, Figures 18-20 show results obtained with vortex r. High streamwise velocities are evident near the wall in Figure 18 at the downwash side of the vortex. Low streamwise velocity fluid is evident away from the wall on the upwash side. Figure 19 shows secondary flow vectors. Clockwise rotating vectors indicate the presence of the vortex. Secondary velocities in the upwash region (left portion of vortex) are directed upwards, away from the wall (+Y direction). The secondary crossflow velocities in downwash region (right portion of vortex) are directed towards the wall (-Y direction). Figure 19 also shows strong secondary velocities between the wall and the vortex. The total pressure field is presented in Figure 20 and shows trends similar to ones shown by the streamwise velocity. Figures 21-23 present results for vortex w. Results for vortices x, y and z are shown in Figures 24-26, Figures 27-29 and Figures 30-32 respectively. Figures 33-35 present results when no vortex is presented. A comparison of these different results show how vortex properties change with different vortex circulation magnitudes.

The results in Figures 36-53 show measurements when film cooling emerges from the row of 13 injection holes. Figures 36-38 present results for vortex r. Figures 39-41 show results for vortex w. Figures 42-44 show results for vortex x. Figures 45-47

present results for vortex y. Figures 48-50 show results for vortex z. Figures 51-53 present results obtained when no vortex generator is employed. The perturbations to the boundary layer are similar to those observed when a single injection hole is employed.

C. MEAN TEMPERATURE SURVEYS

Surveys of mean temperature are shown in Figures 54-83, which provide qualitative information on the distributions of injectant after it emerges from the film cooling holes. These results were obtained using an experimental approach introduced by Ligrani, et al (1989), in which the film injectant is heated to approximately 50 degrees Celsius without providing any heat on the test plate. The temperature field thus shows how the fluid from the injection holes is convected and distorted by the vortex since greater amounts of injectant are indicated by higher temperatures. Experimental results presented in Figures 54-65 show mean temperature surveys conducted at x/d = 41.9 and a blowing ratio = 0.5 for injection from both a single injection hole and a row of 13 injection holes. These surveys are conducted using vortices r, w, x, y, z and no vortex. Figures 66-71 show mean temperature surveys conducted at x/d = 33.6, 54.6 and 75.6 for a single injection hole and at x/d = 33.6, 54.6 and 75.6 for 13 injection holes. These data (in Figures 66-71) are presented for vortices w only. These temperature variations are slightly different from ones which would exist if the wall were heated because of different distributions of turbulent diffusion of injectant heat. However, in spite of this, a good qualitative indication of injectant distributions is obtained because, compared to convection, turbulent diffusion is of secondary importance in organizing relative positions of injectant concentrations.

Data in Figures 54-59 show the influence of vortex circulation on injectant from a single hole. Figures 60-65 show the influence of vortex circulation on injectant from a row of 13 injection holes. In both sets of figures, results are presented for vortices and no vortex. As vortex circulation increases, larger amounts of injectant are swept away from the wall into the vortex upwash region.

Figures 66-68 show injectant distributions with film cooling from a single injection hole at position A (x/d = 33.6), position C (x/d = 54.6) and position D (x/d = 75.6) respectively. Corresponding position B (x/d = 41.9) data are presented in Figure 55. Similar results are presented in Figures 69-71 for the situation in which a row injection holes are employed. As the vortex convects downstream, larger portions of the injectant are convected away from the wall and into vortex upwash regions.

The data in Figures 54-65 are again presented in Figures 72-83, except measured secondary flow vectors are superimposed on each of the latter figures to illustrate how their magnitudes and distributions relate to reorganization of injectant by the different vortices. The same scaling for secondary flow vectors is used for all of the figures.

D. HEAT TRANSFER MEASUREMENTS

In this section, baseline heat transfer data are first discussed. The following heat transfer measurements are then presented in three parts : (1) measurements of boundary layers with an embedded vortex and no film cooling, (2) measurements of boundary layers with film cooling from a single injection hole, with and without an embedded vortex, and (3) measurements of boundary layers with film cooling from a single row of injection holes, with and without an embedded vortex. For the last two parts,

addressed are the influences of the vortices on local heat transfer variations and injectant distributions.

1. Baseline Data Checks

Baseline data with no film injection and no vortex already exist for similar test conditions, Ligrani, et al [Ref. 2]. Repeated measurements of spanwise averaged Stanton number show good agreement (maximum deviation is 5 percent) with the correlation from Kays and Crawford [Ref. 14] for turbulent heat transfer to a flat plate with unheated starting length and constant heat flux boundary condition. Local and spanwise-averaged Stanton numbers with injection at a blowing ratio of 0.5 (and no vortex) also show agreement with earlier results, Ligrani, et al, [Ref. 2].

2. Heat Transfer Measurements : Embedded Vortex with No Film Cooling

Figures 84-88 present development of Stanton number ratios with streamwise distance. Here, Sto is the baseline Stanton number measured in turbulent boundary layer with a two dimensional mean flow field when no vortex and no film cooling are presented. St is then the Stanton number measured when a vortex is present. Each of these figures show the Stanton number ratios for X = 1.15, 1.25, 1.40, 1.60, 1.80, and 2.00 m., which correspond to x/d = 7.4, 17.5, 33.6, 54.6, 75.6, and 96.6, respectively. The figures show St/Sto magnitudes which are less than 1.0 in upwash region, and greater than 1.0 in vortex downwash regions.

Stanton number ratios in Figures 89-94 are presented to illustrate the variations in heat transfer which result as the magnitude of vortex circulation is changed. Data in each figure are given for a different x/d, where x/d ranges from 7.4 to 96.6. If the vortices have no effect on heat transfer, St/Sto ratios in these figures are

Examination of results at any streamwise location for any magnitude of circulation indicates that ratios are greater than 1.0 on the right-hand sides of the figures as a result of vortex downwash regions, and less than 1.0 on left-hand sides due to upwash regions. Between these two regions, St/Sto gradients exist along the length of the test surface. With the exception of data near the gradient for x/d <= 54.6, St/Sto the increases with circulation in the downwash region and decreases with circulation in the upwash region. The largest changes occur as circulation increases from 0.0 m^2/s (no vortex) to 0.019 m^2/s (vortex z), and as circulation increases from 0.019 m^2/s to 0.041 m^2/s (vortex y).

The streamwise coherence of the vortices is evident because ratio magnitudes are significantly different from 1.0 along the entire length of the test plate. In fact, in the downwash region, St/Sto increases with x/d until x/d = 33.6, after which, only very small changes with streamwise distance occur. With these characteristics, these data show agreement with qualitative trends and quantitative magnitudes reported by Eibeck and Eaton [Ref. 1] and Ligrani, et al [Ref. 2].

3. Heat Transfer Measurements : Film Cooling from a Single Injection Hole with and without an Embedded Vortex

Figures 95-100 present surveys to illustrate the influences of the different strength vortices on St/Sto and Stf/Sto. Each figure is given for a different x/d where x/d are equal to 7.4, 17.5, 33.6, 54.6, 75.6 and 96.6. In each figure, St/Sto data are given for vortices r, w, x, y and z, along with Stf/Sto data for no vortex. Comparison of these data thus shows how St/Sto change with vortex strength relative to Stf/Sto.

Results for x/d = 7.4 in Figure 95 evidence significant and complicated interactions between the vortices and the injectant. Near Z/d = 0.0, where the injectant nominally provides protection, St/Sto values are either about the same or slightly higher than Stf/Sto depending on whether the injectant is relatively undisturbed by the vortices or redistributed away form the wall by secondary flows. The former situation results when S <= 0.82 for vortices y and z. The latter situation occurs with stronger vortices r, w and x. At Z larger than 0.0, local St/Sto beneath downwash regions increase with S. The only exception is the S = 0.35 data for vortex z which have about the same magnitudes as when no vortex is presented. St/Sto ratios near vortex upwash regions at Z less than -2.5 cm. are about the same regardless of the magnitude of vortex circulation.

Results for x/d = 17.5 in Figure 96 show the same general qualitative trends as when x/d = 7.4, except for St/Sto minima near Z = 0.0 which show almost no variation with S. The positions of these minima are shifted about 1 cm. away from the nominal location of the injectant at this streamwise location because of vortex secondary flows near the wall.

St/Sto values beneath downwash regions for x/d = 17.5 in Figure 96, x/d = 33.6 in Figure 97 and x/d = 54.6 in Figure 98 are greater than ones for x/d = 7.4 in Figure 95. This is because local heat transfer variations are strongly affected by behavior in the near-wall portions of boundary layer regions where injectant initially accumulates. Some downstream development is then required before enough injectant is disturbed and swept away from the wall by vortex secondary flows to cause high St/Sto. Lower St/Sto are present with the stronger vortices because of a accumulation

of injectant in upwash regions. Less injectant collects in this area with the weaker vortices since they do not have the vitality to rearrange injectant from initial positions beneath vortex downwash regions. For x/d = 33.6 and x/d = 54.6, St/Sto values generally increase with S in downwash regions. The most significant St/Sto changes result as S increases from 0.82 to 1.67. For x/d >= 75.6 in Figures 99 and 100, changes with streamwise distance are quite small. The largest St/Sto values are 1.20-1.22 for S = 3.03. These amount to 22-23 percent increases over ratios with film injection only. In upwash regions, St/Sto data are noticeably lower than Stf/Sto data on the left-hand portions of figures when x/d >= 33.6. For these locations, different data sets follow the same qualitative trends (relative to Stf/Sto data for S = 0.0) with about the same quantitative magnitudes regardless of the value of S.

Figures 101-106 are presented to illustrate the streamwise development of St/Sto relative to Stf/Sto for one particular vortex strength. Results in each figure are given for x/d ranging from 7.4 to 96.6 (X = 1.15 to 2.0 m). The two ratios are plotted together on each figure so that St/Sto values can be compared to Stf/Sto ratios to indicate magnitudes of local perturbations provided to film-cooled boundary layers by the vortices. In the figures, St/Sto are generally higher than Stf/Sto near vortex downwash regions at larger Z, and St/Sto are generally lower than Stf/Sto at smaller Z in the vicinity of vortex upwash regions. Between these two regions, St/Sto gradients exist along the length of the test surface because of the streamwise persistence and coherence of the vortices.

With the upwash passing above the injection hole, results at x/d = 7.4 in Figure 101, 102 and 103 provide evidence that some of the film is lifted slightly off

the surface since the St/Sto local minimum is slightly higher than the Stf/Sto local minimum from the film only. In Figures 104 and 105, St/Sto at x/d = 7.4 are slightly lower than Stf/Sto evidencing an increase in the protection provided by the injectant as it is pushed towards the surface by downwash secondary flows just downstream of the injection location. When x/d >= 33.6, little evidence of the injectant is present except for St/Sto values beneath upwash regions which may be lowered slightly because of accumulation of injection. Figure 106 depicts the boundary layer streamwise development with no embedded vortex. The Stanton number at Z = 0.0 and x/d = 7.4 (X = 1.15 m) shows significant influence of the injectant. These effects are significantly diminished as the boundary layer develops in the streamwise direction. At x/d = 96.6 (X = 2.0 m) the centerline St/Sto and Stf/Sto values are nearly equal to 1.0, indicating that the effects of film cooling are very small.

4. Heat Transfer Measurements : Film Cooling from a Row of Injection Holes with and without an Embedded Vortex

Figures 107-112 present Stanton number ratios illustrating the influence of the different strength vortices on heat transfer in boundary layers film cooled using a row of injection holes. Each figure is given for a different x/d, where x/d equal 7.4, 17.5, 33.6, 54.6, 75.6 and 96.6 (X = 1.15, 1.25, 1.40, 1.60, 1.80 and 2.00 respectively). In each figure, St/Sto data are given for vortices r, w, x, y and z, along with Stf/Sto data for no vortex. One of the most striking aspects of these figures is evident if they are compared with data in Figures 89-94 for no injection. For smaller x/d, St/Sto with injection differ markedly from cases without injection. Initially, at x/d = 7.4 (X = 1.15 m) in Figure 107, the influence of the vortices is minimal if film injection is present.

As x/d increases to 17.5 (X = 1.25 m in Figure 108) and 33.6 (X = 1.4 m in Figure 109), perturbations from the vortices gradually become more apparent, until x/d = 54.6 (X = 1.6 m in Figure 110), when disturbances with injectant are very similar to the perturbations which result without injectant. Thus, initially downstream of injection locations, the film rather than the vortices is most responsible for the spanwise variations of heat transfer. This is because local heat transfer variations are strongly affected by behavior in the near-wall portions of boundary layers regions where injectant initially accumulates. Some downstream development is then required before enough injectant is disturbed and swept away from the wall by vortex secondary flows to cause high St/Sto (even though circulation decreases with streamwise development).

When the vortices influence local St/Sto, qualitative trends in Figures 107-112 are similar to ones in Figures 89-94 for no injection even though the mechanisms which result in changes to wall heat transfer are more complicated. In Figures 107-112, St/Sto are higher than Stf/Sto near vortex downwash regions at larger Z. Because of the downwash and other nearby secondary flows, injectant is depleted, the local boundary layer is thinned, and freestream fluid is convected very near the wall. St/Sto are lower than Stf/Sto at smaller Z in the vicinity of vortex upwash regions. The upwash and nearby secondary flow serve to sweep extra injectant into these regions sometimes giving added thermal protection. In addition, boundary layer fluid and injectant are convected away from the wall, resulting in a thicker local boundary layer. Once the vortices begin to influence local near-wall boundary layer behavior, St/Sto gradients exist along the remaining length of the test surface.

Figures 113-118 show the streamwise development of St/Sto and Stf/Sto for one particular vortex strength. Streamwise development is shown for vortices r, w, x, y, z and no embedded vortex for x/d ranging from 7.4 to 96.6. As for Figures 101-106, the two ratios are plotted together on each set of graphs so that St/Sto values can be compared to Stf/Sto ratios to indicate magnitudes of local perturbations provided to film-cooled boundary layers by the vortices.

E. FLOW VISUALIZATION RESULTS

Figures 119 and 120 present surface flow visualization results. The photographs show how an oil-pigment suspension placed on the test surface is rearranged and distorted by the vortices and film injection. In each photograph, the test surface spanwise centerline is labelled. The negative Z direction lies to the left of this symbol, while the positive Z lies to the right. The arrow shown at the top of most photographs indicates the spanwise position of the vortex generator at x = 0.48 m. This arrow is not present in photographs of flow patterns for turbulent boundary layers with no embedded vortex. The wide horizontal band visible in the middle of the photographs is due to a probe access slot in the test section top wall.

Figure 119 shows surface flow visualization when a single injection hole is employed. Labels a, b, c, d, and e correspond to the vortices r, w, x, y, and no vortex, respectively. The vortex upwash region below the centerline symbol is indicated by the bright area in these photographs. Here, white pigment accumulates on the test surface after secondary flow velocities have swept it in the transverse direction. The dark area in these photographs corresponds to vortex downwash regions. Evidence of film

injectant is not discernable in photographs a and b, in contrast to photographs c, d and e, wherein some evidence of injectant is evident.

Figure 120 shows surface flow visualization when a row injection holes is employed with vortices r, w, x, y, z and no vortex. These vortex configurations correspond to labels a, b, c, d, e and f, respectively. In these photographs, the dark regions show the path of vortex downwash regions and the bright areas just to the right of these dark regions correspond to vortex upwash regions. Streamwise paths of the film-cooling jets are also evident in these photographs, as indicated by narrow dark lines.

IV. SUMMARY AND CONCLUSIONS

Results are presented which illustrate the effects of single embedded longitudinal vortices on heat transfer and injectant downstream of a single of film-cooling hole and a row of film-cooling holes in the turbulent boundary layer. Attention is focussed on the changes resulting as circulation magnitudes of the vortices are varied from 0.0 to 0.144 m^2/s. The ratio of vortex core diameter to hole diameter is about 1.5-1.6, and the blowing ratio is approximately 0.5. The film-cooling hole is oriented 30 degrees with respect to the test surface. Stanton numbers are measured on a constant heat flux surface with a non-dimensional temperature parameter θ of about 1.5. The situation is studied with the injection hole beneath the vortex upwash. The vortices pass well within 2.9 vortex core diameters of the centerline of the injection hole.

To qualify the influences of the vortices on the injectant, the parameter S is used, defined as the ratio of vortex circulation to injection hole diameter times mean injectant velocity. The most important conclusion is that the magnitude of parameter S determines whether perturbations to local heat transfer and injection distributions are significant. S is varied from 0 to 3.03 for a single injection hole and from 0 to 2.82 for a row of injection holes. When S is greater than 1.0-1.5, injectant is swept into the vortex upwash and above the vortex core by secondary flows, and St/Sto data show little evidence of injectant beneath the vortex core and downwash near the wall for x/d up to 17.5 (for a single injection hole) and for x/d up to 7.4 and in some cases, 17.5 (for a row of injection holes). For larger x/d with such situations, the vortices

cause local Stanton numbers in the film-cooled boundary layers to be augmented by as much as 23 percent relative to film-cooled layers with no vortices for a single injection hole and 25 percent for a row of injection holes.

When S is less than 1.0-1.5, some injectant may remain near the wall beneath vortex core and downwash regions where it continues to provide some thermal protection. For a single injection hole with the weakest vortices studied (S = 0.35), evidence of injectant is evident for x/d values as large as 75.6. For a row of injection holes with S = 0.26, Stanton number ratios substantially less than 1.0 indicate that thermal protection is provided for x/d value at least up to 96.6. For S = 0.91, Stanton number ratios substantially less than 1.0 indicate that thermal protection is provided for x/d values up to about 54.6.

In some cases, the protection provided by film cooling is augmented because of the vortex when secondary flows cause extra injection to accumulate in one area, usually near the vortex upwash.

APPENDIX A

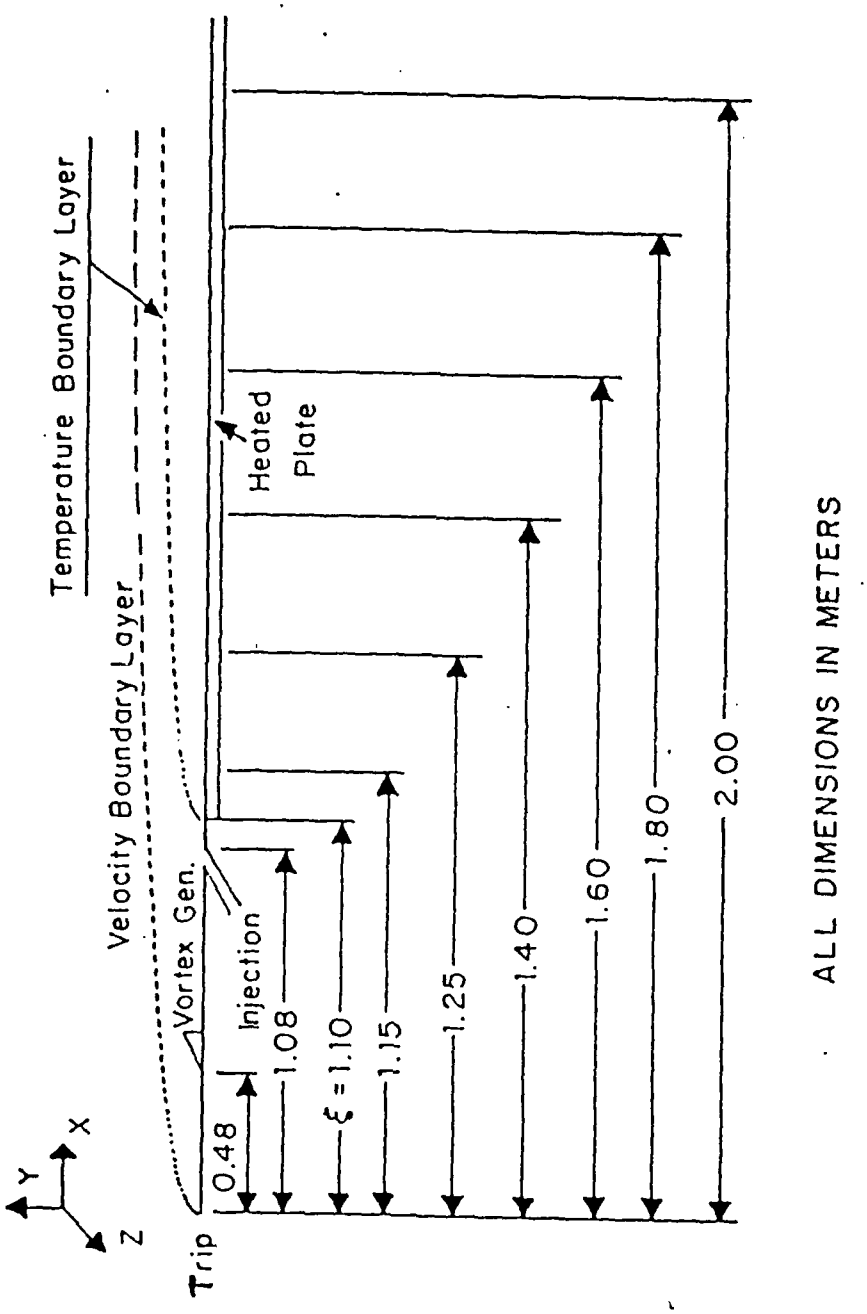

Figure 1 Test Section Coordinate System

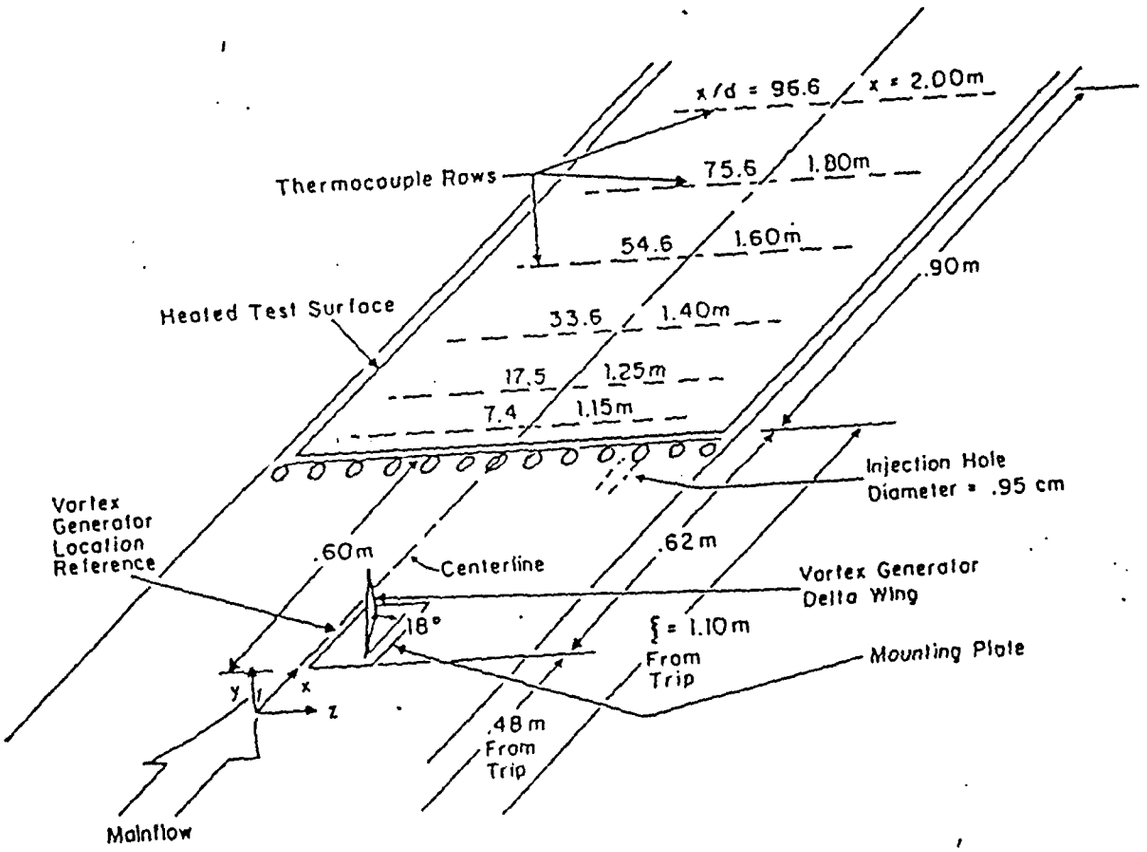

Figure 2 Top View Schematic of Wind Tunnel Test Section

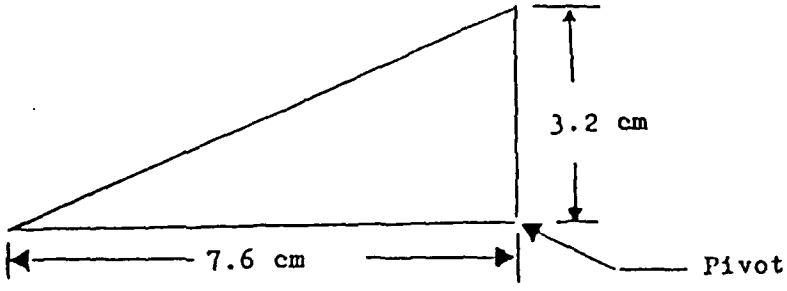

Half Delta Wing

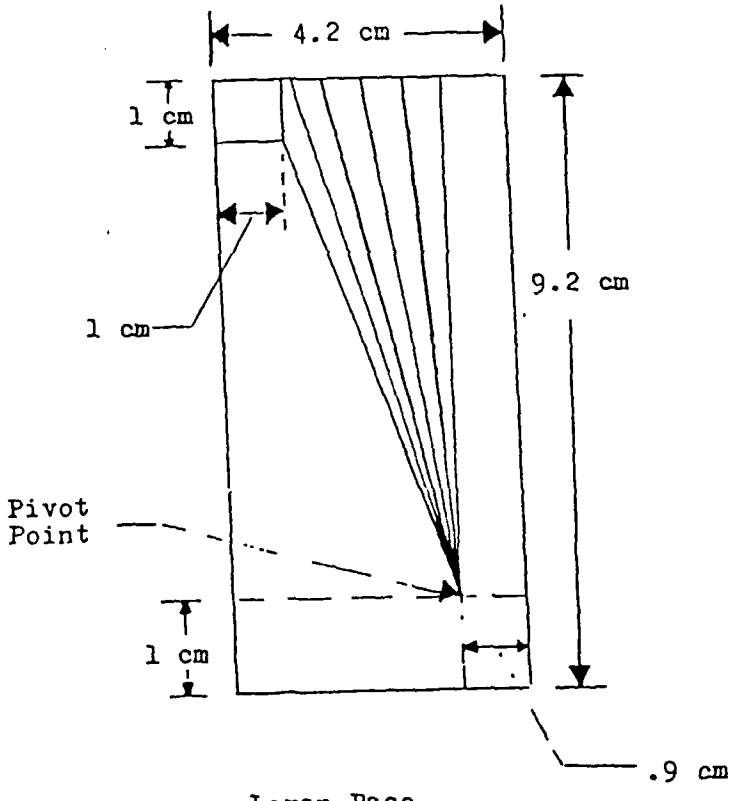

Lexan Base
(mounting plate)

Figure 3 Vortex Generator Details

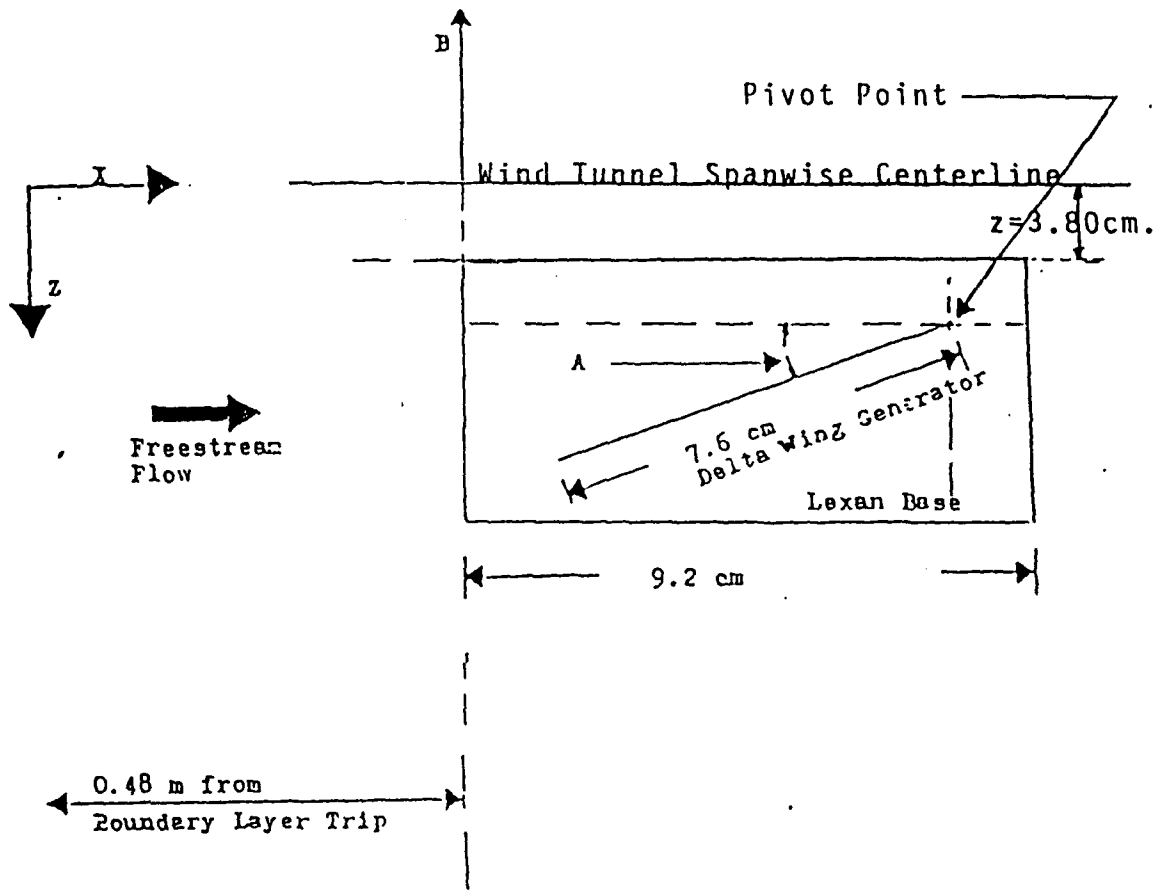

Figure 4 Vortex Generator Orientation in X-Z for Various Vortex Generator Angles

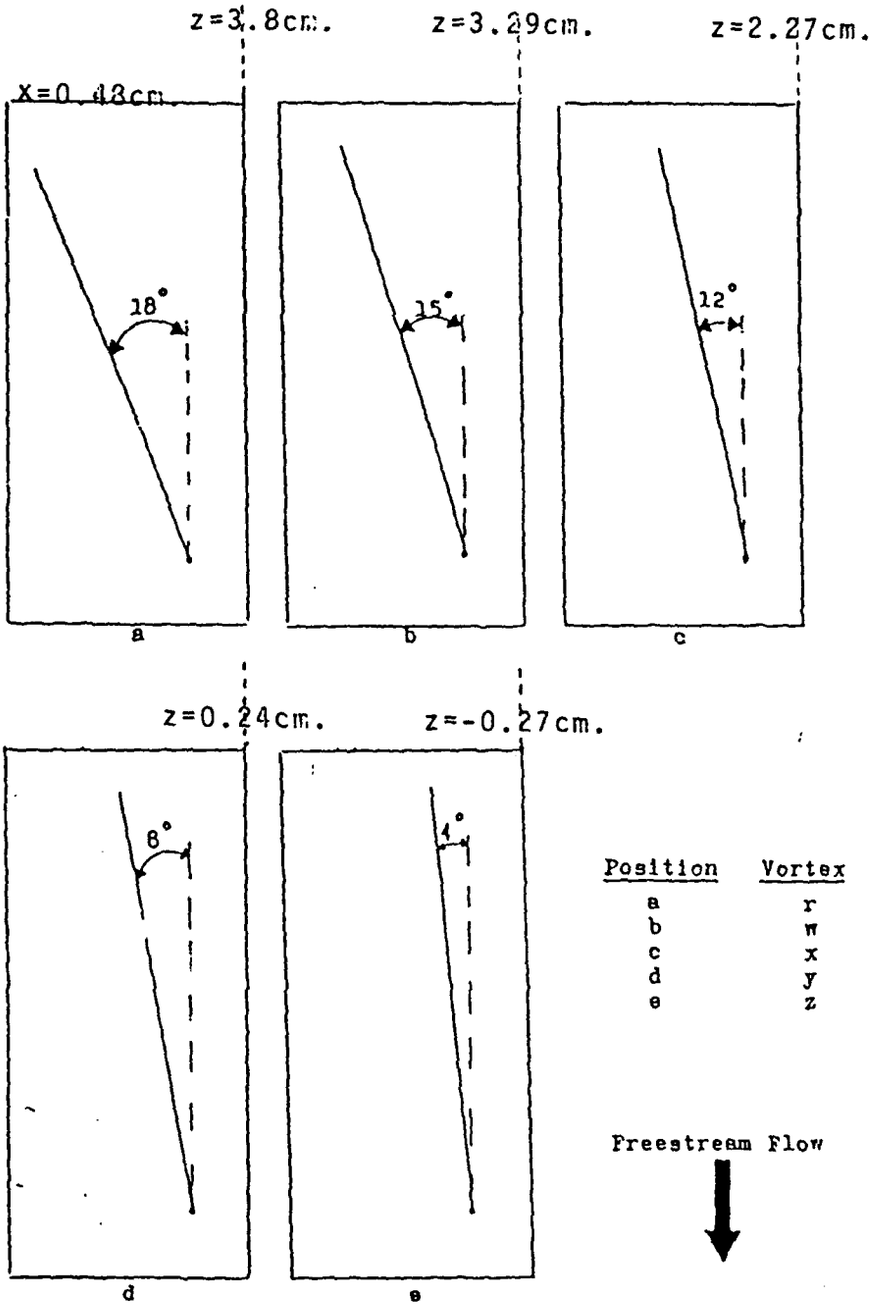

Figure 5 Coordinate Location of Vortex Generator Mounting Plate for Various Vortex Generator Angles

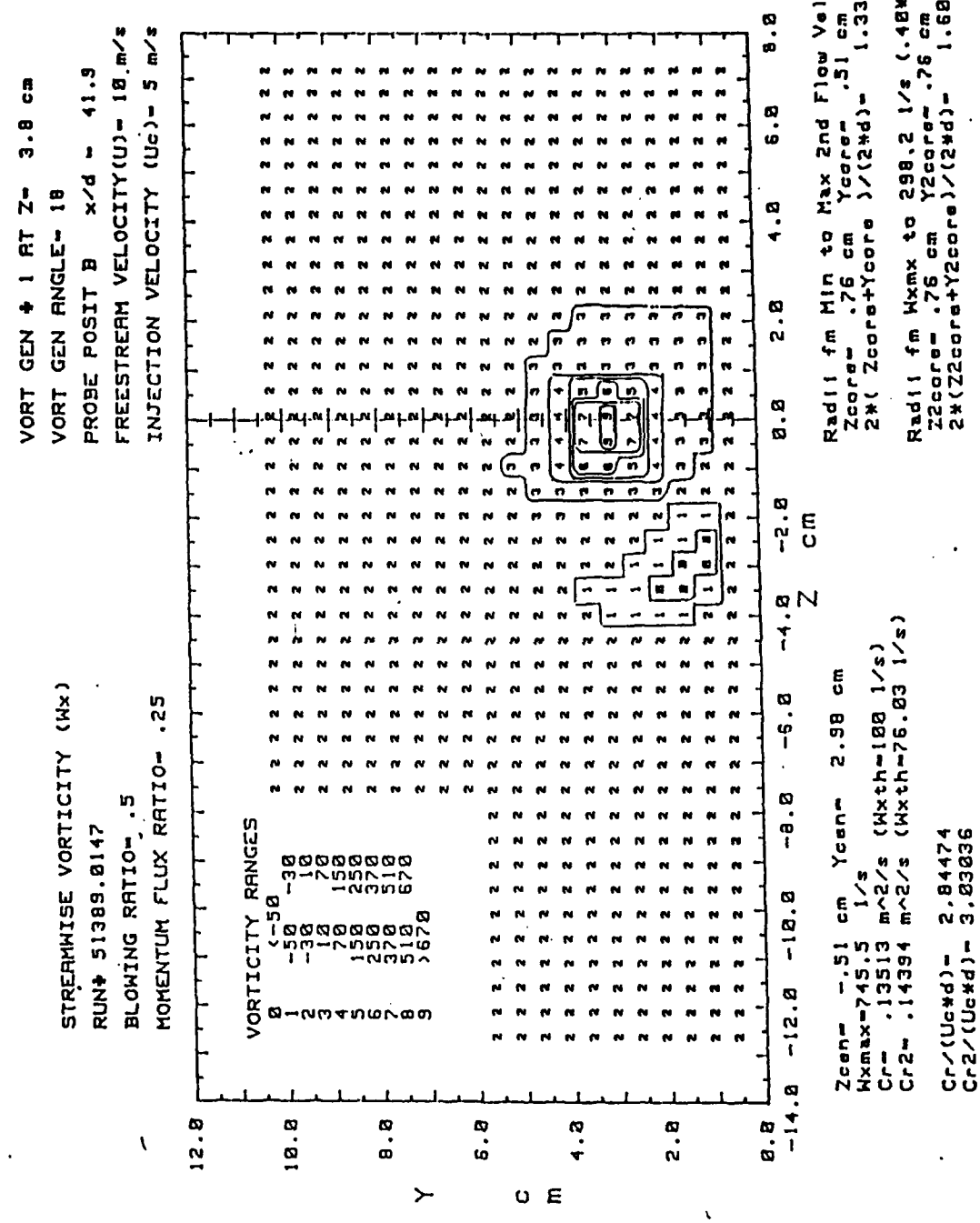

Figure 6 Streamwise Vorticity Distributions, A Single Film Cooling Hole, m = 0.5, x/d = 41.9, Vortex r

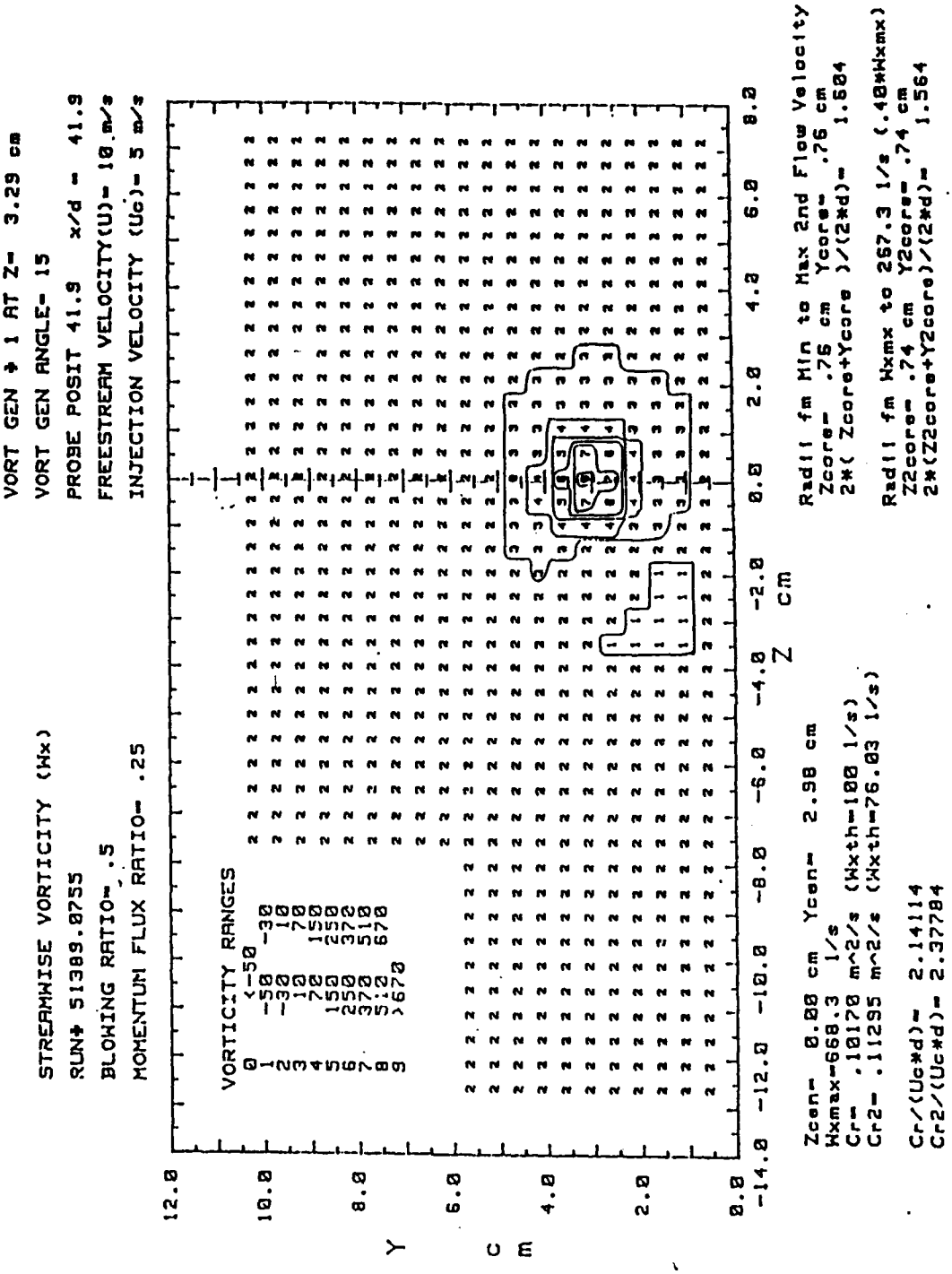

Figure 7 Streamwise Vorticity Distributions, A Single Film Cooling Hole, m = 0.5, x/d = 41.9, Vortex w

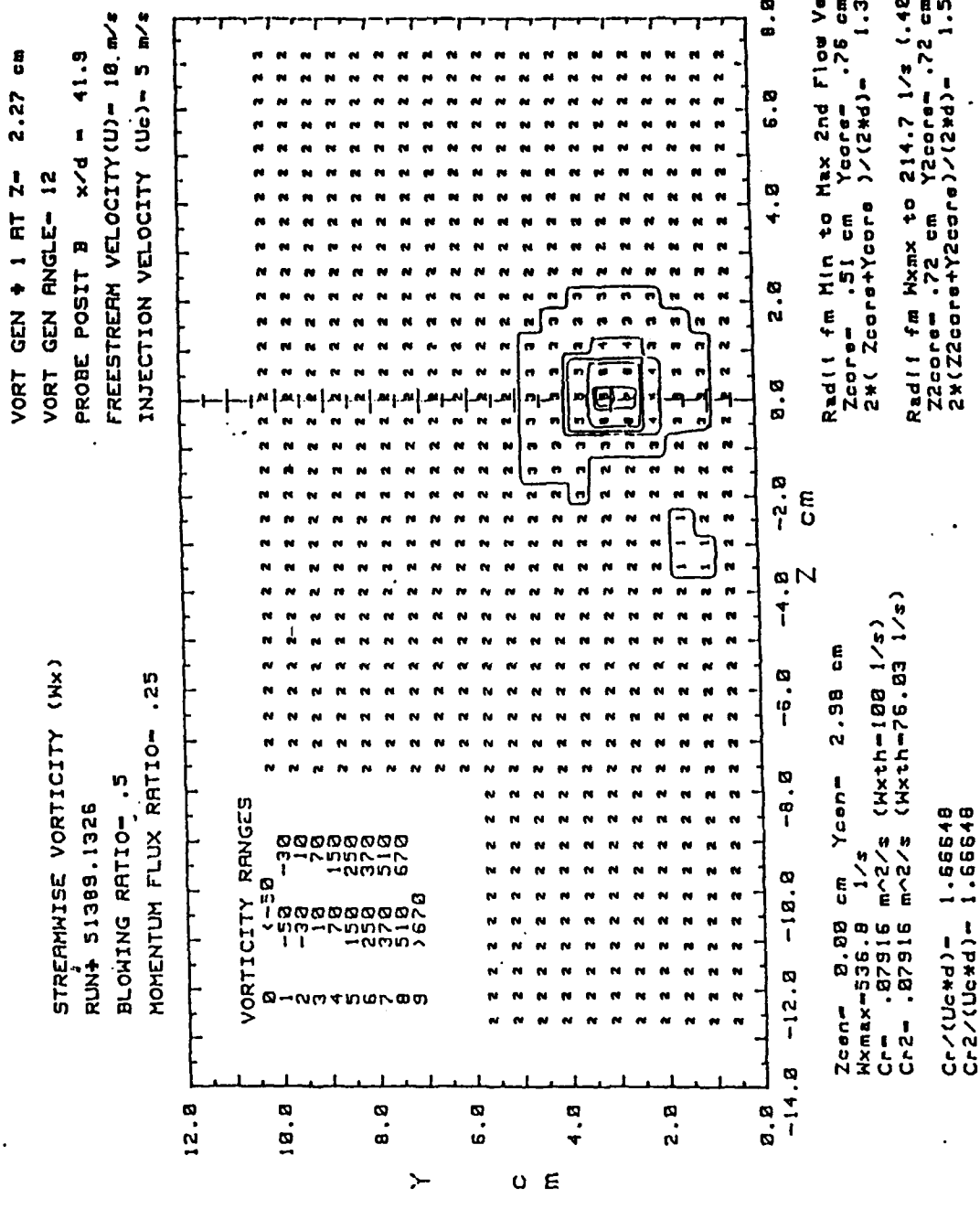

Figure 8 Streamwise Vorticity Distributions, A Single Film Cooling Hole, m = 0.5, x/d = 41.9, Vortex x

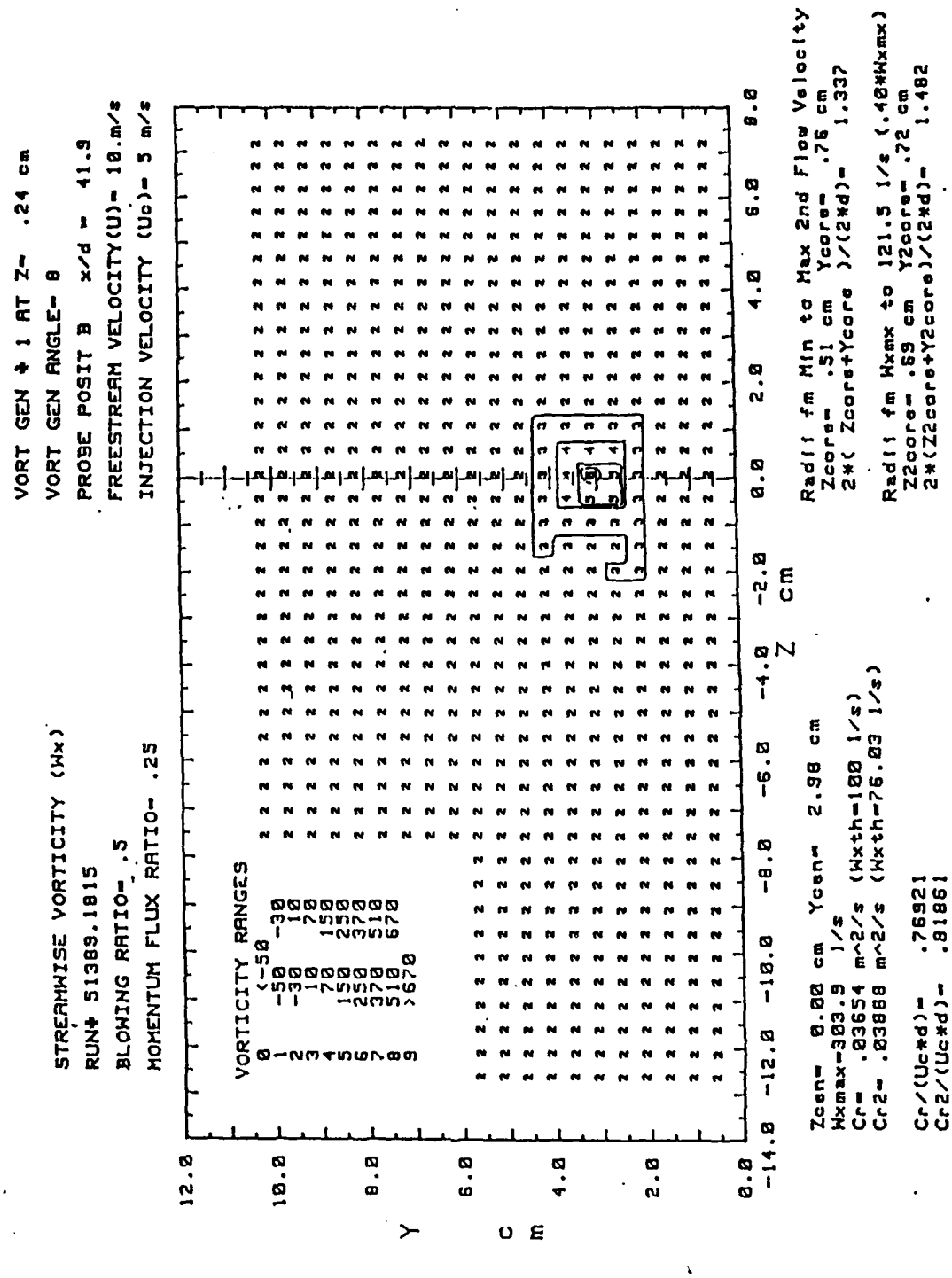

Figure 9 Streamwise Vorticity Distributions, A Single Film Cooling Hole, m = 0.5, x/d = 41.9, Vortex y

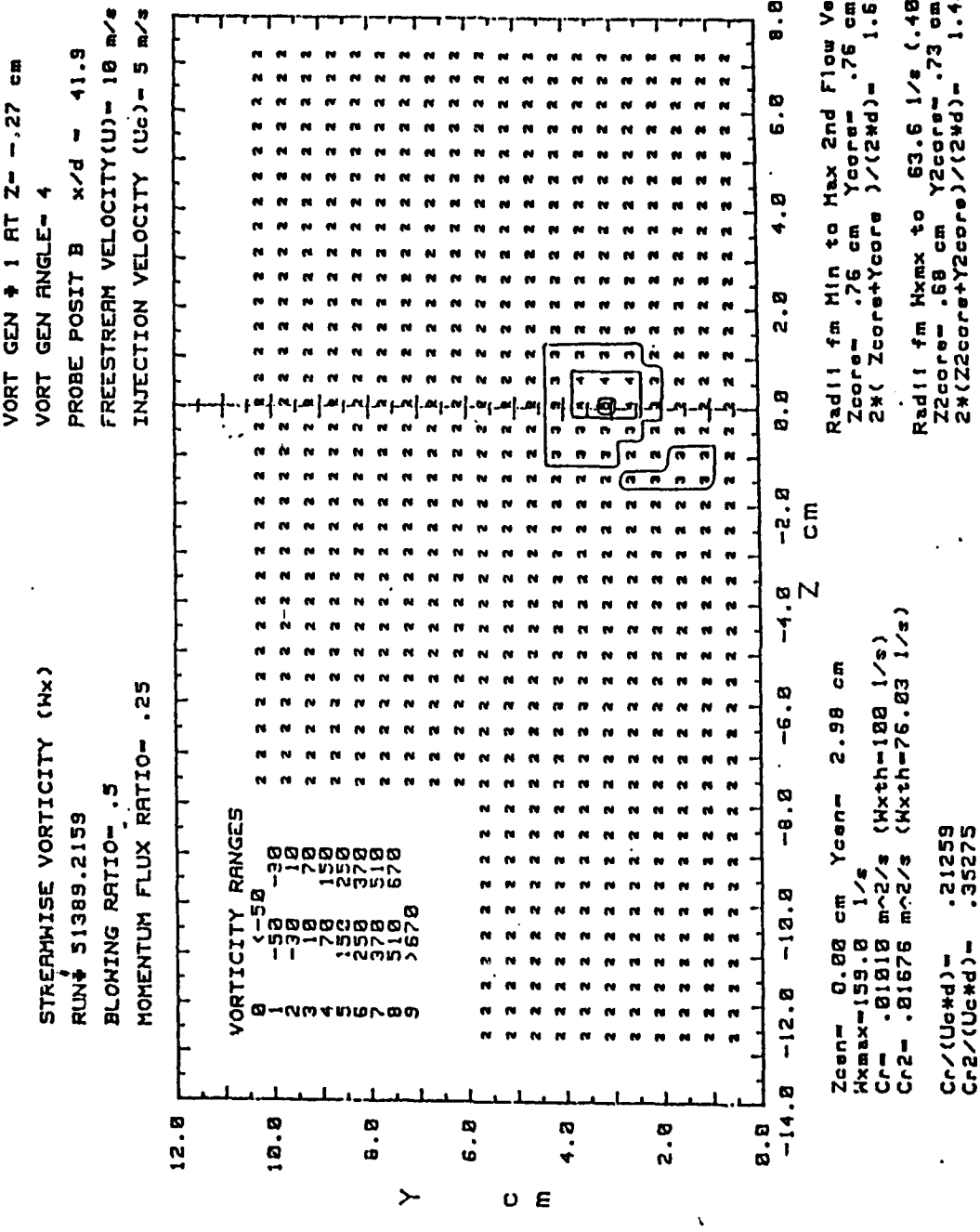

Figure 10 Streamwise Vorticity Distributions, A Single Film Cooling Hole, m = 0.5, x/d = 41.9, Vortex z

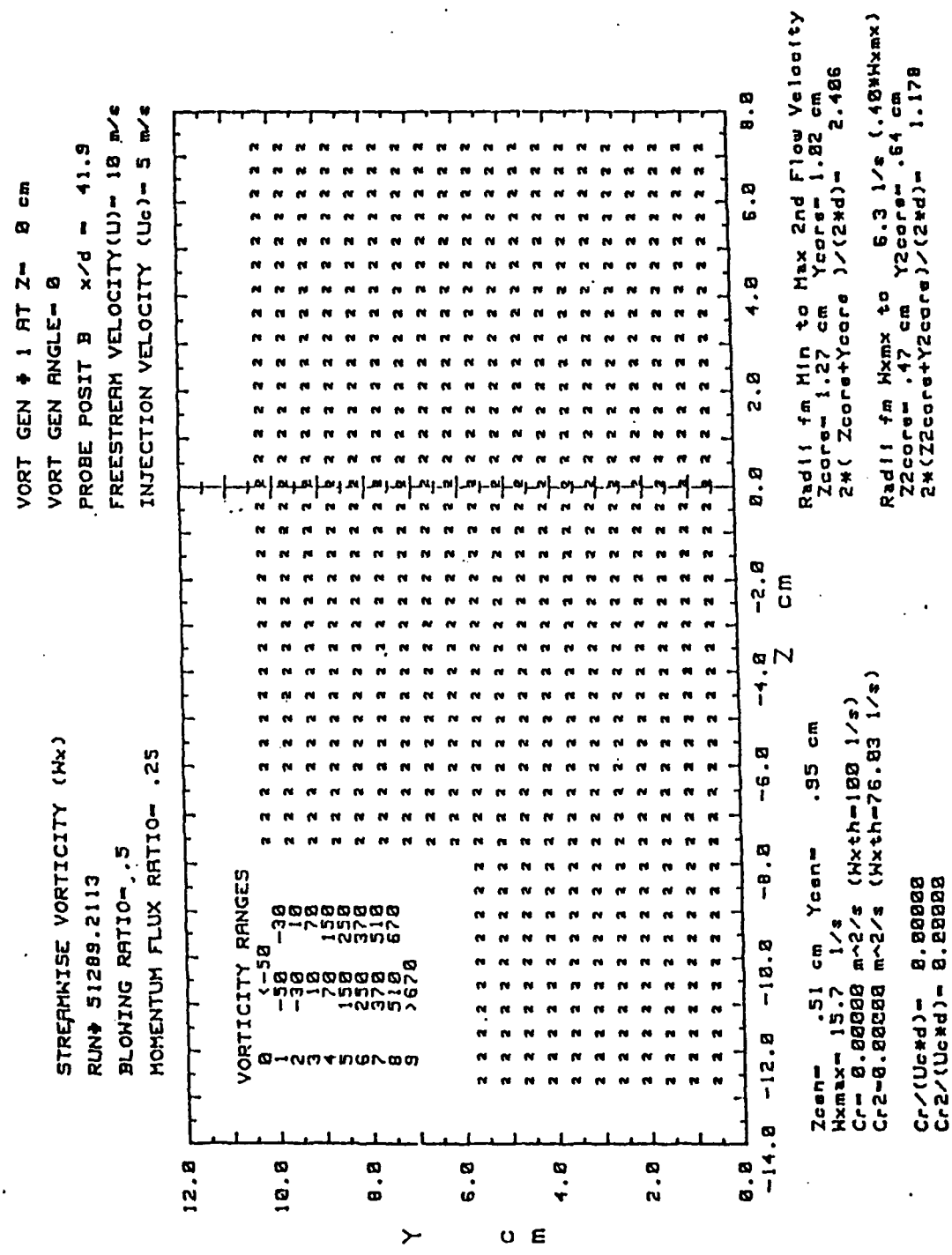

Figure 11 Streamwise Vorticity DIstributions, A Single Film Cooling Hole, m = 0.5, x/d = 41.9, No Vortex Generator

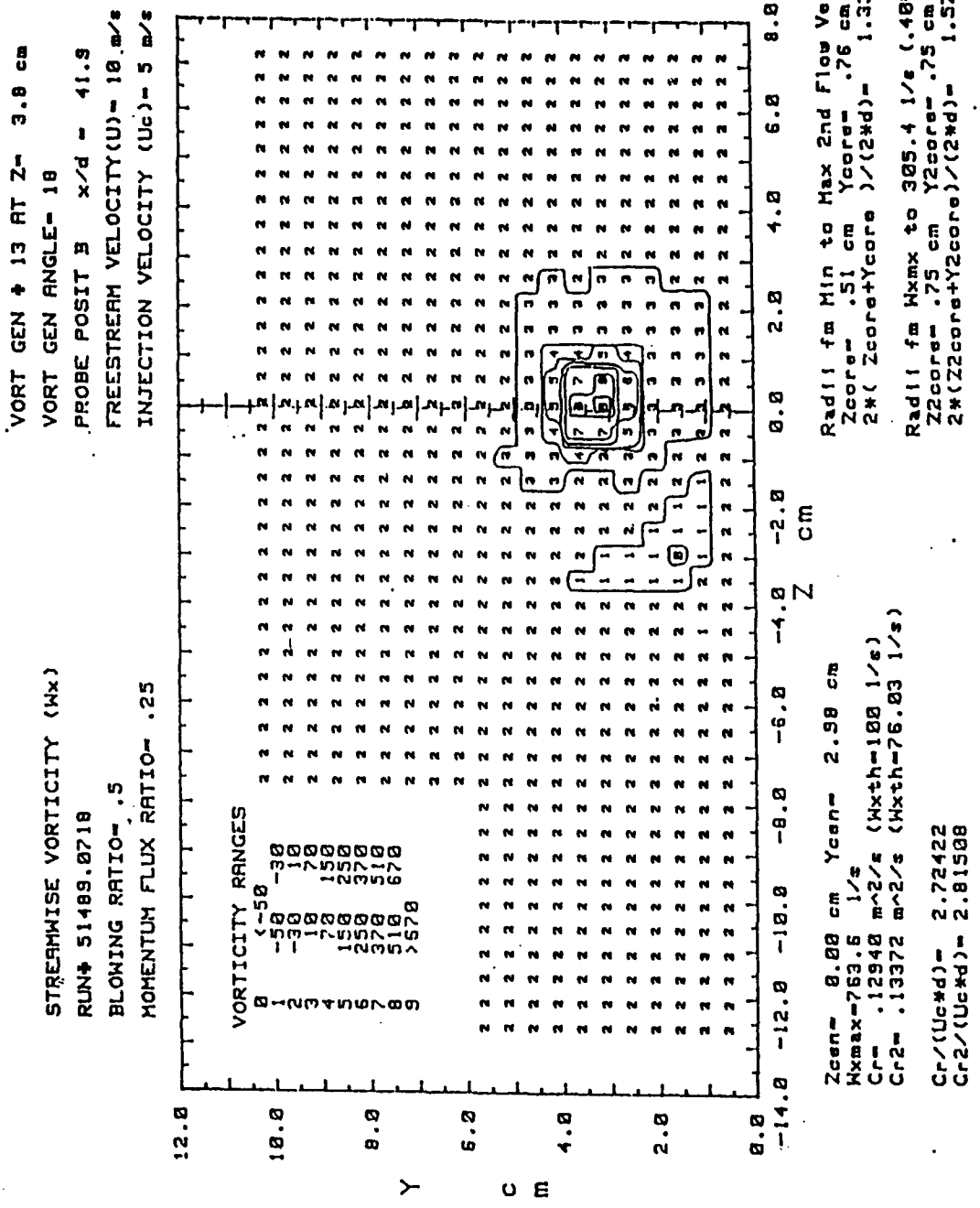

Figure 12 Streamwise Vorticity Distributions, 13 Film Cooling Holes, m = 0.5, x/d = 41.9, Vortex r

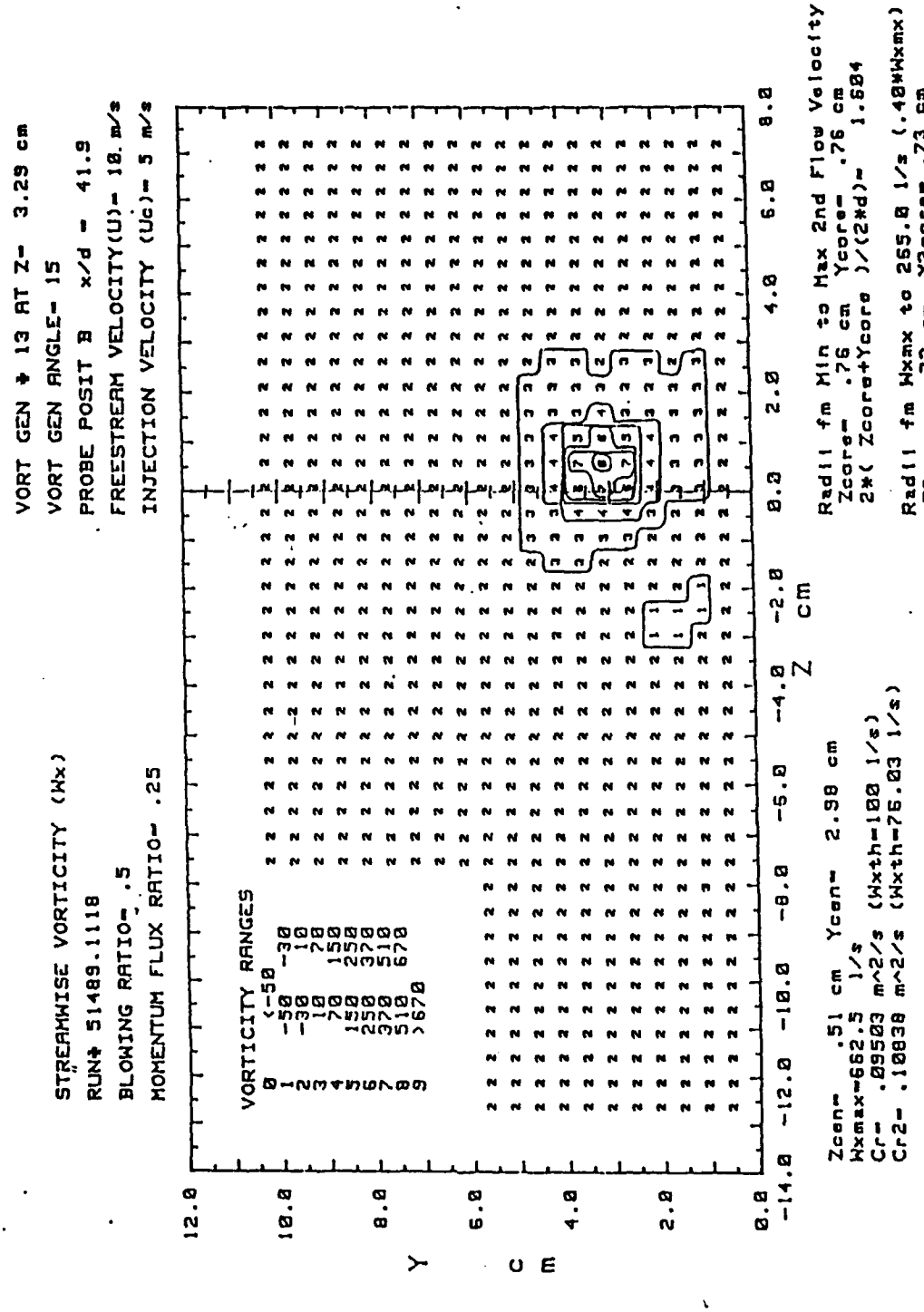

Figure 13 Streamwise Vorticity Distributions, 13 Film Cooling Holes, m = 0.5, x/d = 41.9, Vortex w

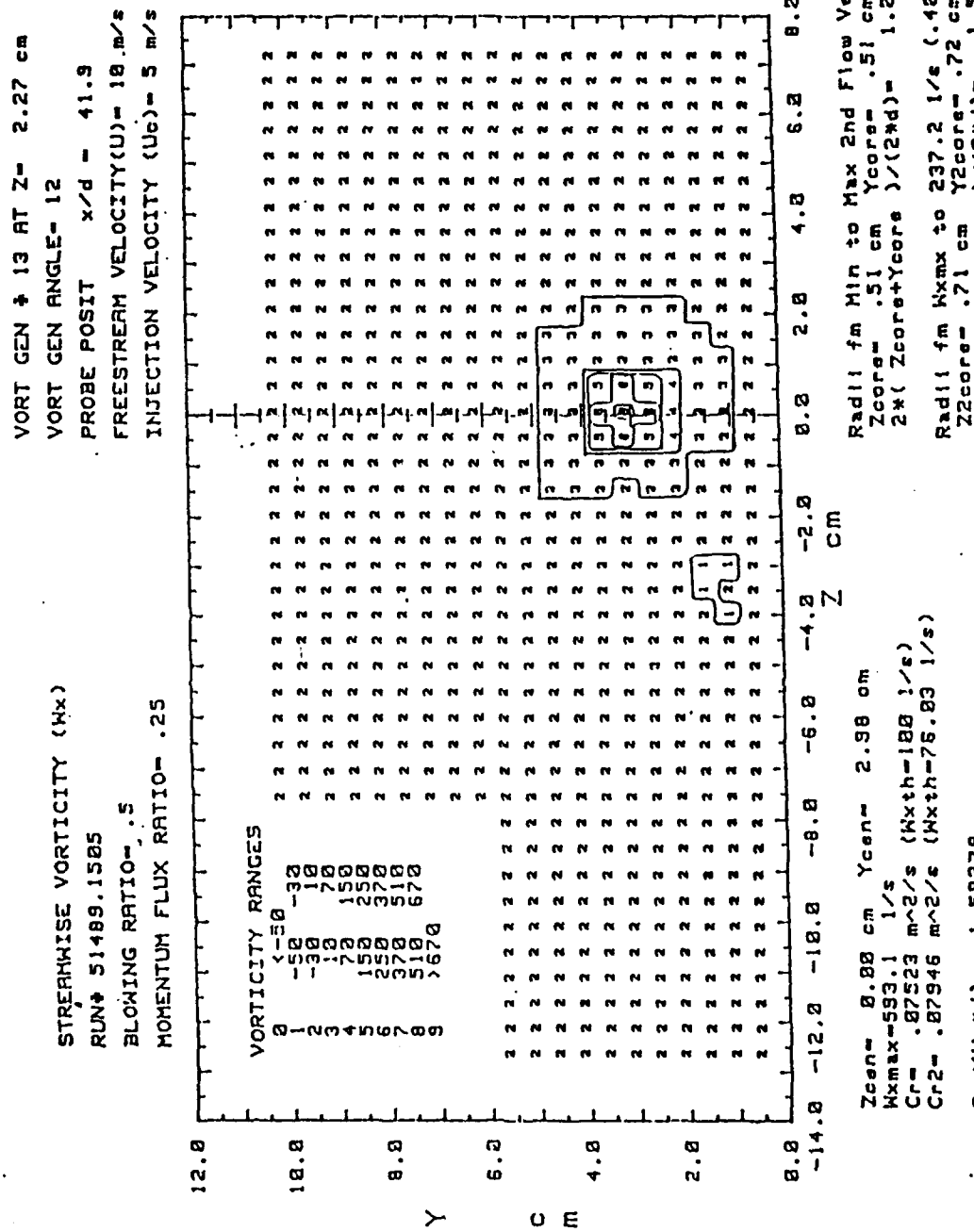

Figure 14 Streamwise Vorticity Distributions, 13 Film Cooling Holes, m = 0.5, x/d = 41.9, Vortex x

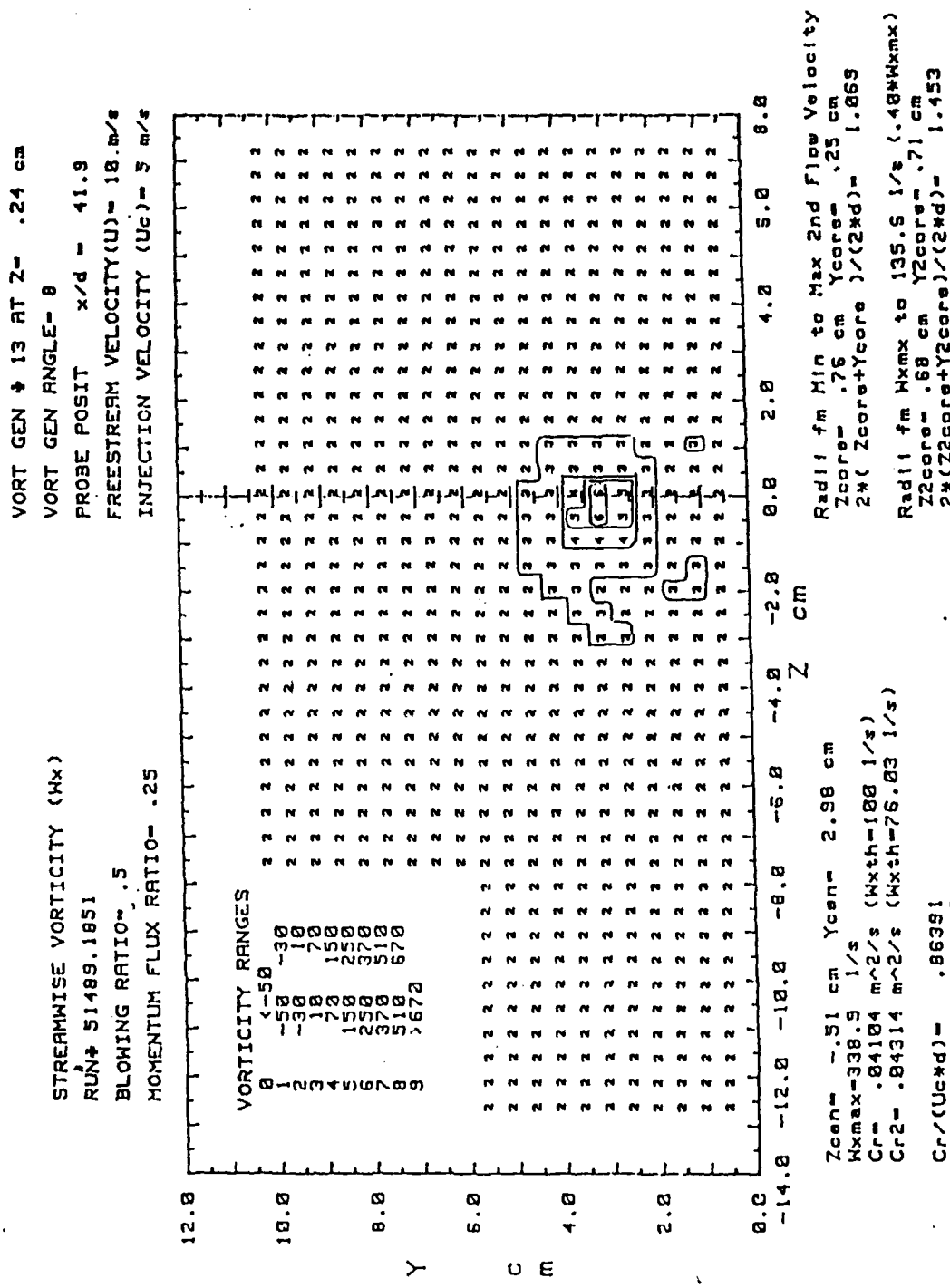

Figure 15 Streamwise Vorticity Distributions, 13 Film Cooling Holes, m = 0.5 x/d = 41.9, Vortex y

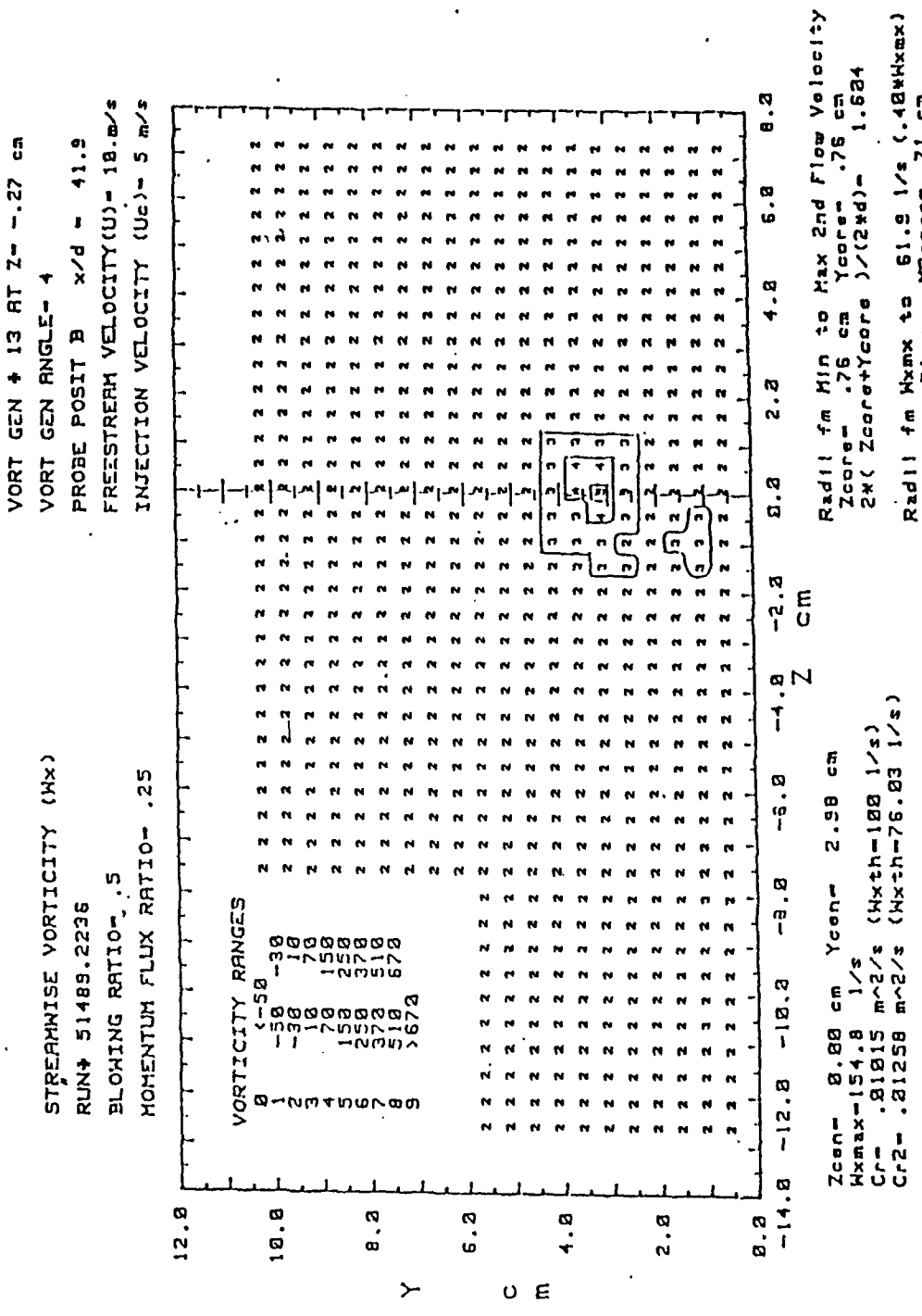

Figure 16 Streamwise Vorticity Distributions, 13 Film Cooling Holes, m = 0.5, x/d = 41.9, Vortex z

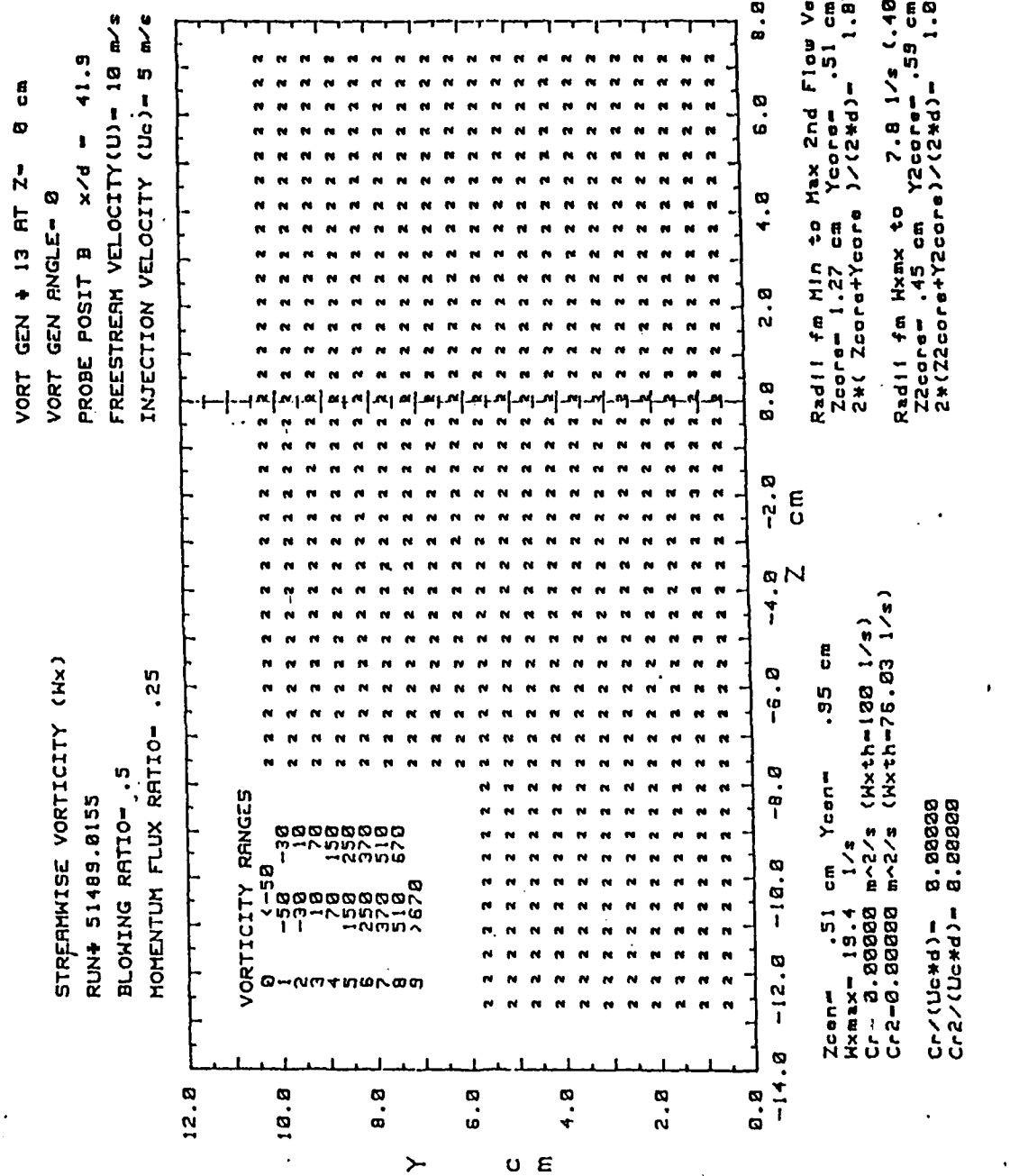

Figure 17 Streamwise Vorticity Distributions. 13 Film Cooling Holes, m = 0.5, x/d = 41.9, No Vortex Generator

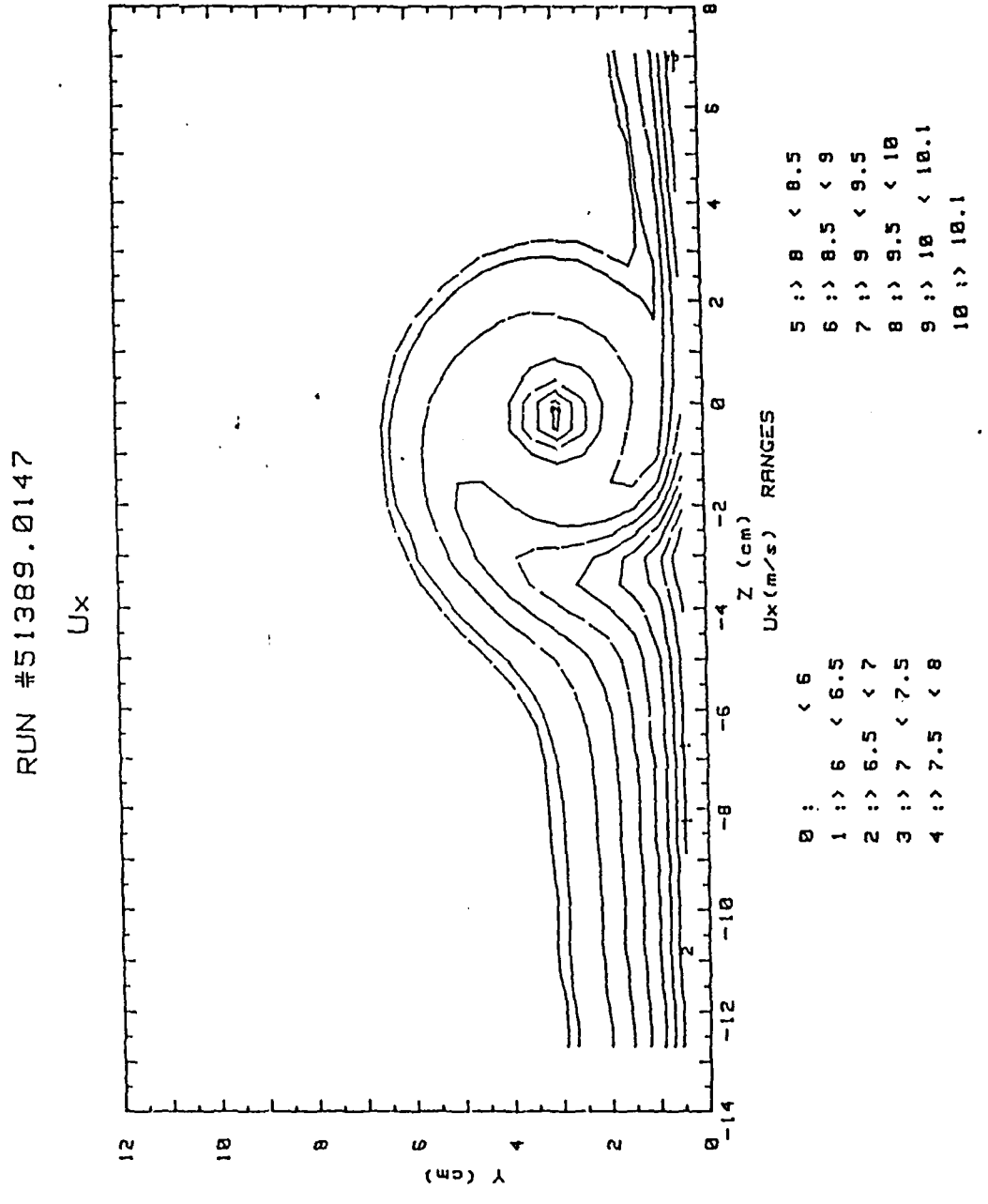

Figure 18 Streamwise Velocity Distributions for A Single Injection Hole, m = 0.5, x/d = 41.9, Vortex r

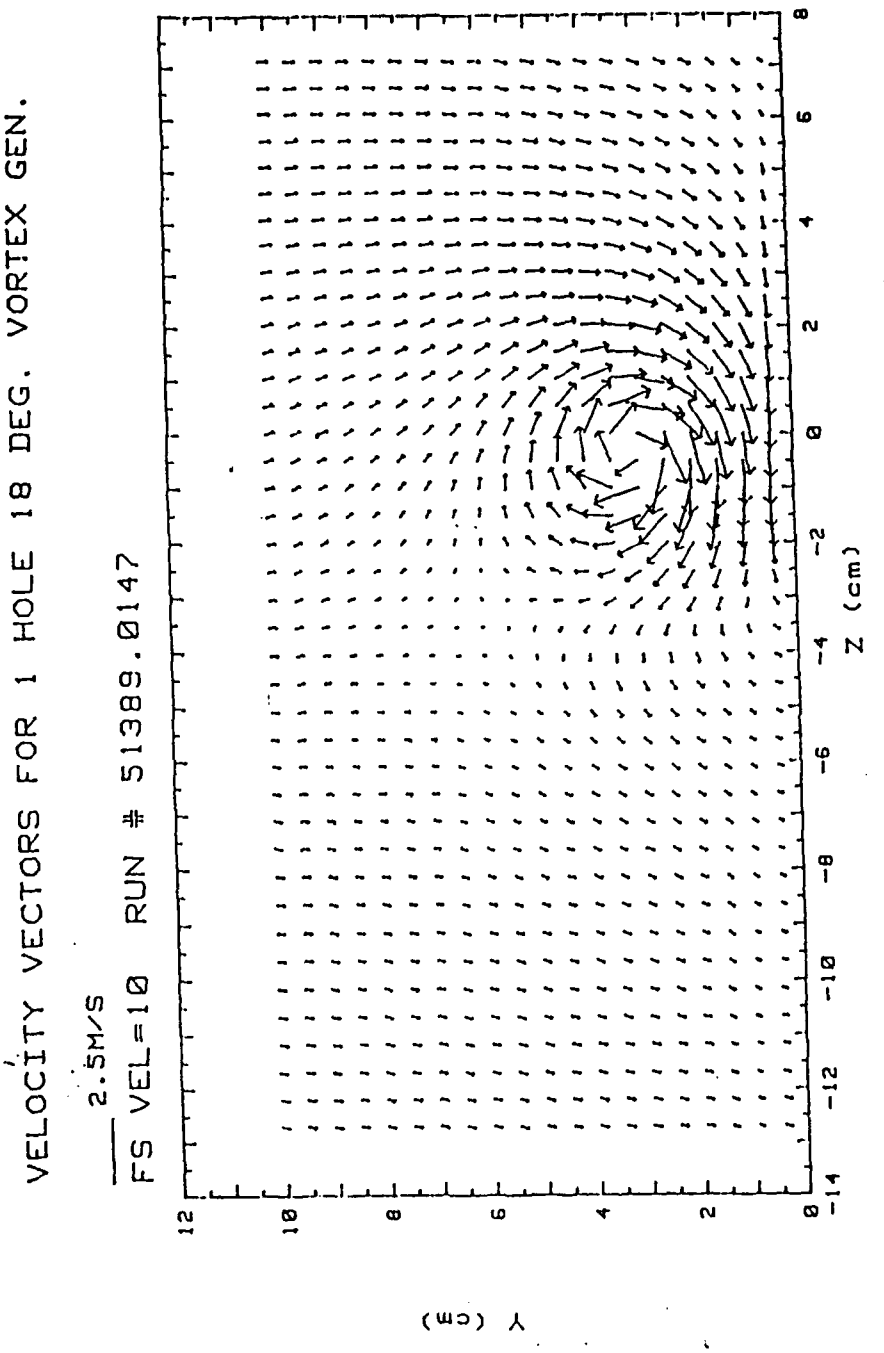

Figure 19 Secondary Flow Vectors Field for A Single Injection Hole, m = 0.5, x/d = 41.9, Vortex r

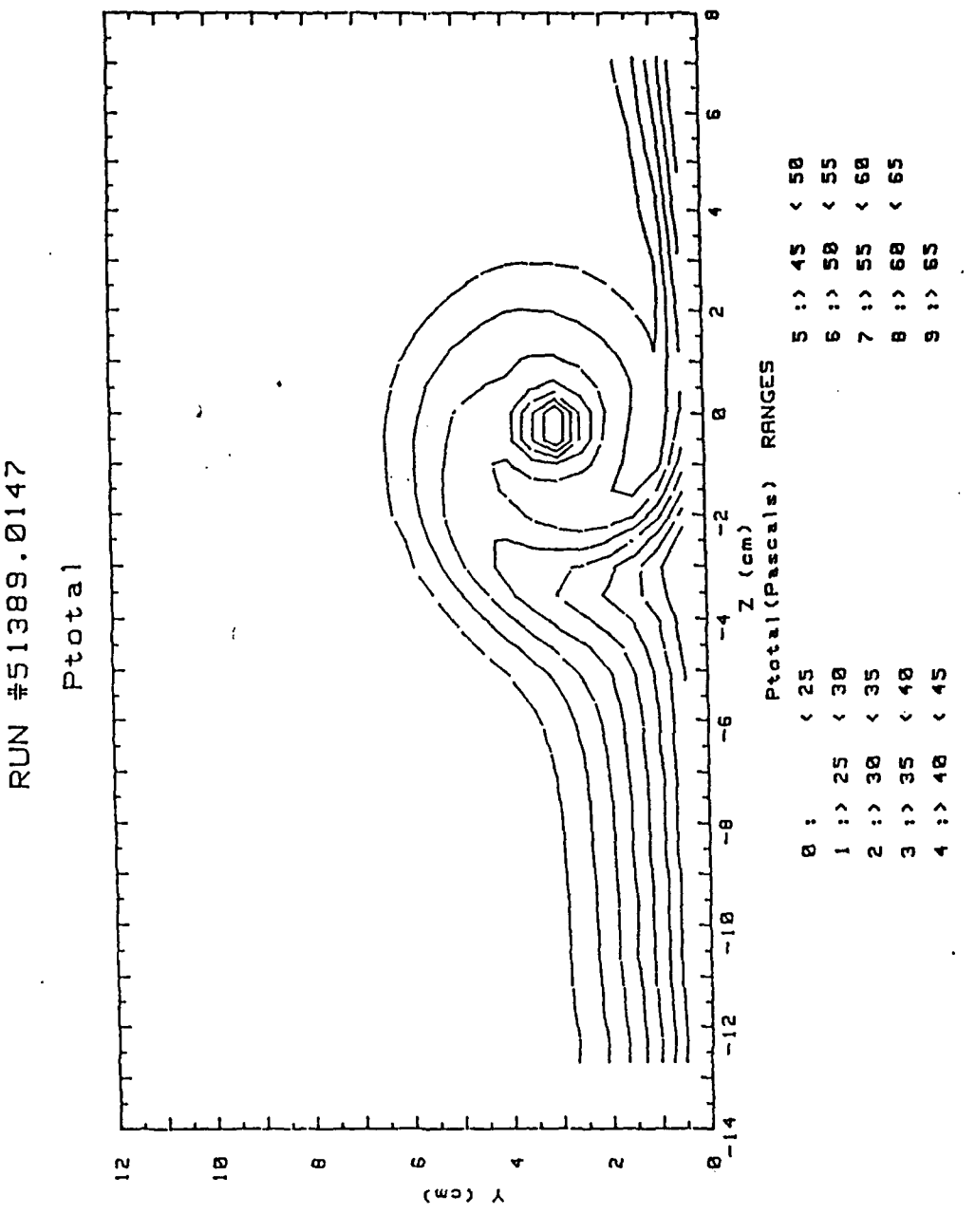

Figure 20 Total Pressure Field for A Single Injection Hole, m = 0.5, x/d = 41.9, Vortex r

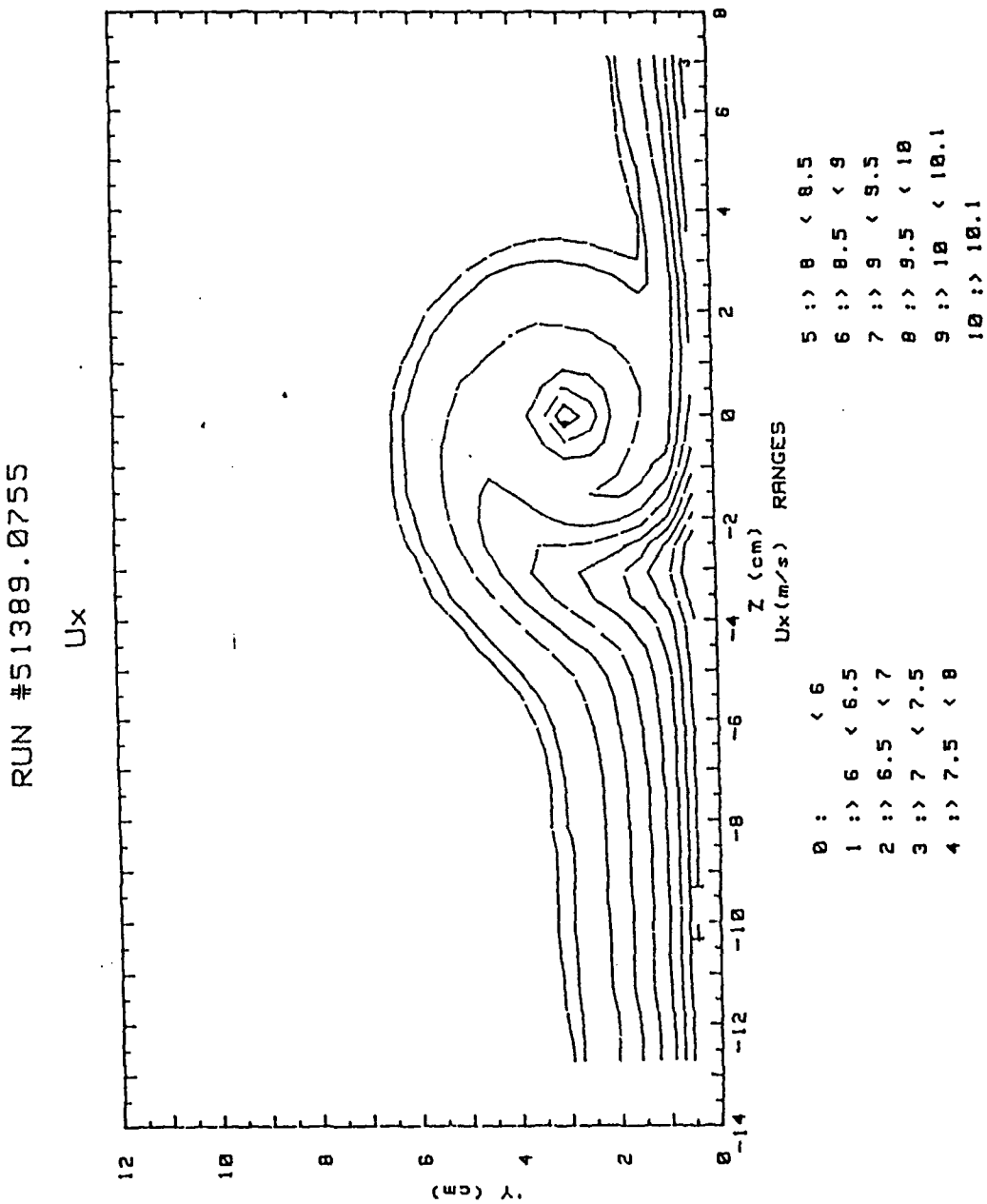

Figure 21 Streamwise Velocity Distributions for A Single Injection Hole, m = 0.5, x/d = 41.9, Vortex w

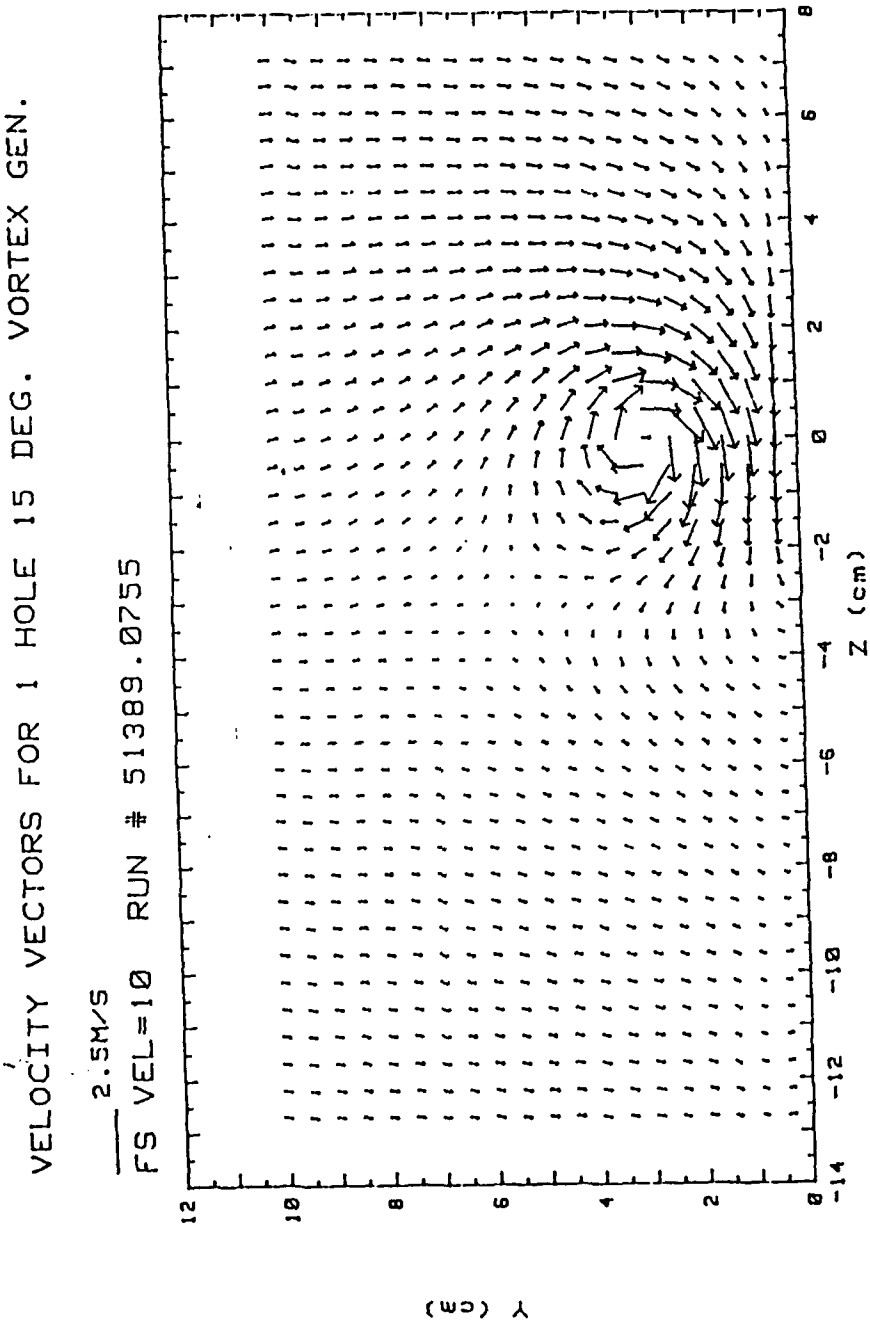

Figure 22 Secondary Flow Vectors Field for A Single Injection Hole, m = 0.5, x/d = 41.9, Vortex w

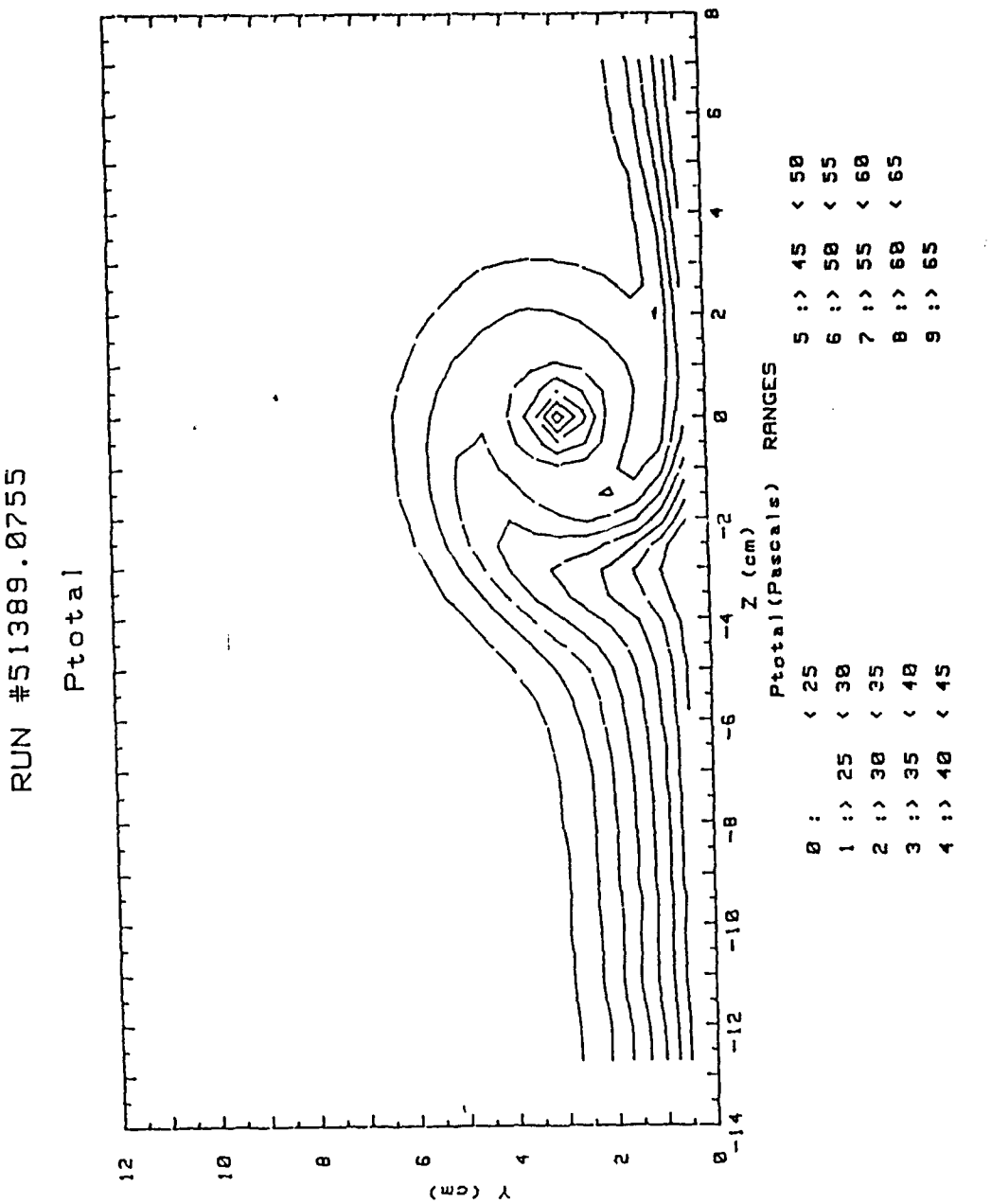

Figure 23 Total Pressure Field for A Single Injection Hole, m = 0.5, x/d = 41.9, Vortex w

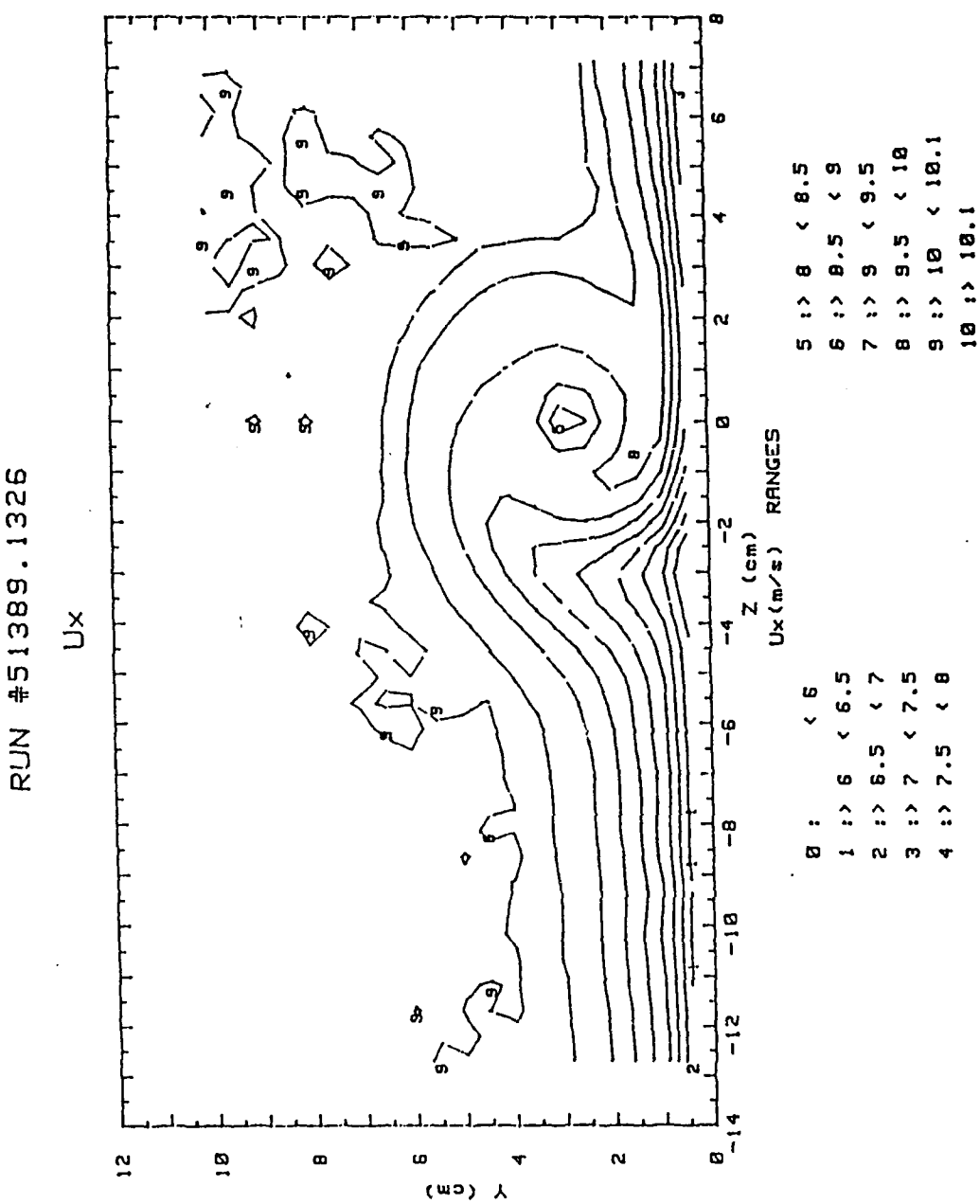

Figure 24 Streamwise Velocity Distributions for A Single Injection Hole, m = 0.5, x/d = 41.9, Vortex x

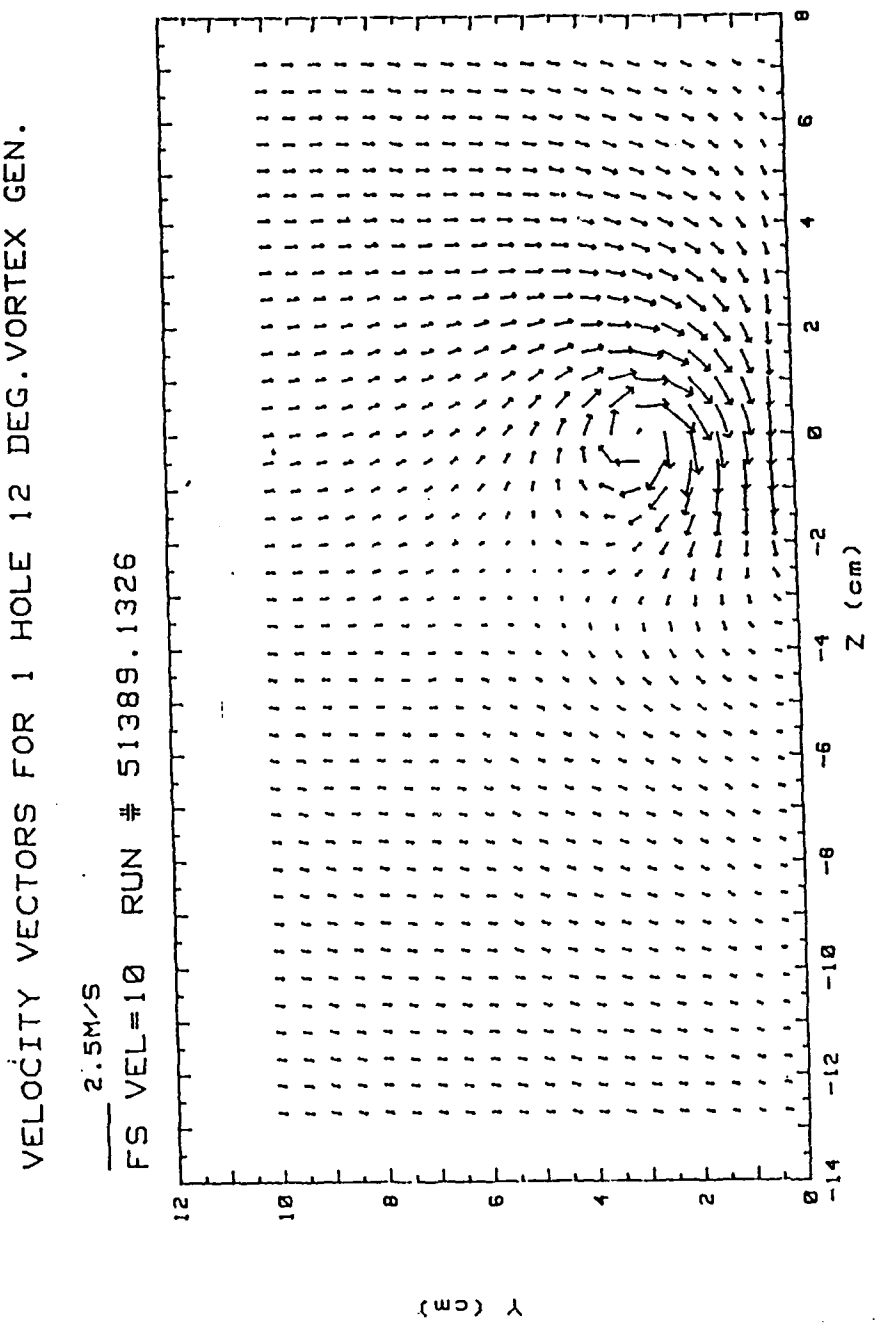

Figure 25 Secondary Flow Vectors Field for A Single Injection Hole, m = 0.5, x/d = 41.9, Vortex x

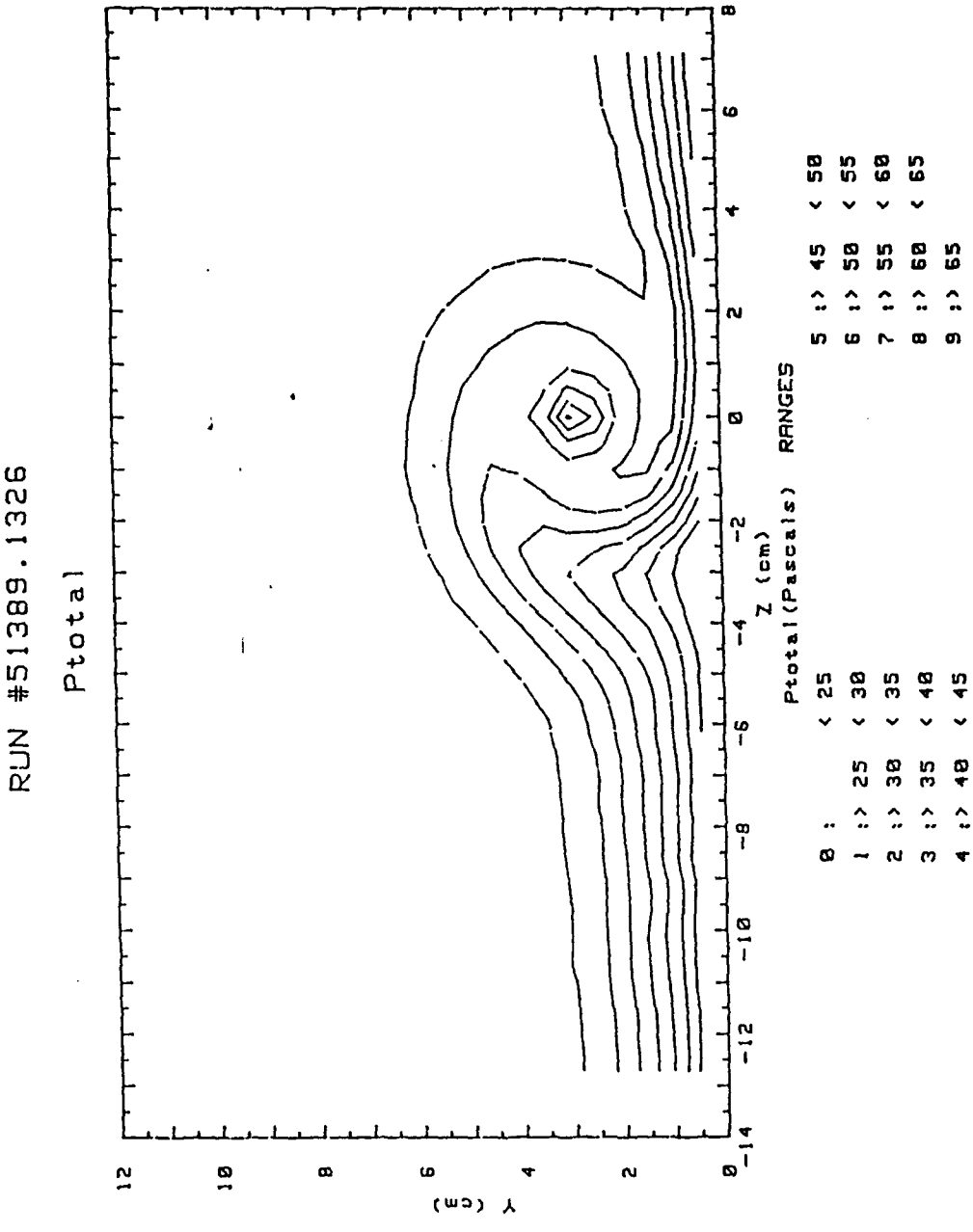

Figure 26 Total Pressure Field for A Single Injection Hole, m = 0.5, x/d = 41.9, Vortex x

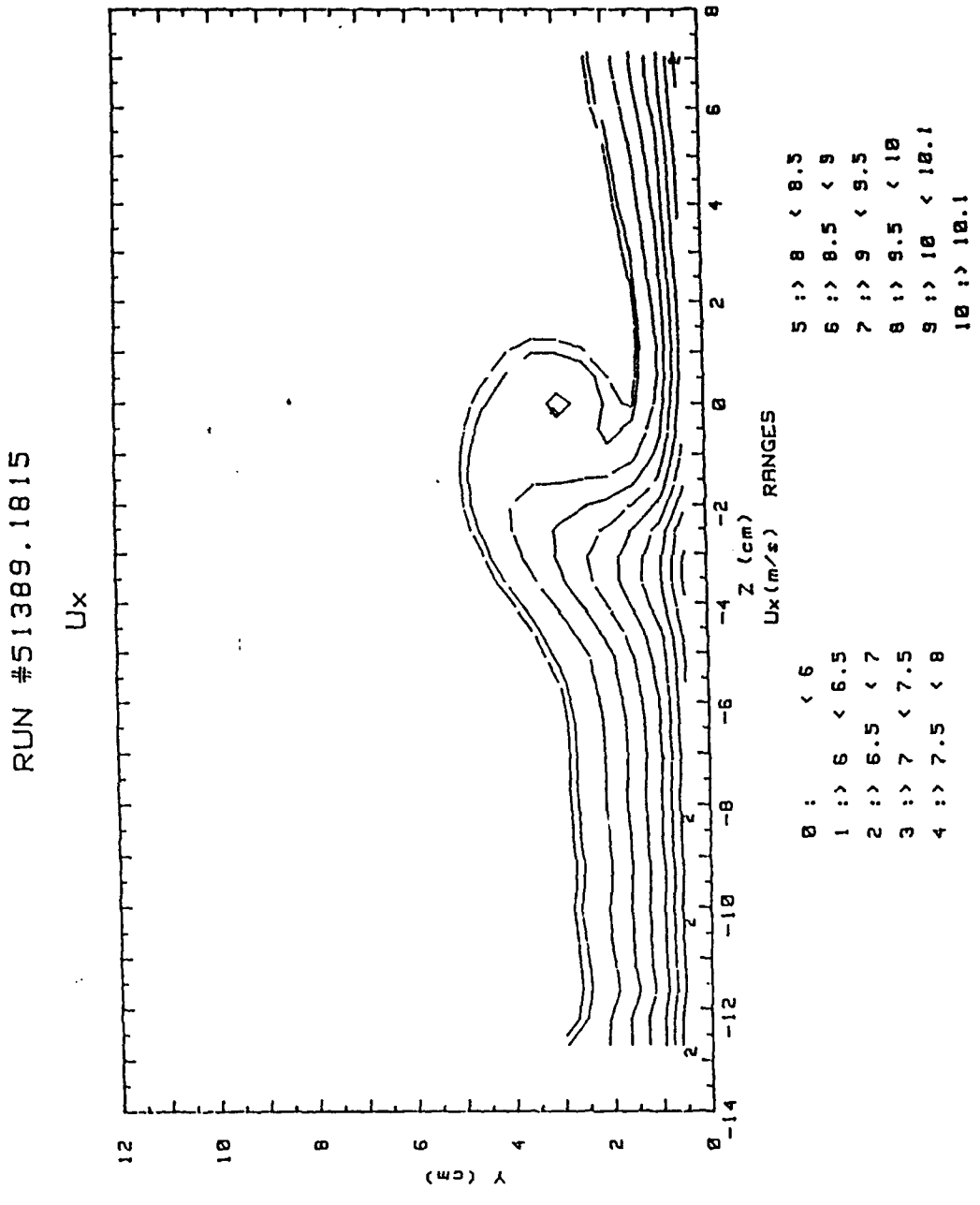

Figure 27 Streamwise Velocity Distributions for A Single Injection Hole, m = 0.5, x/d = 41.9, Vortex y

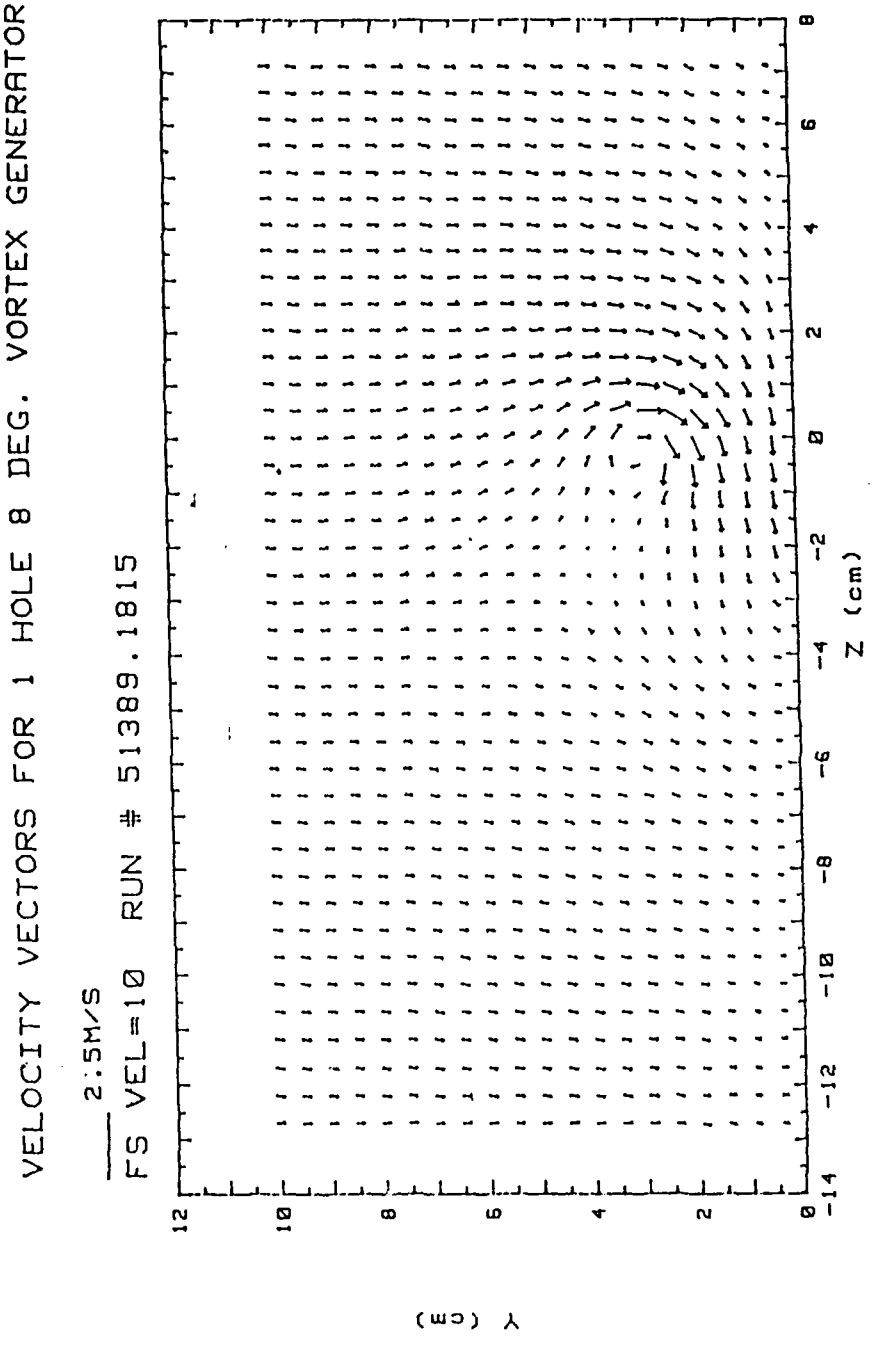

Figure 28 Secondary Flow Vectors Field for A Single Injection Hole, m = 0.5, x/d = 41.9, Vorex y

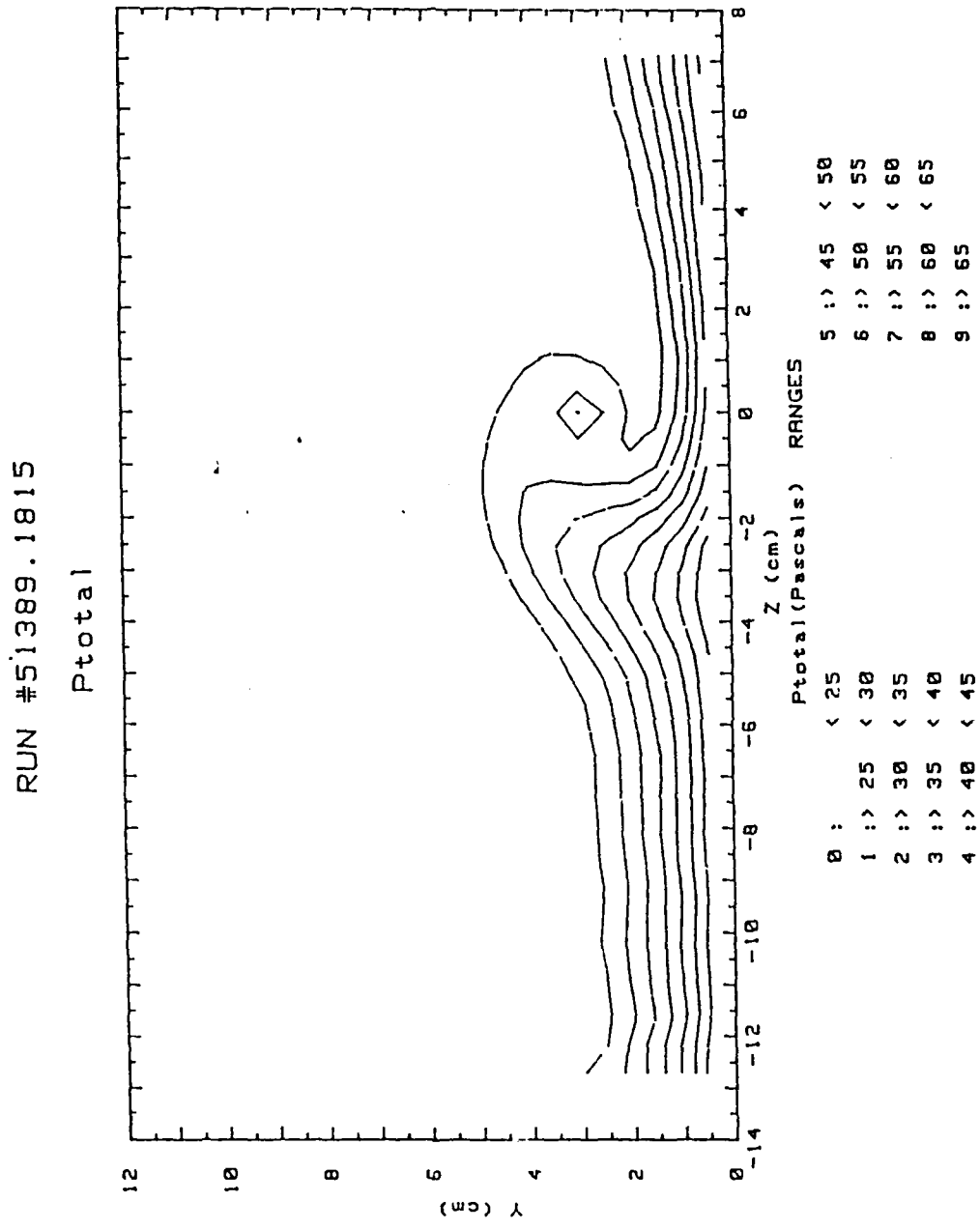

Figure 29 Total Pressure Field for A Single Injection Hole, m = 0.5, x/d = 41.9, Vortex y

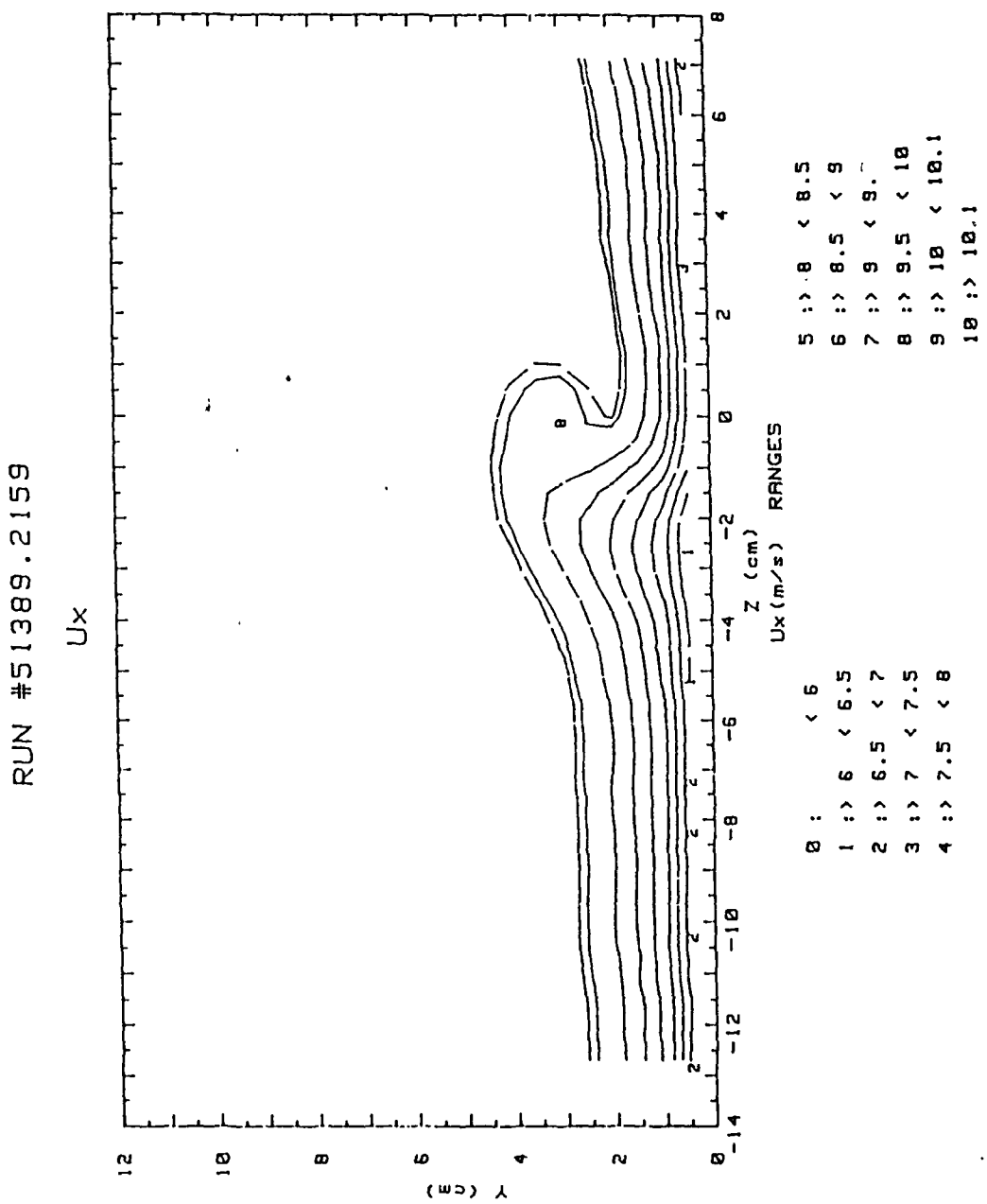

Figure 30 Streamwise Velocity Distributions for A Single Injection Hole, m = 0.5, x/d = 41.9, Vortex z

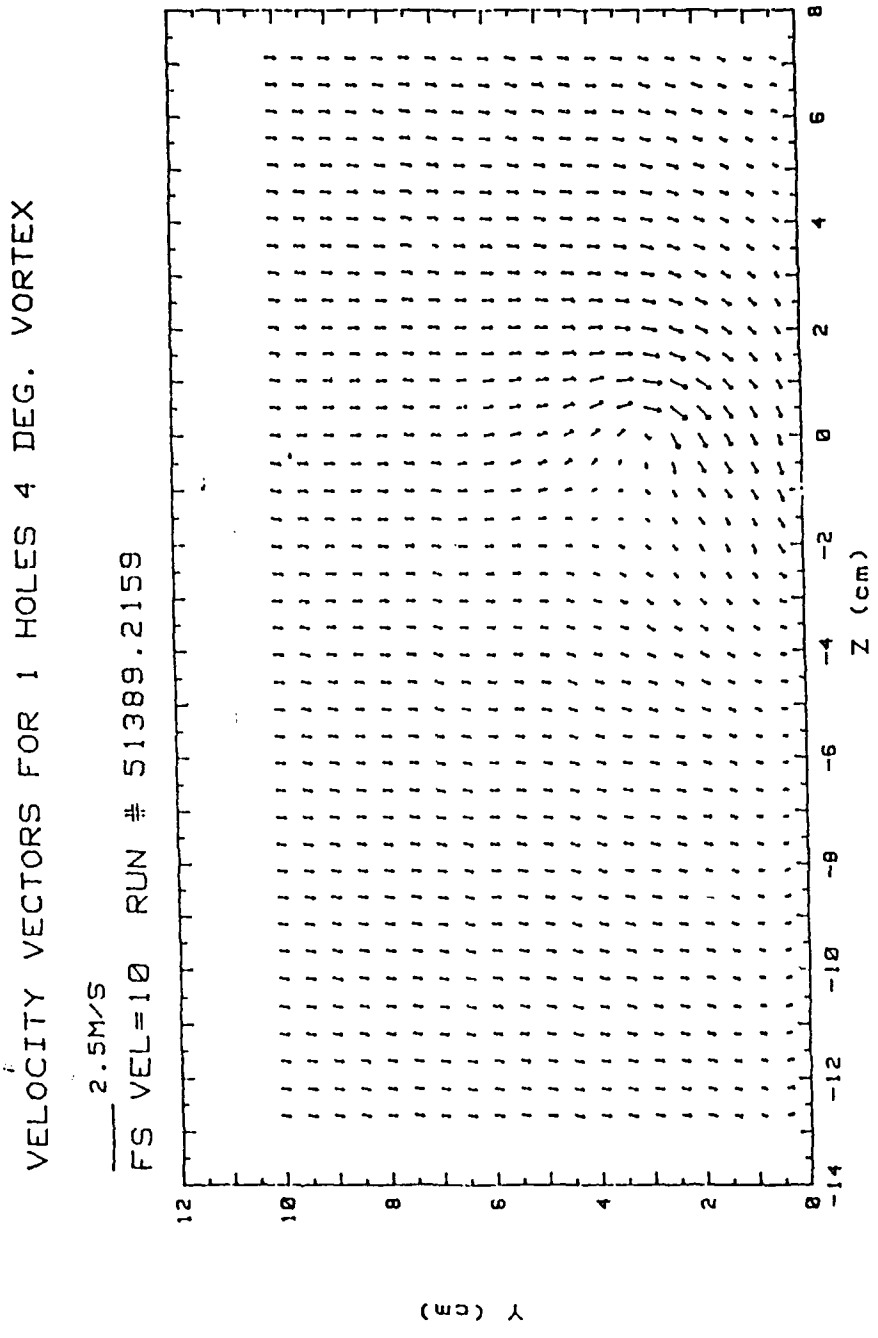

Figure 31 Secondary Flow Vectors Field for A Single Injection Hole, m = 0.5, x/d = 41.9, Vorex z

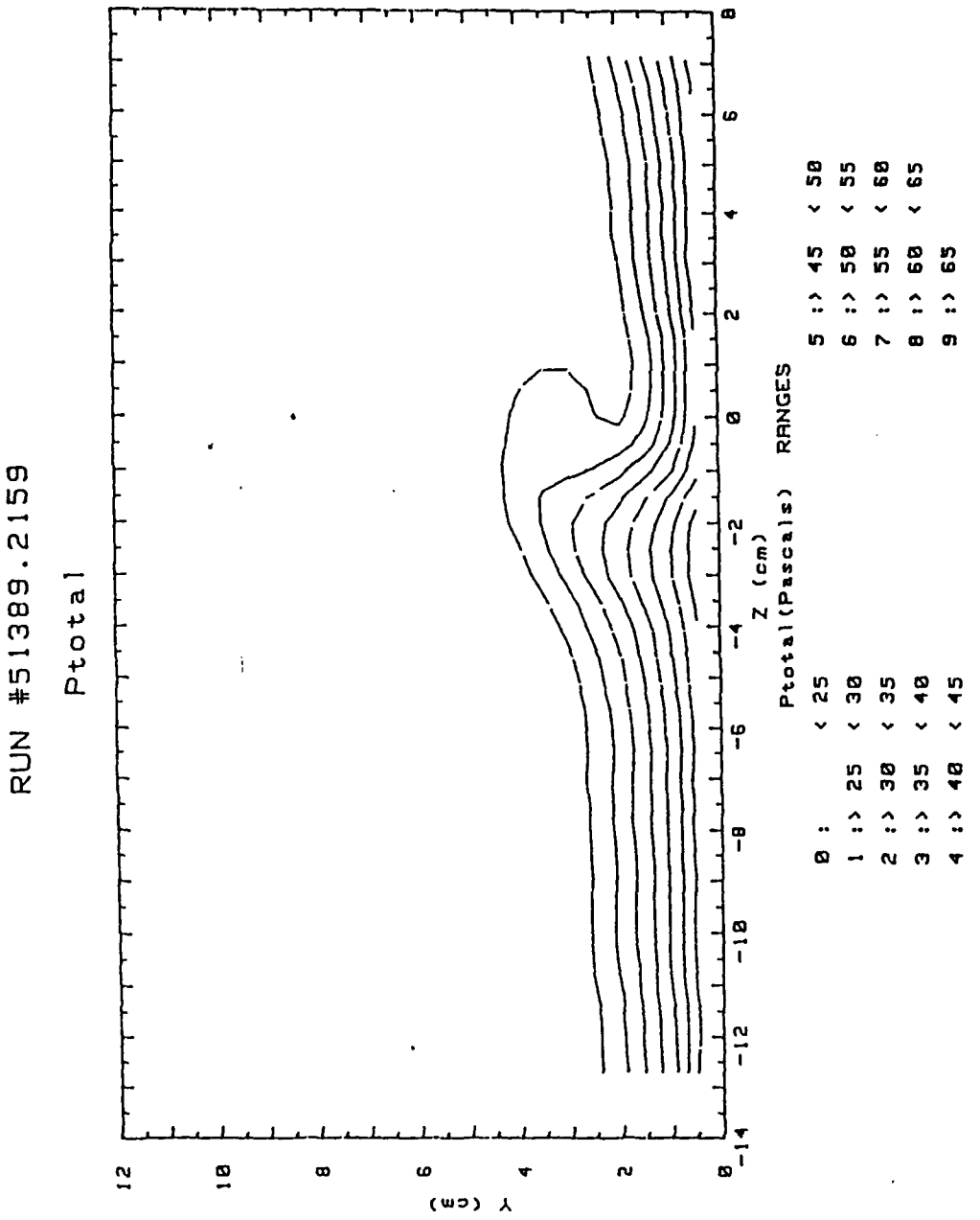

Figure 32 Total Pressure Field for A Single Injection Hole, m = 0.5, x/d = 41.9, Vortex z

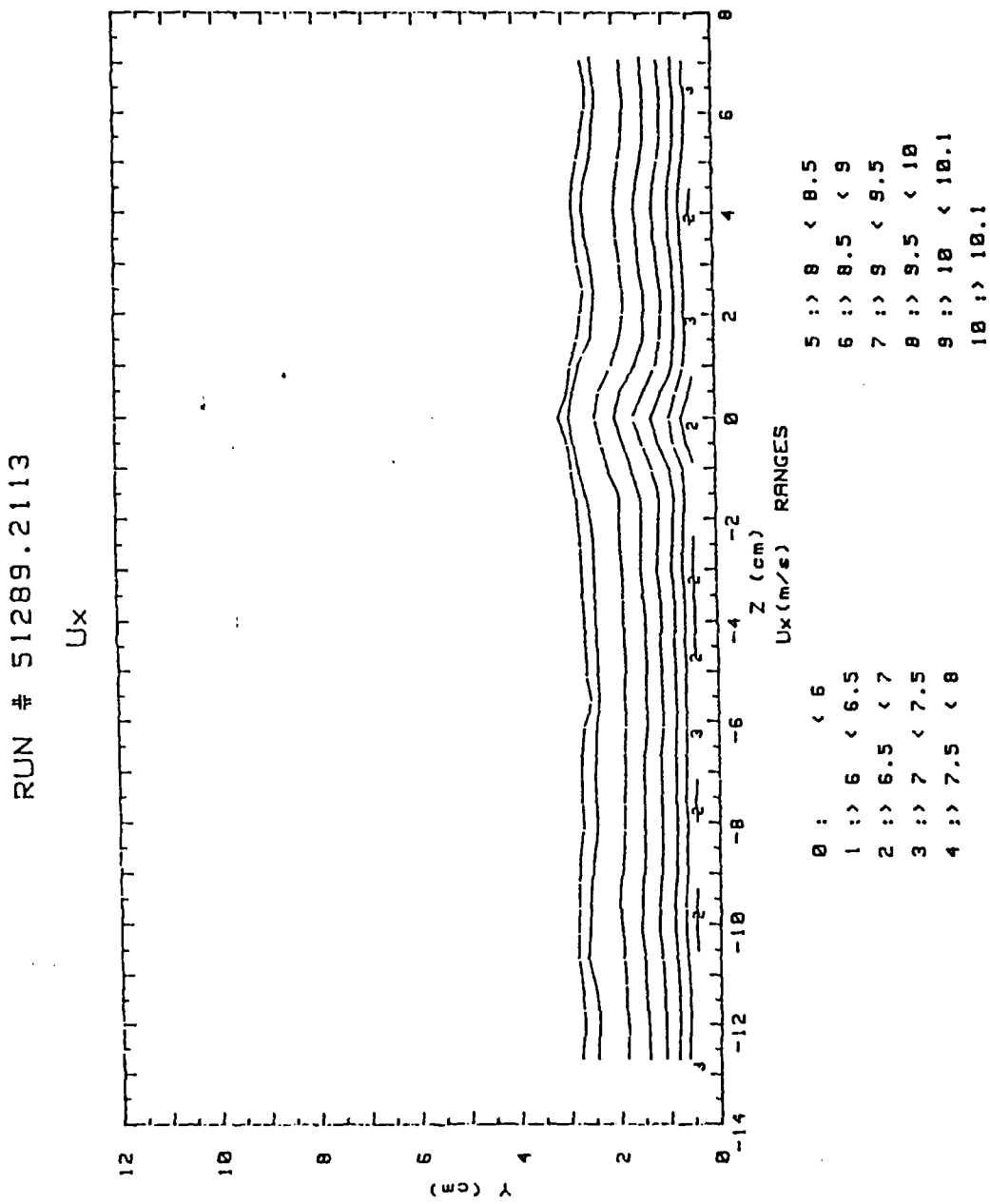

Figure 33 Streamwise Velocity Distributions for A Single Injection Hole, m = 0.5, x/d = 41.9, No Vortex Generator

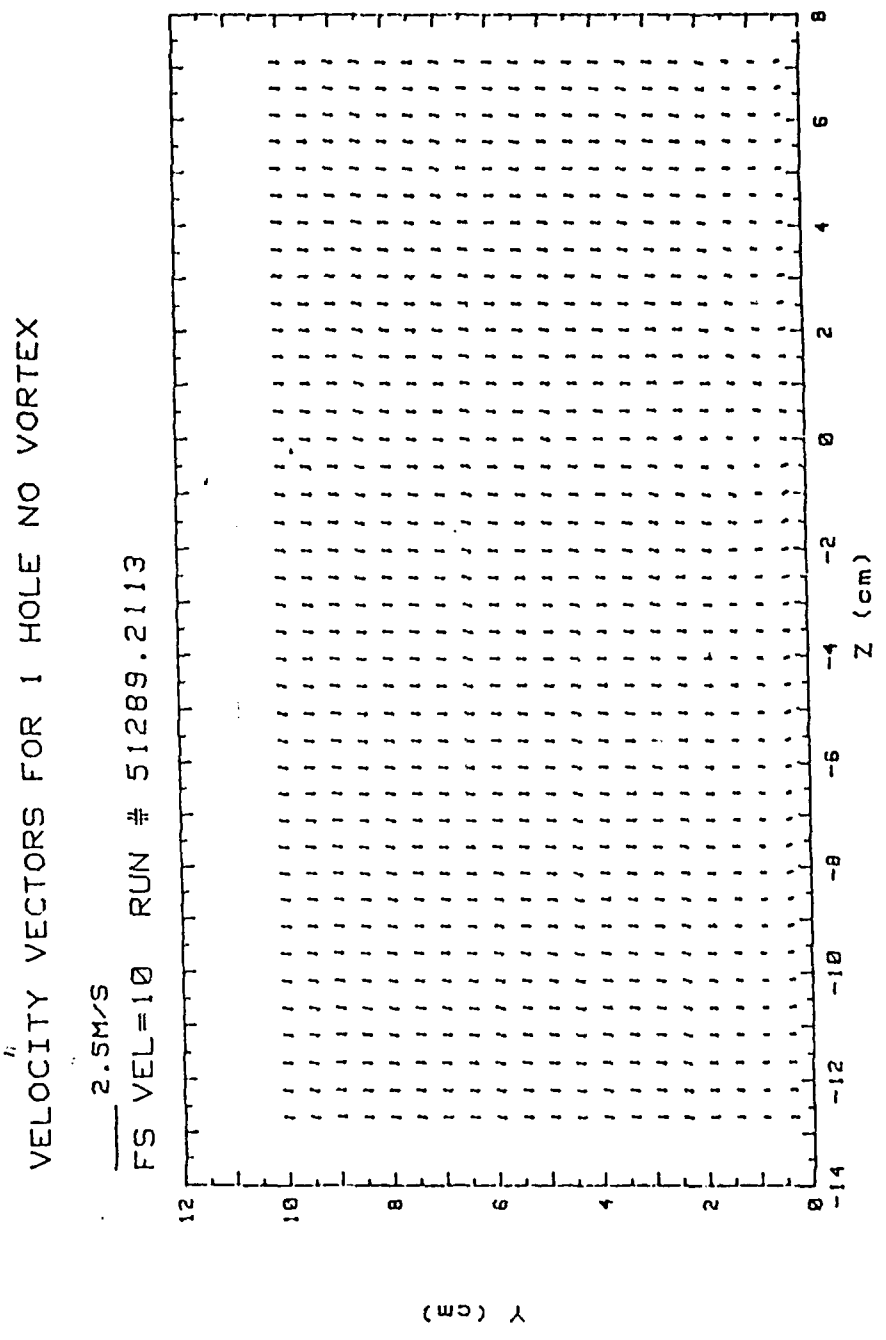

Figure 34 Secondary Flow Vectors Field for A Single Injection Hole, m = 0.5, x/d = 41.9, No Vortex Generator

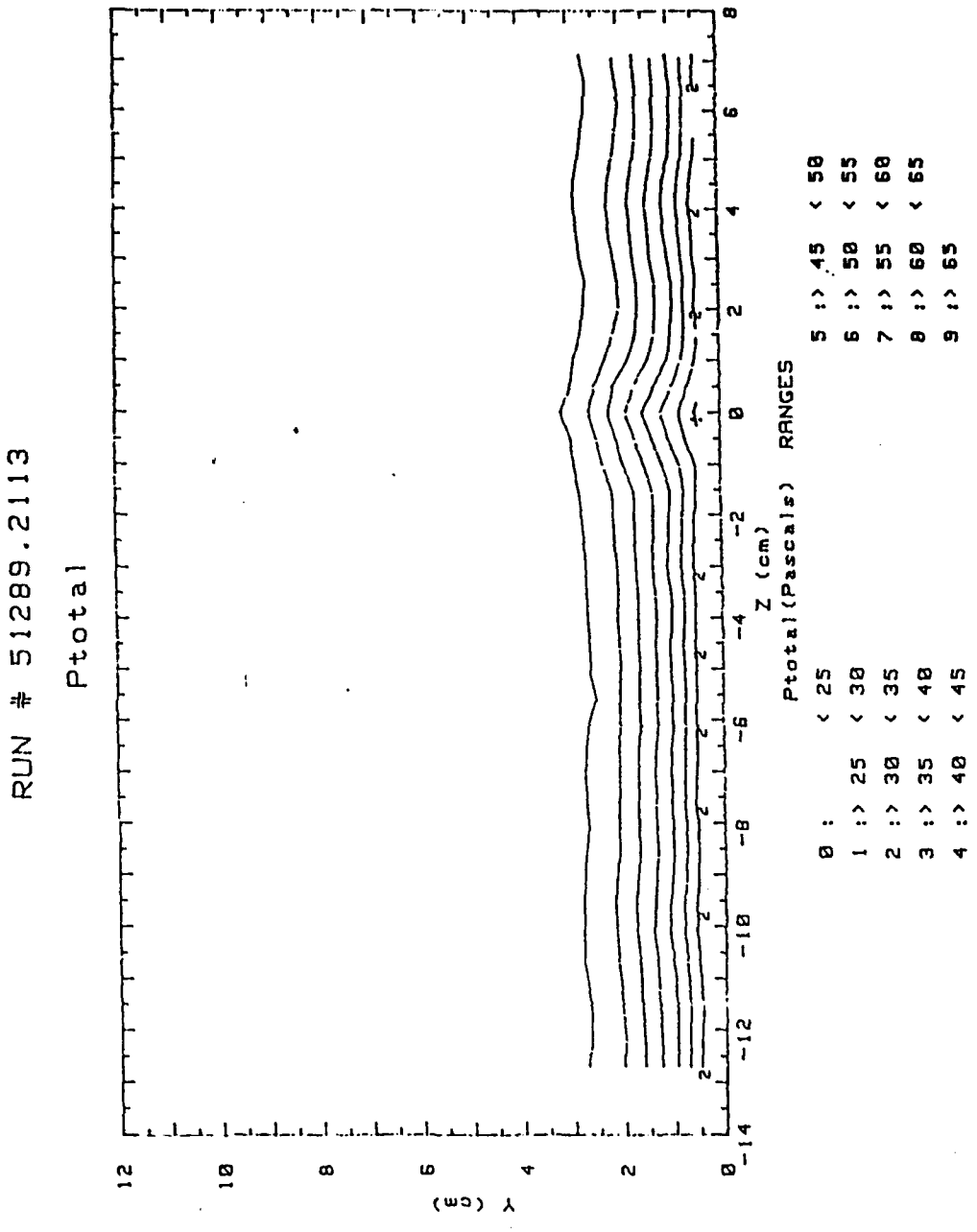

Figure 35 Total Pressure Field for A Single Injection Hole, m = 0.5, x/d = 41.9, No Vortex Generator

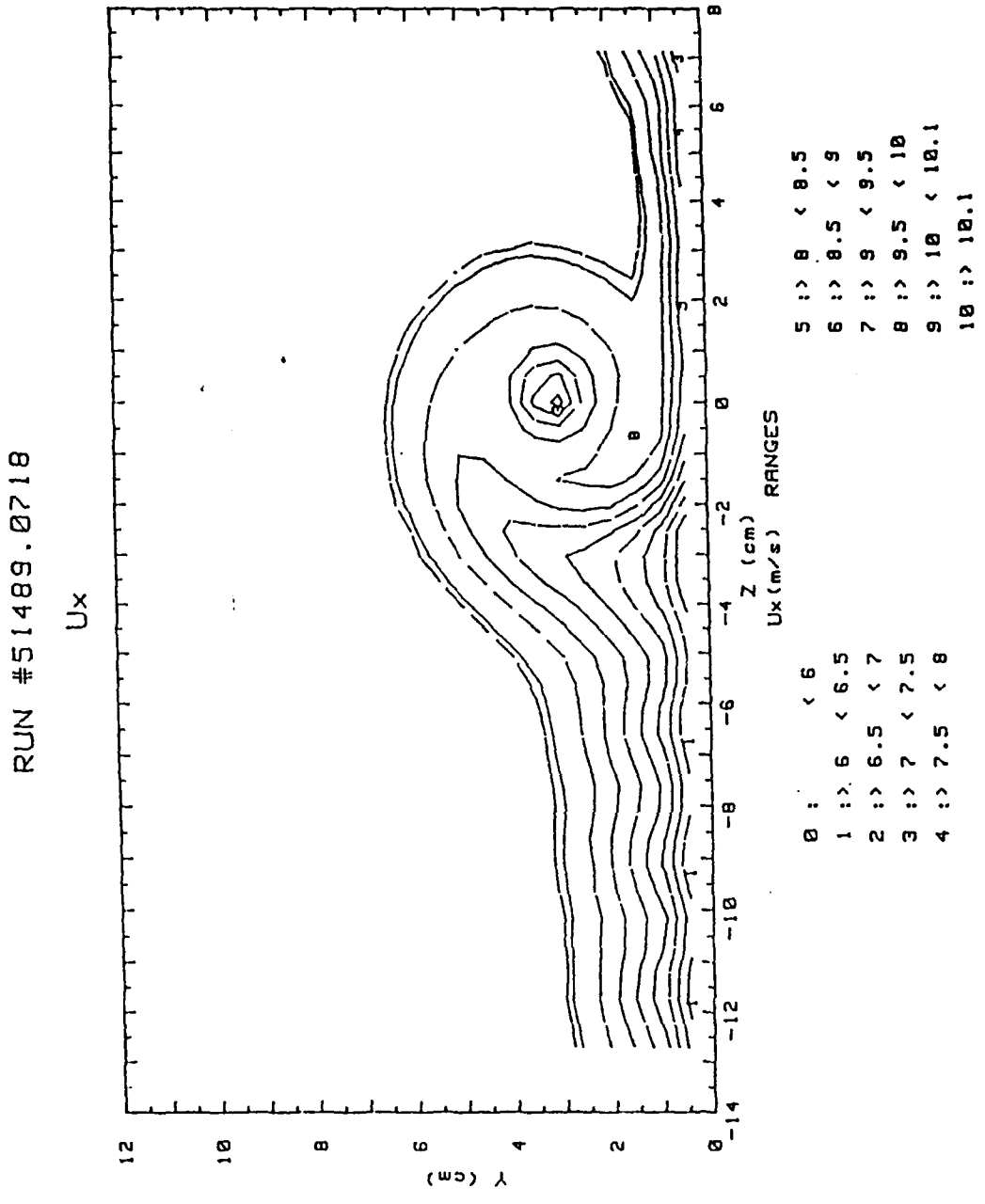

Figure 36 Streamwise Velocity Distributions for 13 Injection Holes, m = 0.5, x/d = 41.9, Vortex r

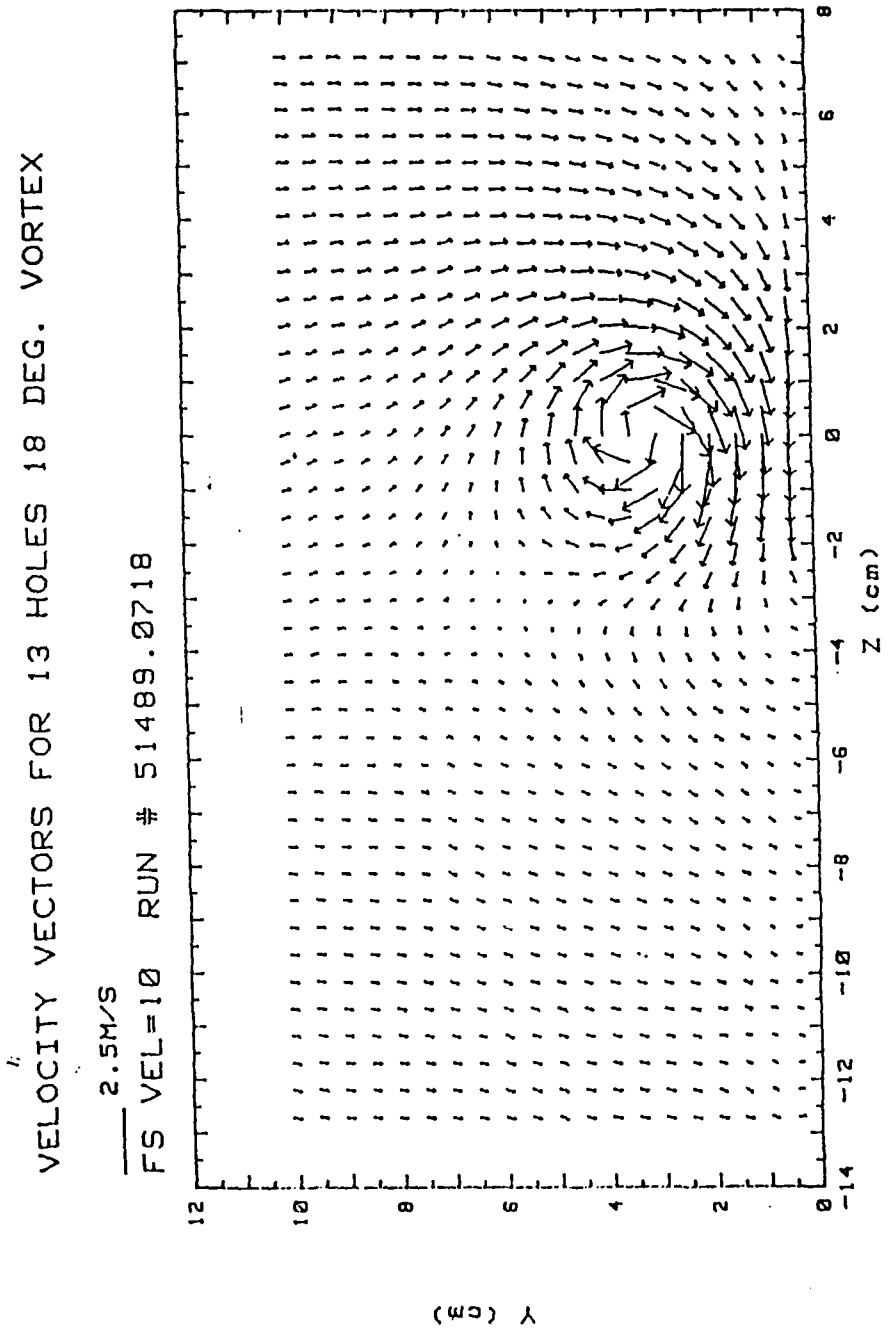

Figure 37 Secondary Flow Vectors Field for 13 Injection Holes, m = 0.5, x/d = 41.9, Vortex r

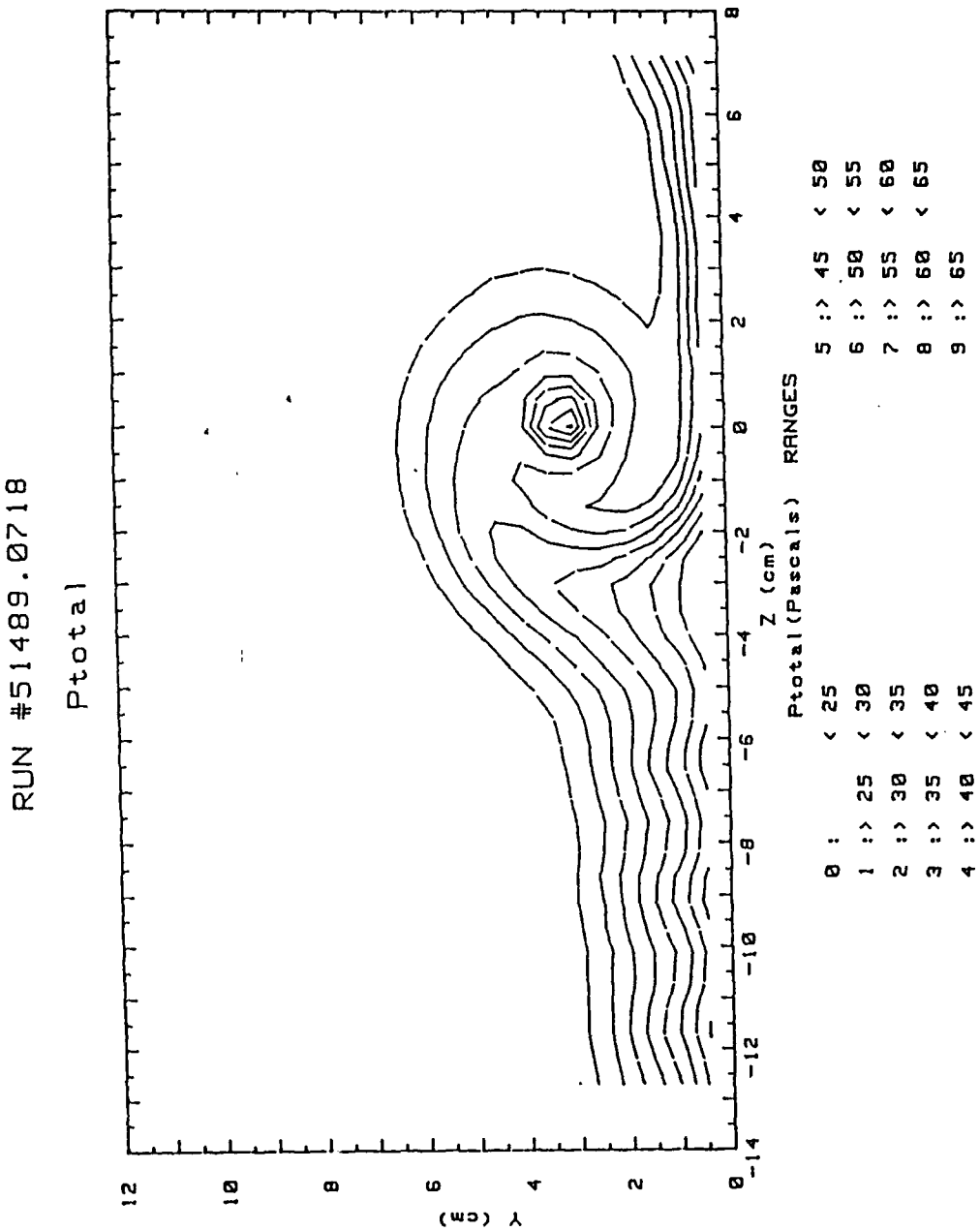

Figure 38 Total Pressure Field for 13 Injection Holes, m = 0.5, x/d = 41.9, Vortex r

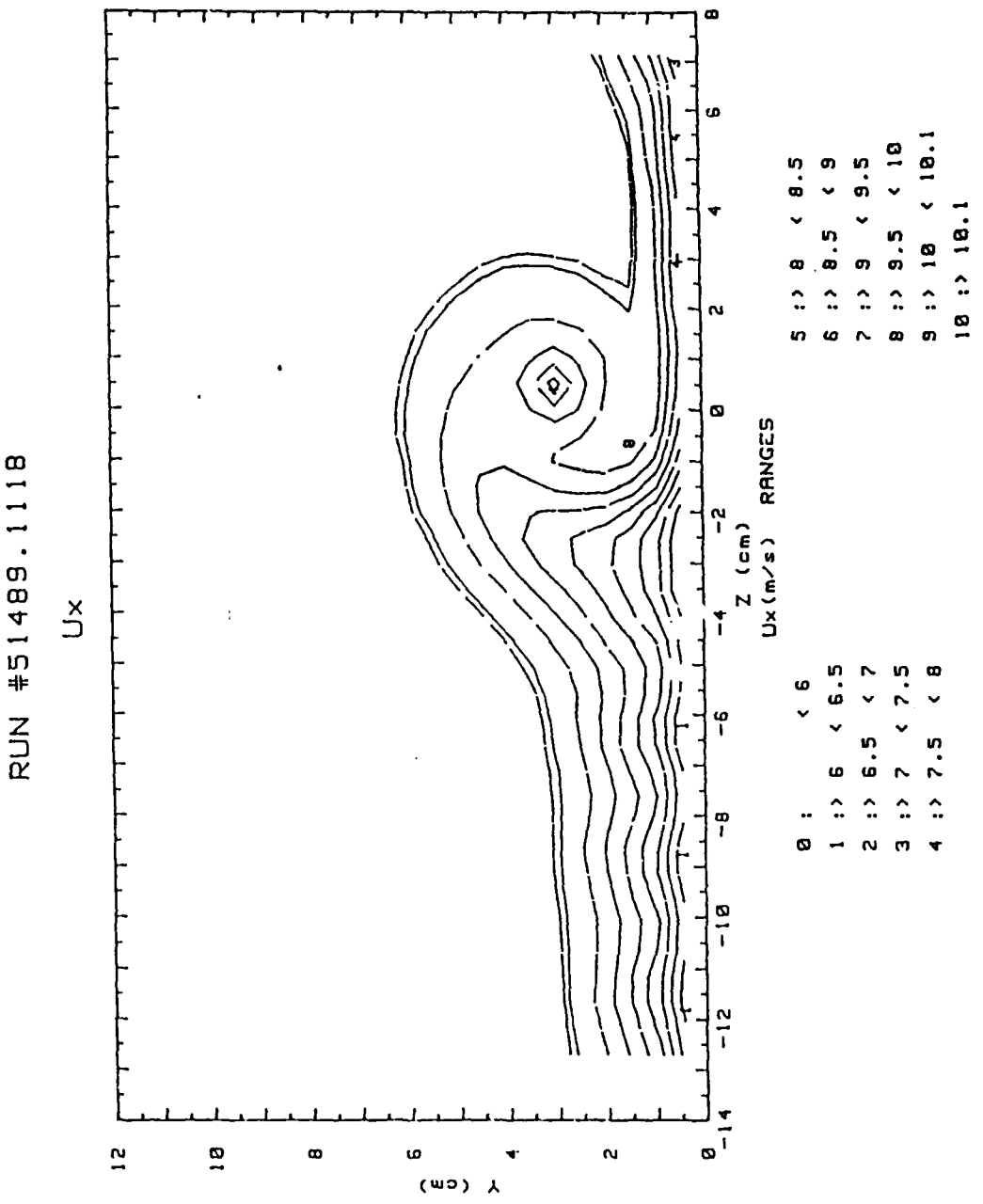

Figure 39 Streamwise Velocity Distributions for 13 Injection Holes, m = 0.5, x/d = 41.9, Vortex w

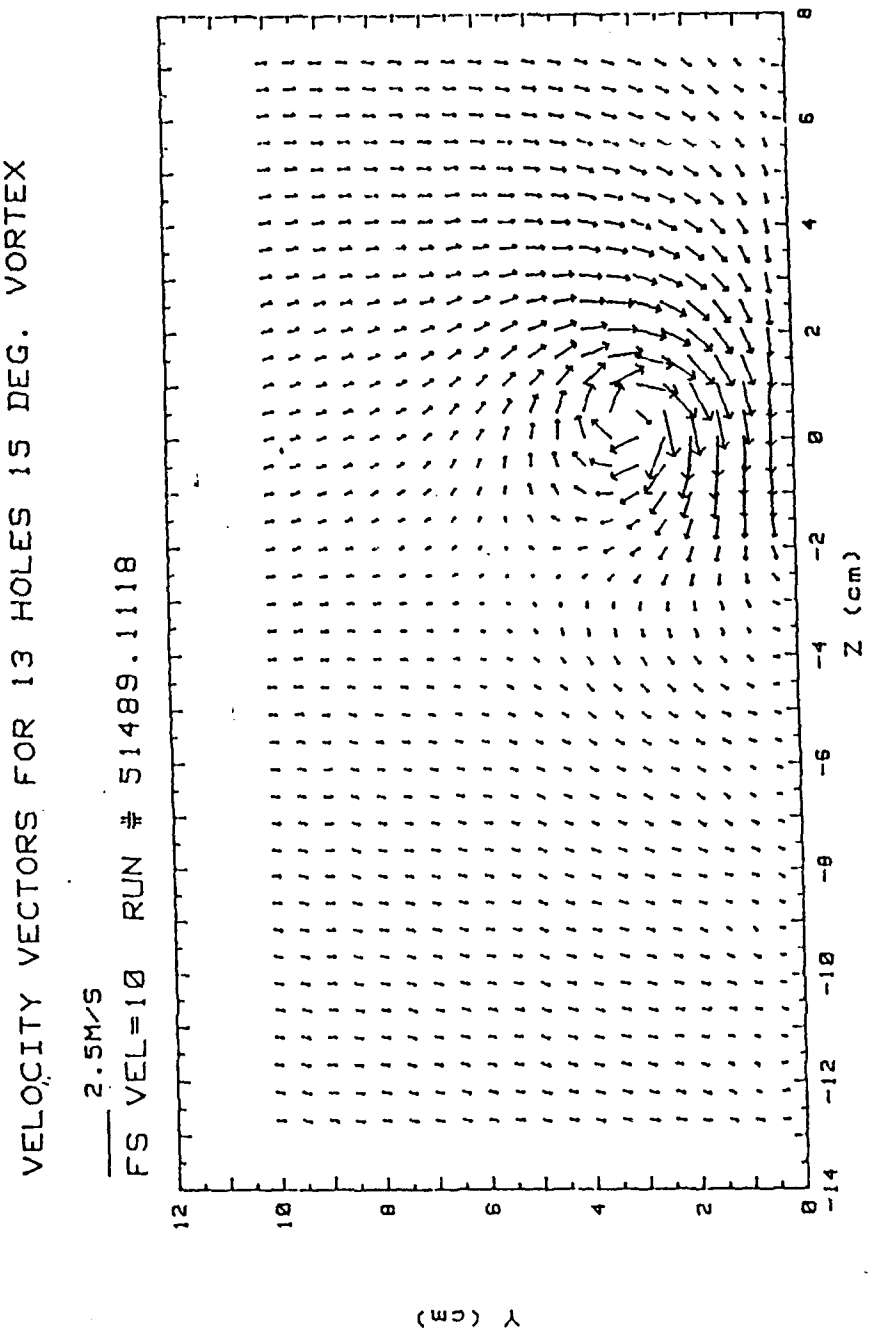

Figure 40 Secondary Flow Vectors Field for 13 Injection Holes, m = 0.5, x/d = 41.9, Vortex w

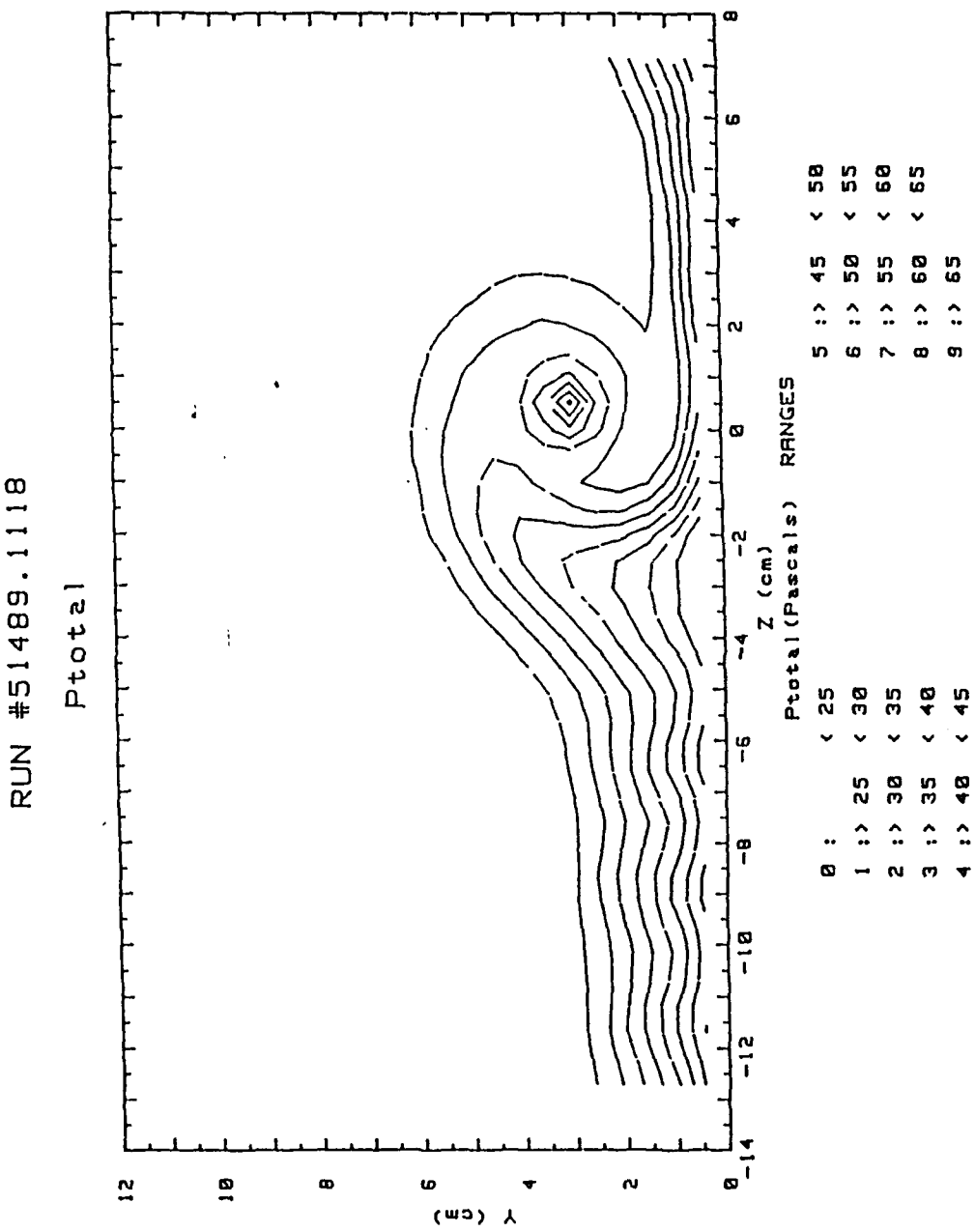

Figure 41 Total Pressure Field for 13 Injection Holes, m = 0.5, x/d = 41.9, Vortex w

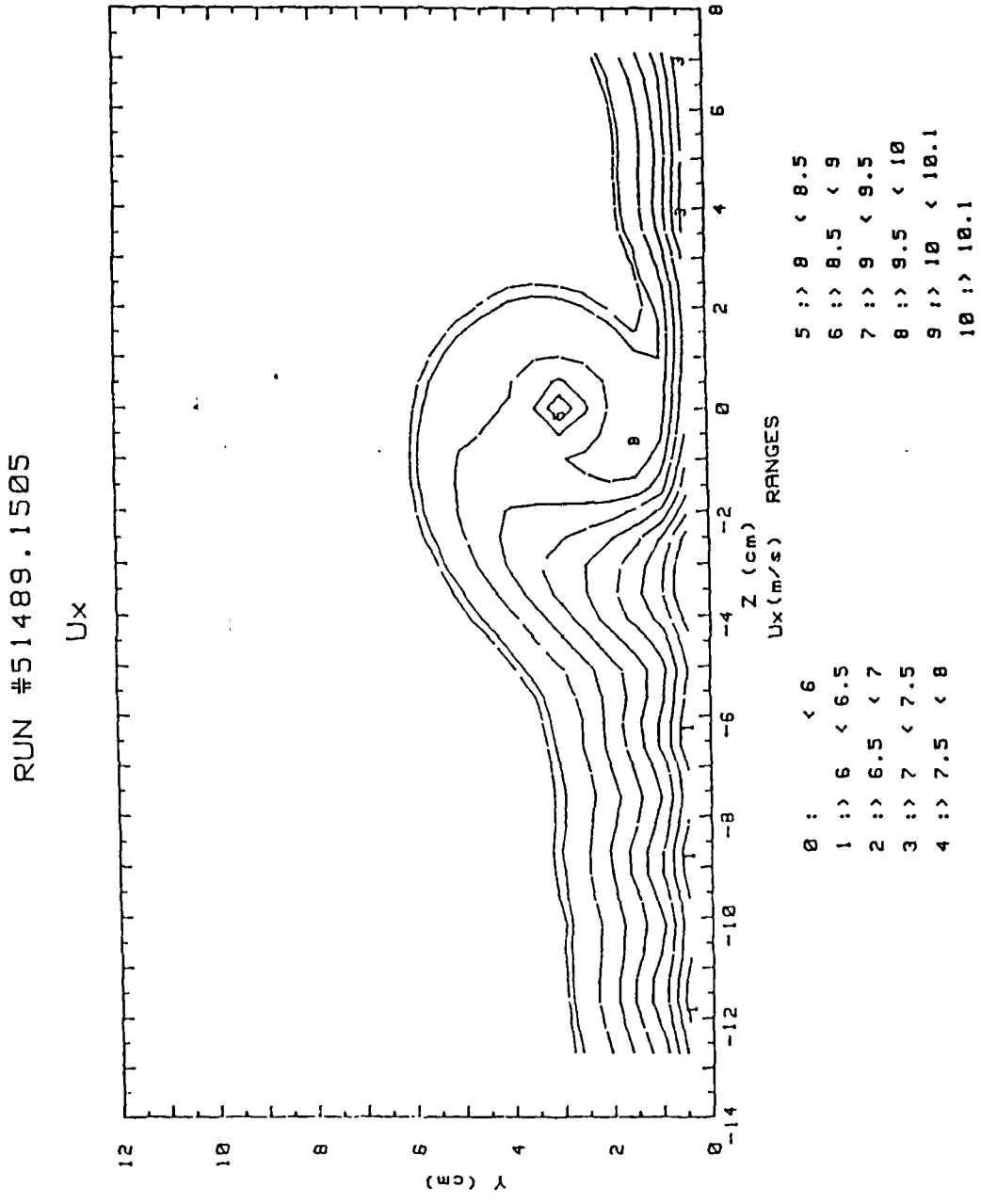

Figure 42 Streamwise Velocity Distributions for 13 Injection Ho' .s, m = 0.5, x/d = 41.9, Vortex x

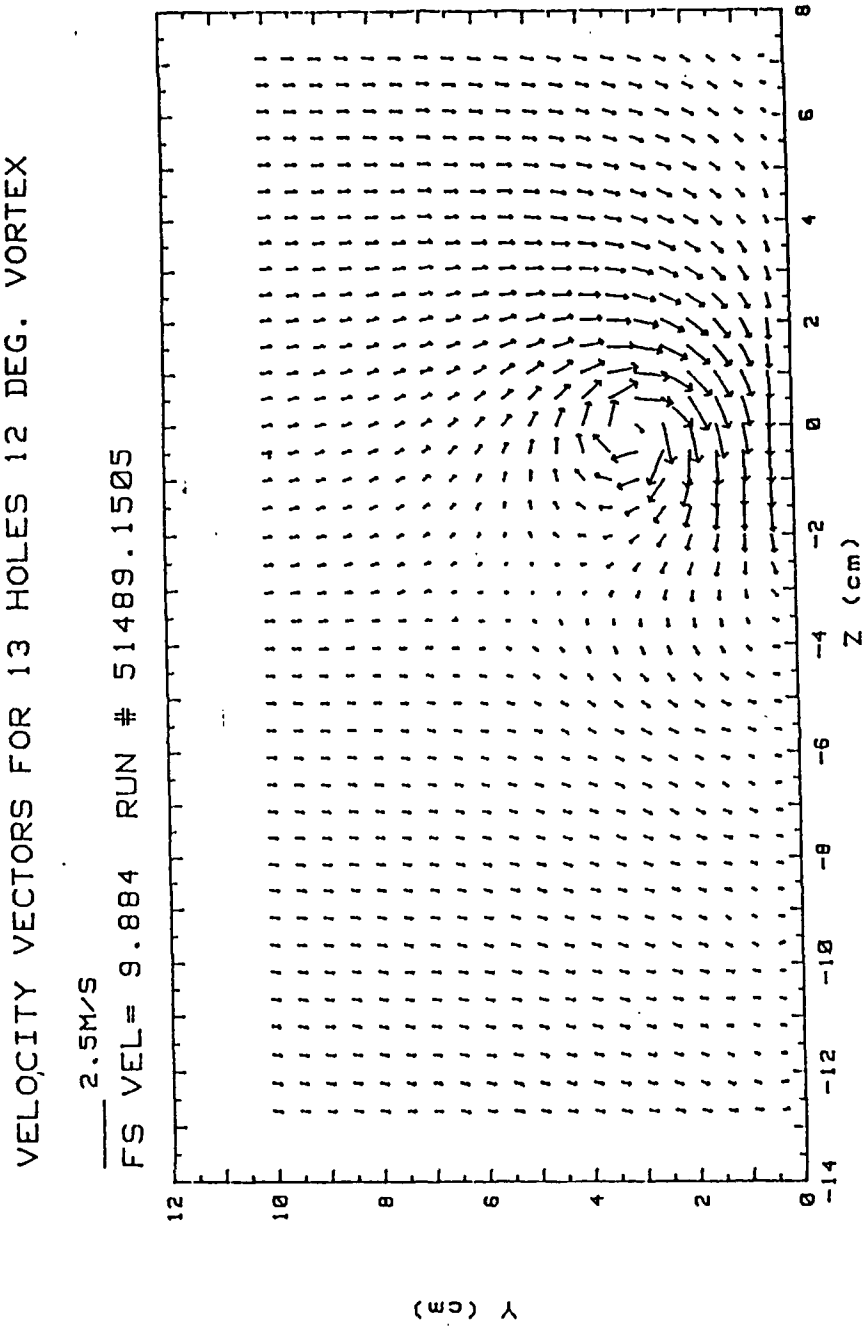

Figure 43 Secondary Flow Vectors Field for 13 Injection Holes, m = 0.5, x/d = 41.9, Vortex x

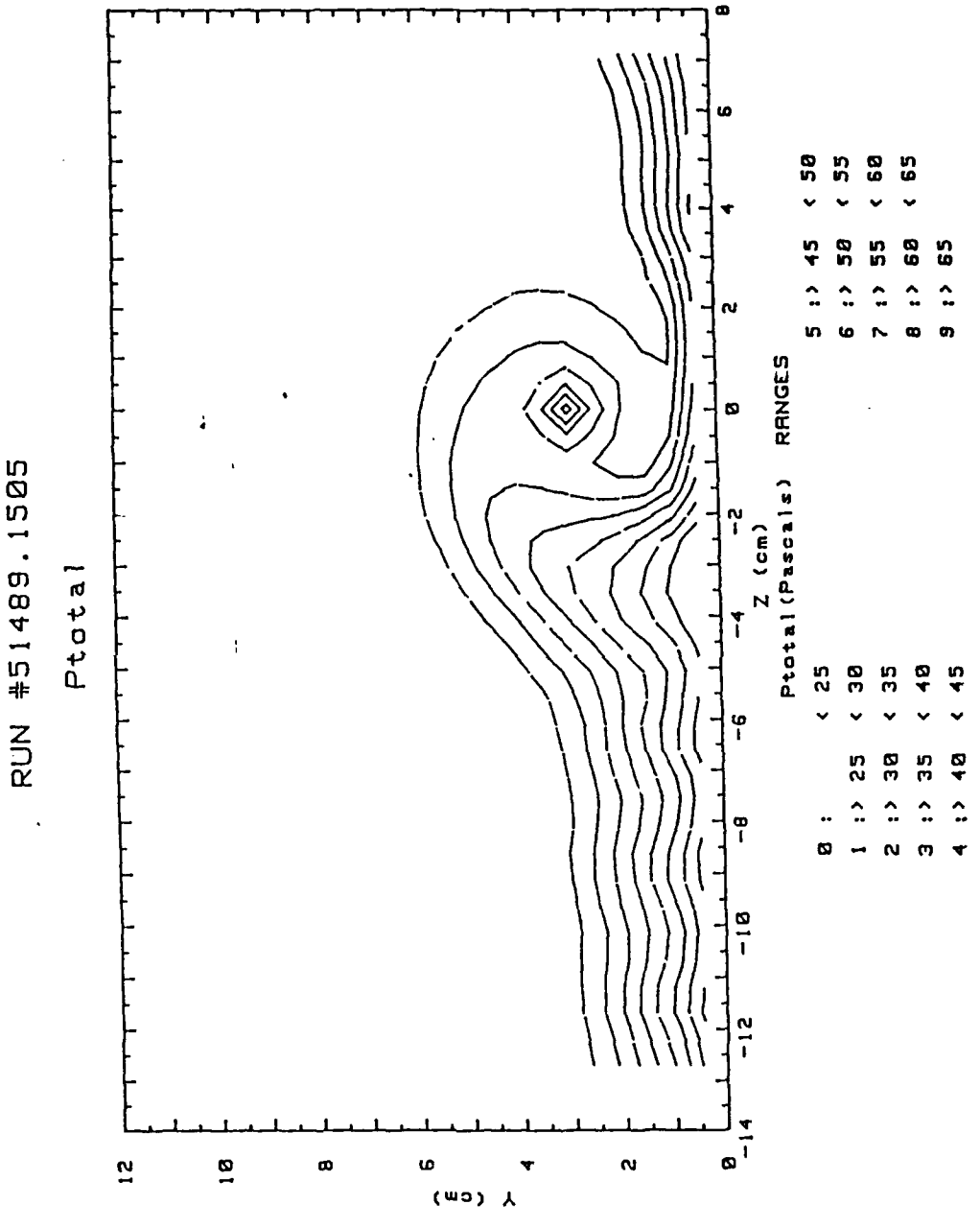

Figure 44 Total Pressure Field for 13 Injection Holes, m = 0.5, x/d = 41.9, Vortex x

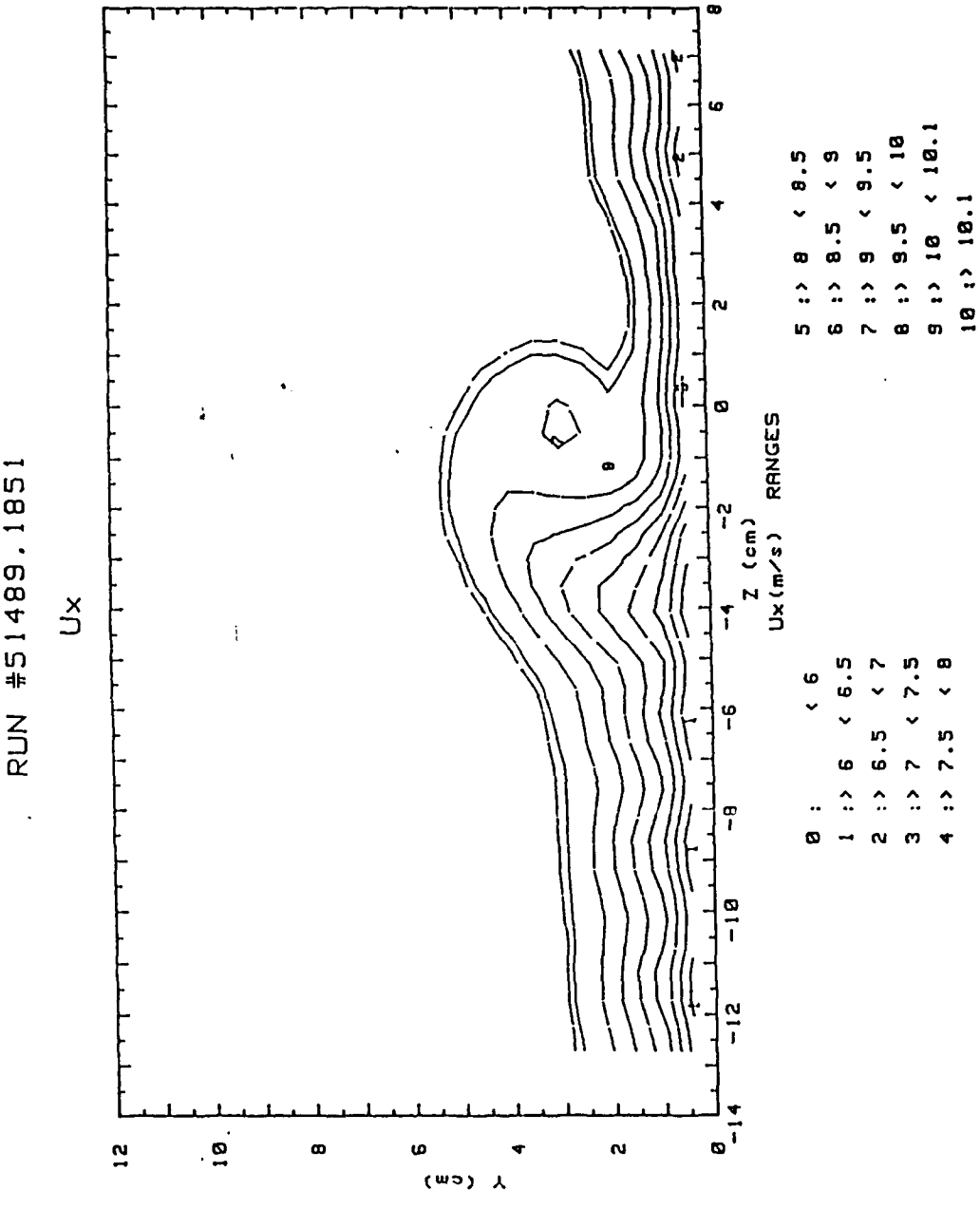

Figure 45 Streamwise Velocity Distributions for 13 Injection Holes, m = 0.5, x/d = 41.9, Vortex y

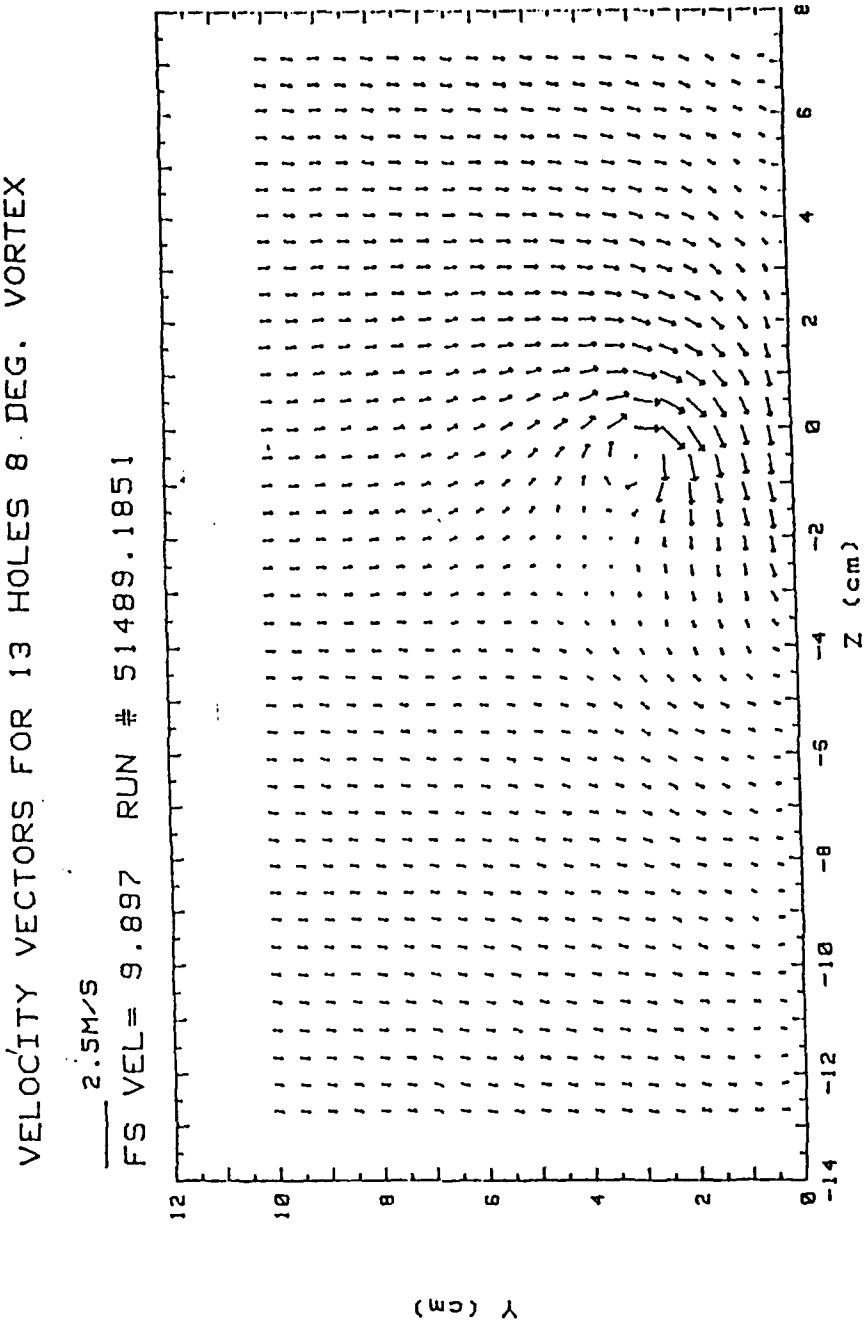

Figure 46 Secondary Flow Vectors Field for 13 Injection Holes, m = 0.5, x/d = 41.9, Vorex y

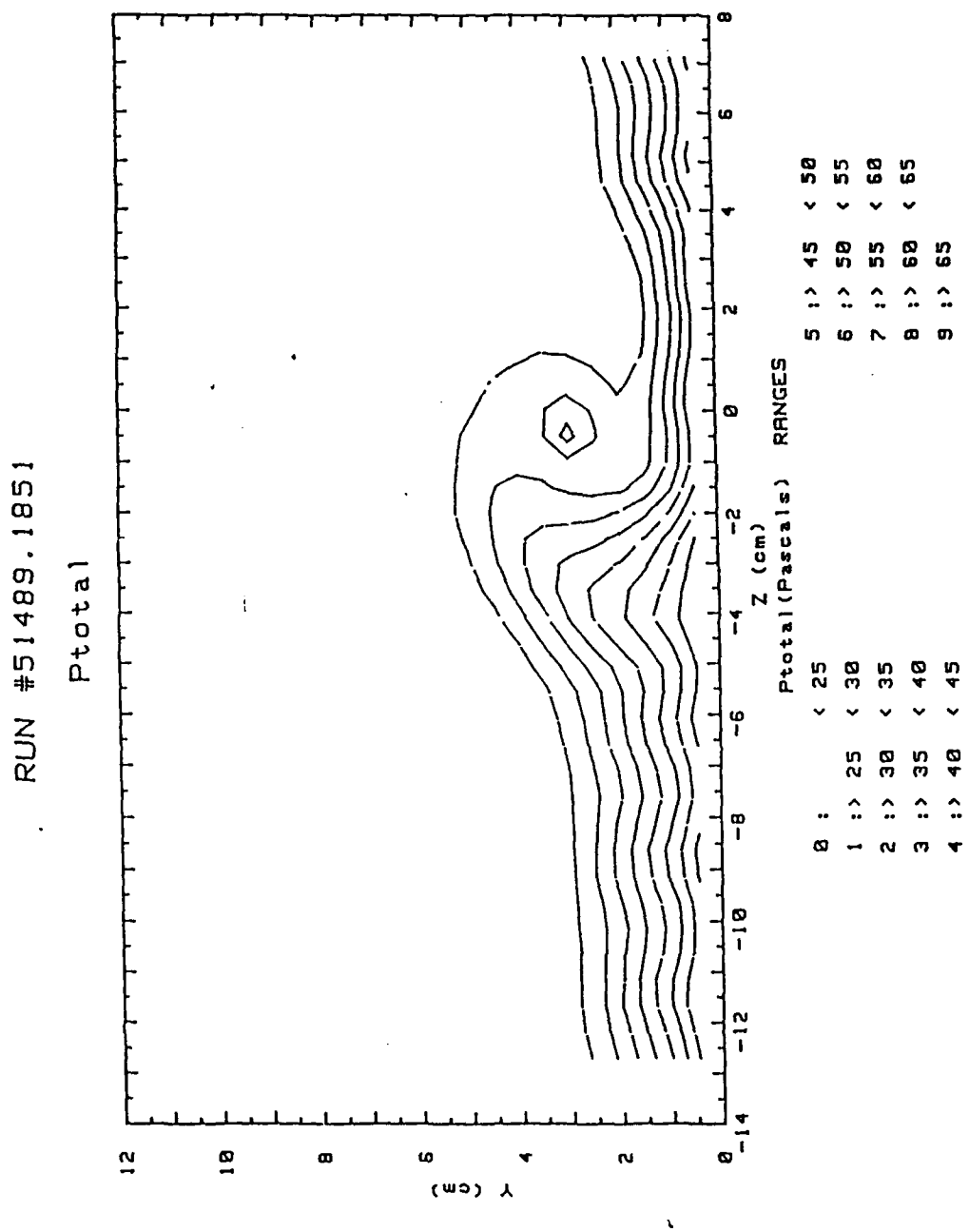

Figure 47 Total Pressure Field for 13 Injection Holes, m = 0.5, x/d = 41.9, Vortex y

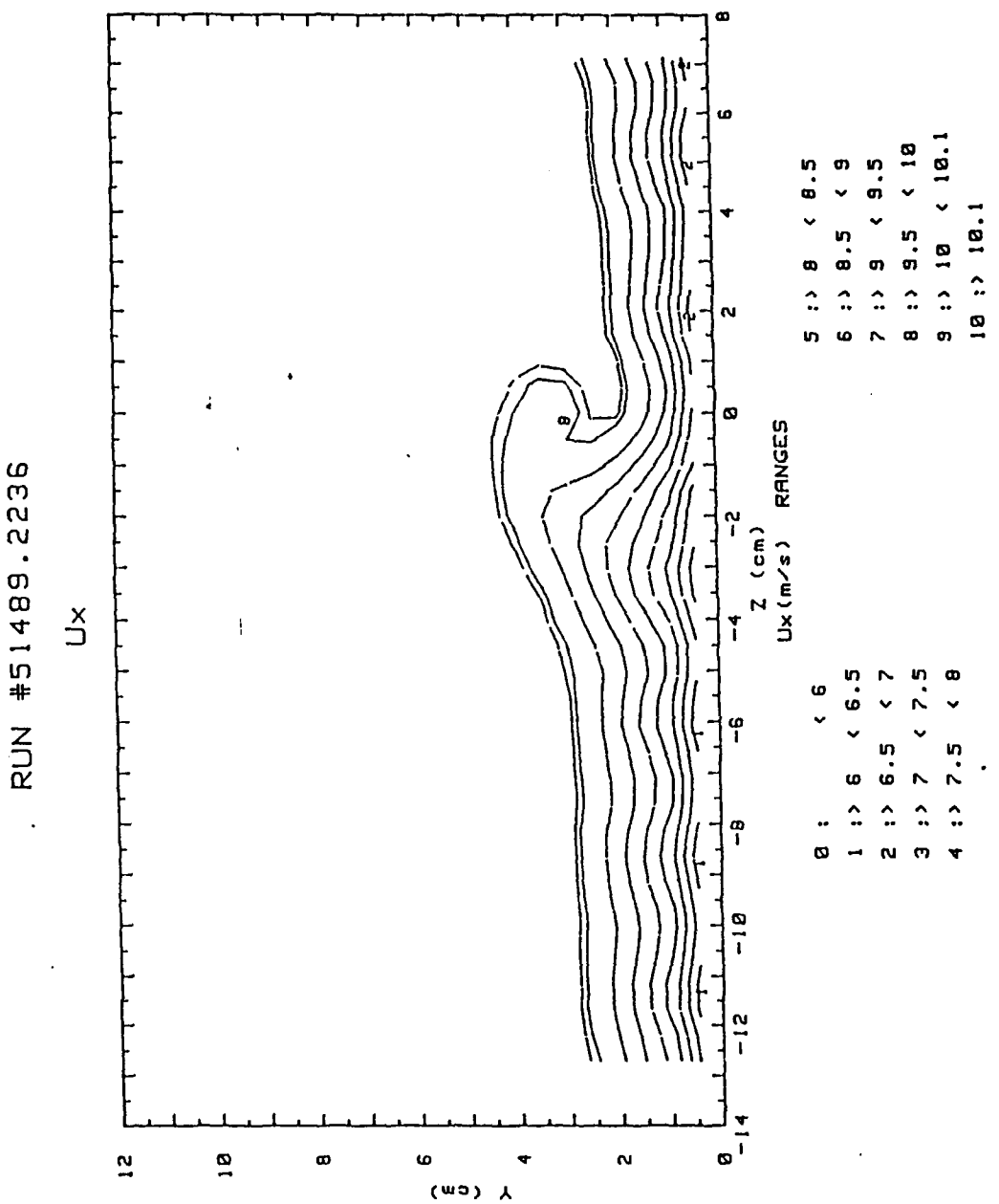

Figure 48 Streamwise Velocity Distributions for 13 Injection Holes, m = 0.5, x/d = 41.9, Vortex z

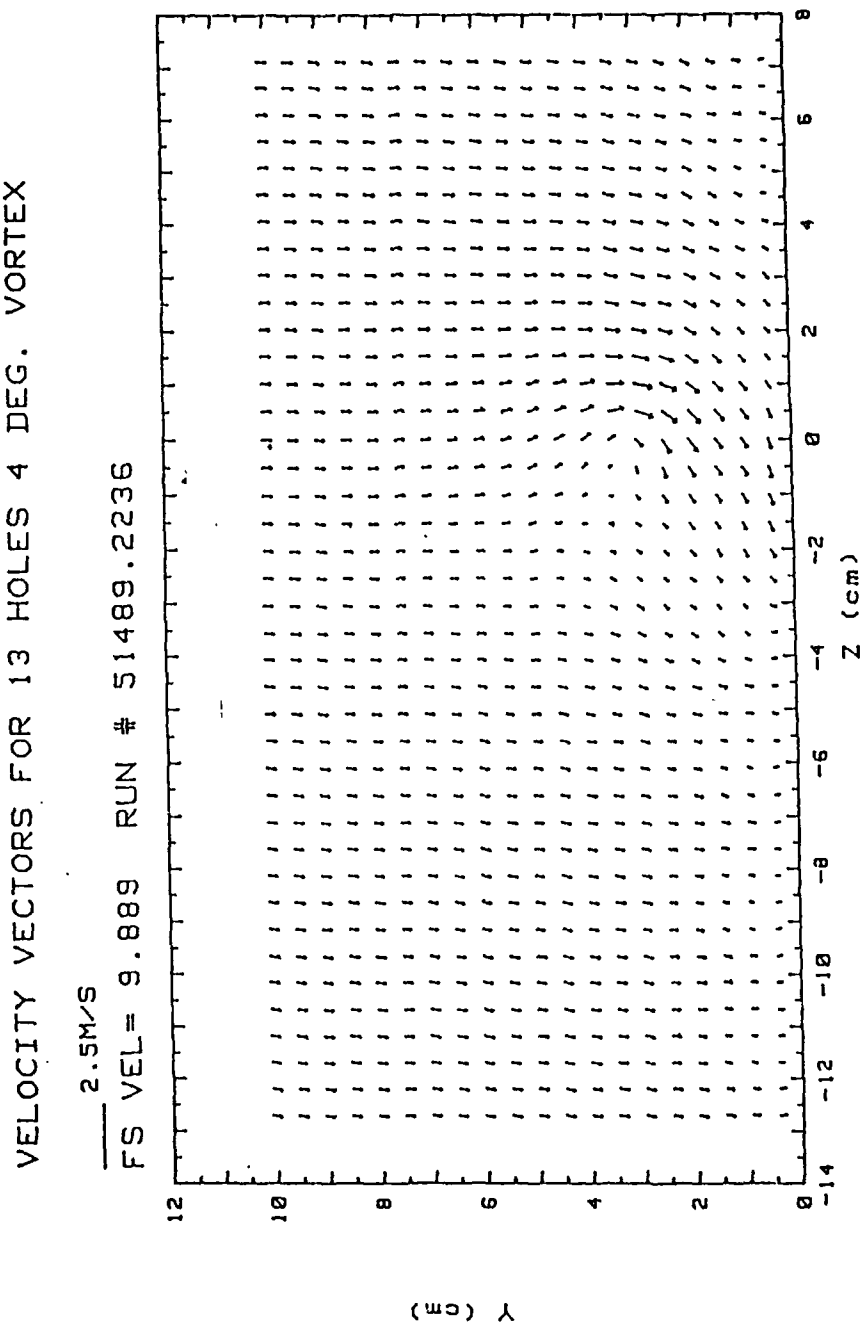

Figure 49 Secondary Flow Vectors Field for 13 Injection Holes, m = 0.5, x/d = 41.9, Vortex z

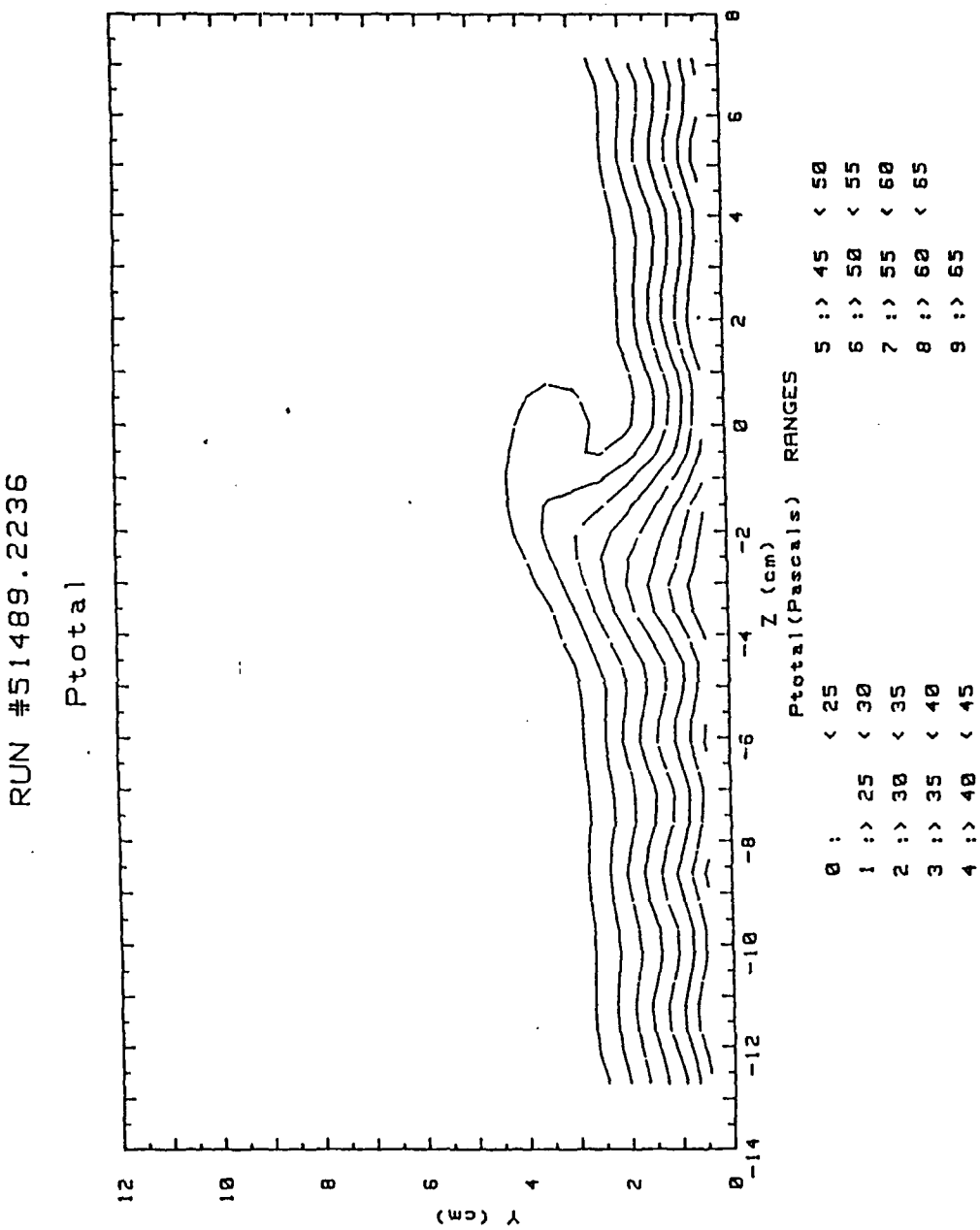

Figure 50 Total Pressure Field for 13 Injection Holes, m = 0.5, x/d = 41.9, Vortex z

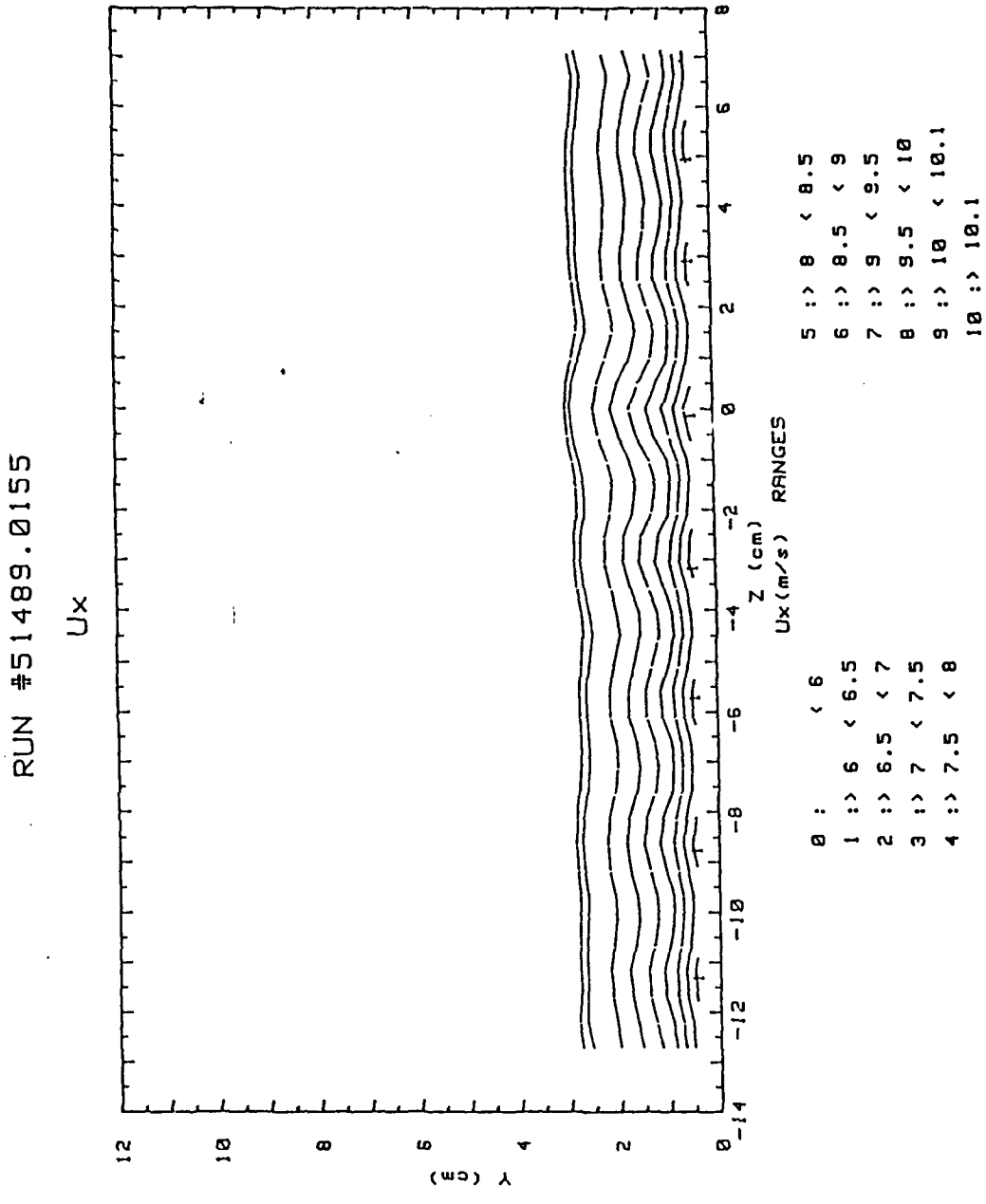

Figure 51 Streamwise Velocity Distributions for 13 Injection Holes, m = 0.5, x/d = 41.9, No Vortex Generator

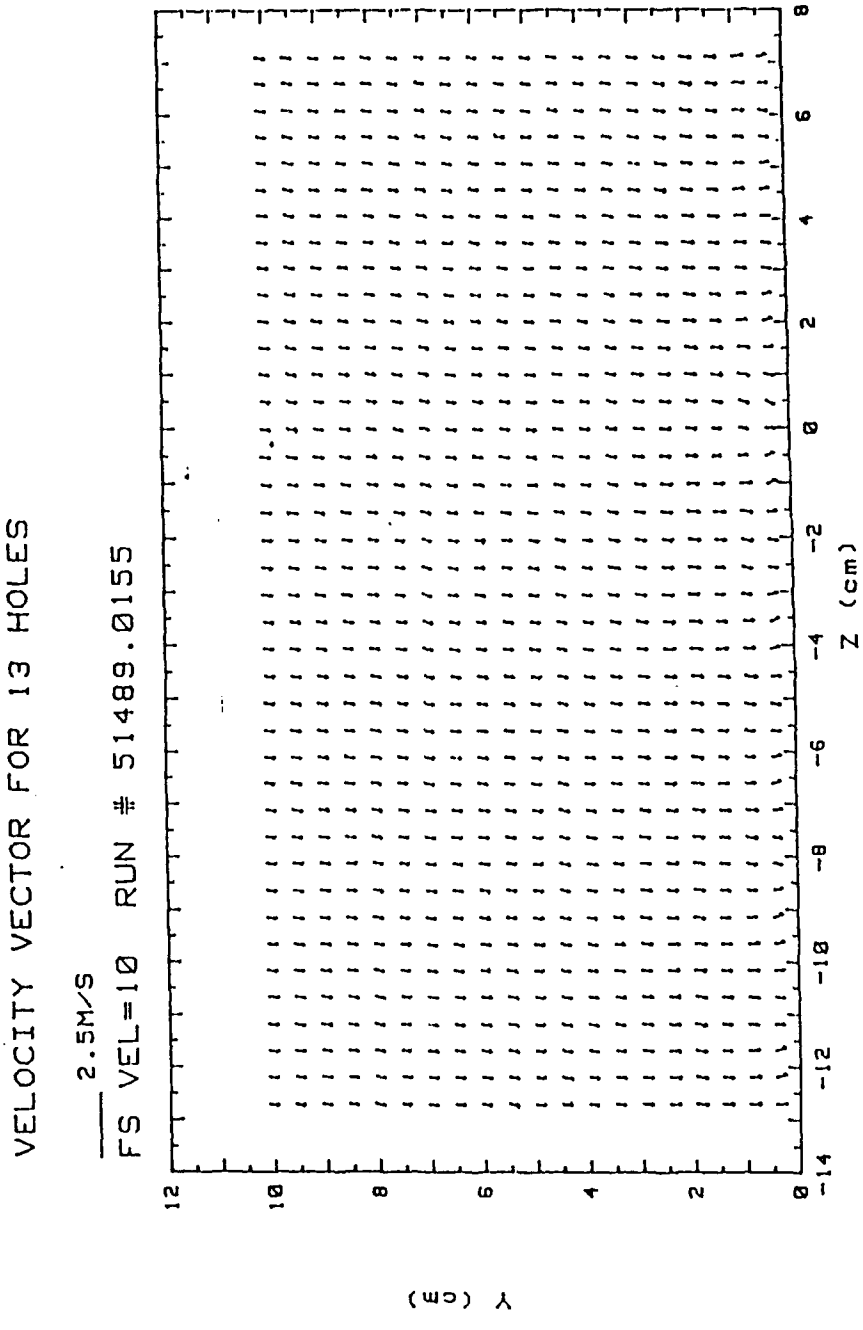

Figure 52 Secondary Flow Vectors Field for 13 Injection Holes, m = 0.5, x/d = 41.9, No Vortex Generator

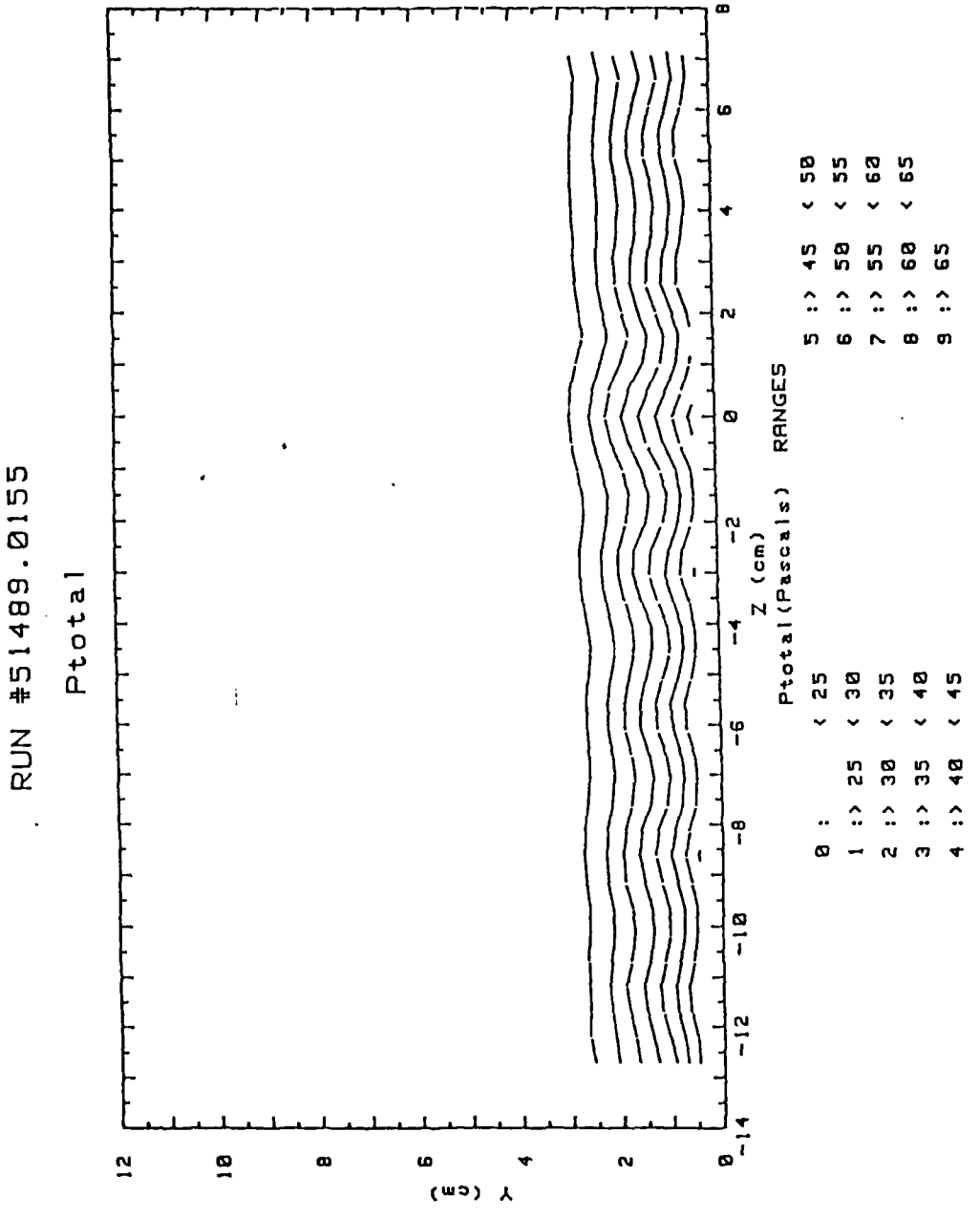

Figure 53 Total Pressure Field for 13 Injection Holes, m = 0.5, x/d = 41.9, No Vortex Generator

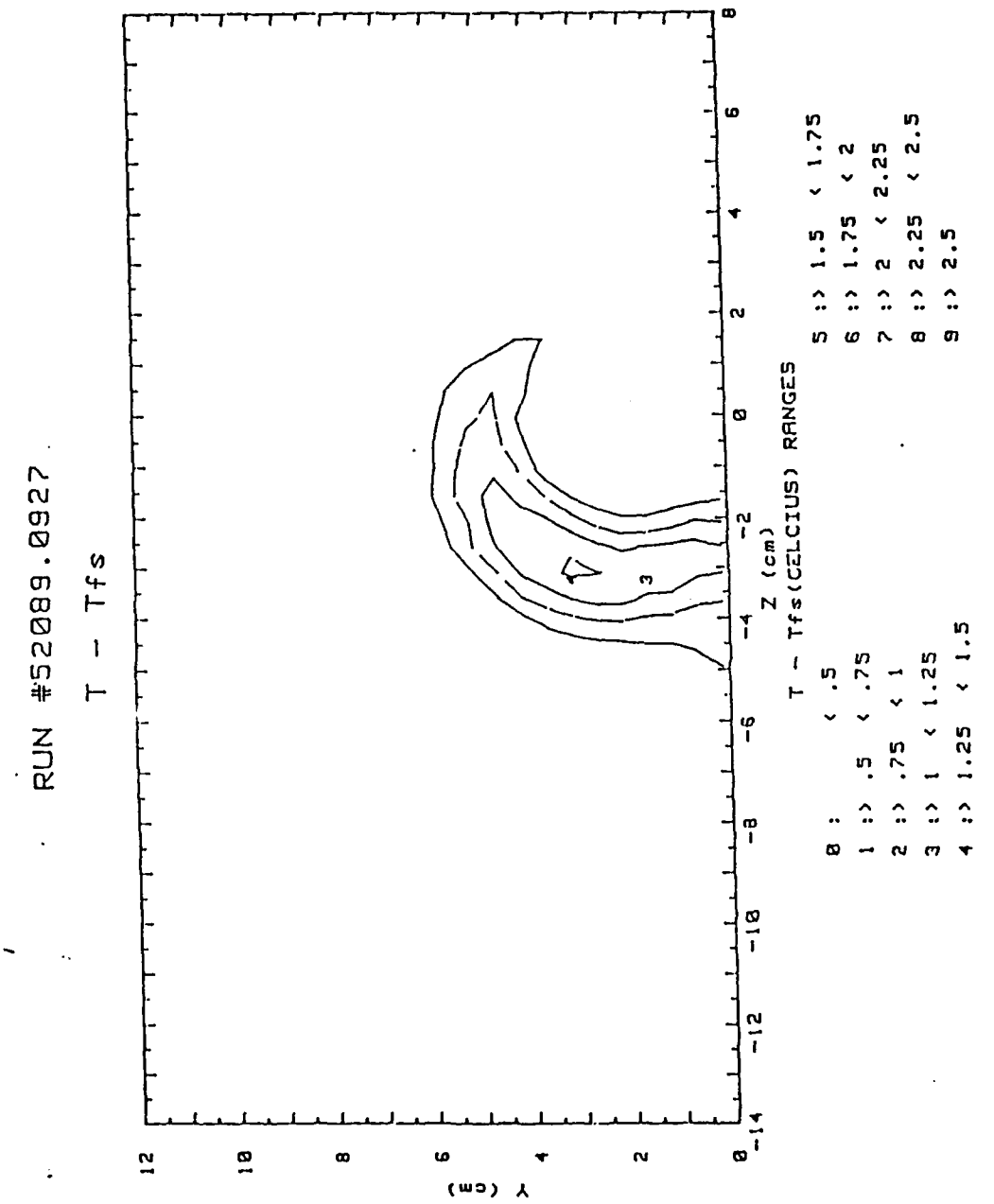

Figure 54 Local Temperature Distribution, A Single Injection Hole, m = 0.5, x/d = 41.9, Vortex r

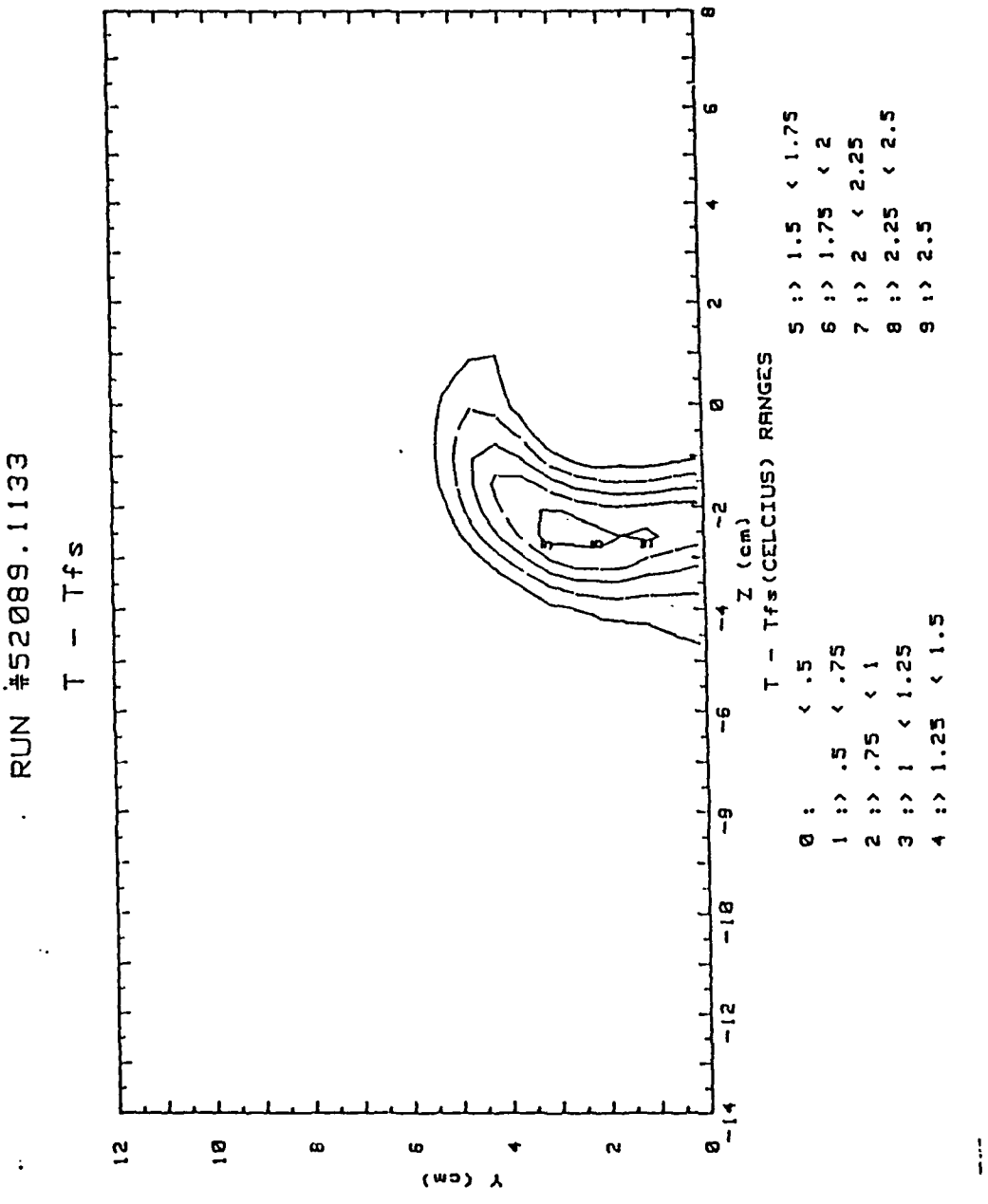

Figure 55 Local Temperature Distribution, A Single Injection Hole, m = 0.5, x/d = 41.9, Vortex w

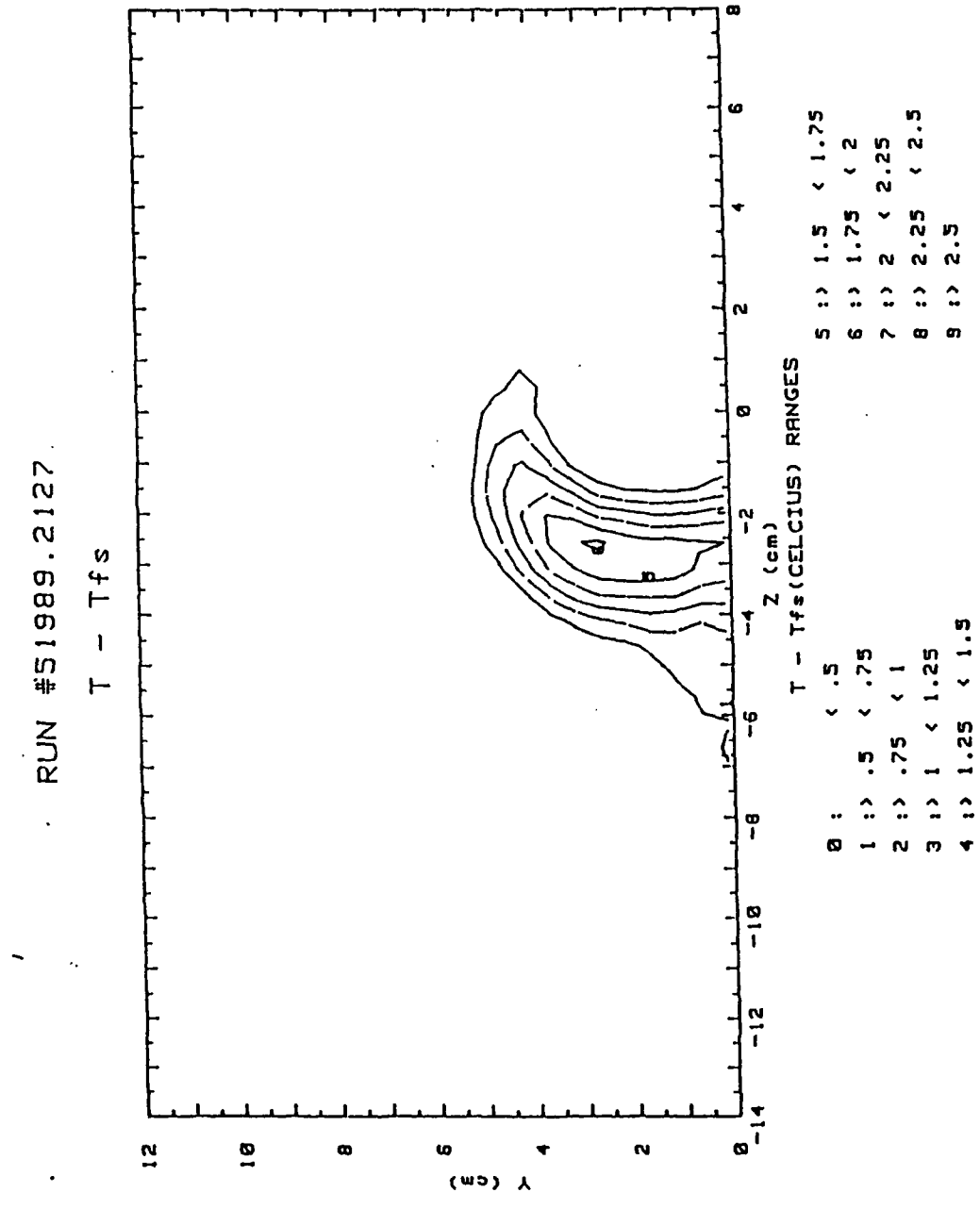

Figure 56 Local Temperature Distribution, A Single Injection Hole, m = 0.5, x/d = 41.9, Vortex x

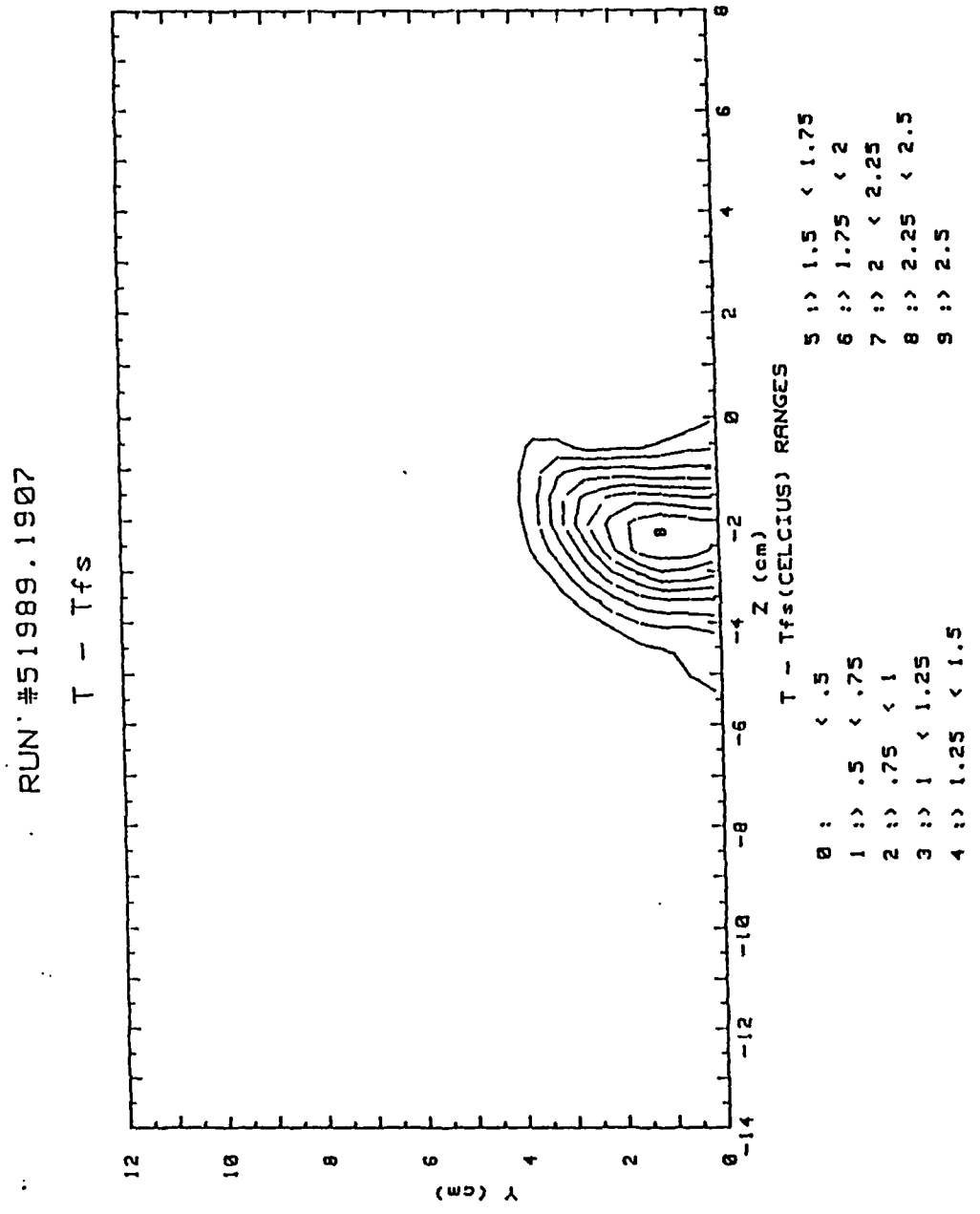

Figure 57 Local Temperature Distribution, A Single Injection Hole, m = 0.5, x/d = 41.9, Vortex y

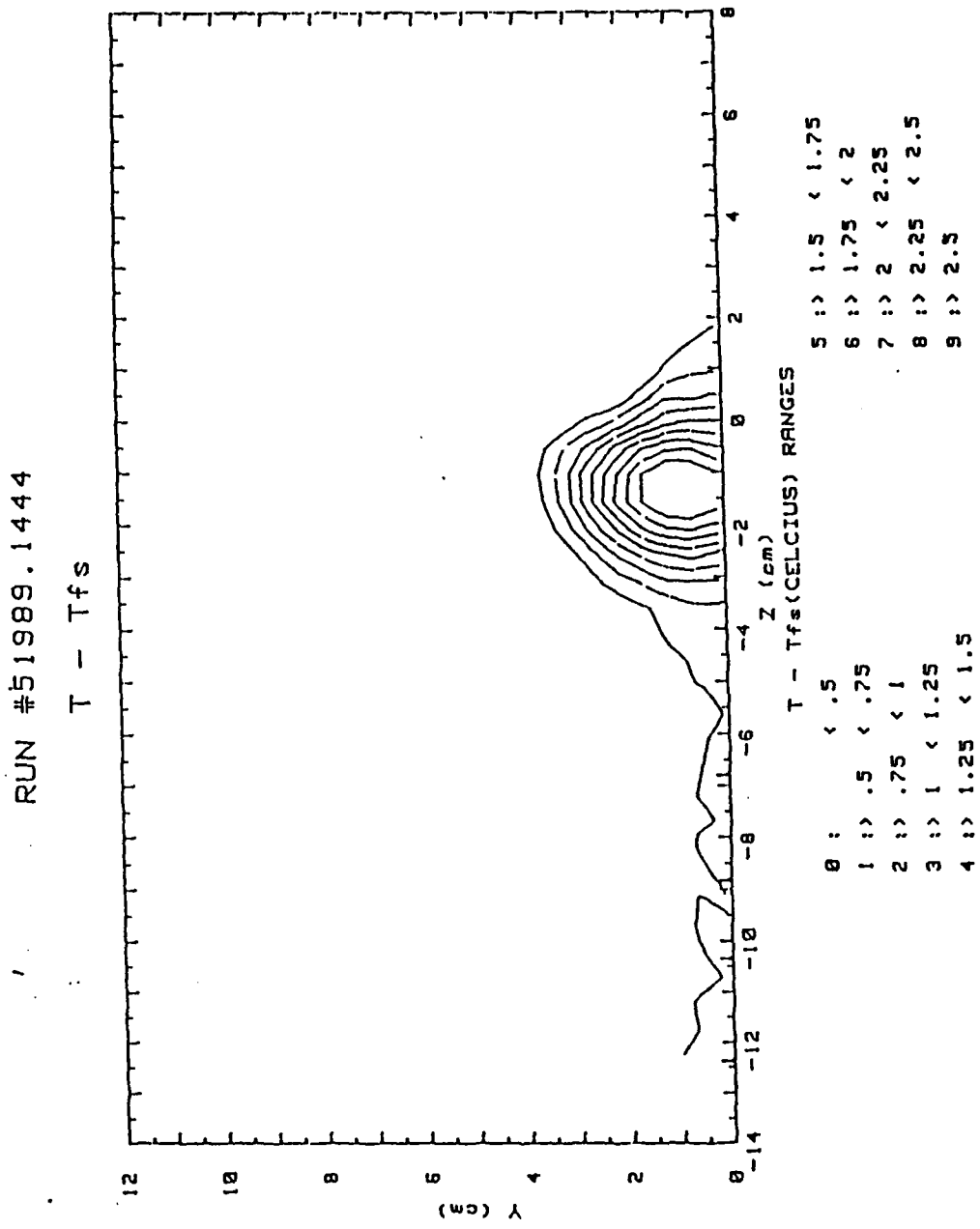

Figure 58 Local Temperature Distribution. A Single Injection Hole, m = 0.5, x/d = 41.9, Vortex z

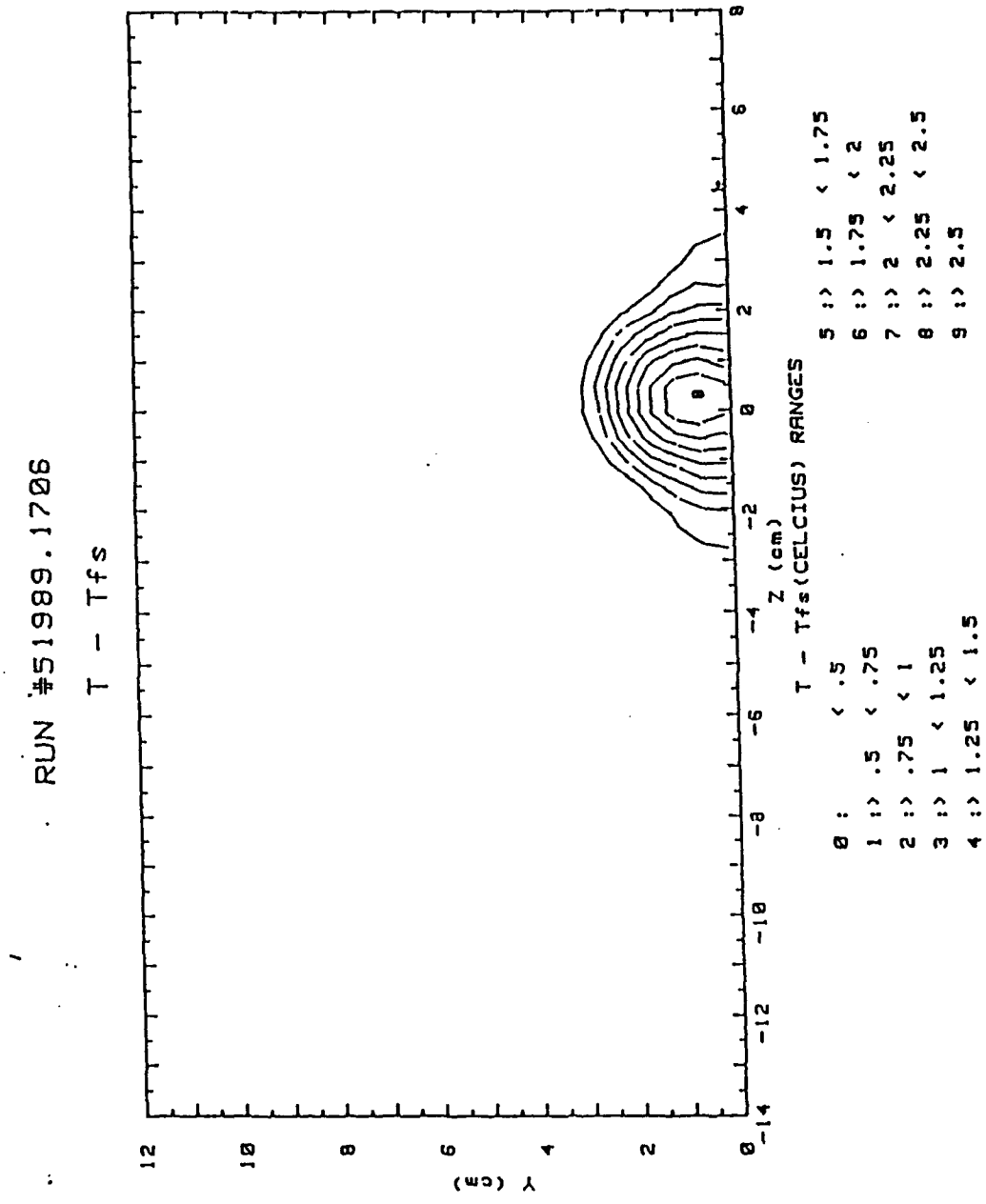

Figure 59 Local Temperature Distribution, A Single Injection Hole, m = 0.5, x/d = 41.9, No Vortex Generator

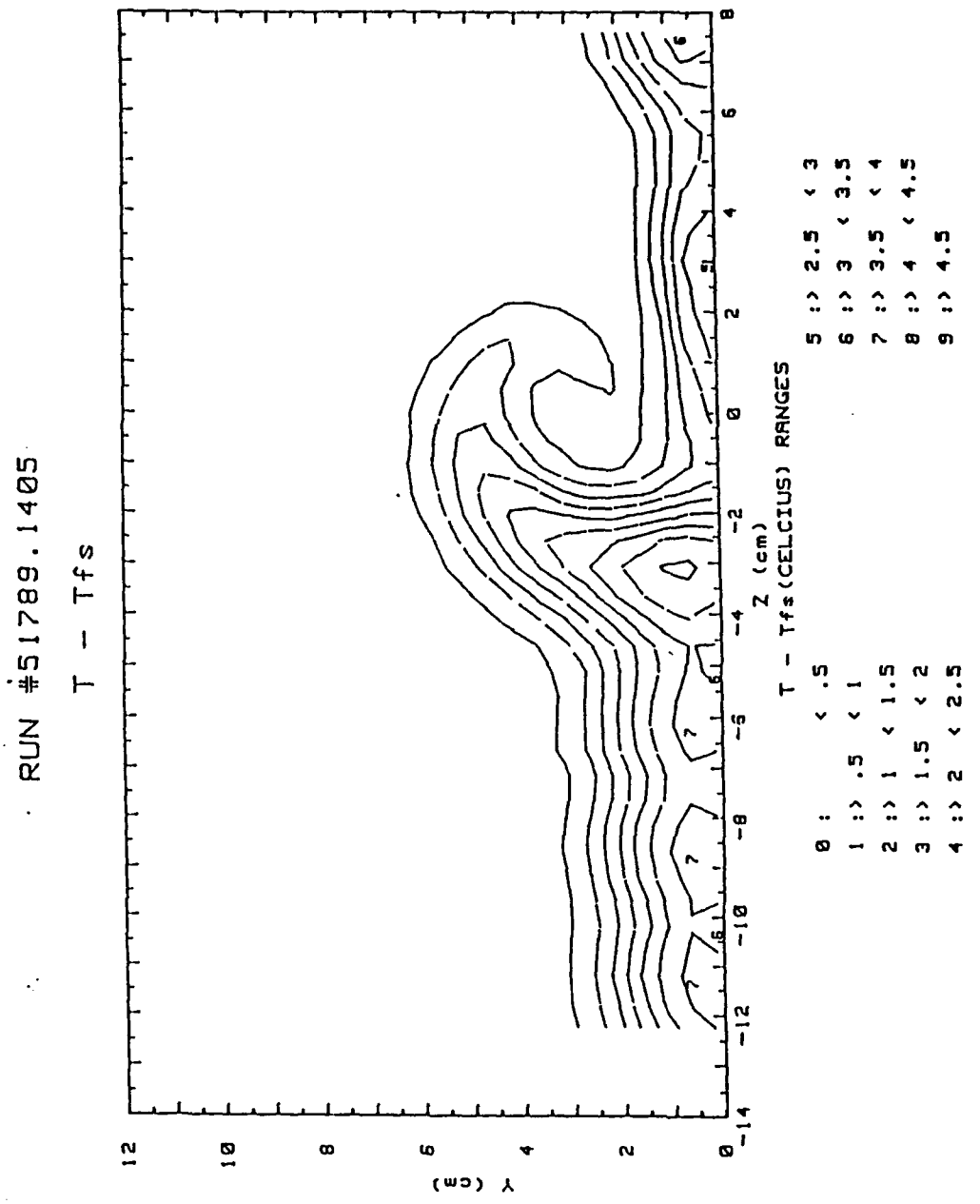

Figure 60 Local Temperature Distribution, 13 Injection Holes, m = 0.5, x/d = 41.9, Vortex r

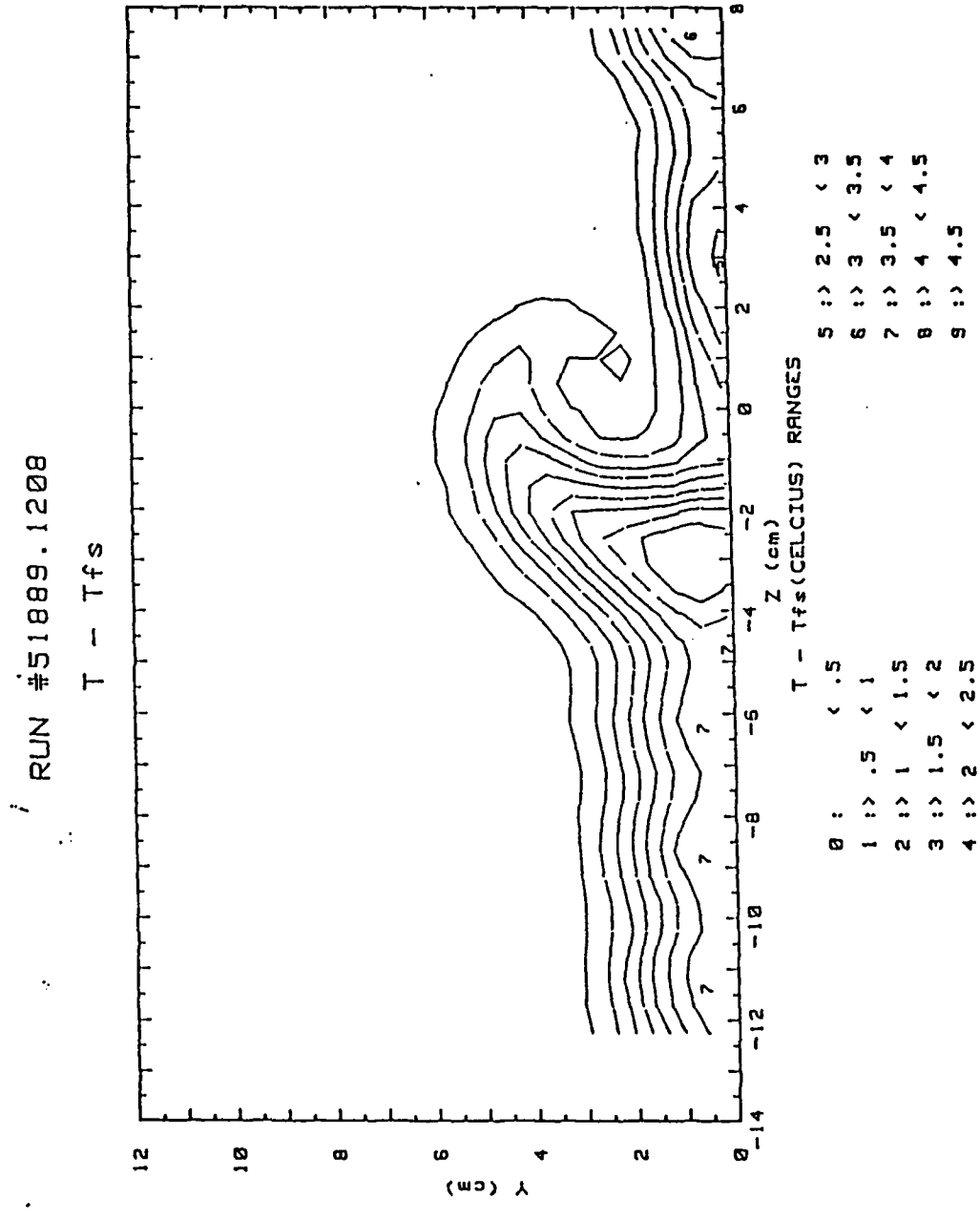

Figure 61 Local Temperature Distribution, 13 Injection Holes, m = 0.5, x/d = 41.9, Vortex w

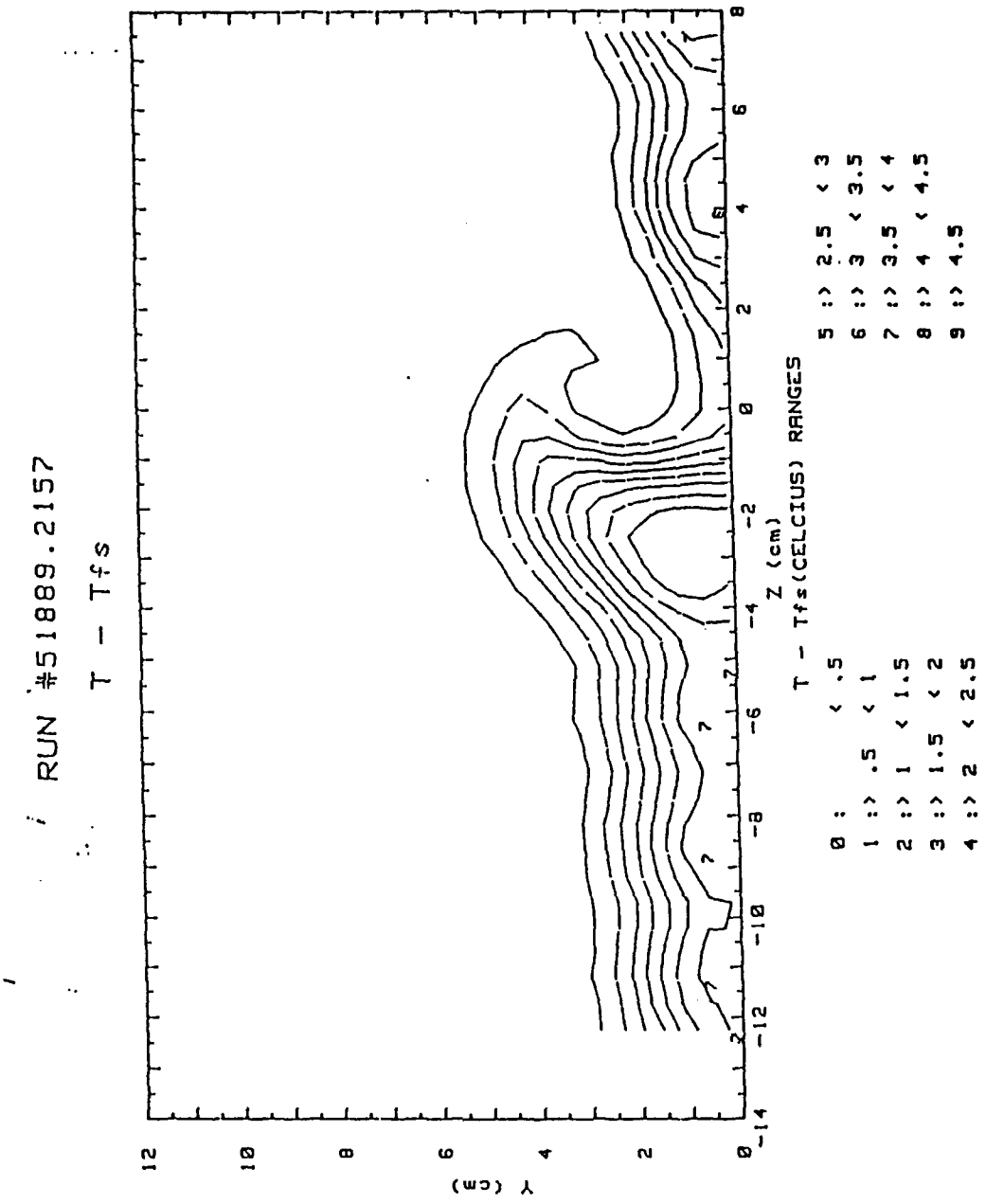

Figure 62 Local Temperature Distribution, 13 Injection Holes, m = 0.5, x/d = 41.9, Vortex x

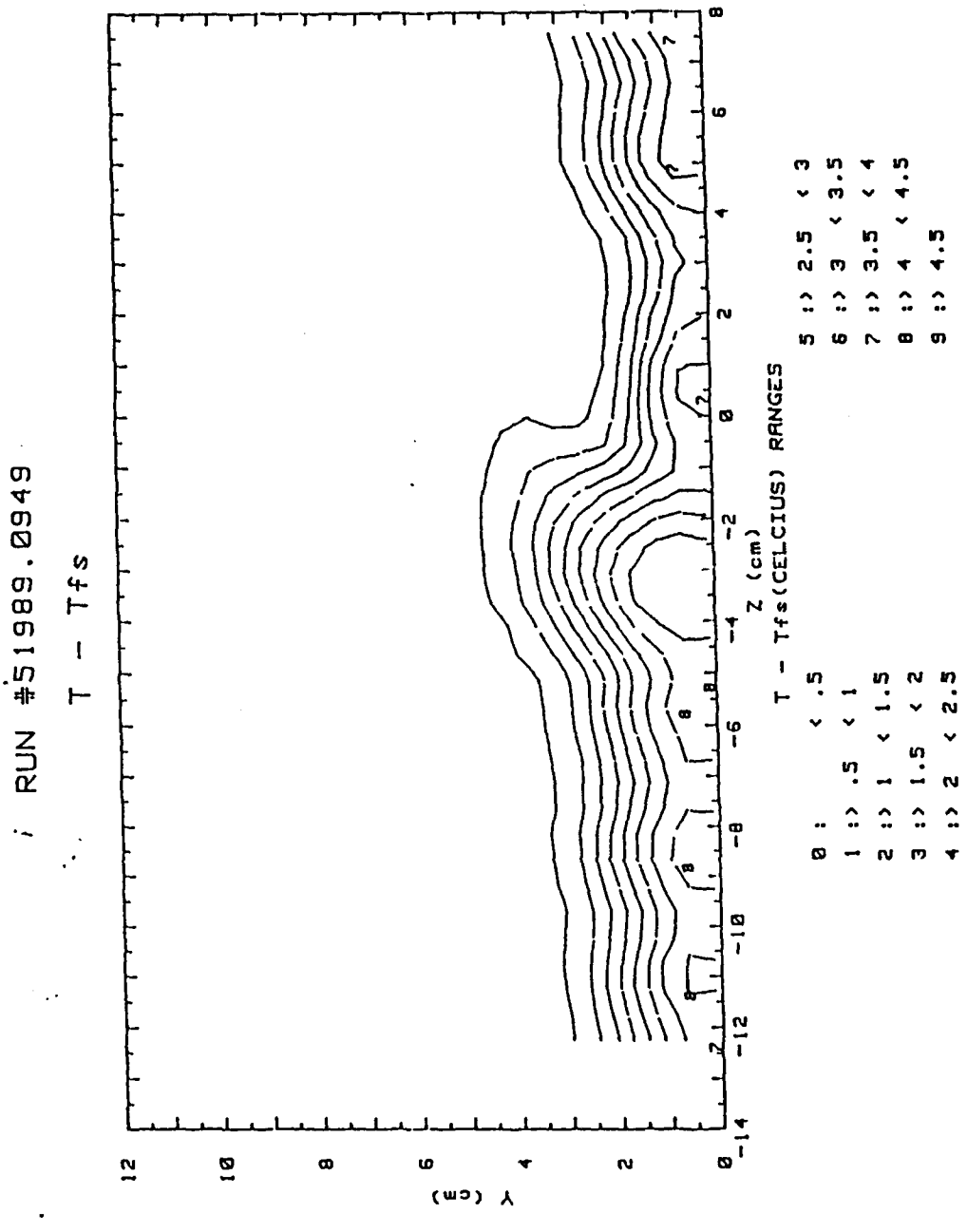

Figure 63 Local Temperature Distribution, 13 Injection Holes, m = 0.5, x/d = 41.9, Vortex y

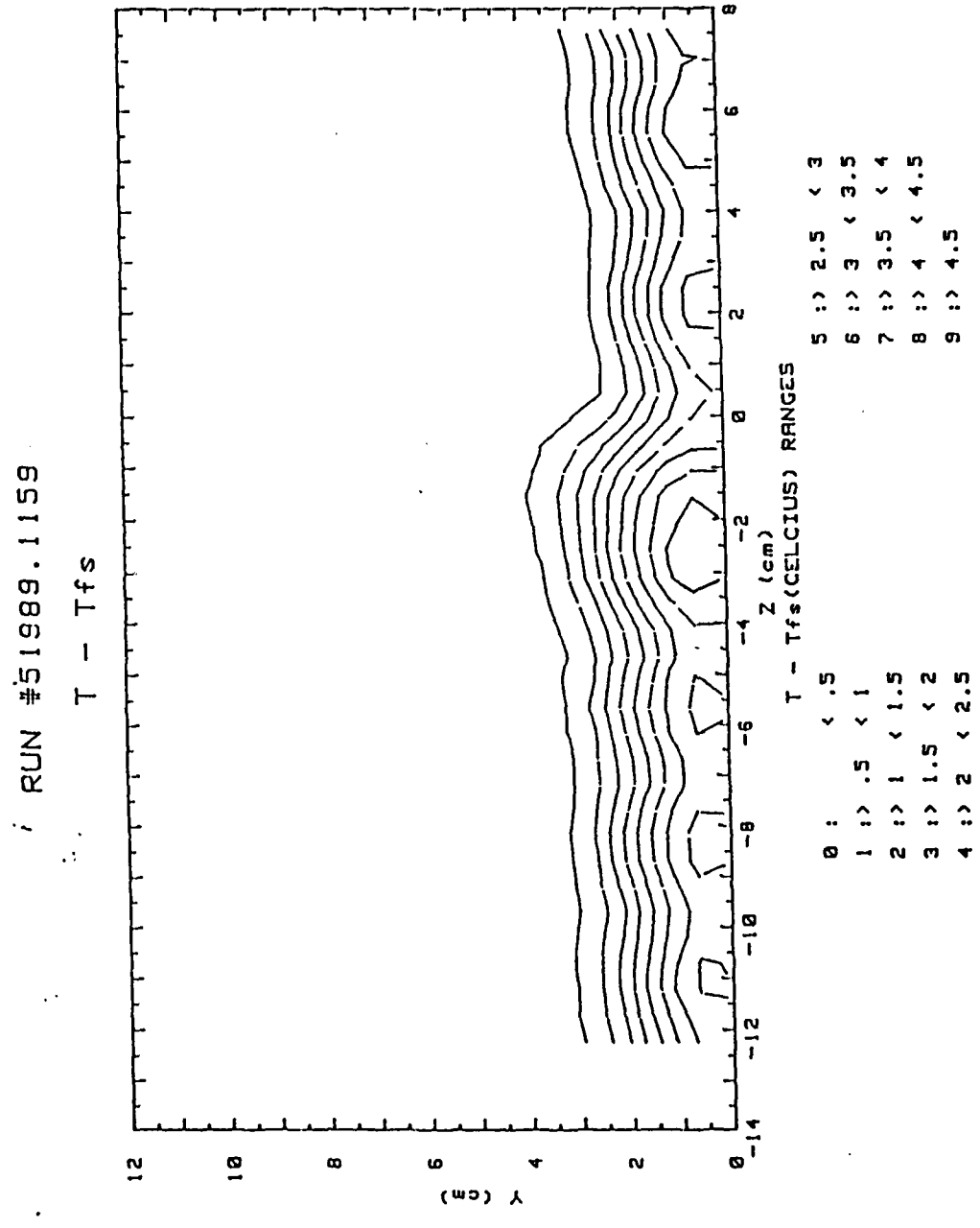

Figure 64 Local Temperature Distribution, 13 Injection Holes, m = 0.5, x/d = 41.9, Vortex z

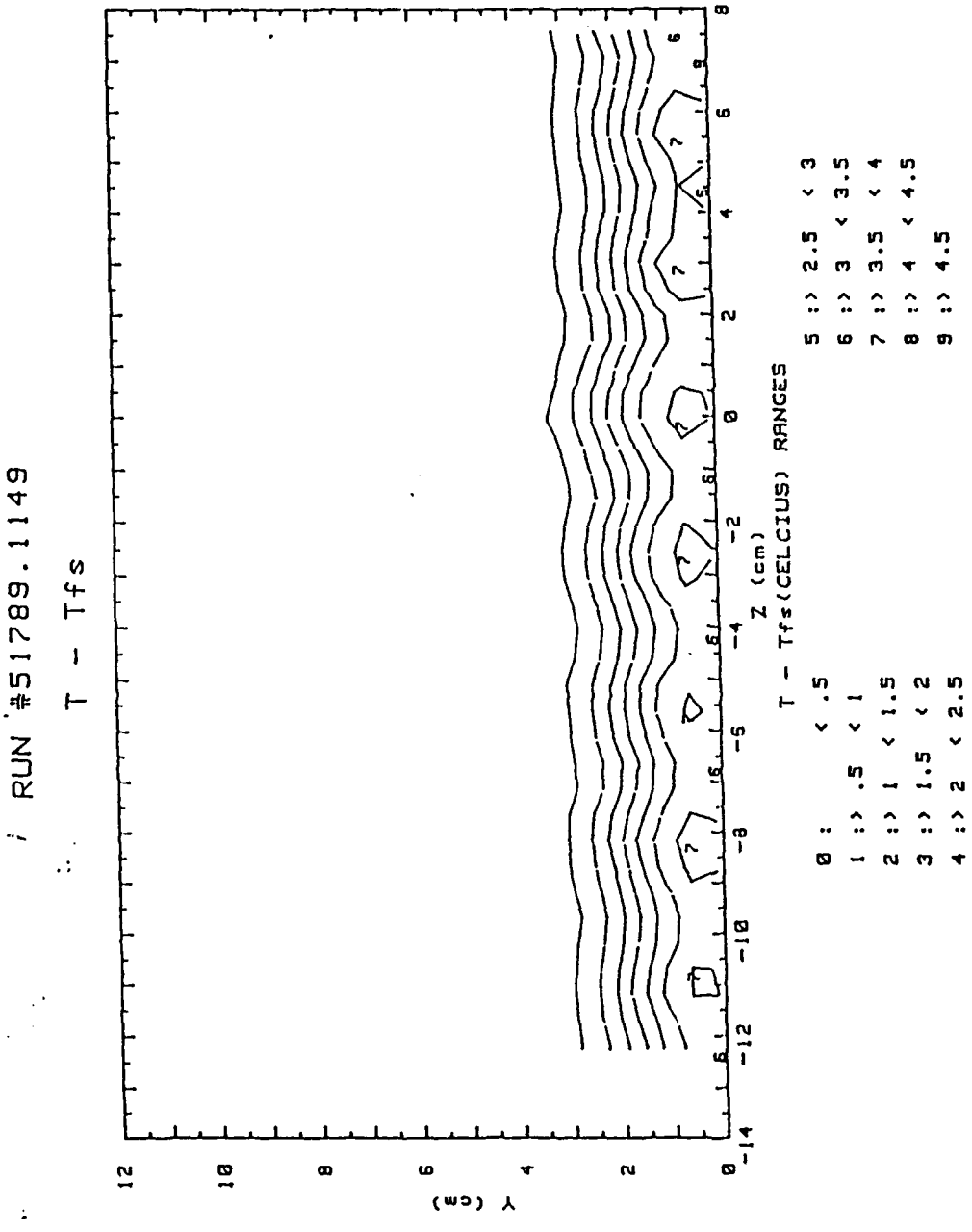

Figure 65 Local Temperature Distribution, 13 Injection Holes, m = 0.5, x/d = 41.9, No Vortex Generator

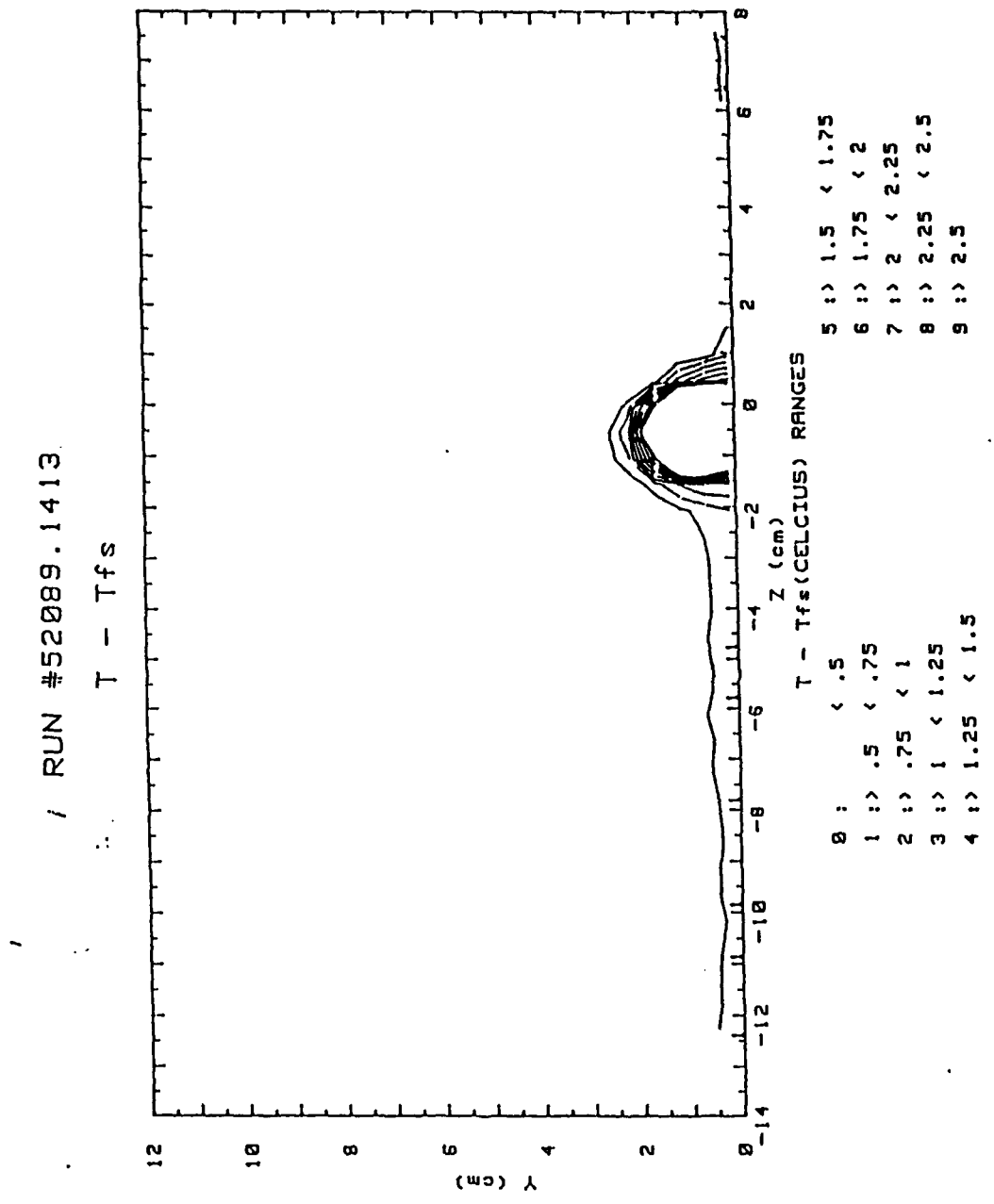

Figure 66 Local Temperature Distribution, A Single Injection Hole, m = 0.5, x/d = 33.6, Vortex w

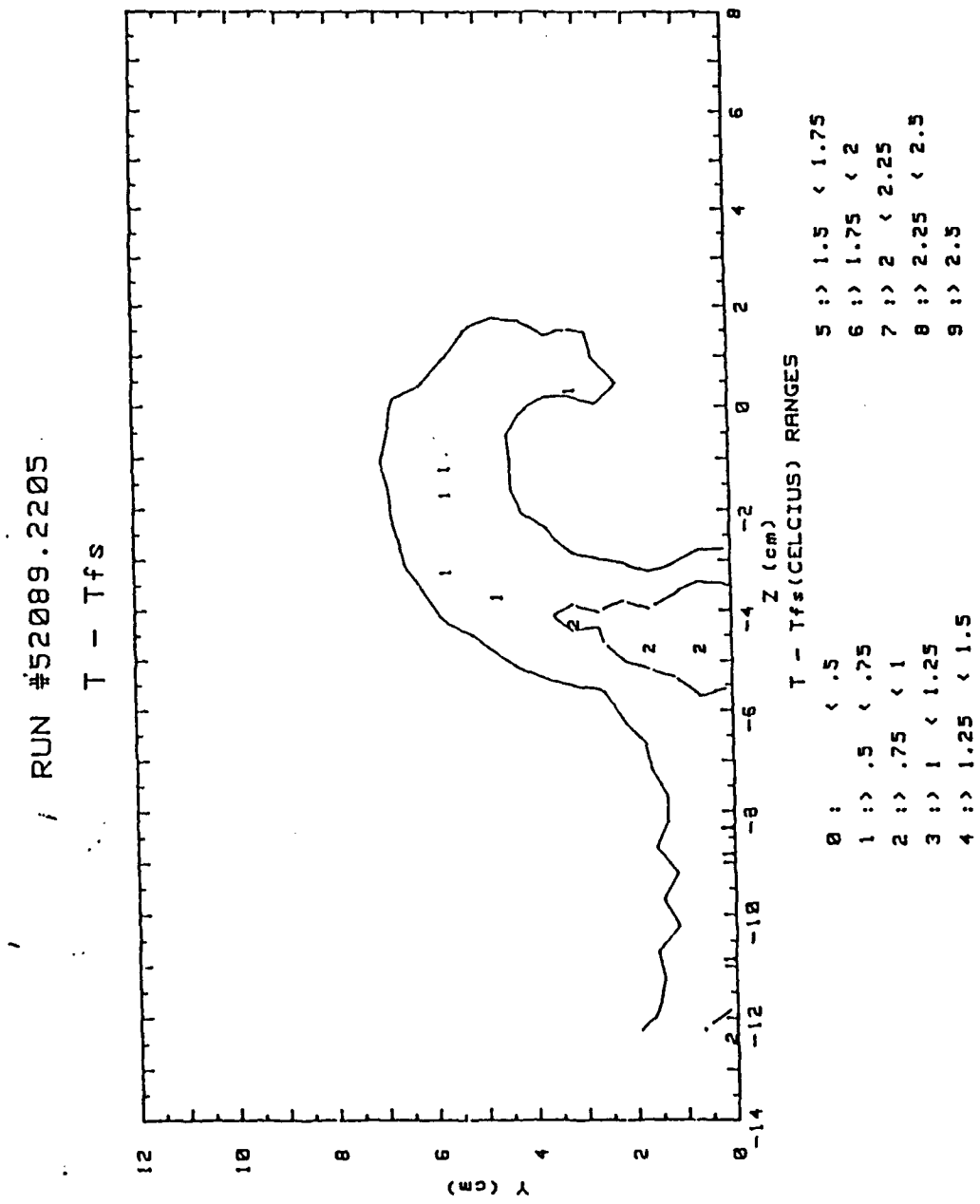

Figure 67 Local Temperature Distribution, A Single Injection Hole, m = 0.5, x/d = 54.6, Vortex w

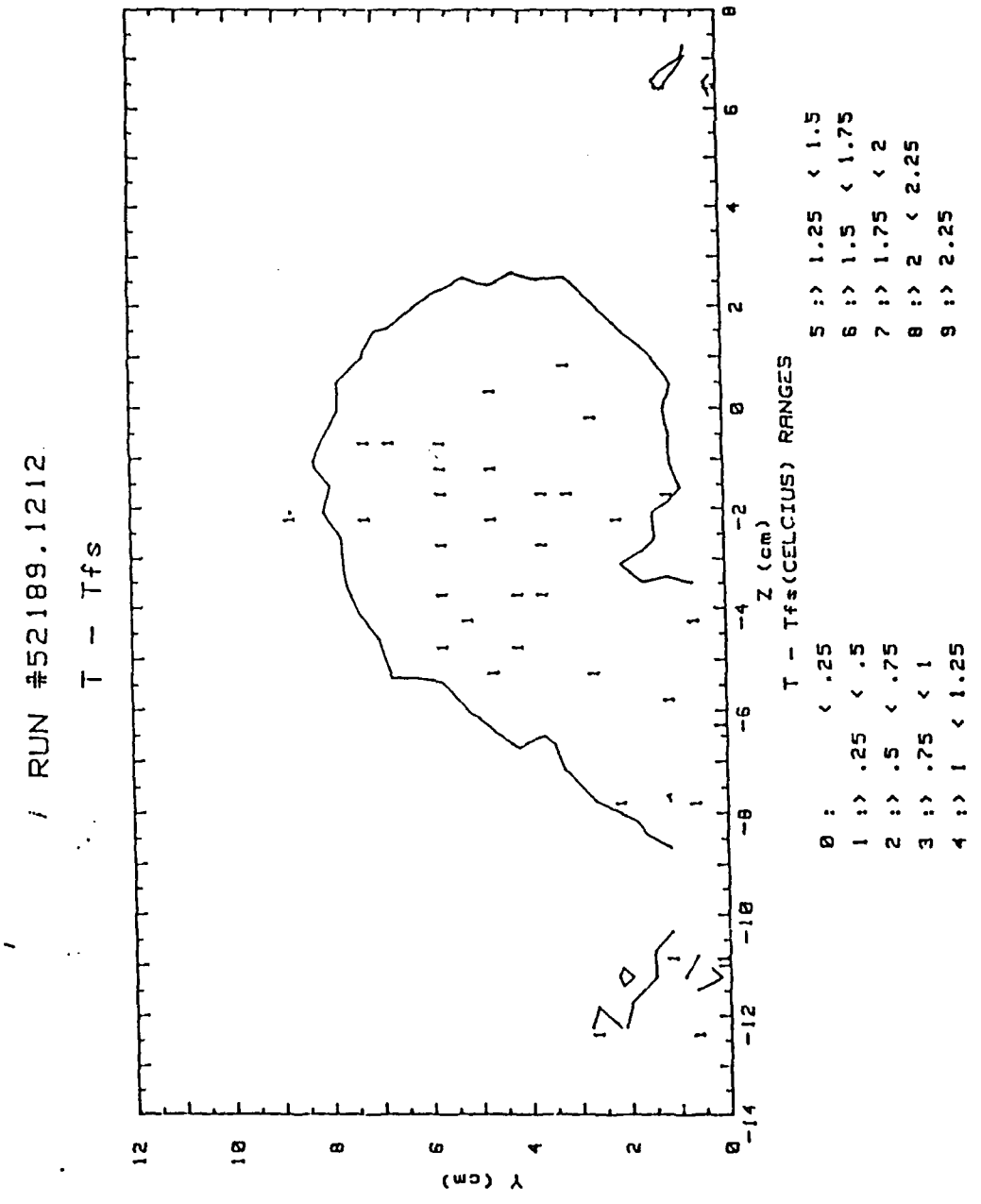

Figure 68 Local Temperature Distribution, A Single Injection Hole, m = 0.5, x/d = 75.6, Vortex w

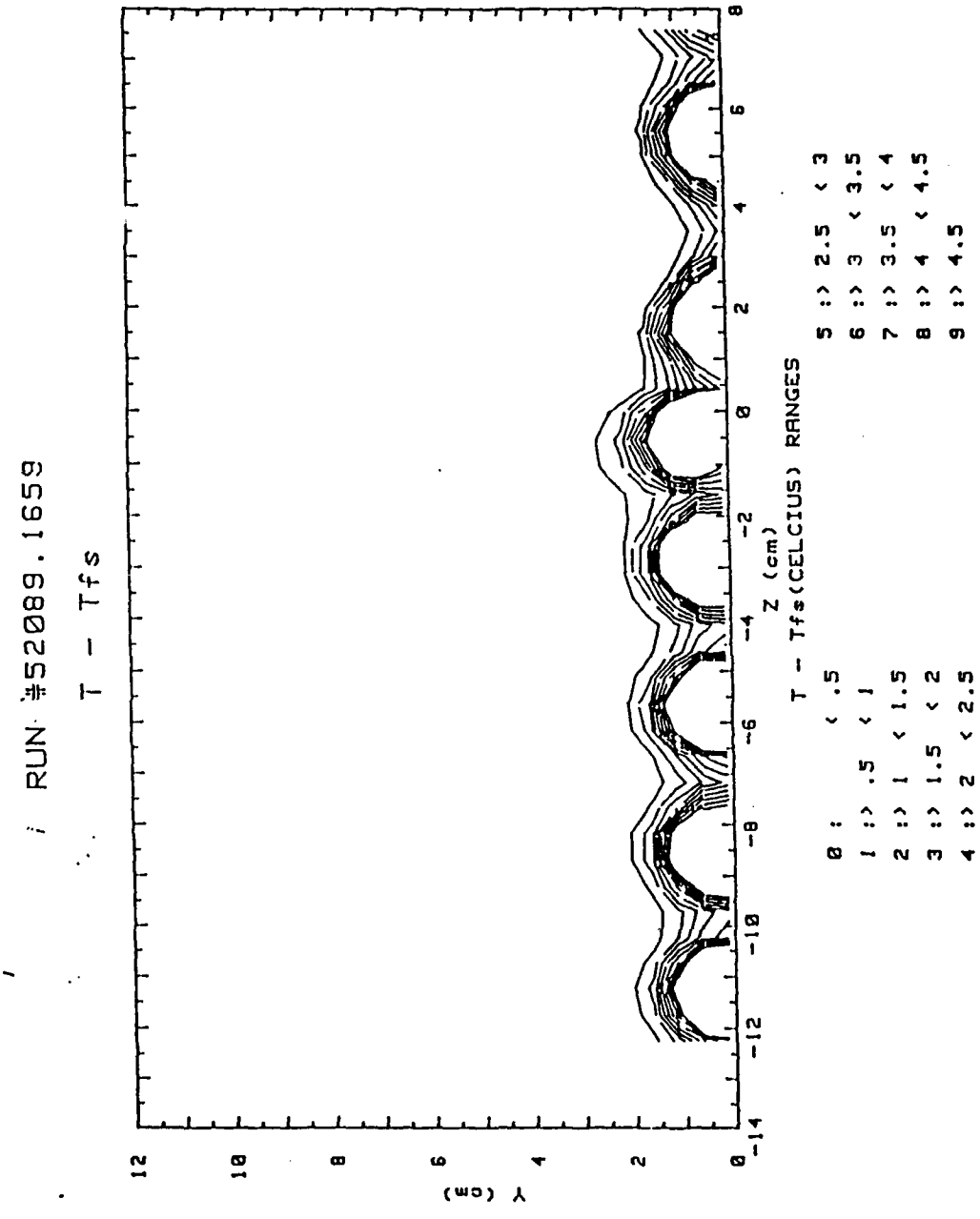

Figure 69 Local Temperature Distribution, 13 Injection Holes, m = 0.5, x/d = 33.6, Vortex w

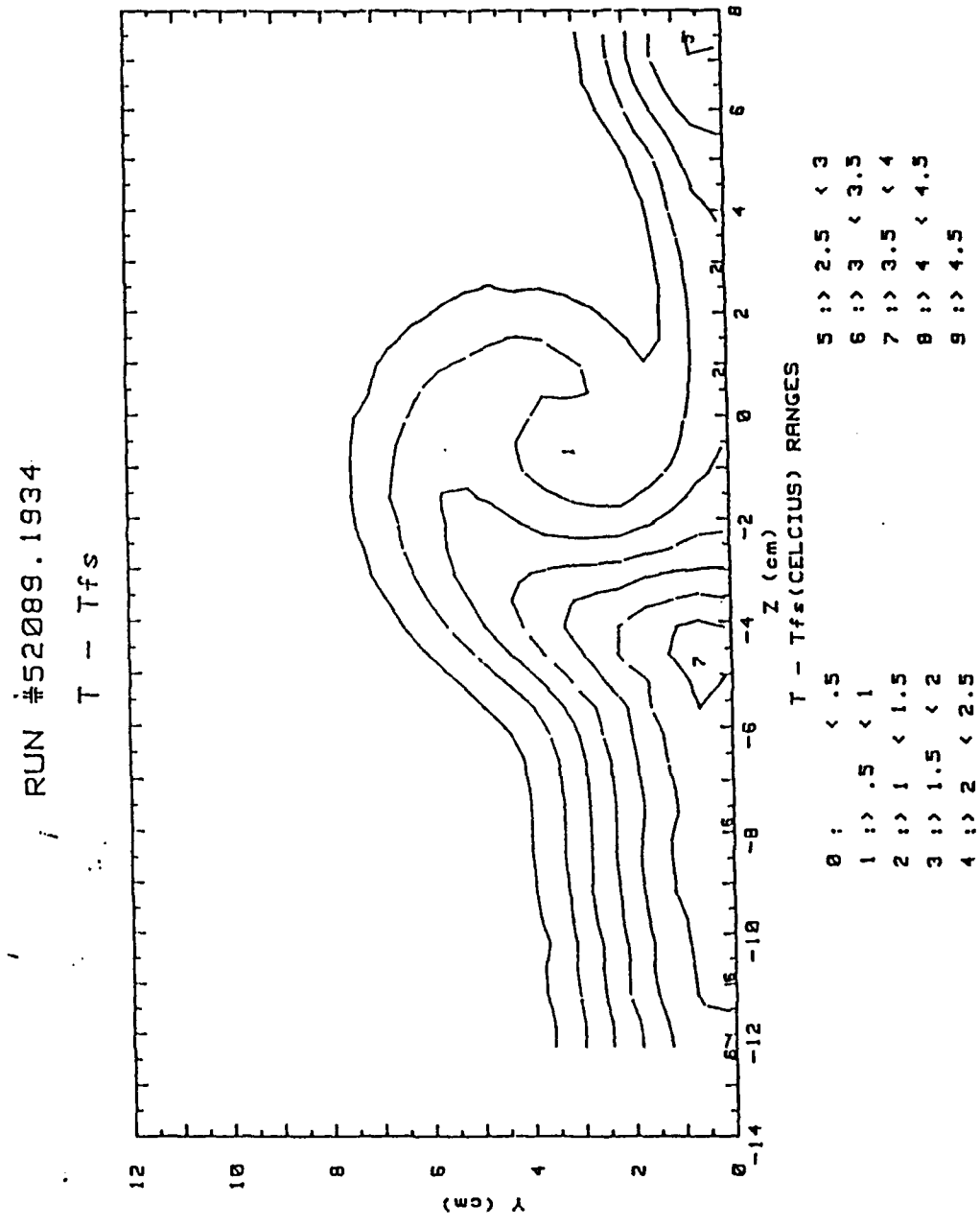

Figure 70 Local Temperature Distribution, 13 Injection Holes, m = 0.5, x/d = 54.6, Vortex w

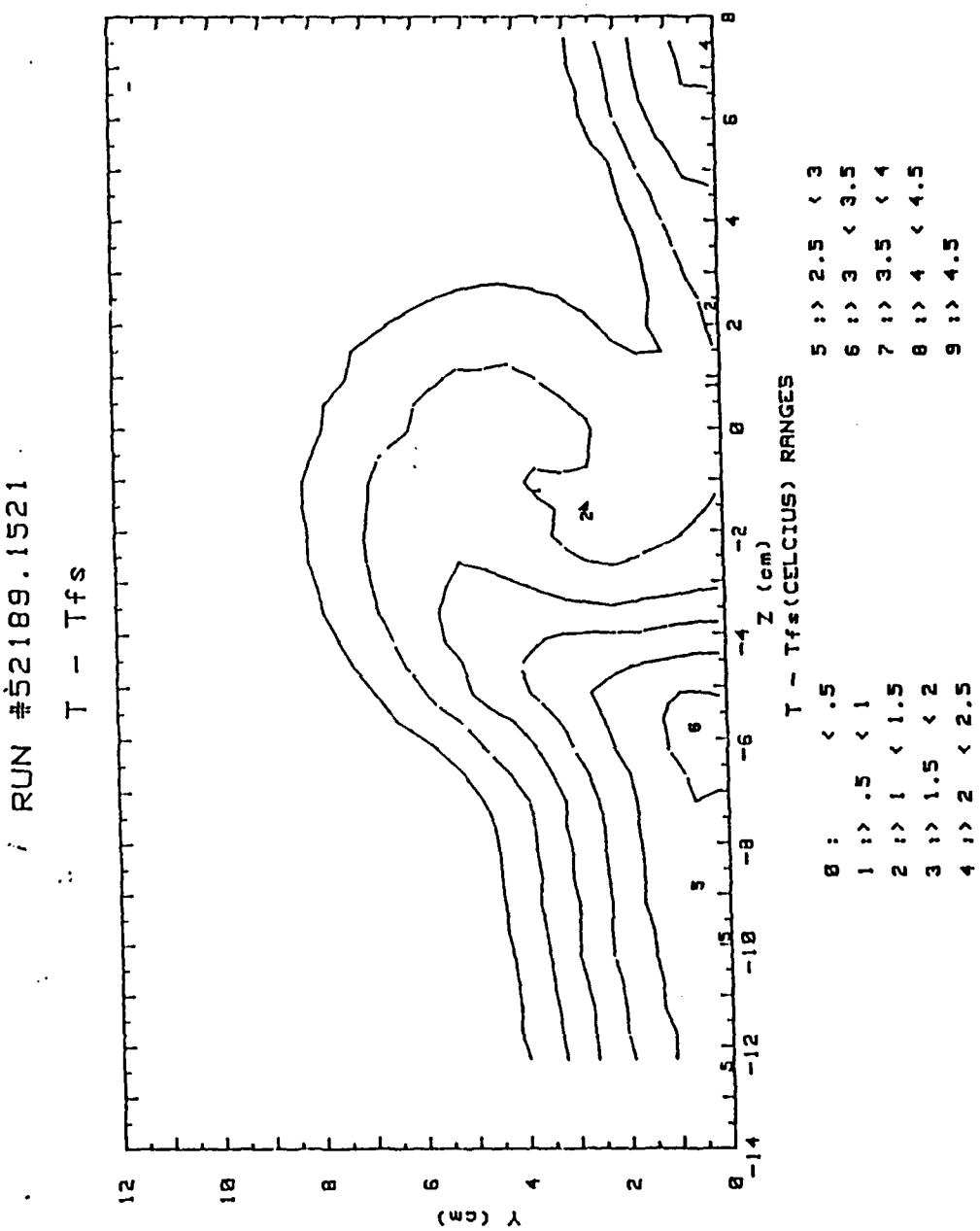

Figure 71 Local Temperature Distribution, 13 Injection Holes, m = 0.5, x/d = 75.6, Vortex w

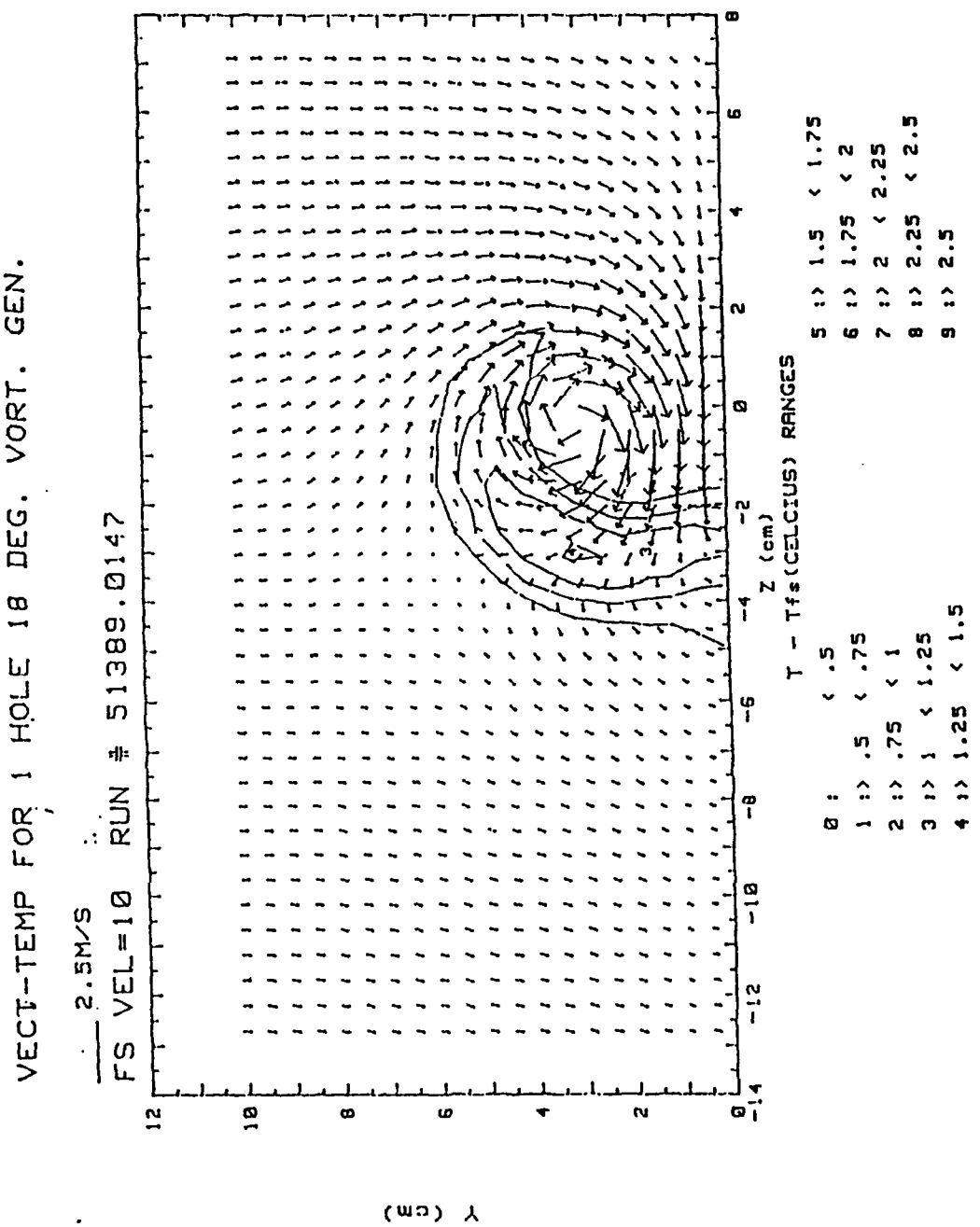

Figure 72 Secondary Flow Vector Field-Local Temperature Distribution, A Single Injection Hole, vortex r
m = 0.5, x/d = 41.9

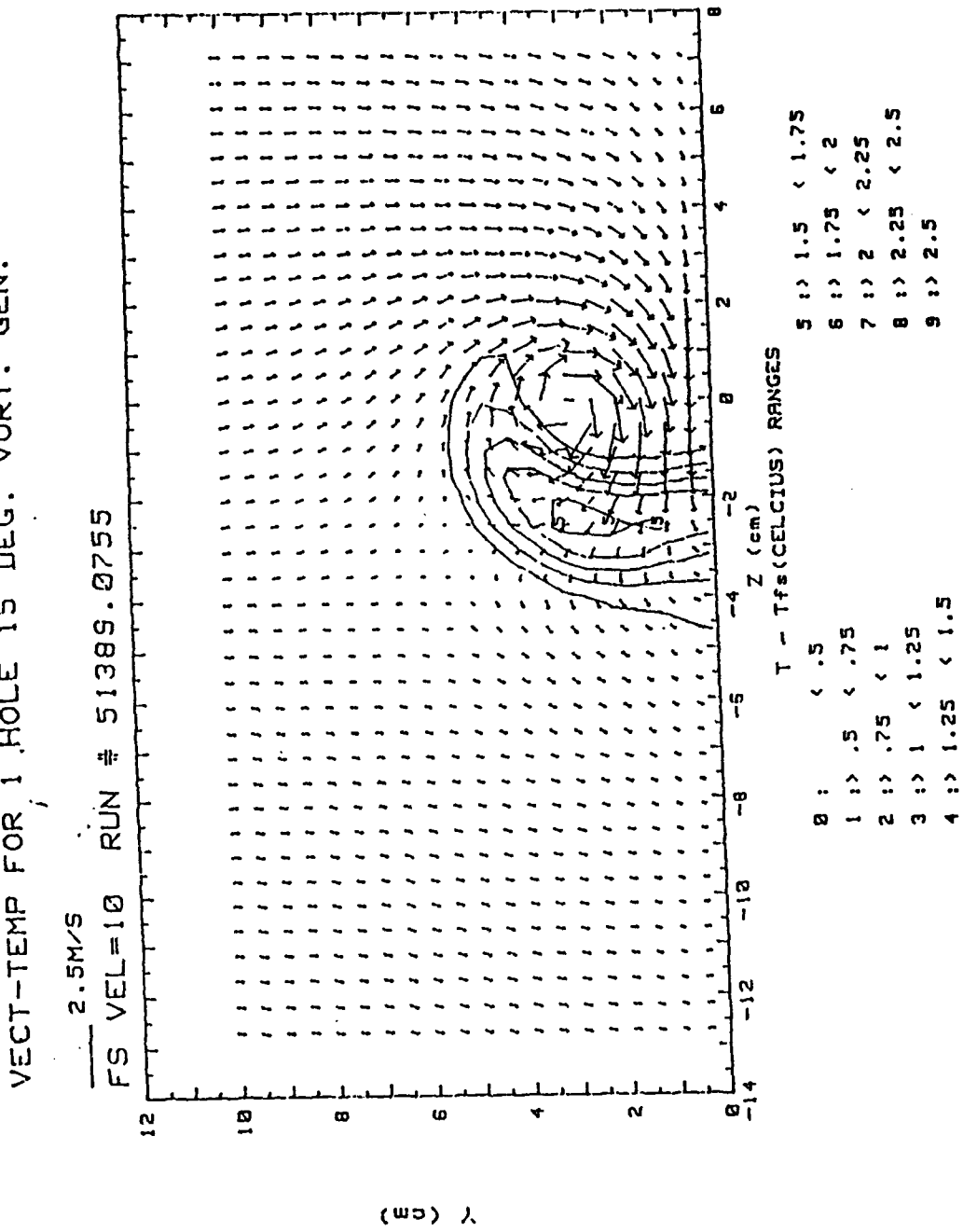

Figure 73 Secondary Flow Vector Field-Local Temperature Distribution, A Single Injection Hole, vortex w
m = 0.5, x/d = 41.9

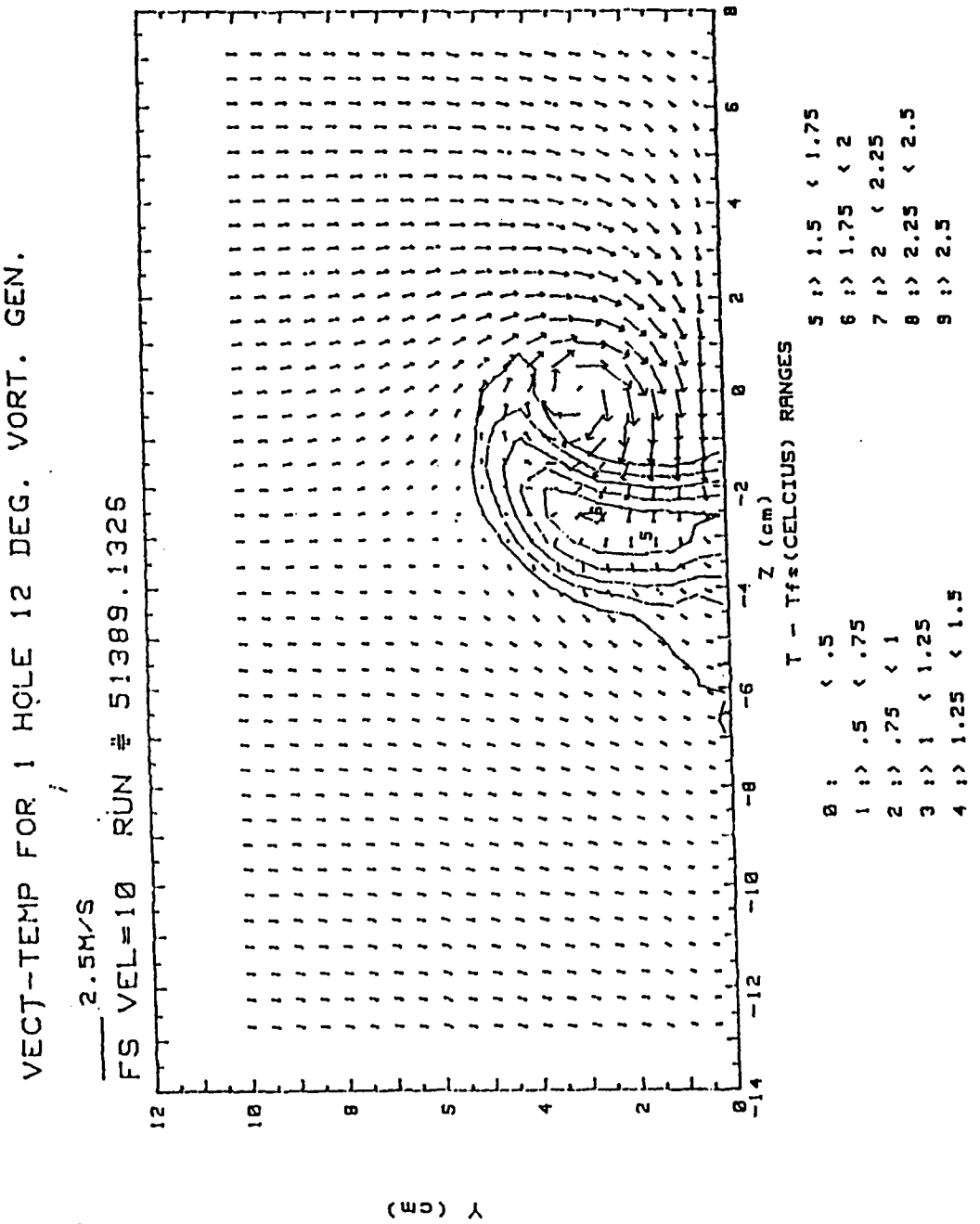

Figure 74 Secondary Flow Vector Field-Local Temperature Distribution, A Single Injection Hole, vortex *x*, m = 0.5, x/d = 41.9

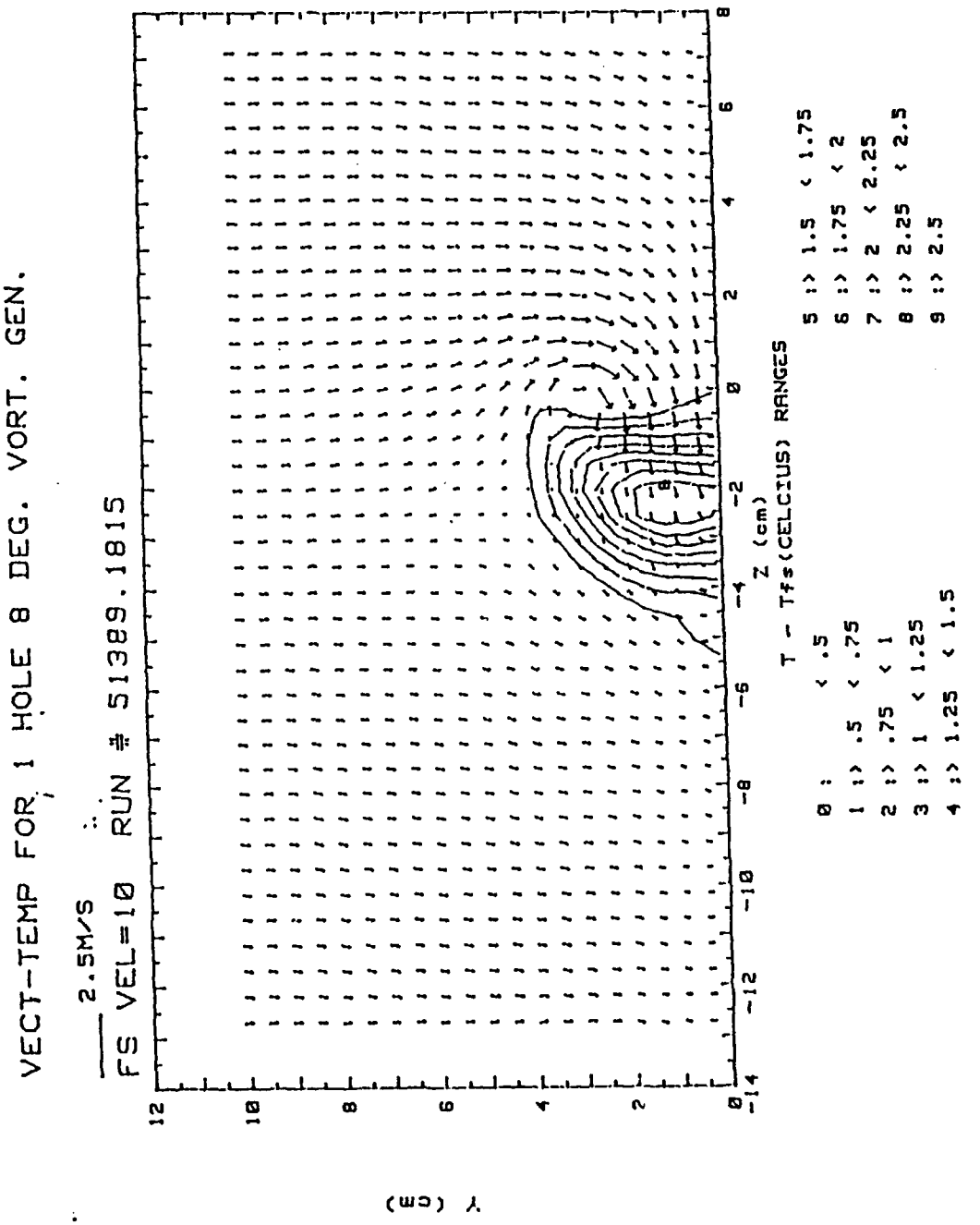

Figure 75 Secondary Flow Vector Field-Local Temperature Distribution, A Single Injection Hole, vortex y, m = 0.5, x/d = 41.9

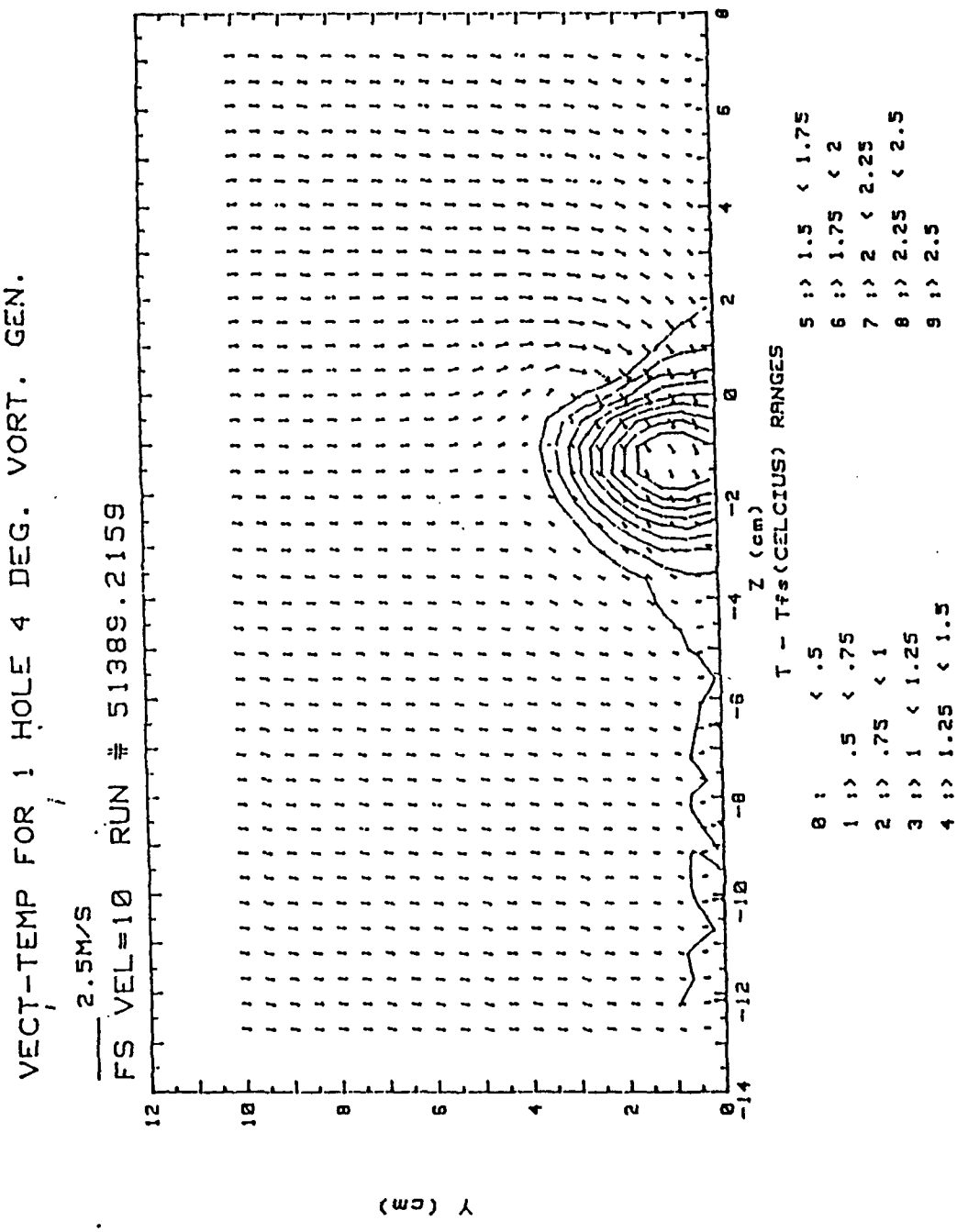

Figure 76 Secondary Flow Vector Field-Local Temperature Distribution, A Single Injection Hole, vortex z, m = 0.5, x/d = 41.9

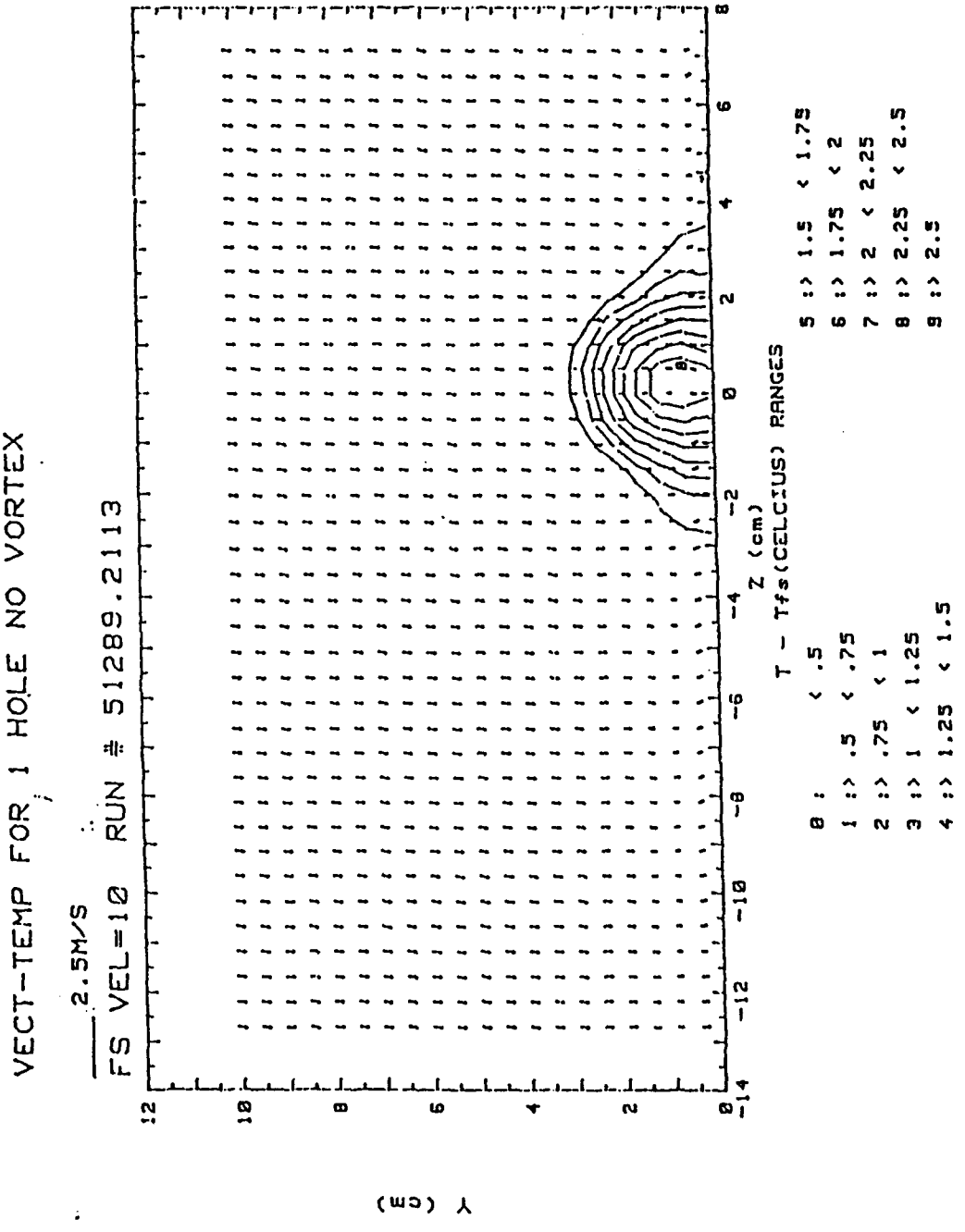

Figure 77 Secondary Flow Vector Field-Local Temperature Distribution, A Single Injection Hole, No Vortex Generator, m = 0.5, x/d = 41.9

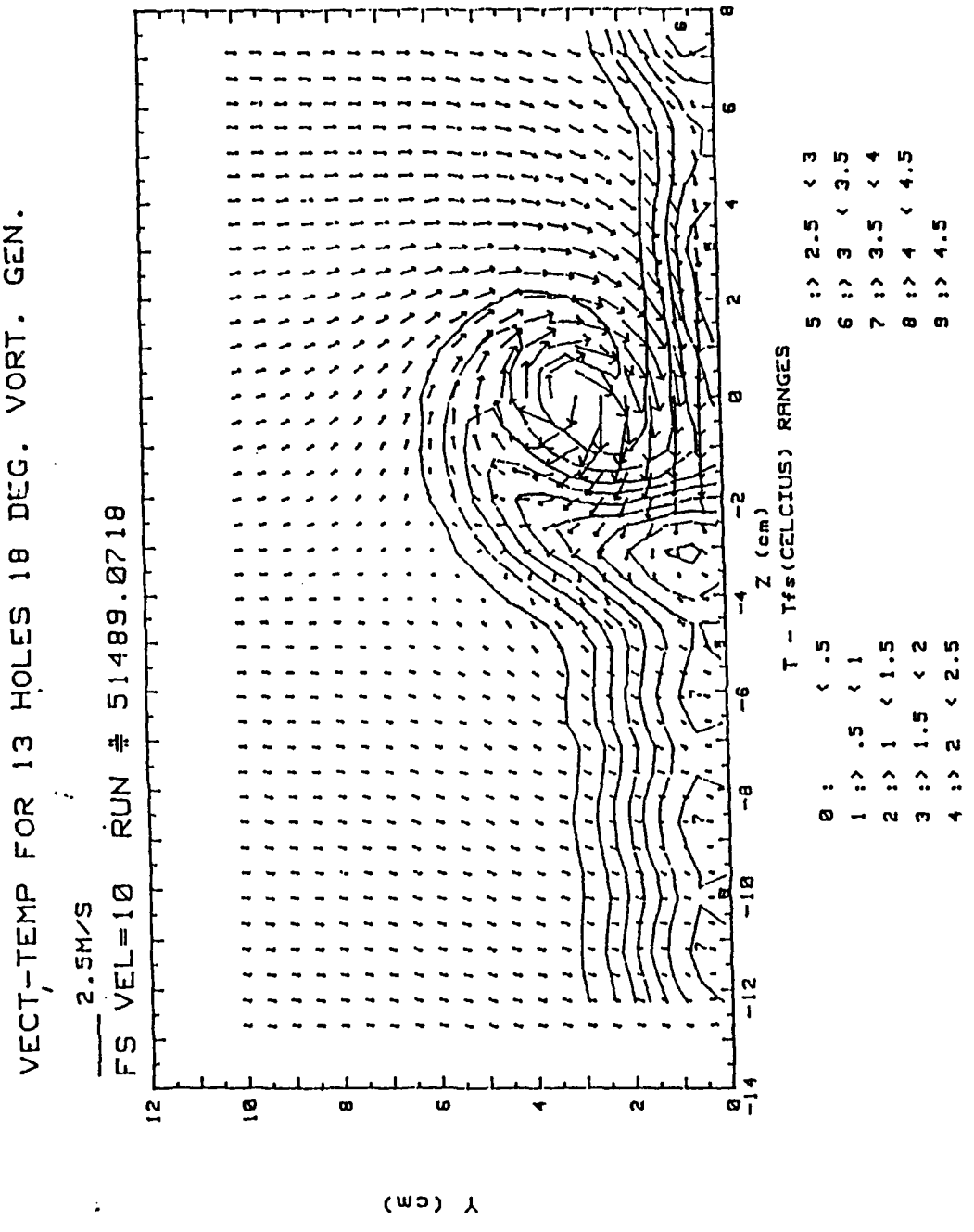

Figure 78 Secondary Flow Vector Field-Local Temperature Distribution, 13 Injection Holes, Vortex r, m = 0.5, x/d = 41.9

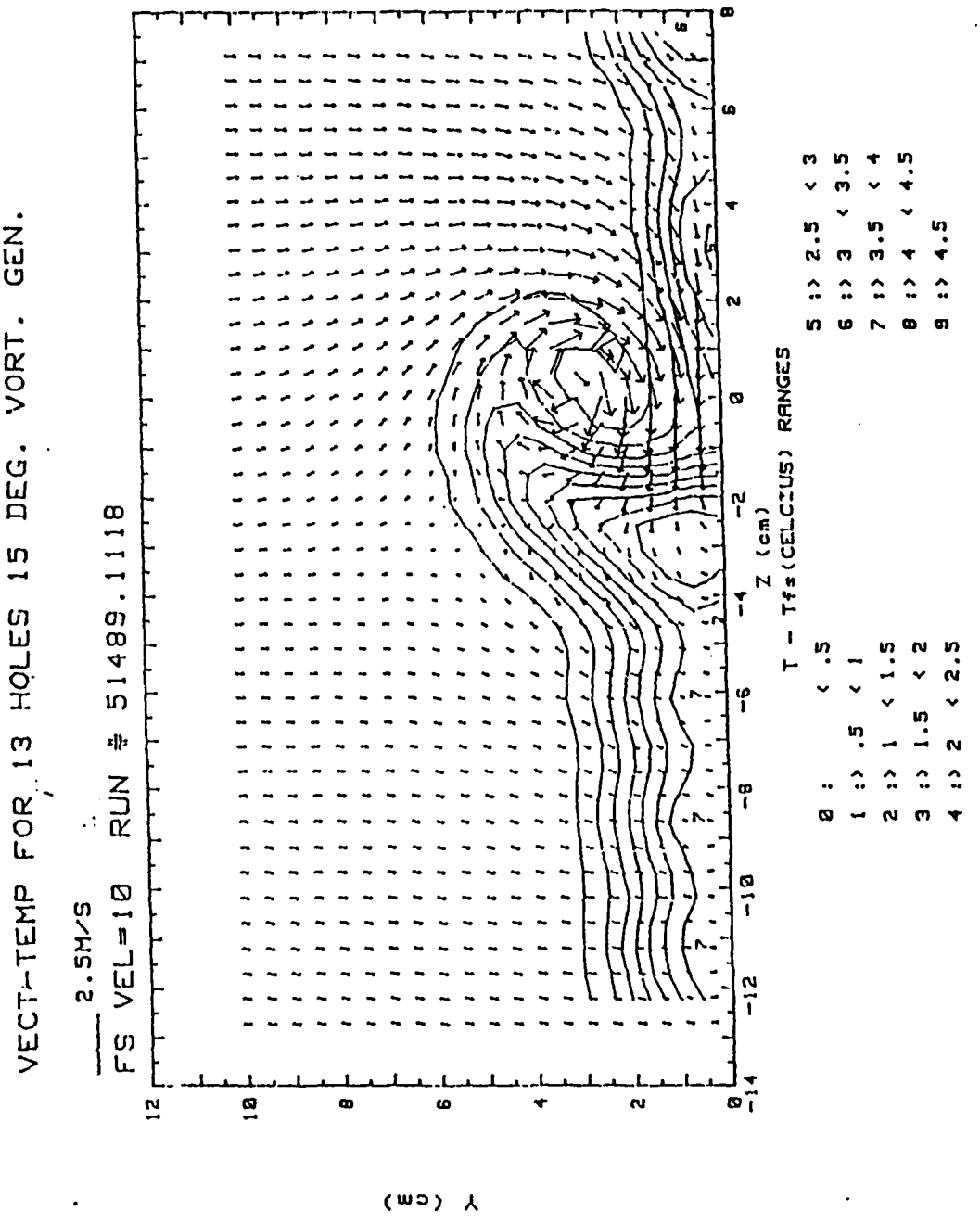

Figure 79 Secondary Flow Vector Field-Local Temperature Distribution, 13 Injection Holes, Vortex w, m = 0.5, x/d = 41.9

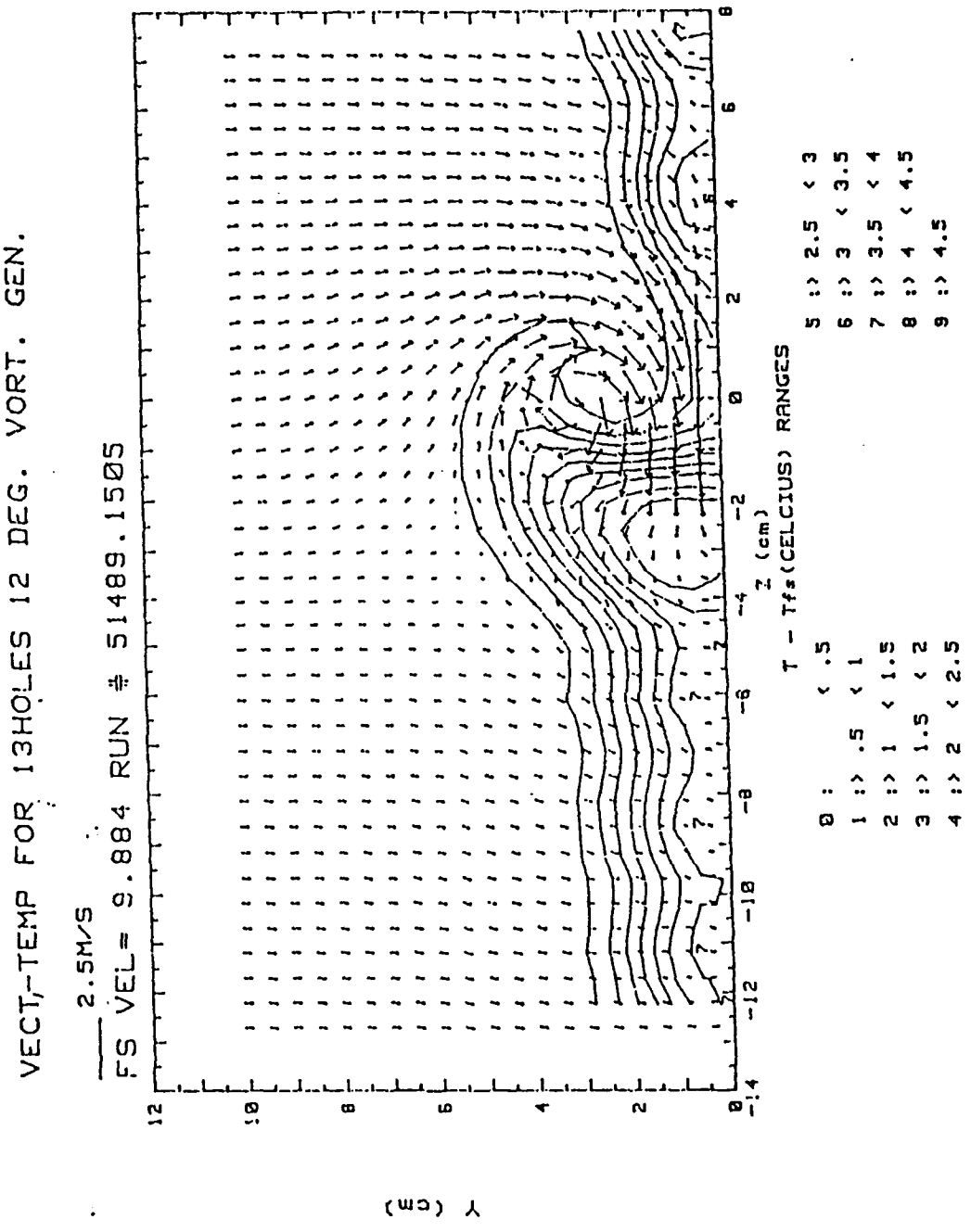

Figure 80 Secondary Flow Vector Field-Local Temperature Distribution, 13 Injection Holes, Vortex x, m = 0.5, x/d = 41.9

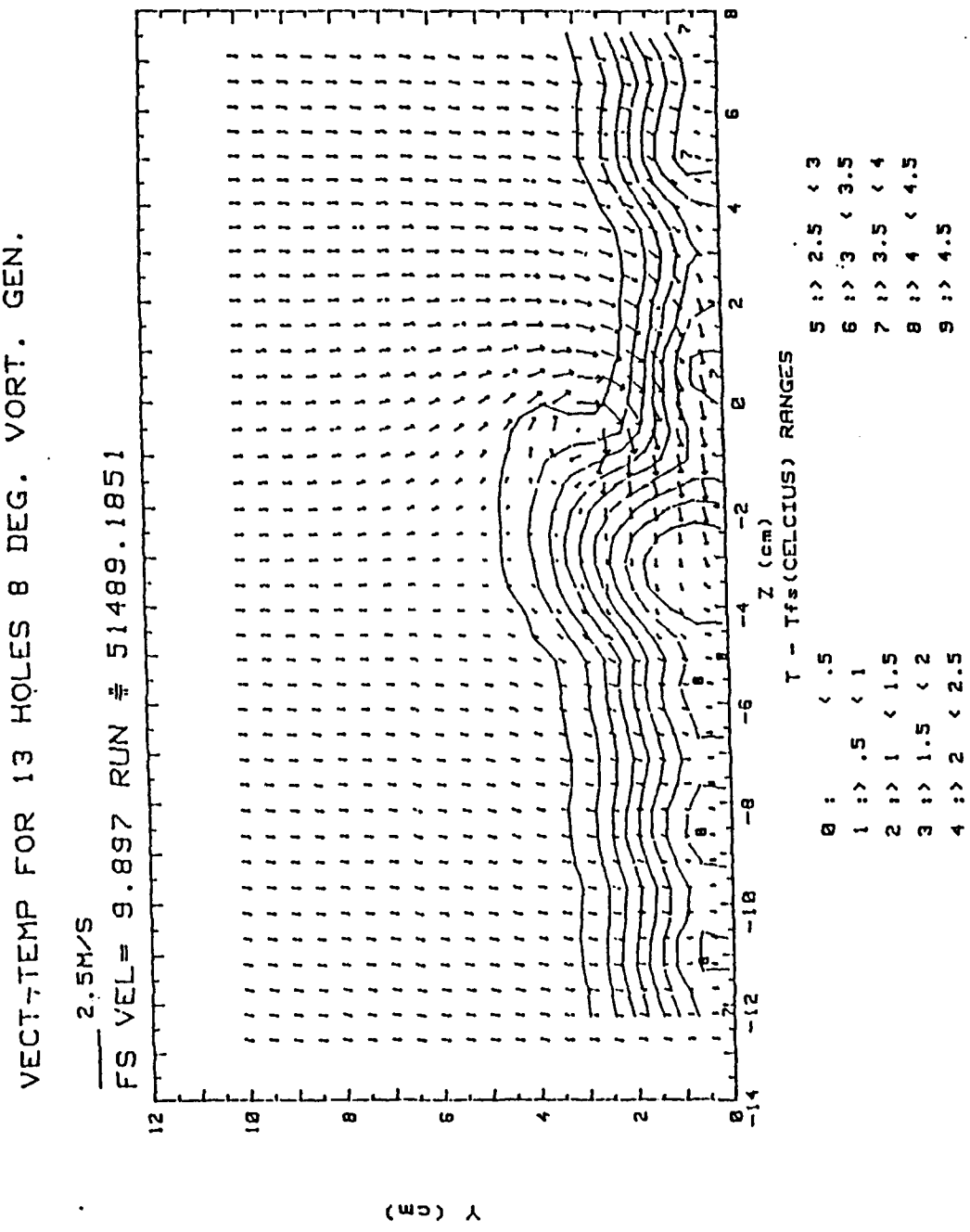

Figure 81 Secondary Flow Vector Field-Local Temperature Distribution, 13 Injection Holes, Vortex y, m = 0.5, x/d = 41.9

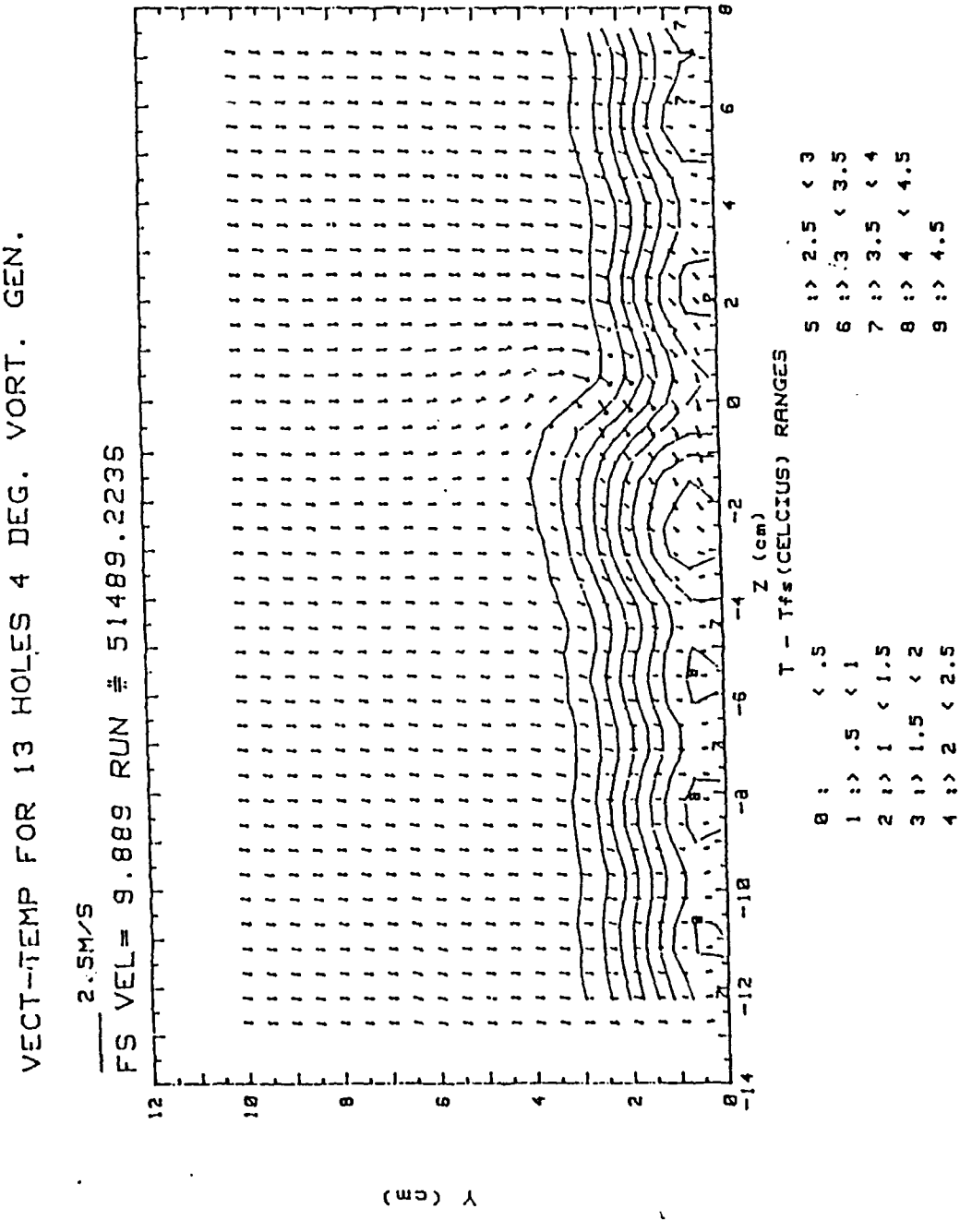

Figure 82 Secondary Flow Vector Field-Local Temperature Distribution, 13 Injection Holes, Vortex z, m = 0.5, x/d = 41.9

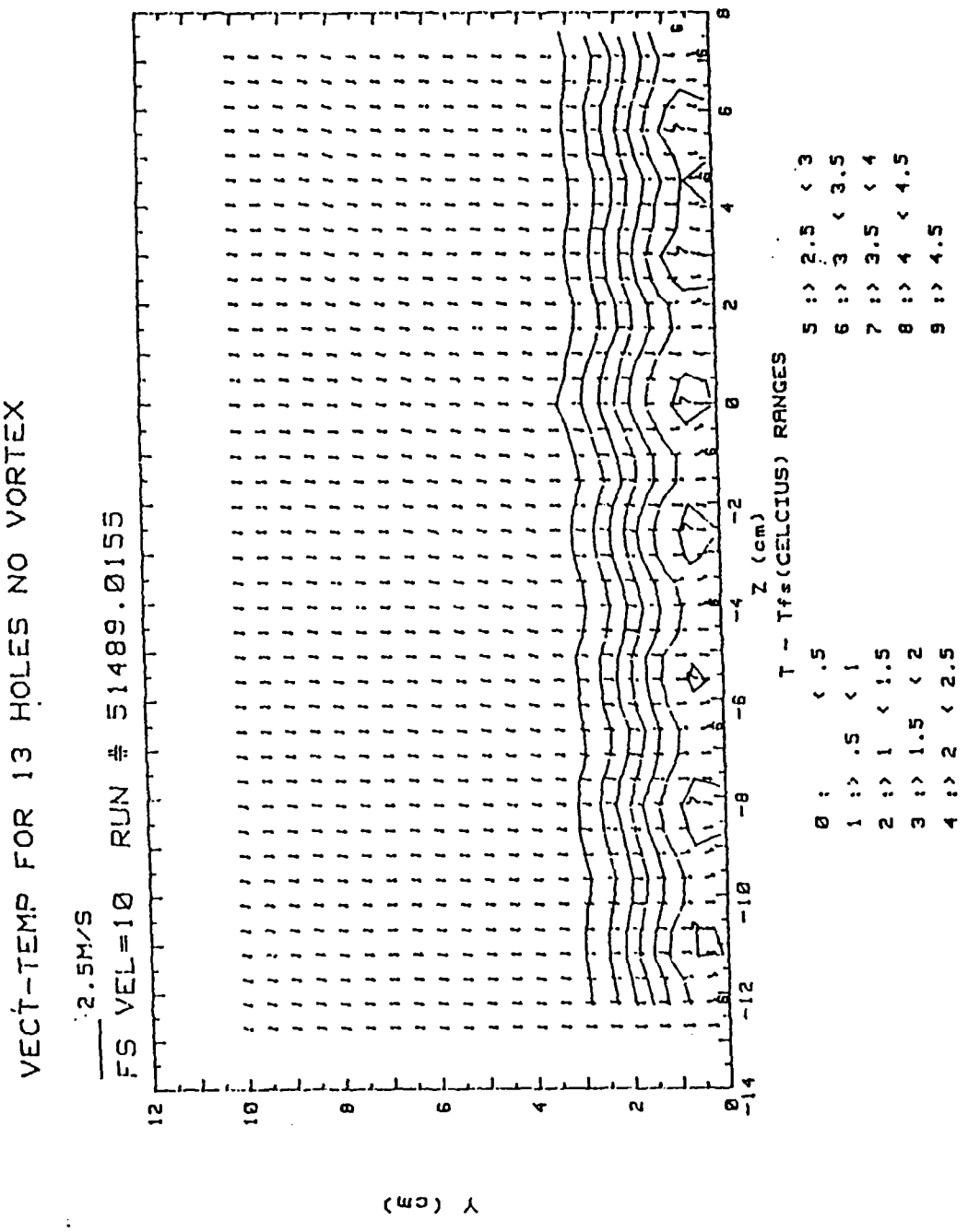

Figure 83 Secondary Flow Vector Field-Local Temperature Distribution, 13 Injection Holes, No Vortex Generator, m = 0.5, x/d = 41.9

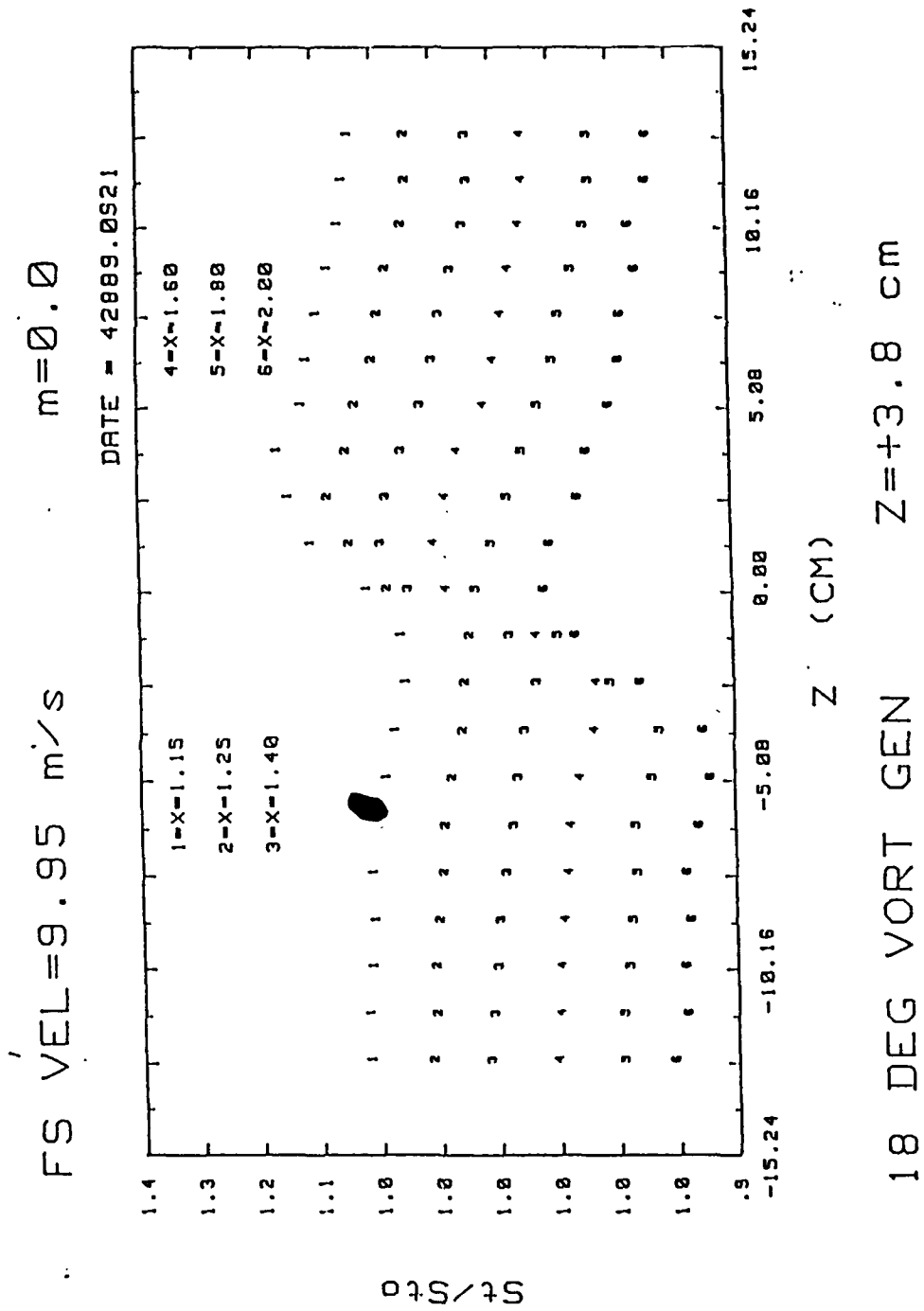

Figure 84 Stanton Number Development with Streamwise Distance, No Film-Cooling, Vortex r

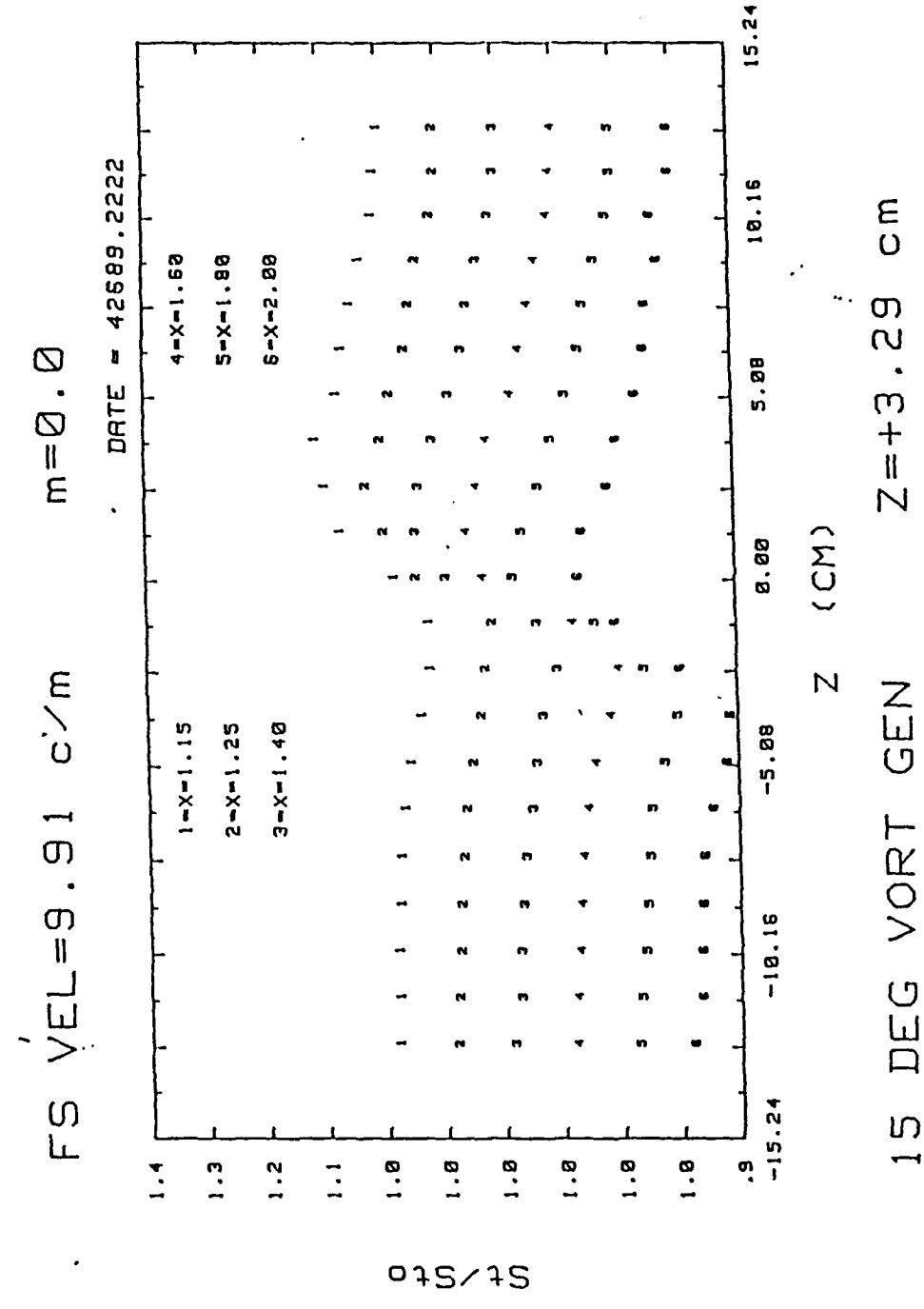

Figure 85 Stanton Number Development with Streamwise Distance, No Film-Cooling, Vortex w

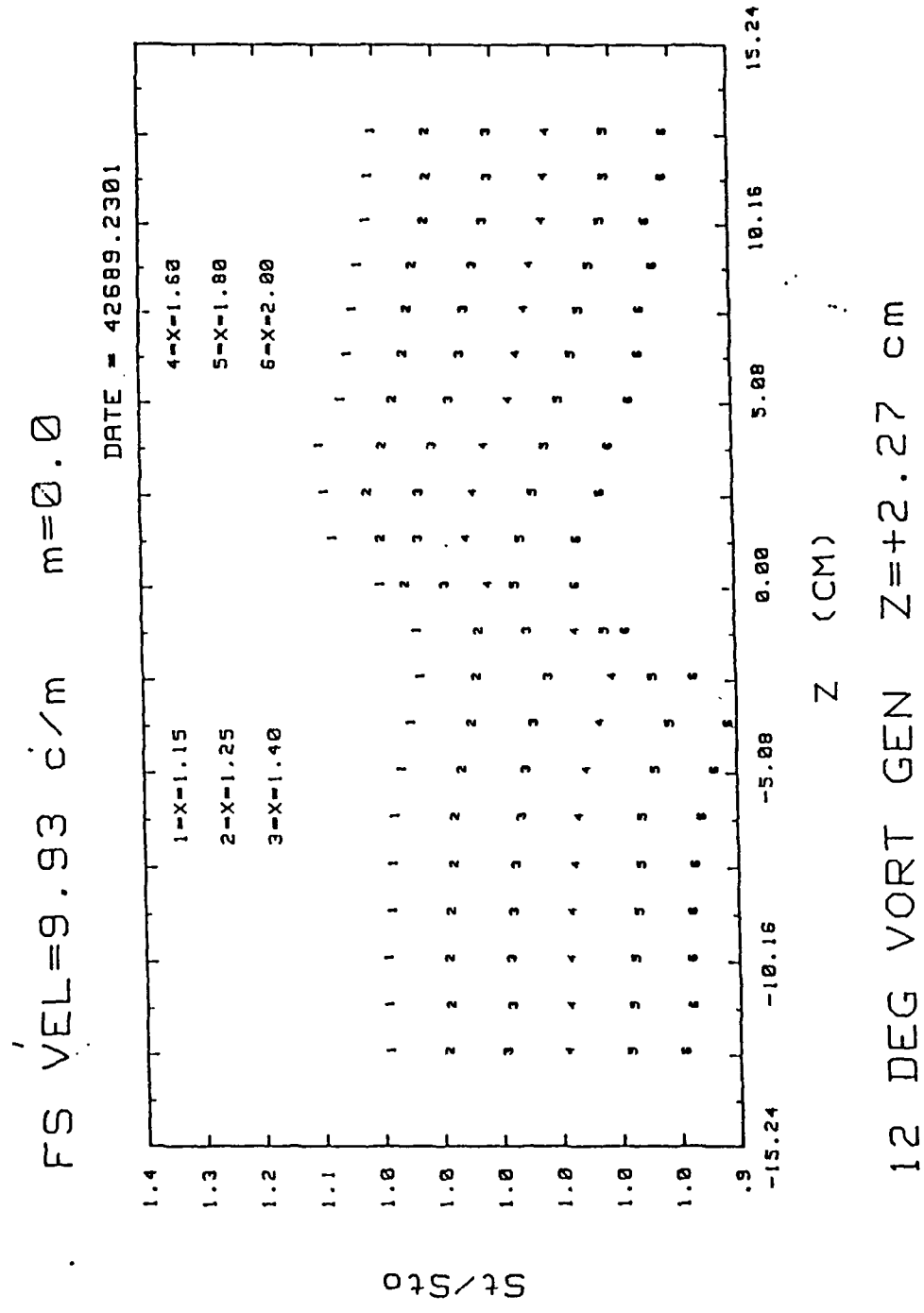

Figure 86 Stanton Number Development with Streamwise Distance, No Film-Cooling, Vortex x

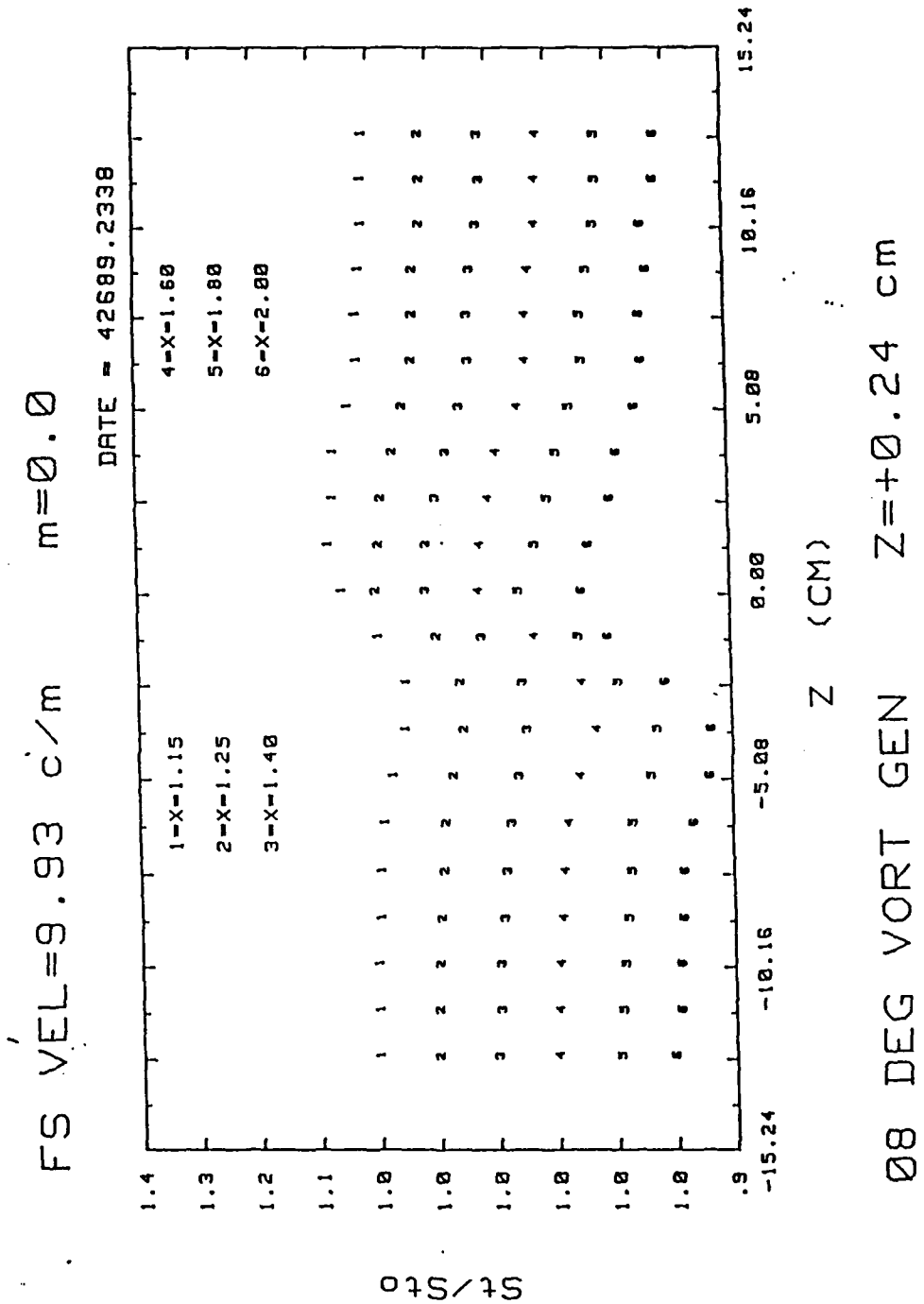

Figure 87 Stanton Number Development with Streamwise Distance, No Film-Cooling, Vortex y

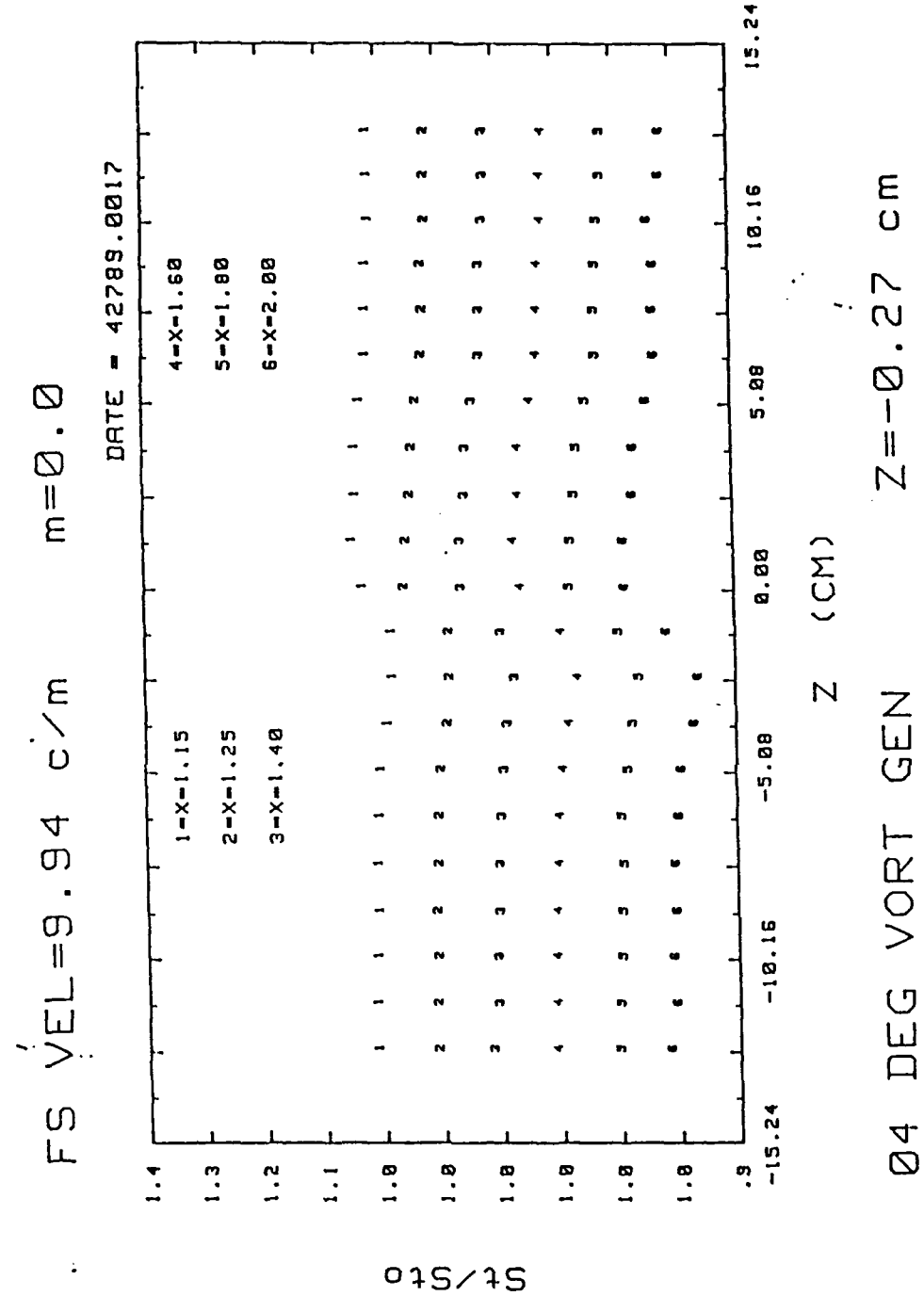

Figure 88 Stanton Number Development with Streamwise Distance, No Film-Cooling, Vortex z

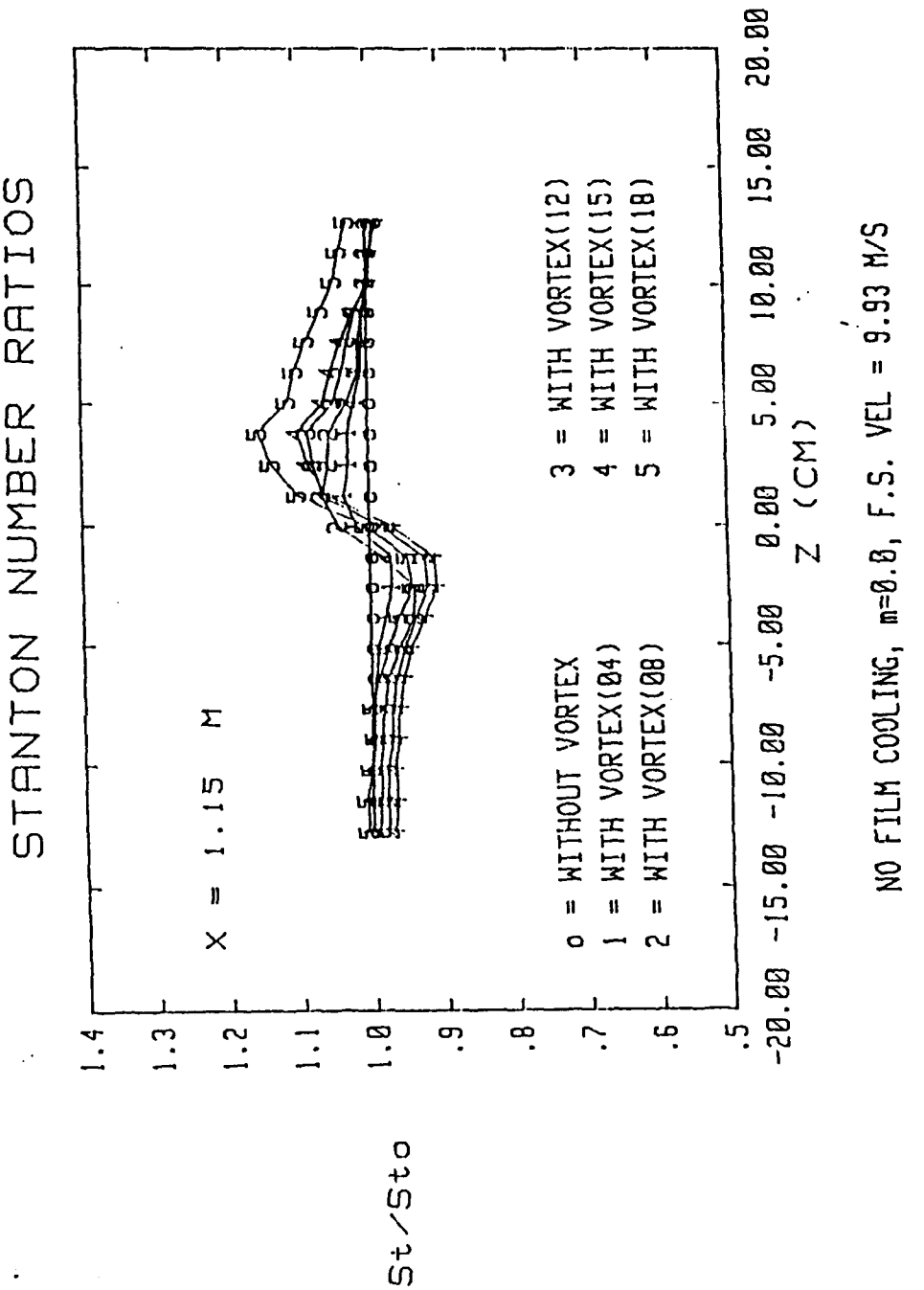

Figure 89 Spanwise Variation of St/Sto Ratios, No Film-Cooling, X = 1.15 m

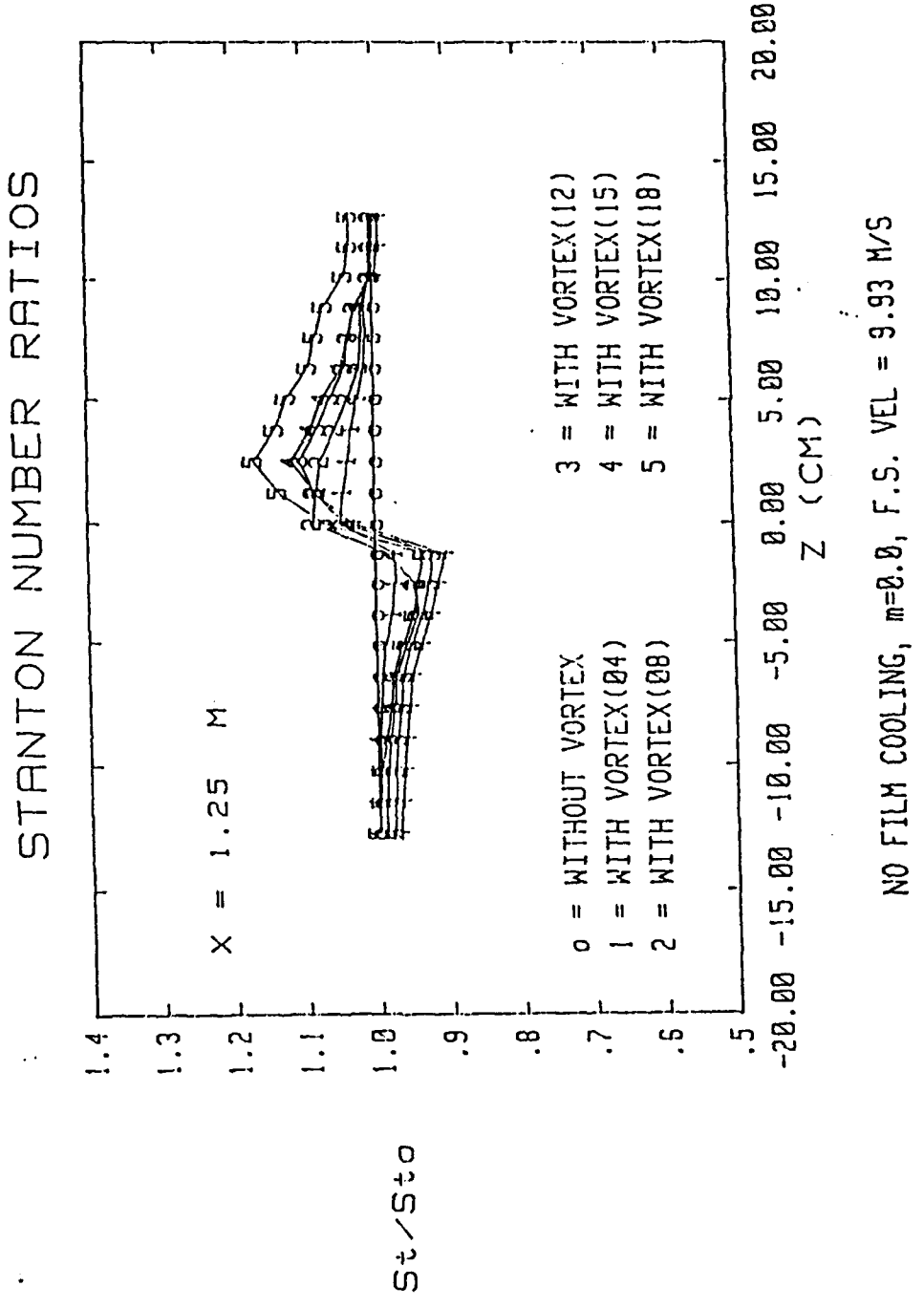

Figure 90 Spanwise Variation of St/Sto Ratios, No Film-Cooling, X = 1.25 m

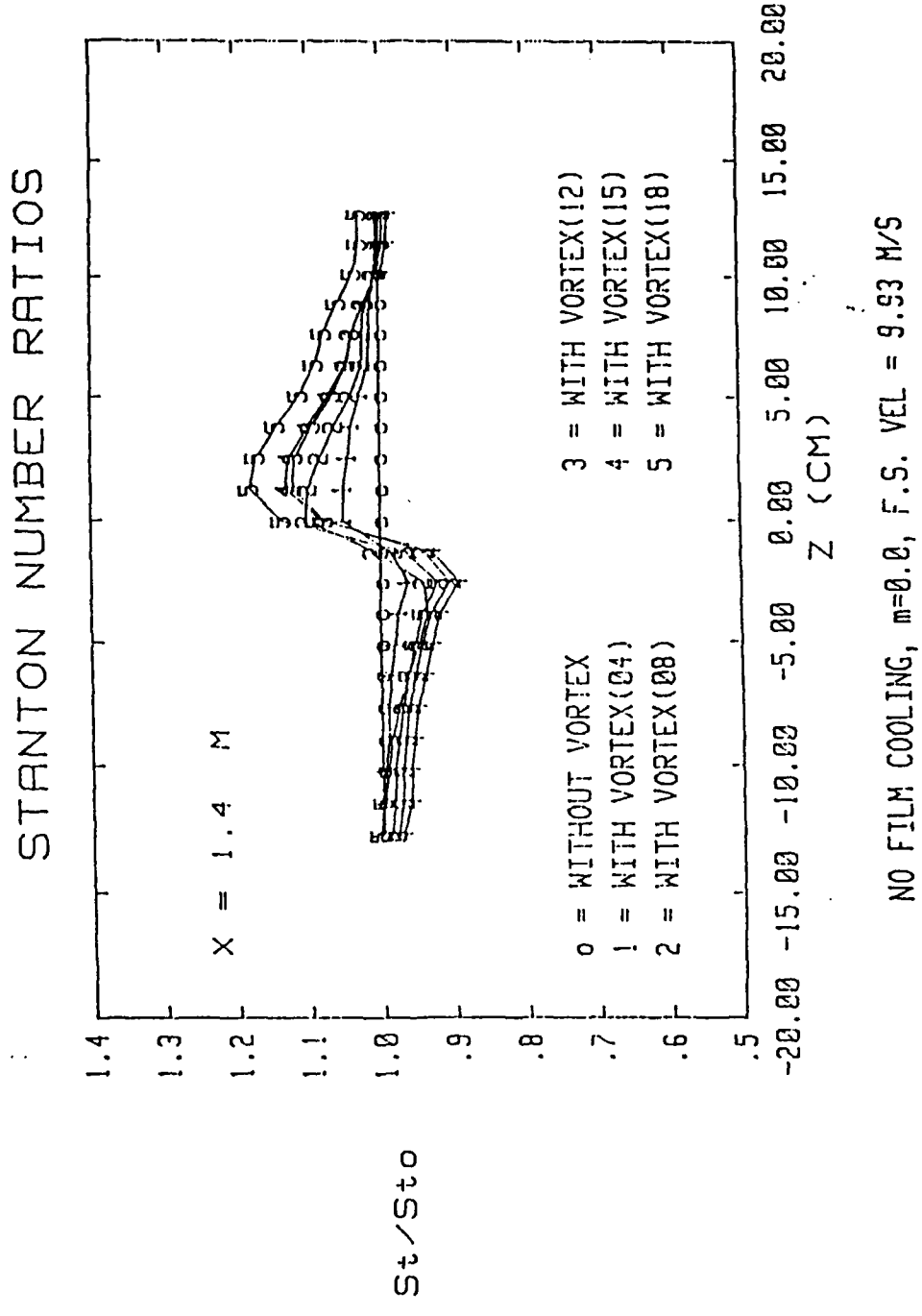

Figure 91 Spanwise Variation of St/Sto Ratios, No Film-Cooling, X = 1.40 m

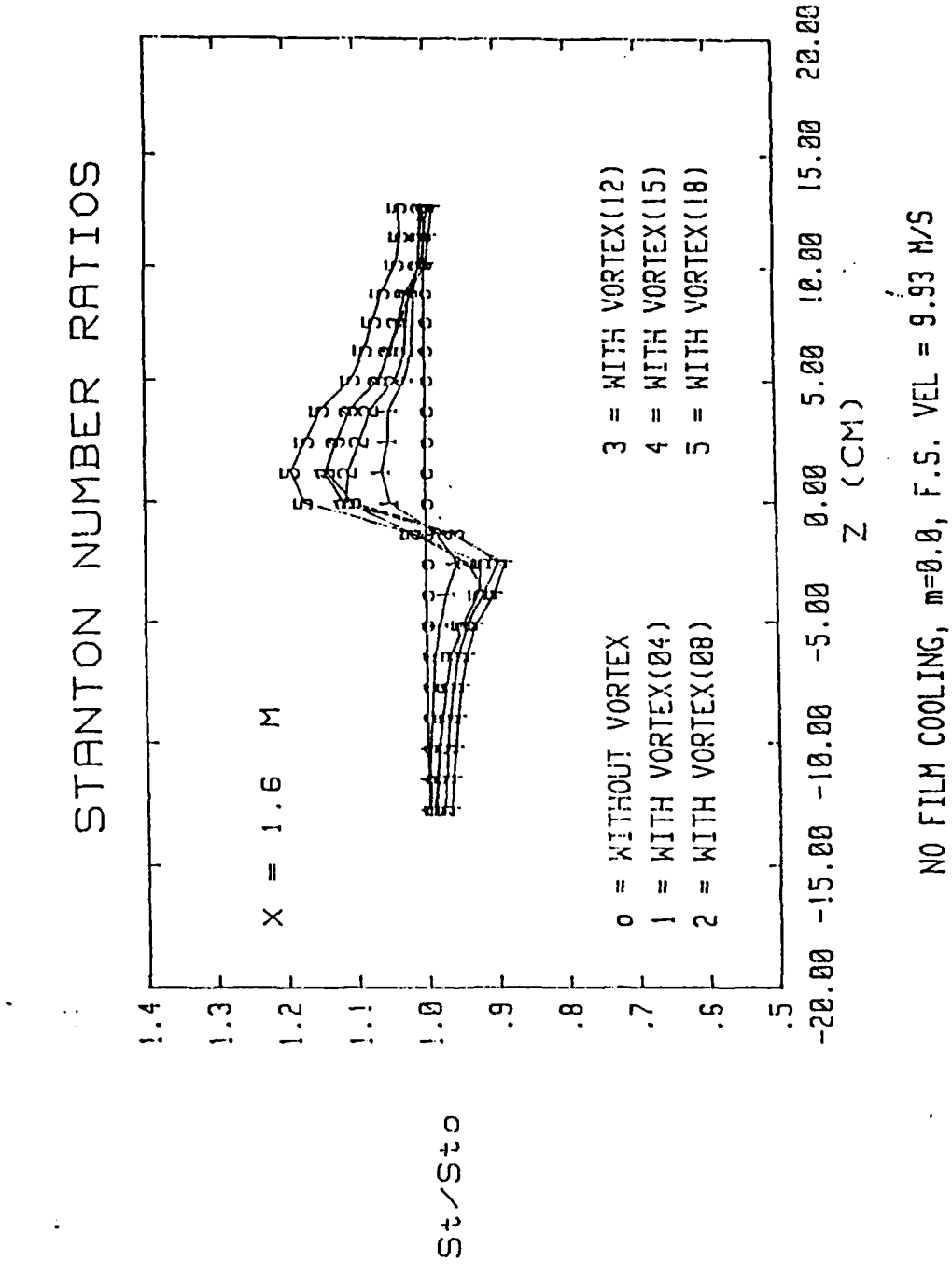

Figure 92 Spanwise Variation of St/Sto Ratios, No Film-Cooling, X = 1.60 m

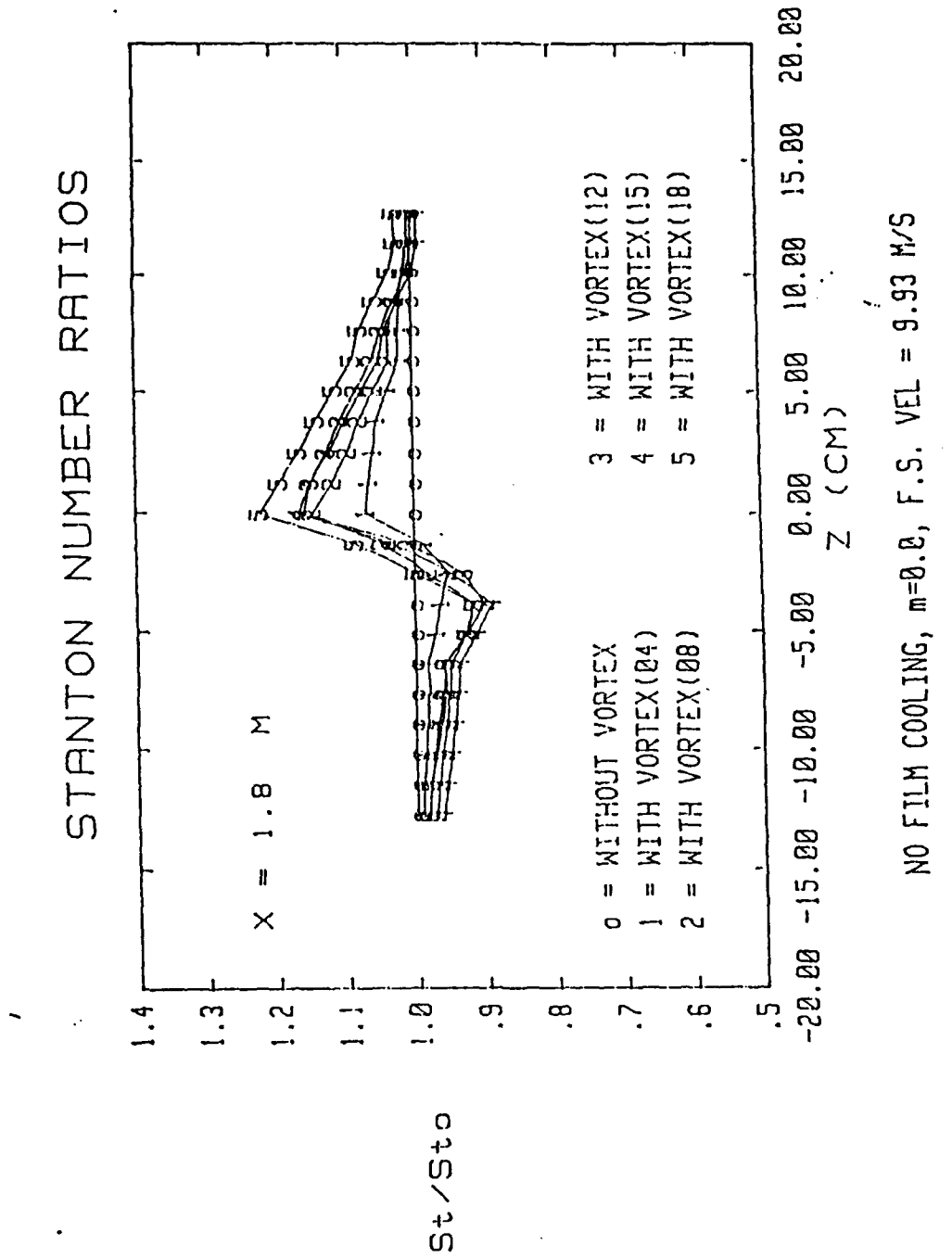

Figure 93 Spanwise Variation of St/Sto Ratios, No Film-Cooling, X = 1.80 m

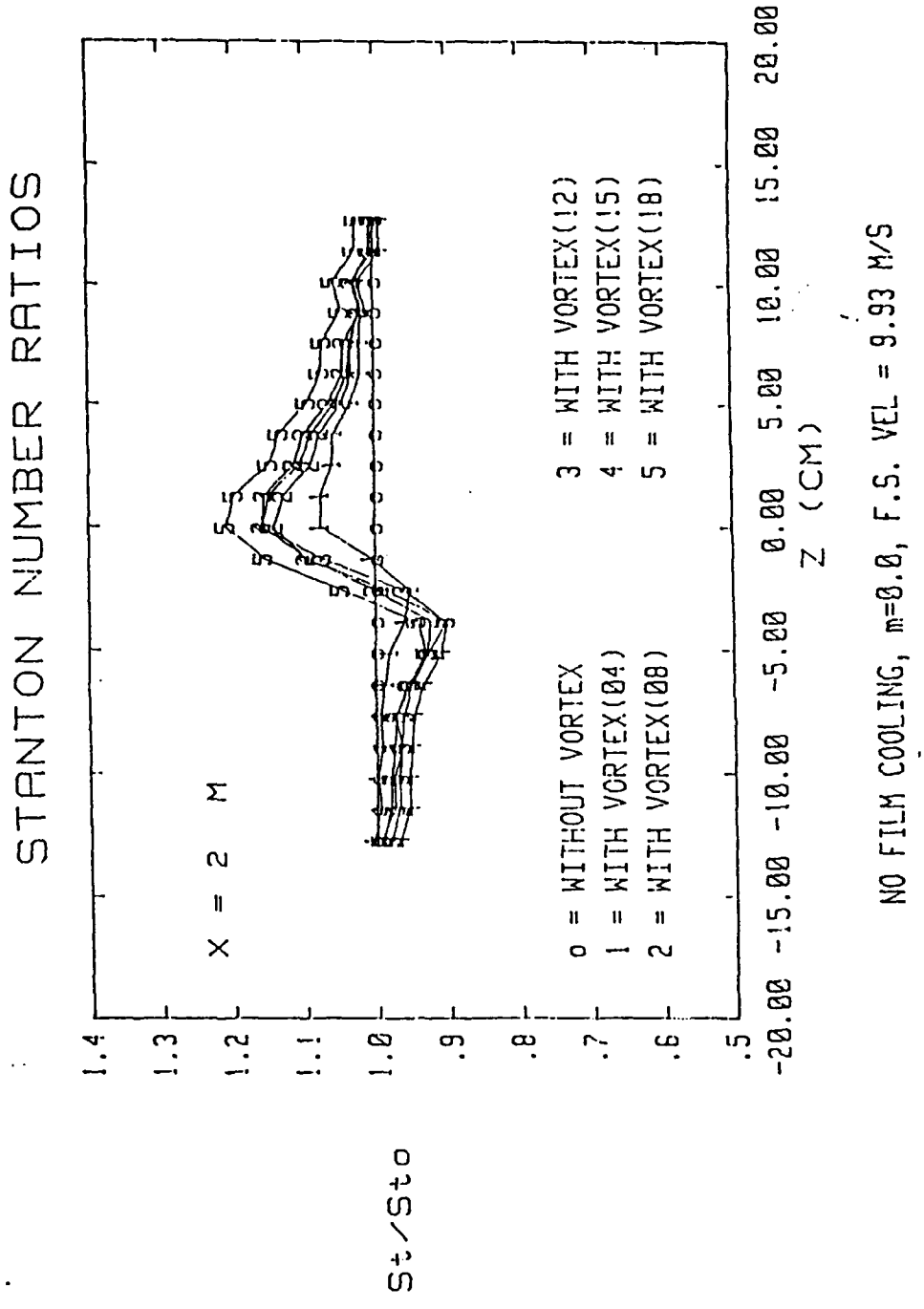

Figure 94 Spanwise Variation of St/Sto Ratios, No Film-Cooling, X = 2.00 m

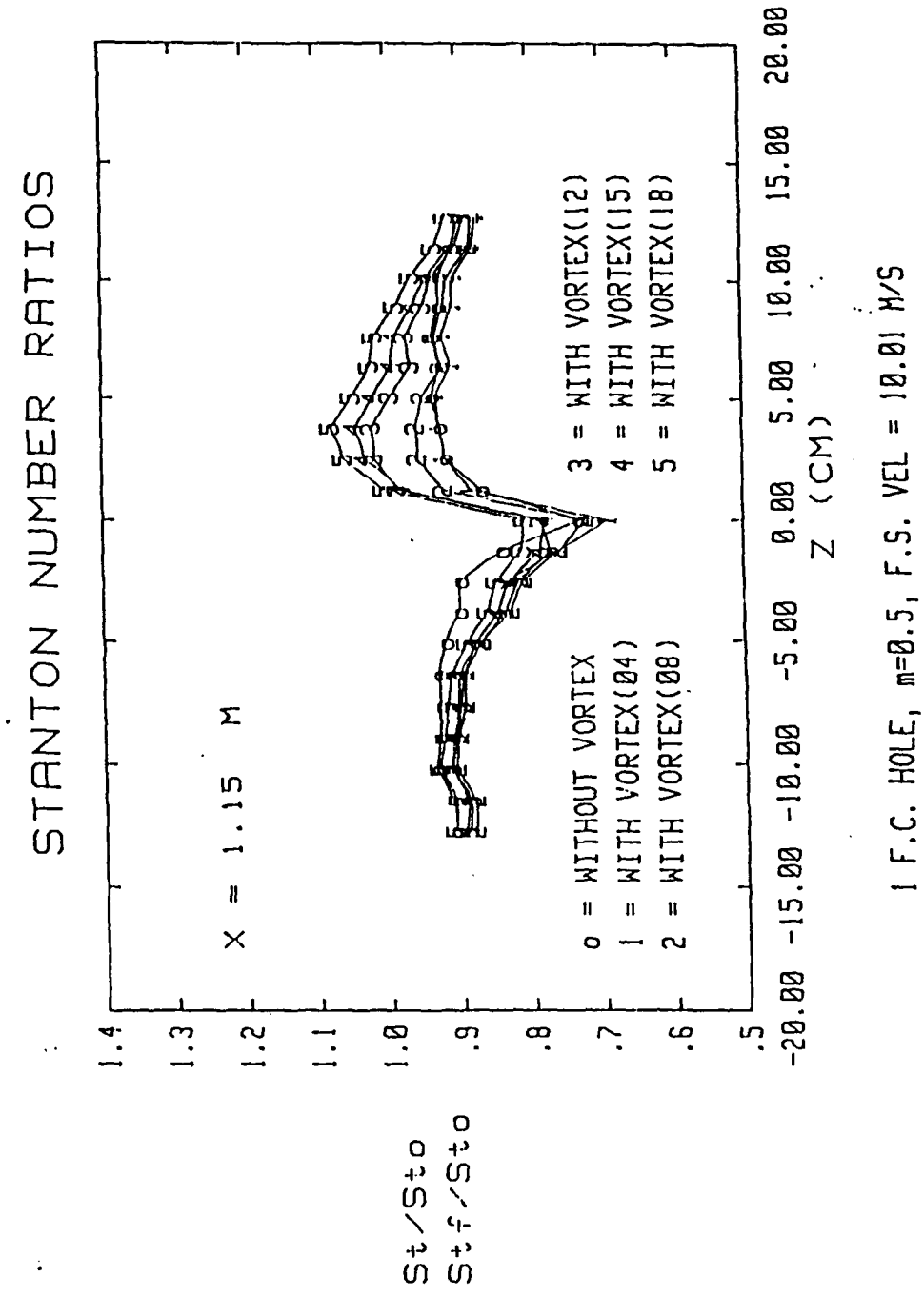

Figure 95 Spanwise Variation of St/Sto and Stf/Sto Ratios, A Single Film-Cooling Hole, X = 1.15 m

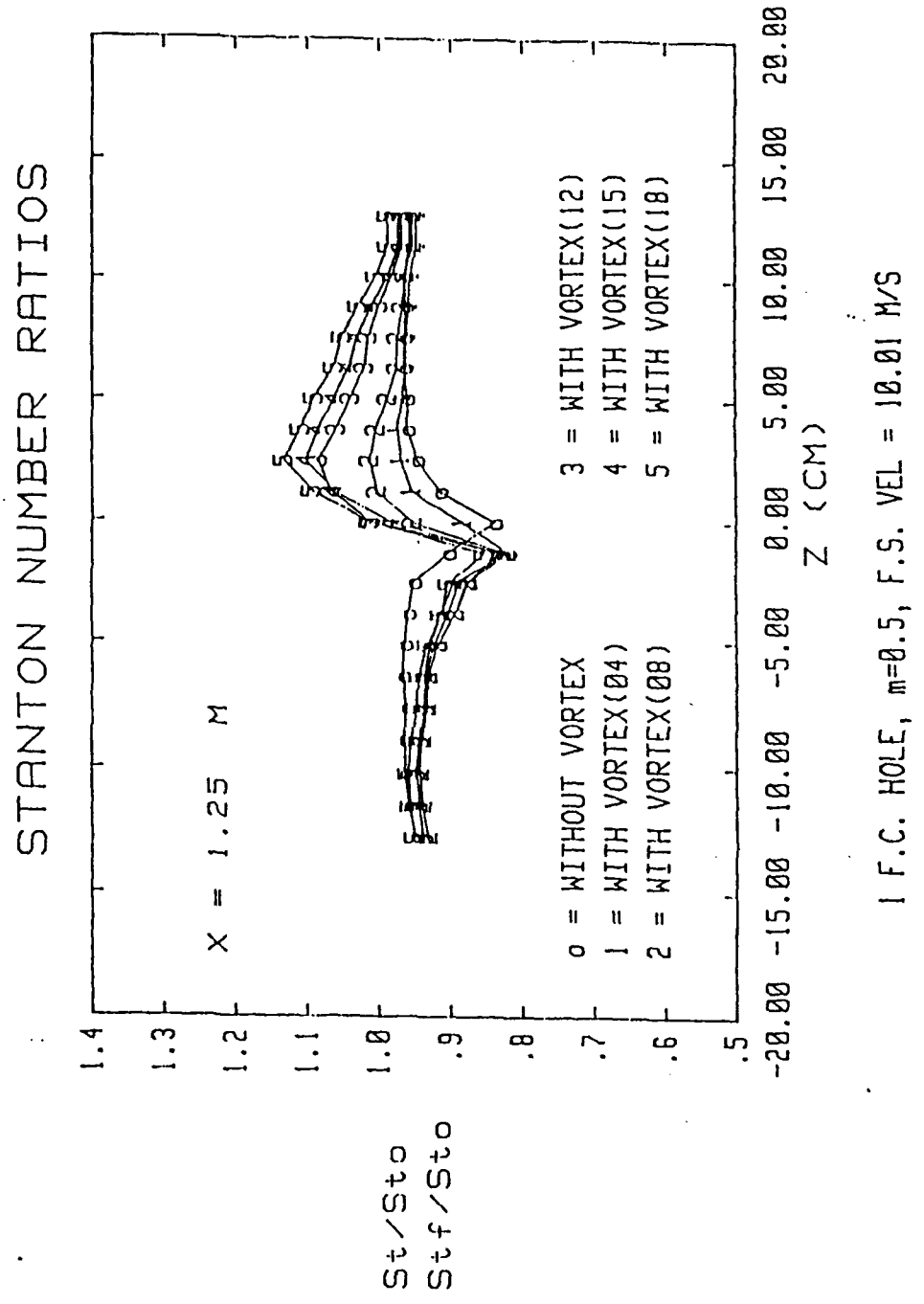

Figure 96 Spanwise Variation of St/Sto and Stf/Sto Ratios, A Single Film-Cooling Hole, X = 1.25 m

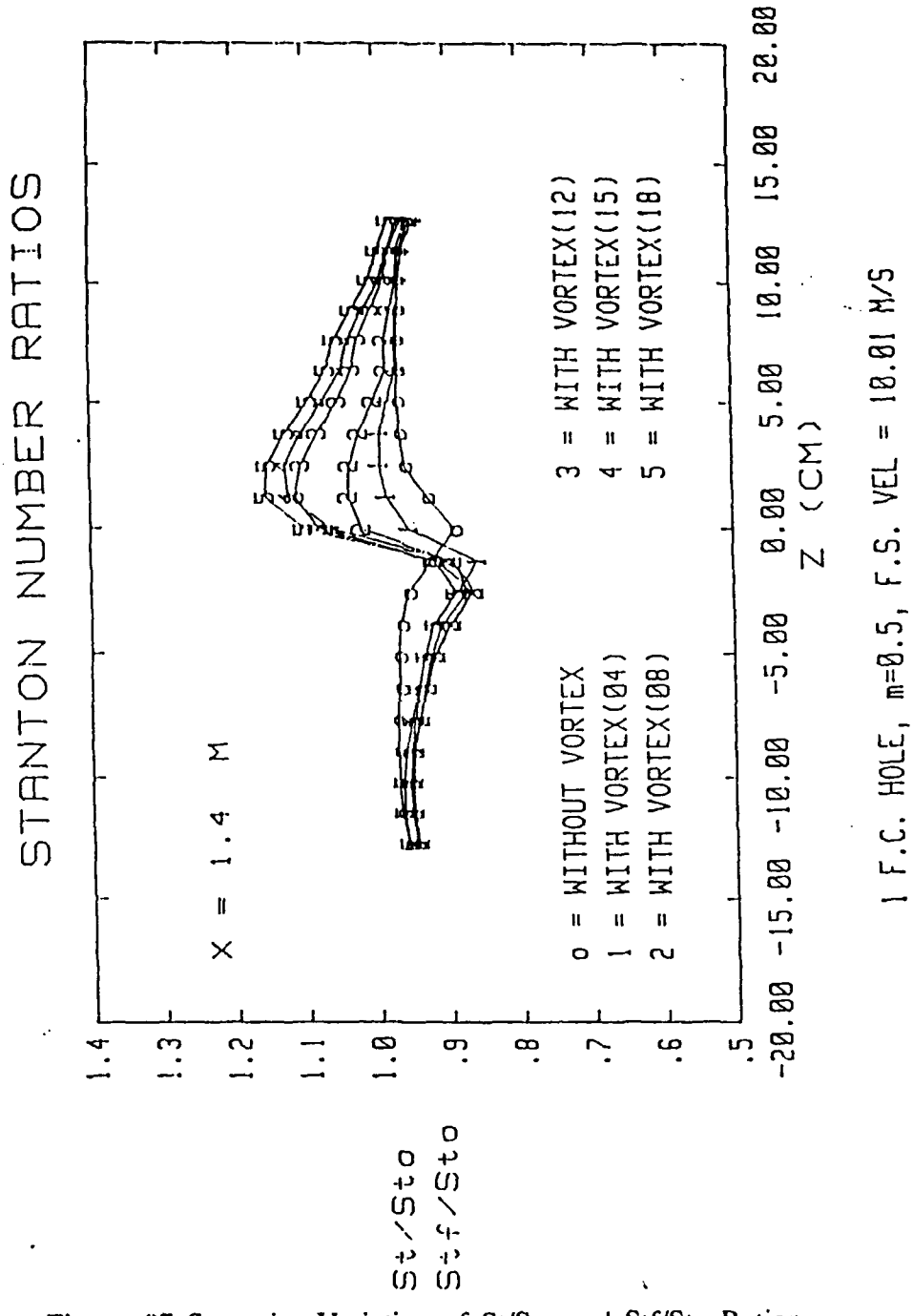

Figure 97 Spanwise Variation of St/Sto and Stf/Sto Ratios, A Single Film-Cooling Hole, X = 1.40 m

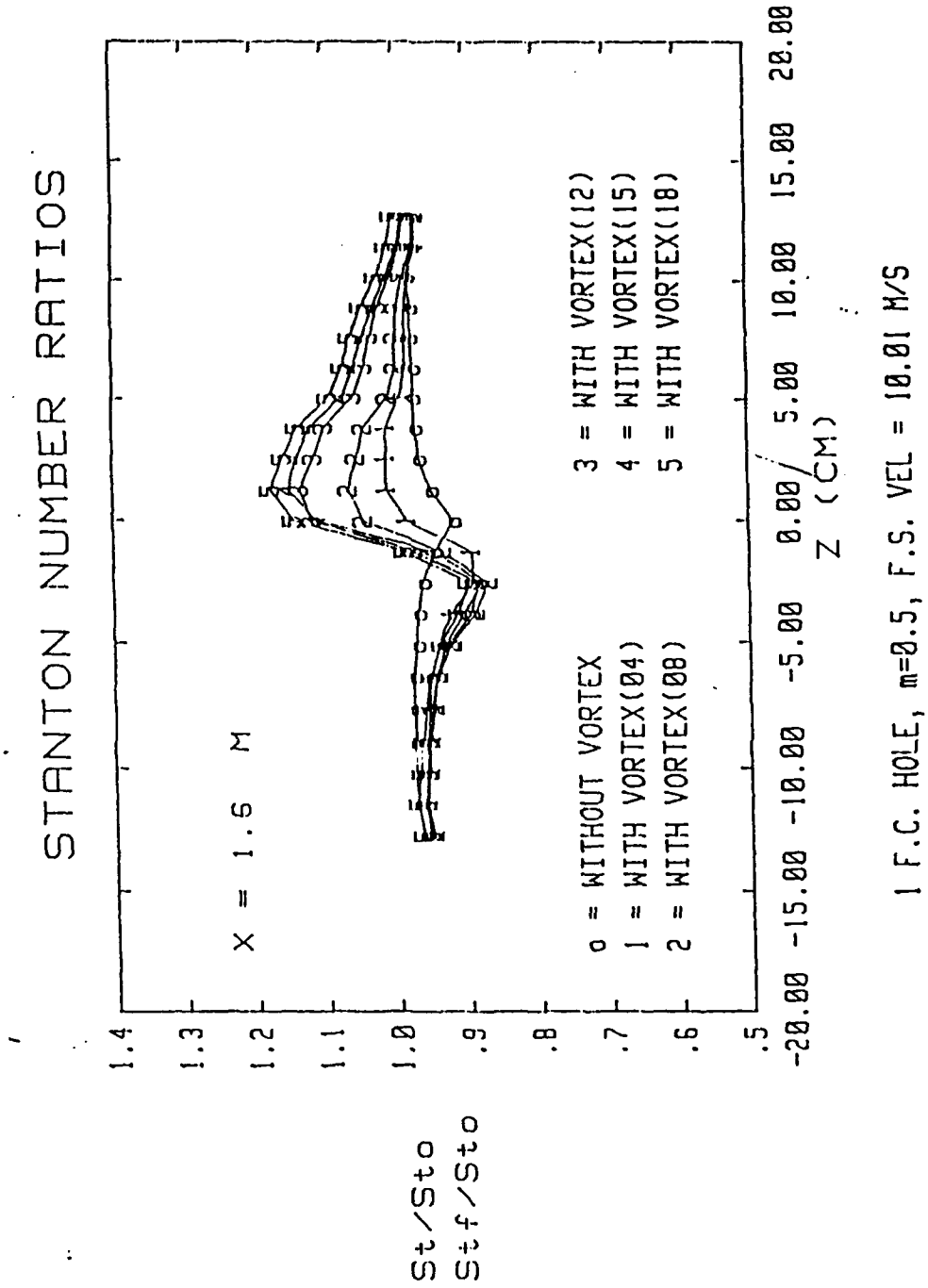

Figure 98 Spanwise Variation of St/Sto and Stf/Sto Ratios, A Single Film-Cooling Hole, X = 1.60 m

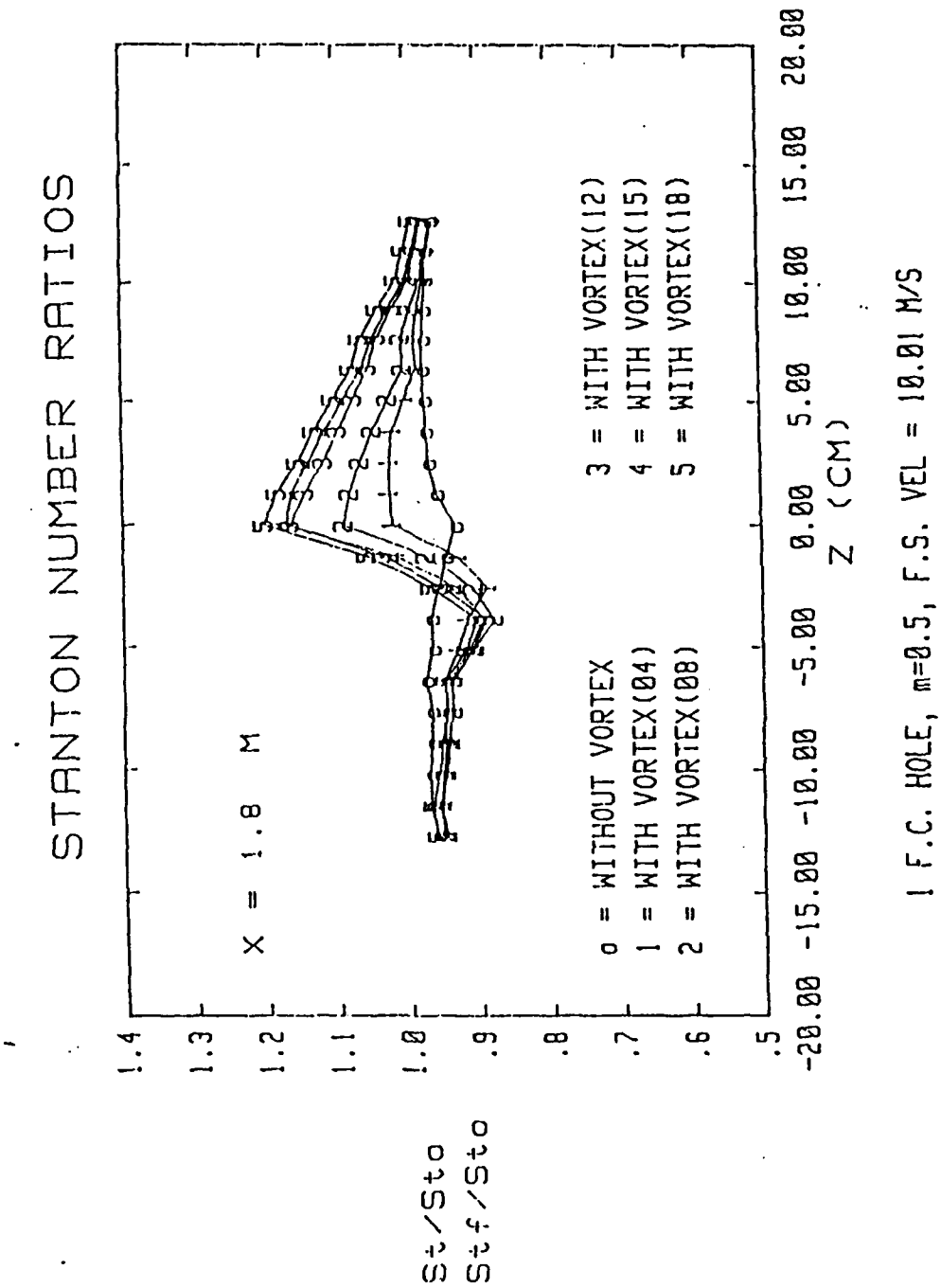

Figure 99 Spanwise Variation of St/Sto and Stf/Sto Ratios, A Single Film-Cooling Hole, X = 1.80 m

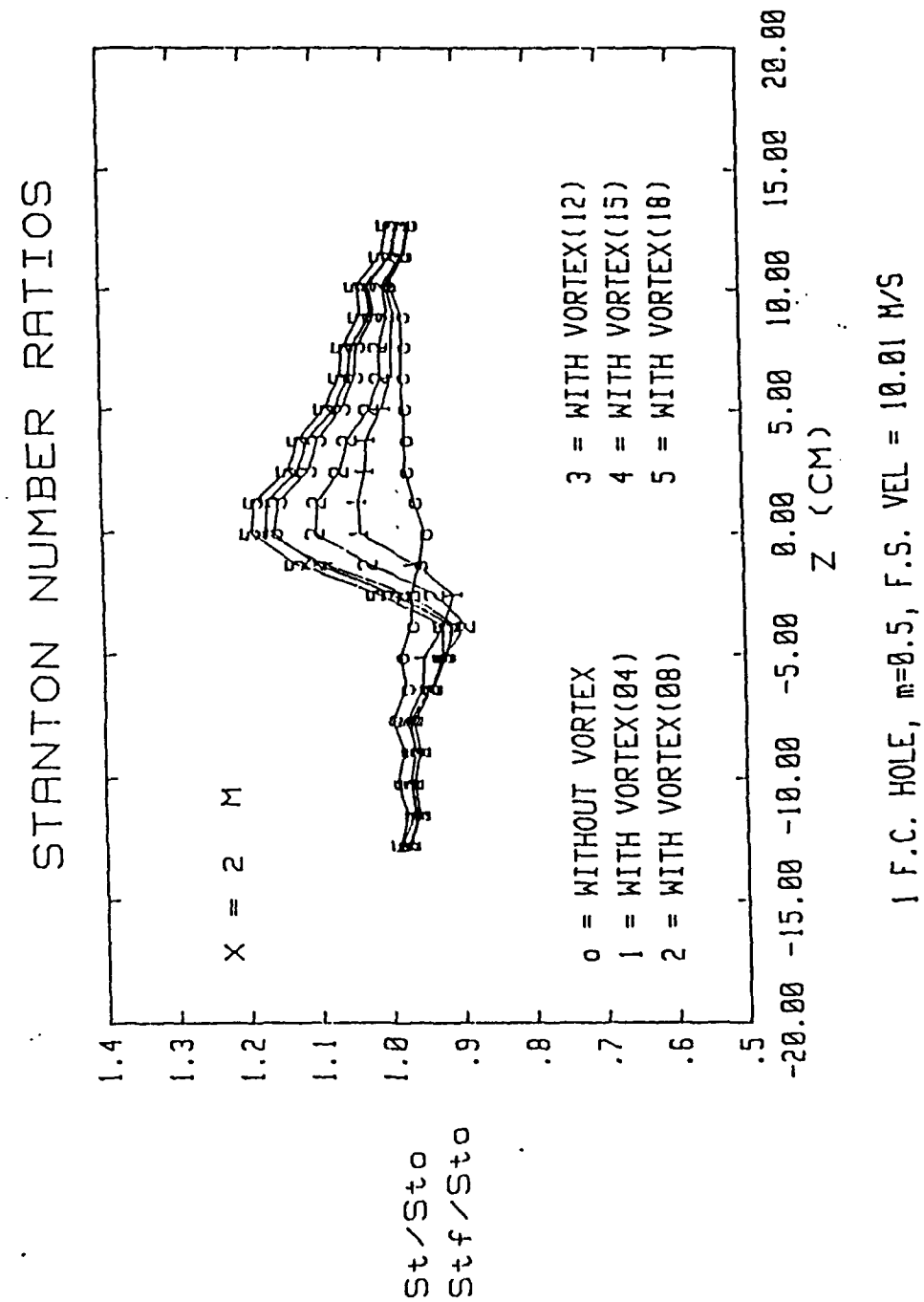

Figure 100 Spanwise Variation of St/Sto and Stf/Sto Ratios, A Single Film-Cooling Hole, X = 2.00 m

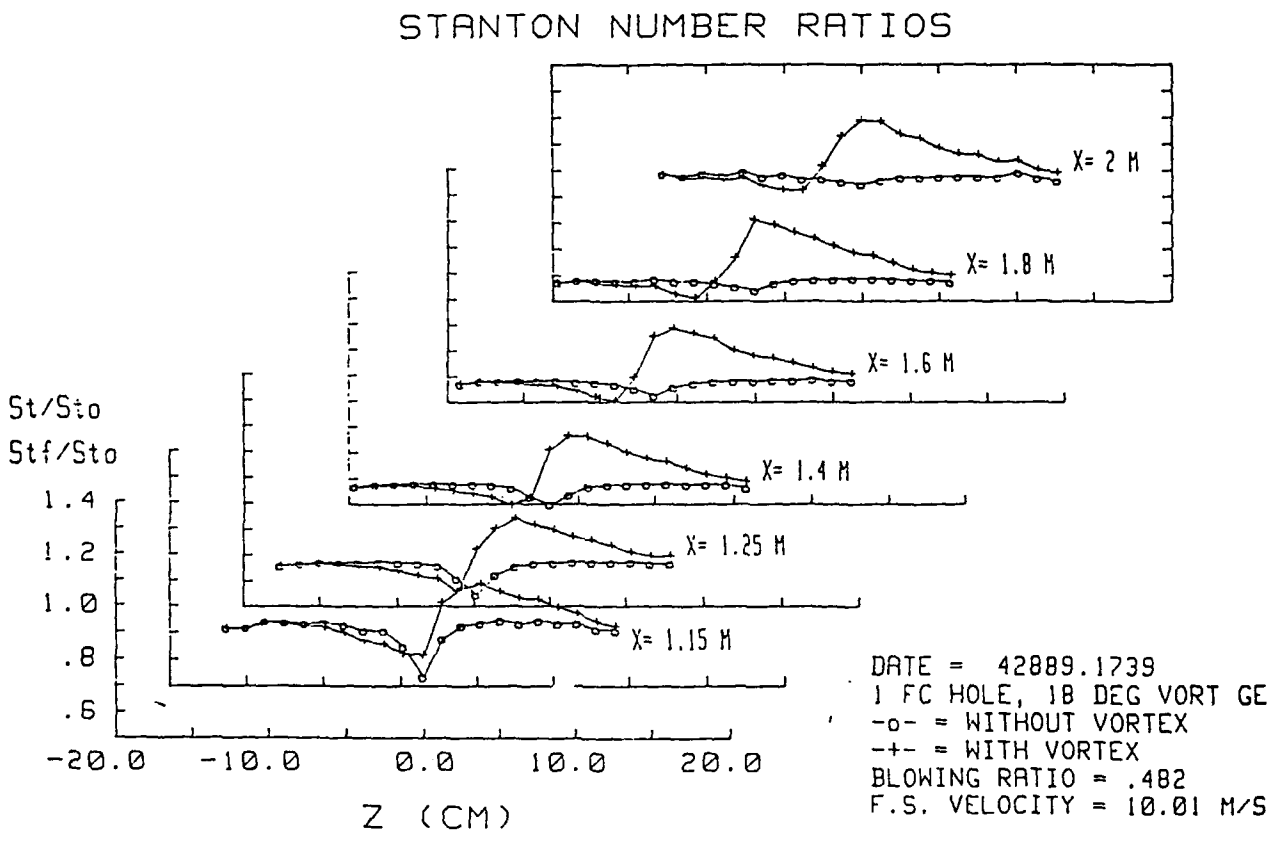

Figure 101 Local Stanton Number Ratios in Boundary Layers with Film-Cooling, with and without an embedded Vortex, A Single Injection Hole, m = 0.482, Vortex r

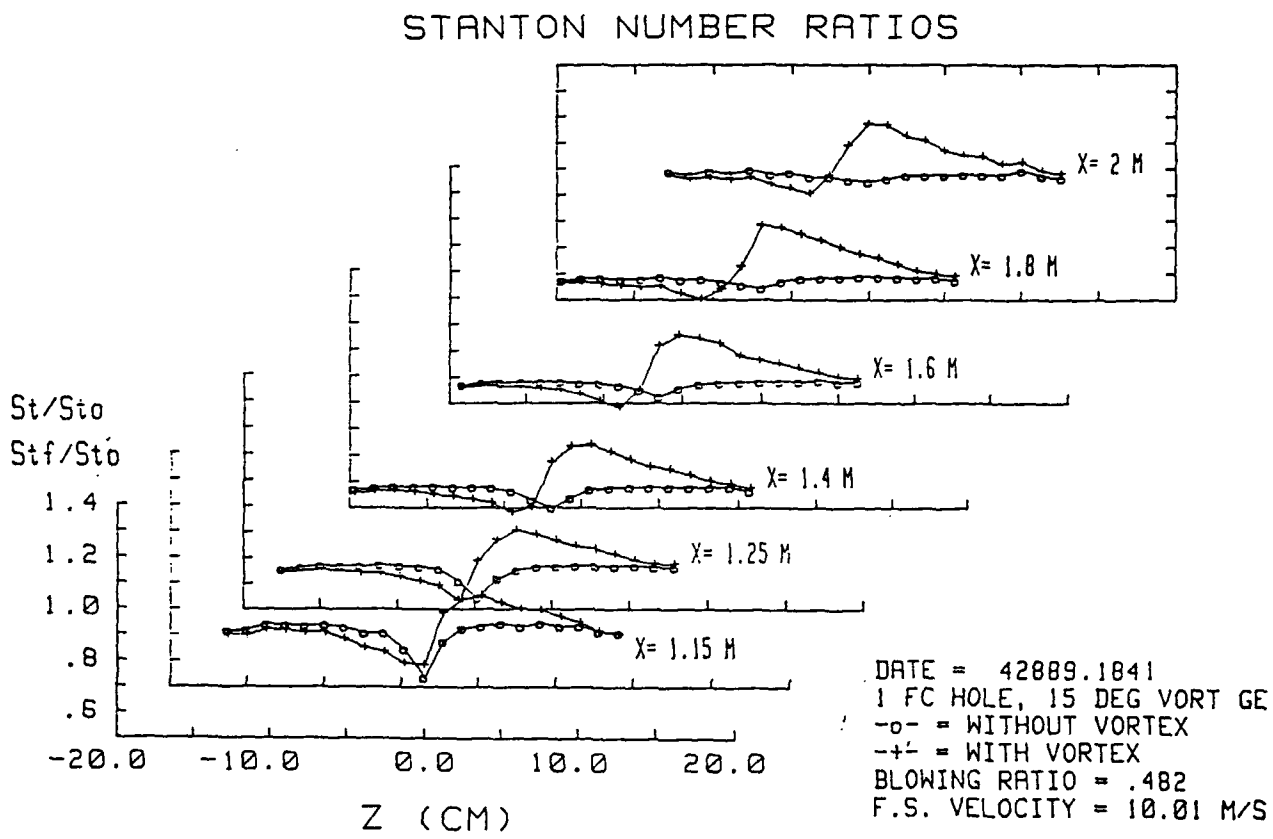

Figure 102 Local Stanton Number Ratios in Boundary Layers with Film-Cooling, with and without an embedded Vortex, A Single Injection Hole, m = 0.482, Vortex w

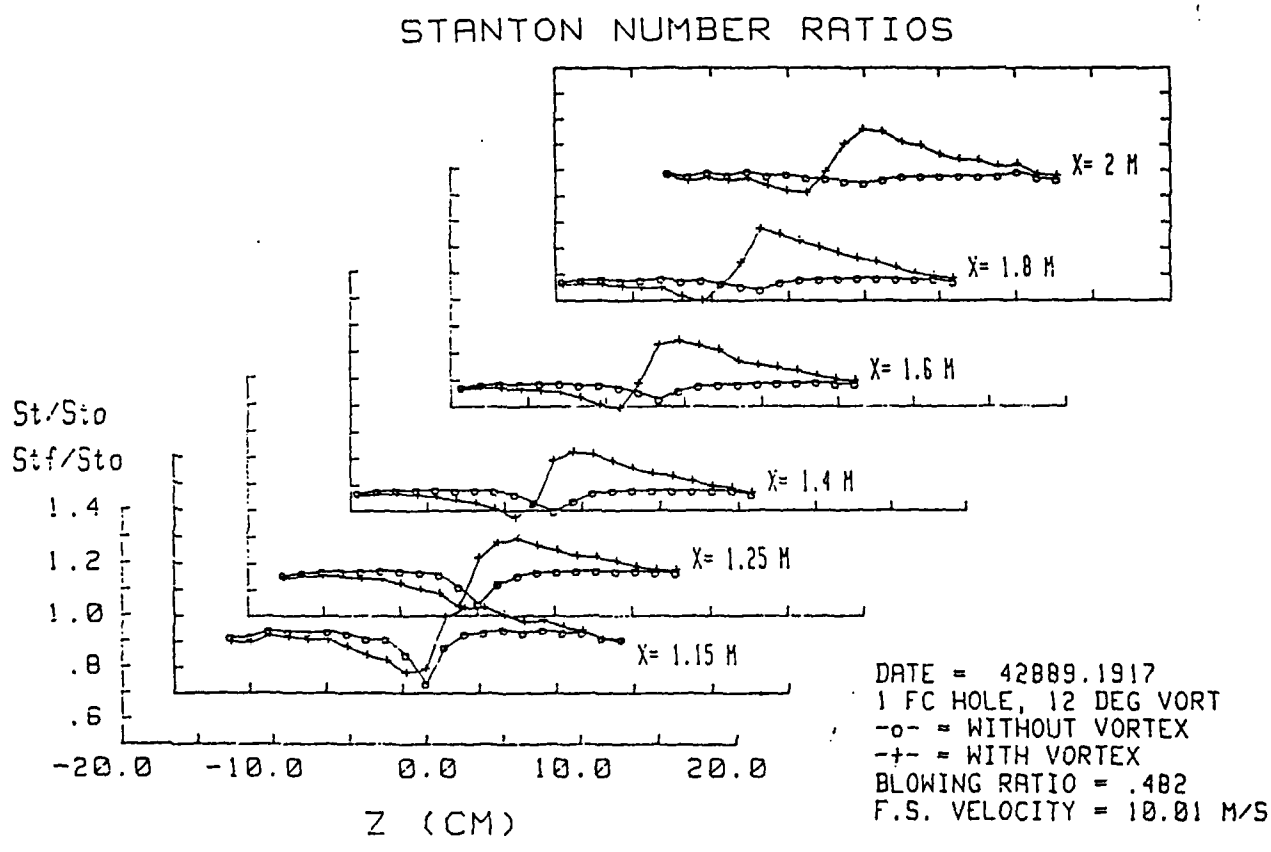

Figure 103 Local Stanton Number Ratios in Boundary Layers with Film-Cooling, with and without an embedded Vortex, A Single Injection Hole, m = 0.482, Vortex x

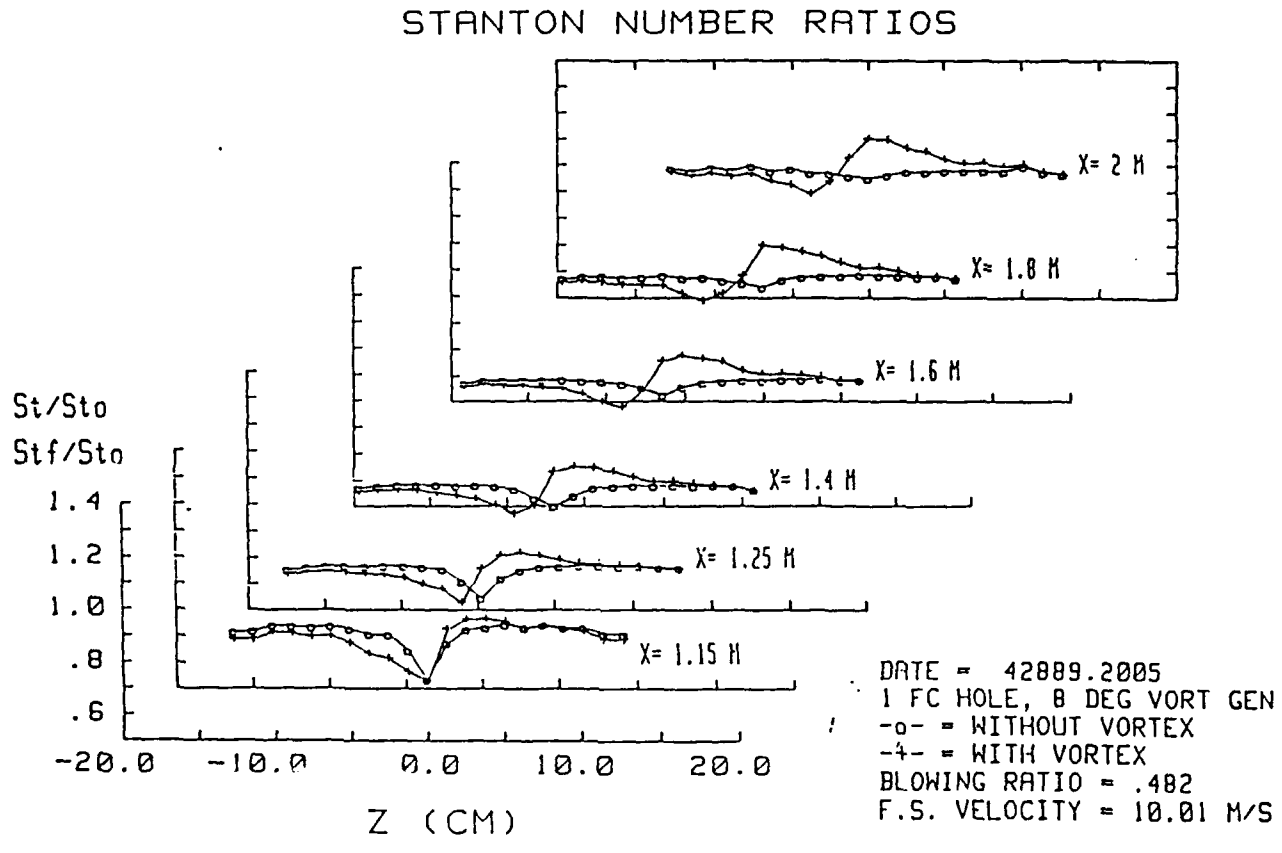

Figure 104 Local Stanton Number Ratios in Boundary Layers with Film-Cooling, with and without an embedded Vortex, A Single Injection Hole, m = 0.482, Vortex y

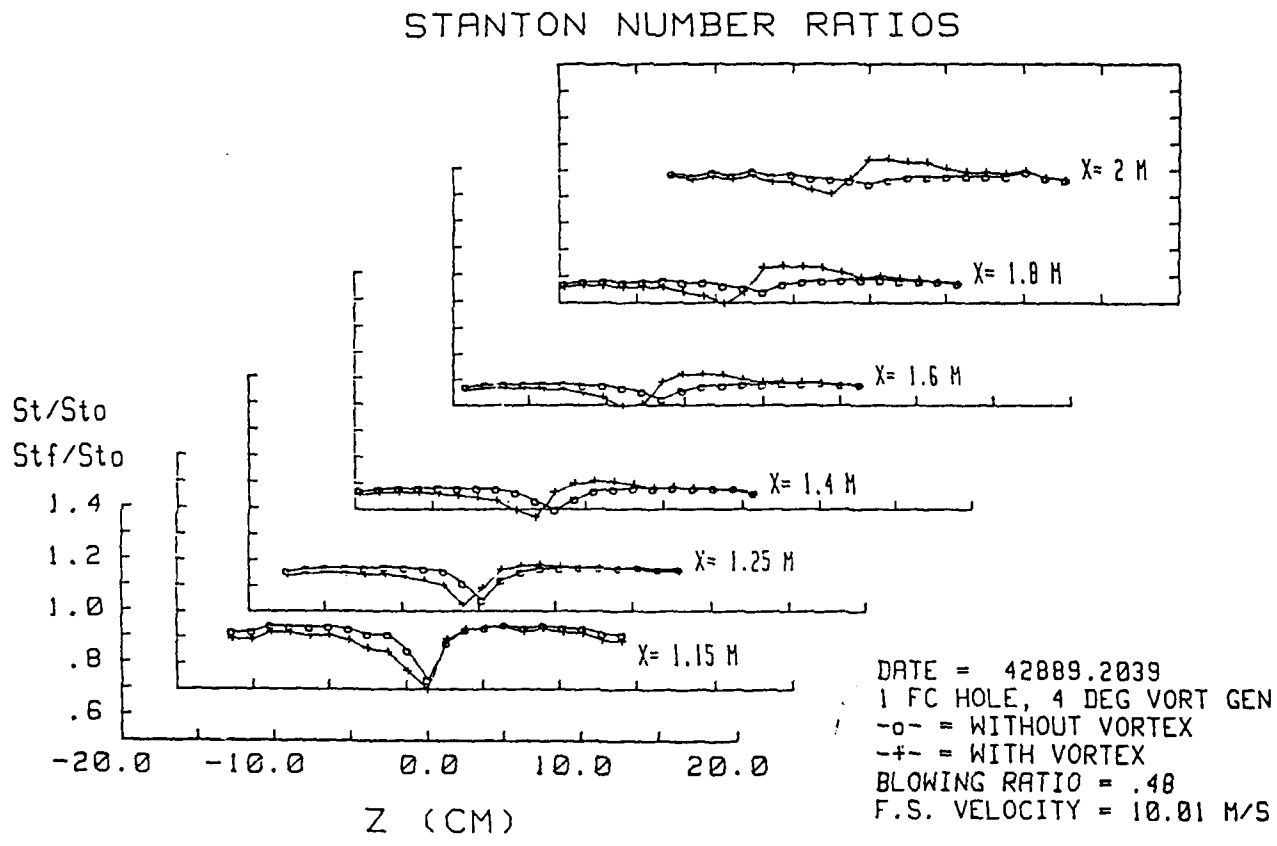

Figure 105 Local Stanton Number Ratios in Boundary Layers with Film-Cooling, with and without an embedded Vortex, A Single Injection Hole, m = 0.480, Vortex z

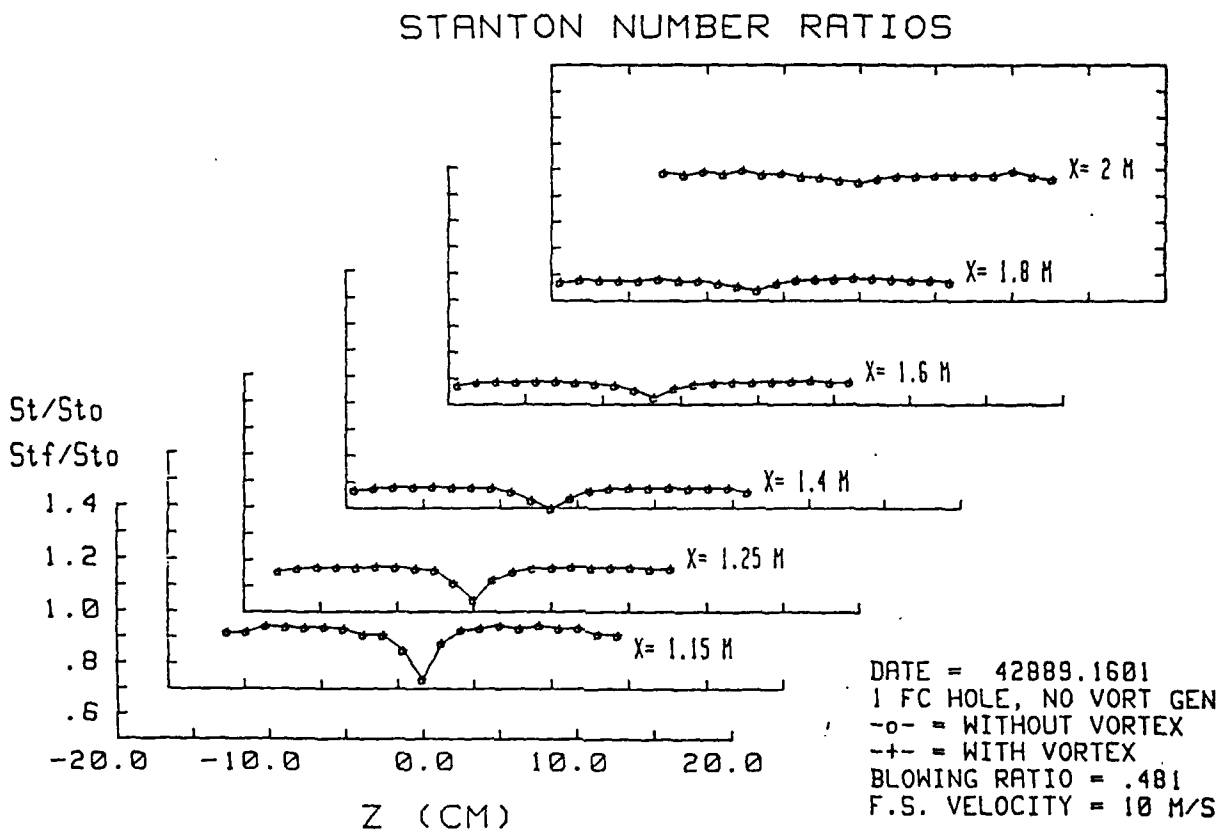

Figure 106 Local Stanton Number Ratios in Boundary Layers with Film-Cooling, with and without an embedded Vortex, A Single Injection Hole, m = 0.481, No Vortex Generator

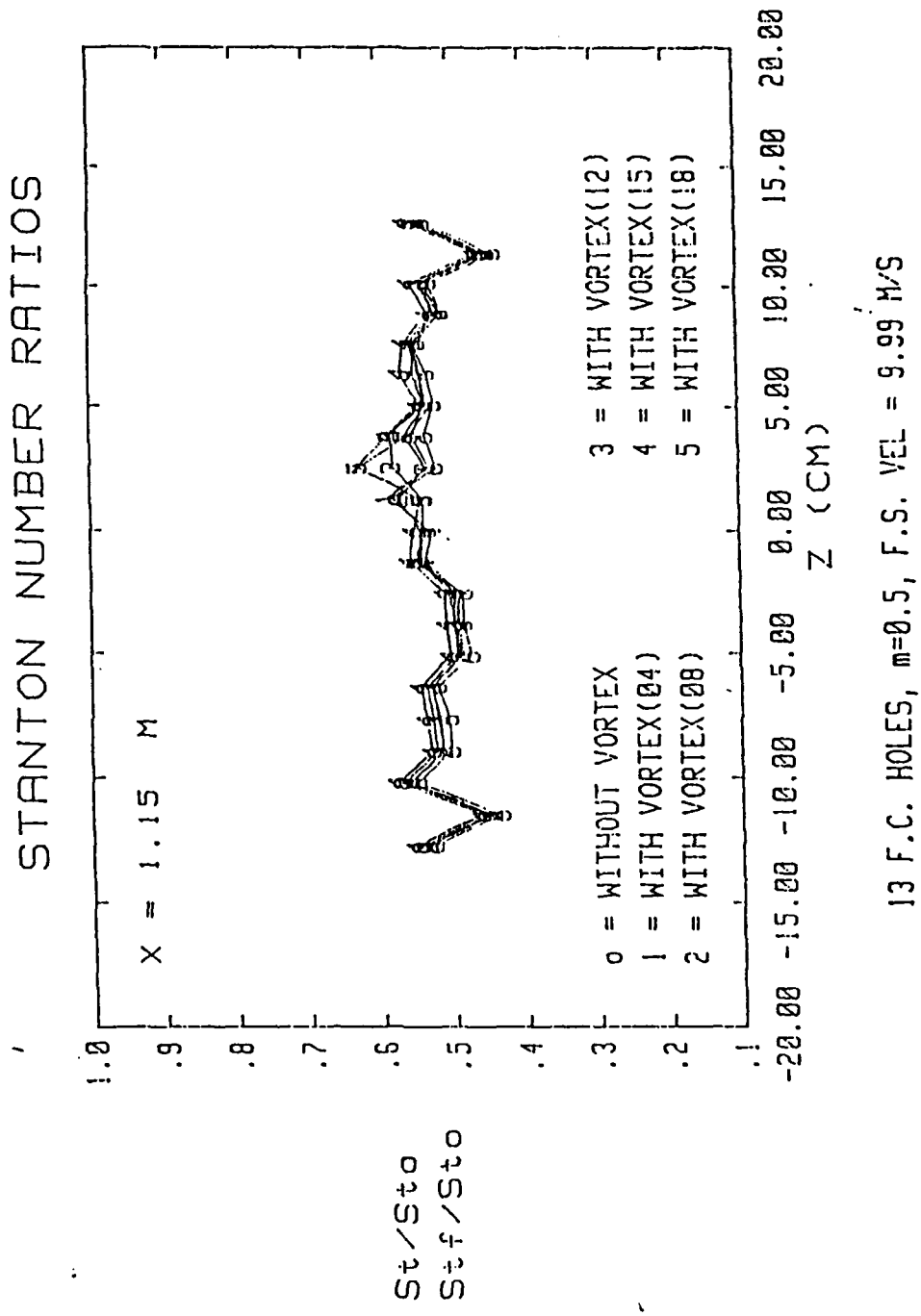

Figure 107 Spanwise Variation of St/Sto and Stf/Sto Ratios, 13 Film-Cooling Holes, X = 1.15 m

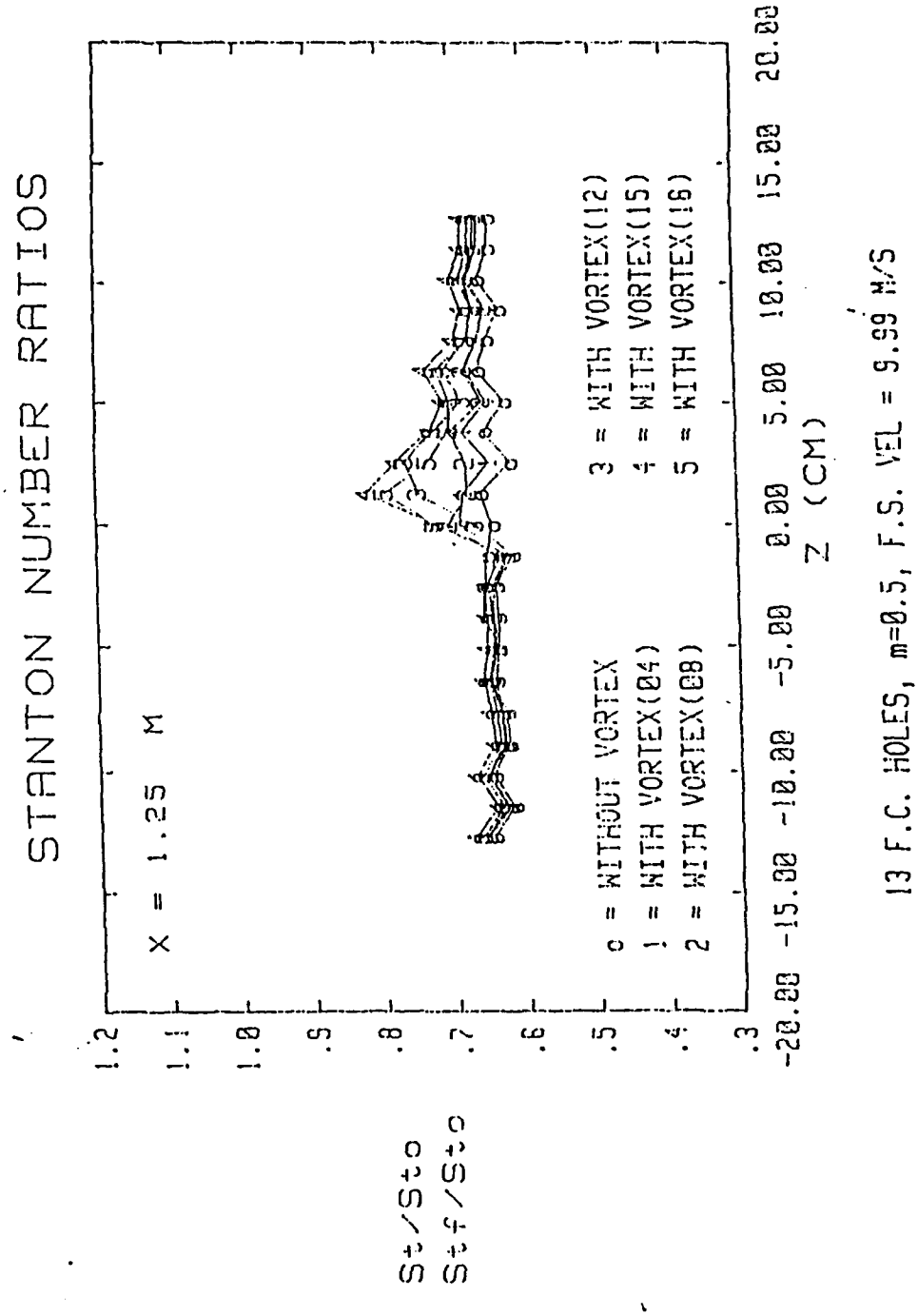

Figure 108 Spanwise Variation of St/Sto and Stf/Sto Ratios, 13 Film-Cooling Holes, X = 1.25 m

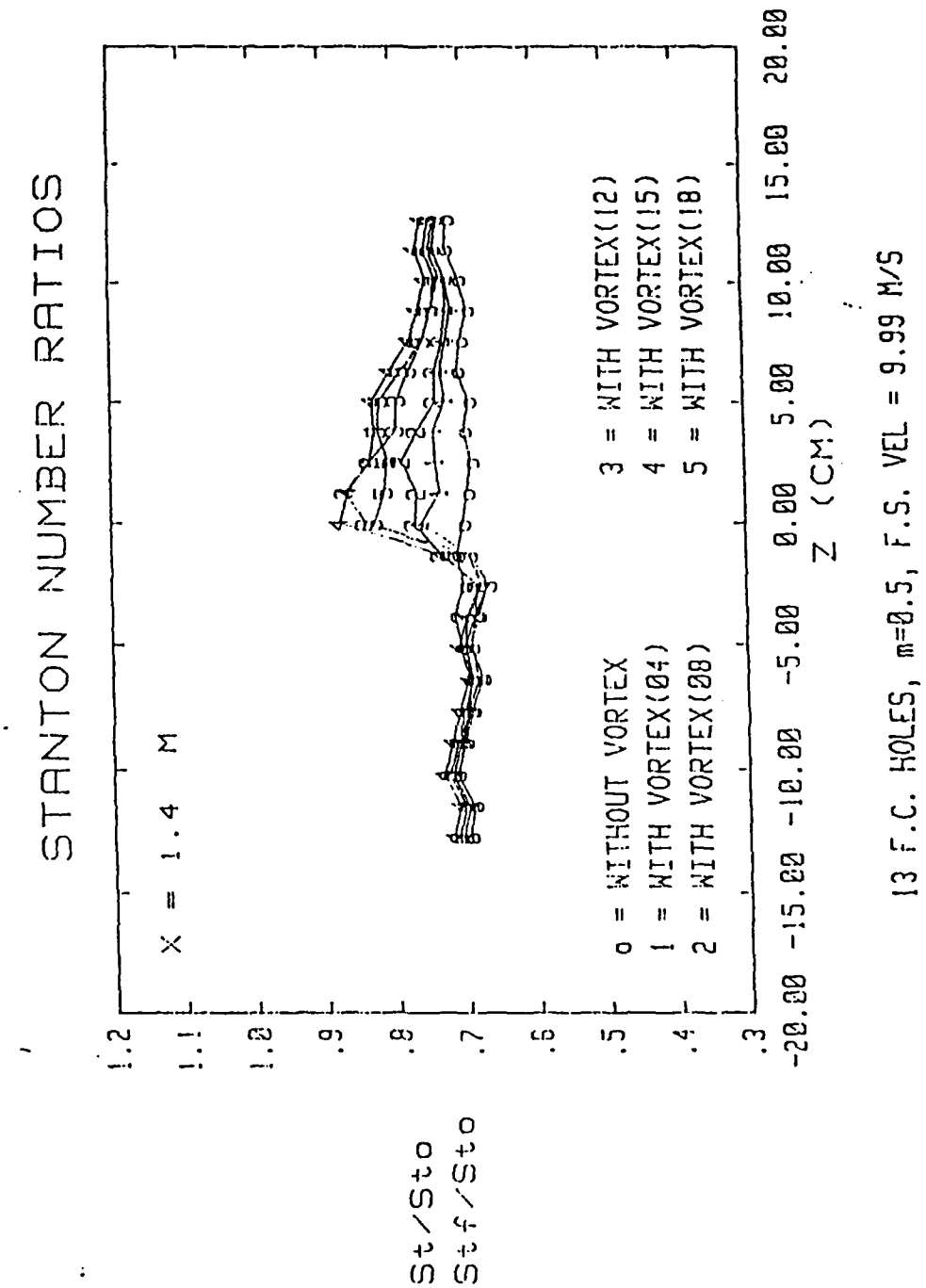

Figure 109 Spanwise Variation of St/Sto and Stf/Sto Ratios, 13 Film-Cooling Holes, X = 1.40 m

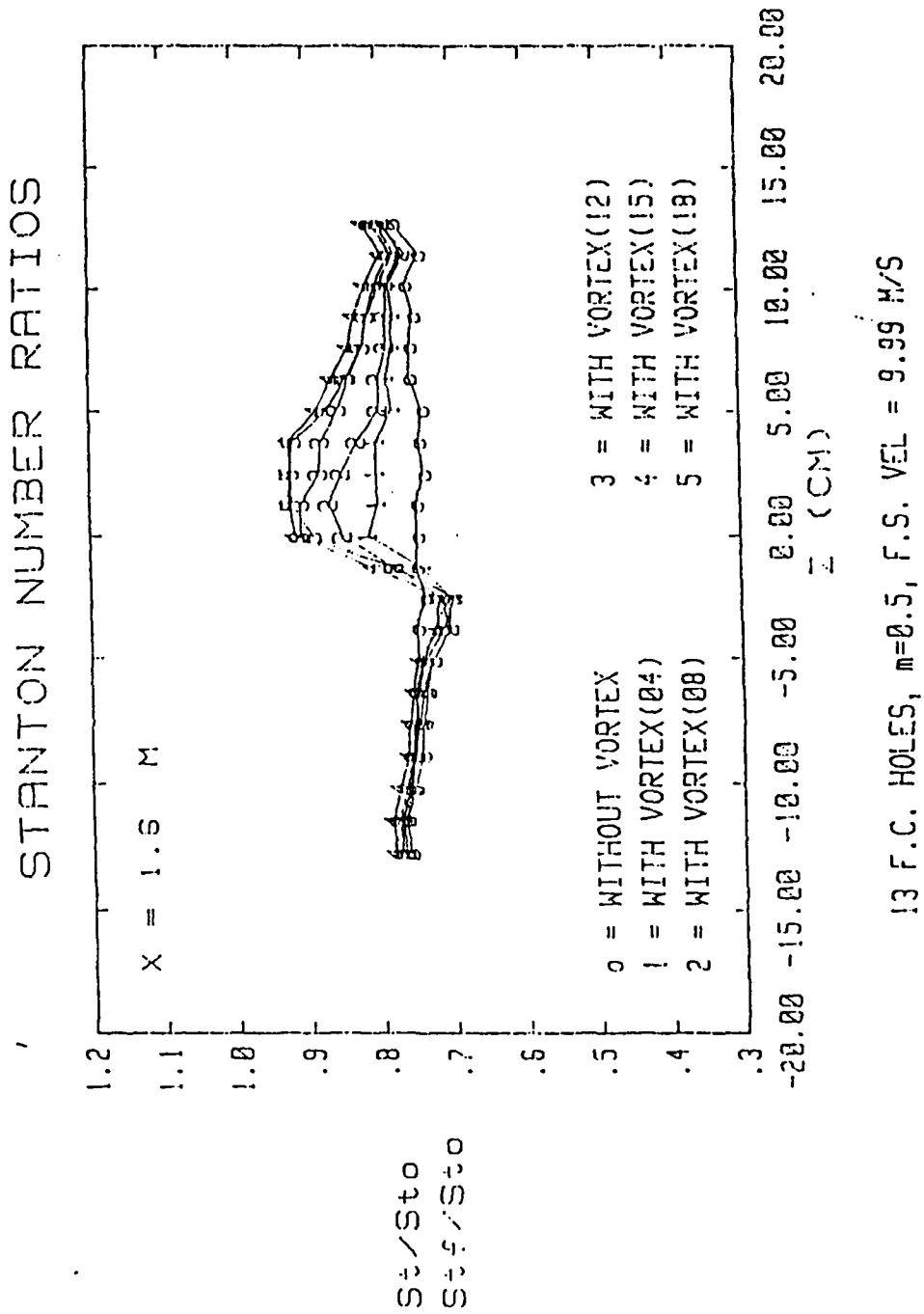

Figure 110 Spanwise Variation of St/Sto and Stf/Sto Ratios, 13 Film-Cooling Holes, X = 1.60 m

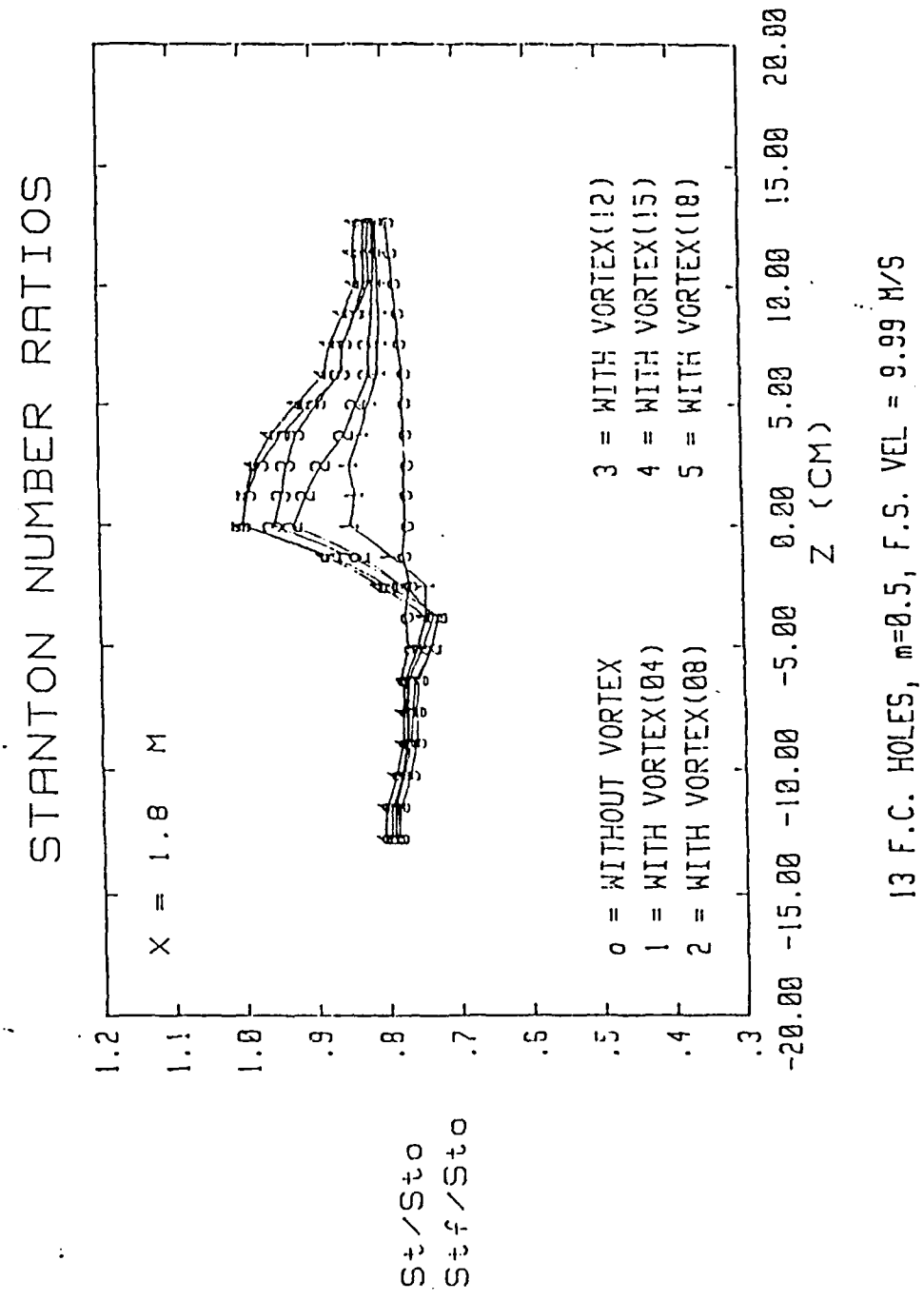

Figure 111 Spanwise Variation of St/Sto and Stf/Sto Ratios, 13 Film-Cooling Holes, X = 1.80 m

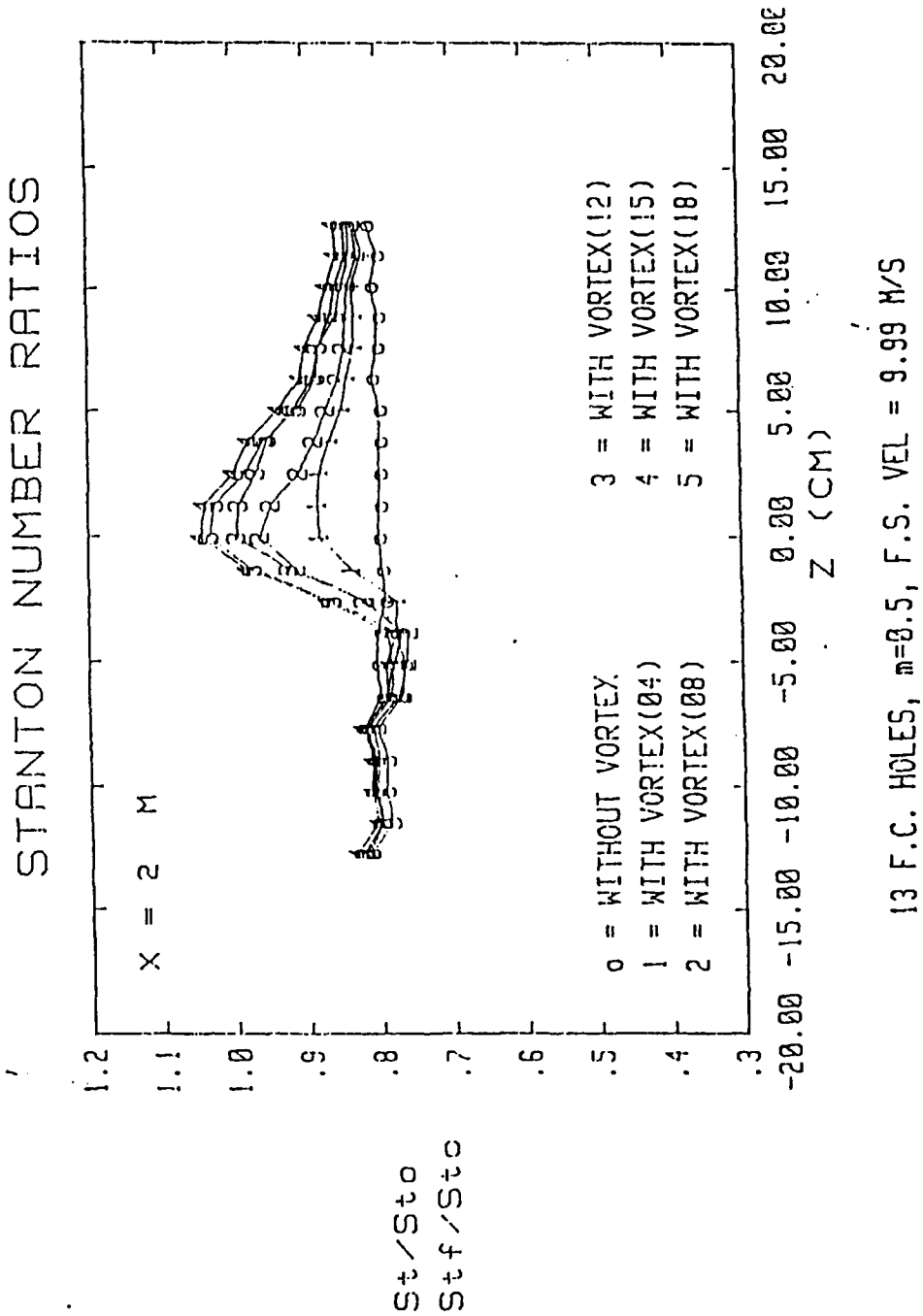

Figure 112 Spanwise Variation of St/Sto and Stf/Sto Ratios, 13 Film-Cooling Holes, X = 2.00 m

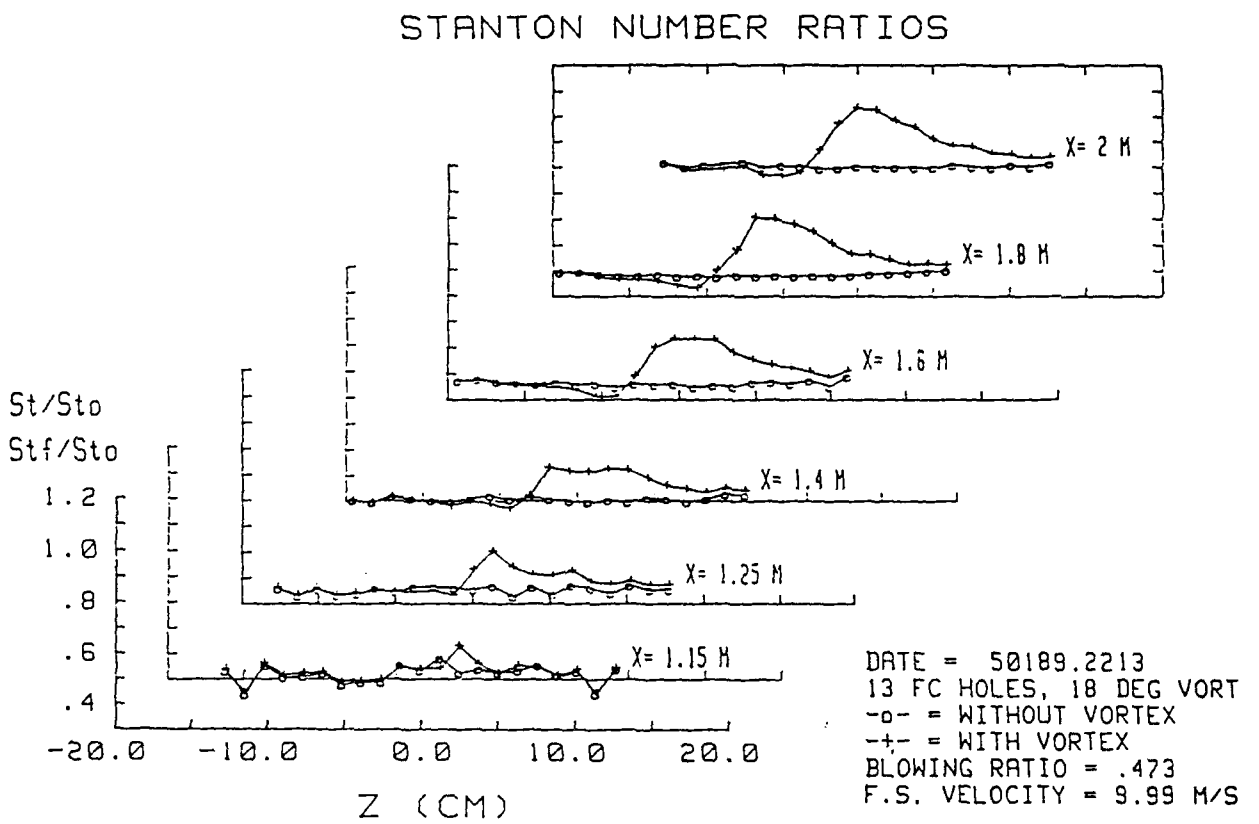

Figure 113 Local Stanton Number Ratios in Boundary Layers with Film-Cooling, with and without an embedded Vortex, 13 Injection Holes, m = 0.473, Vortex *r*

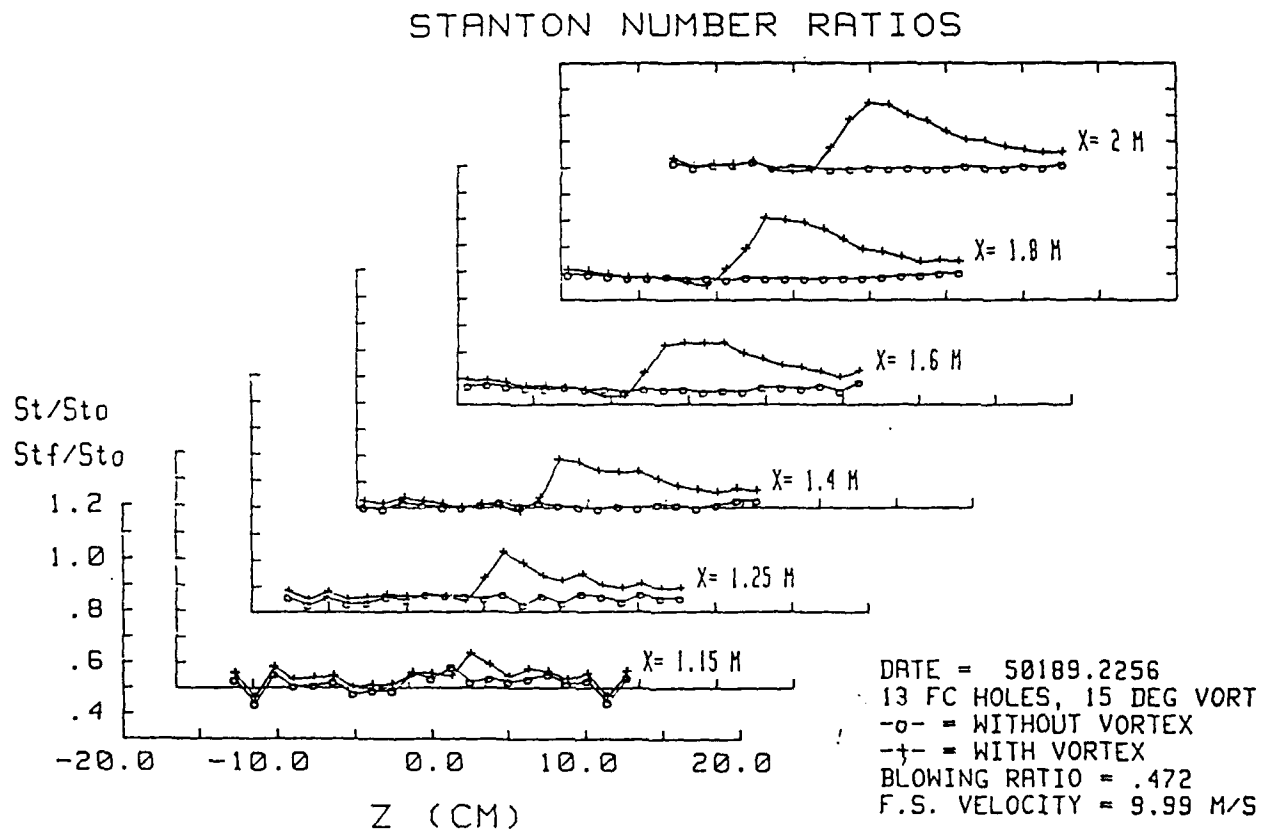

Figure 114 Local Stanton Number Ratios in Boundary Layers with Film-Cooling, with and without an embedded Vortex, 13 Injection Holes, m = 0.472, Vortex w

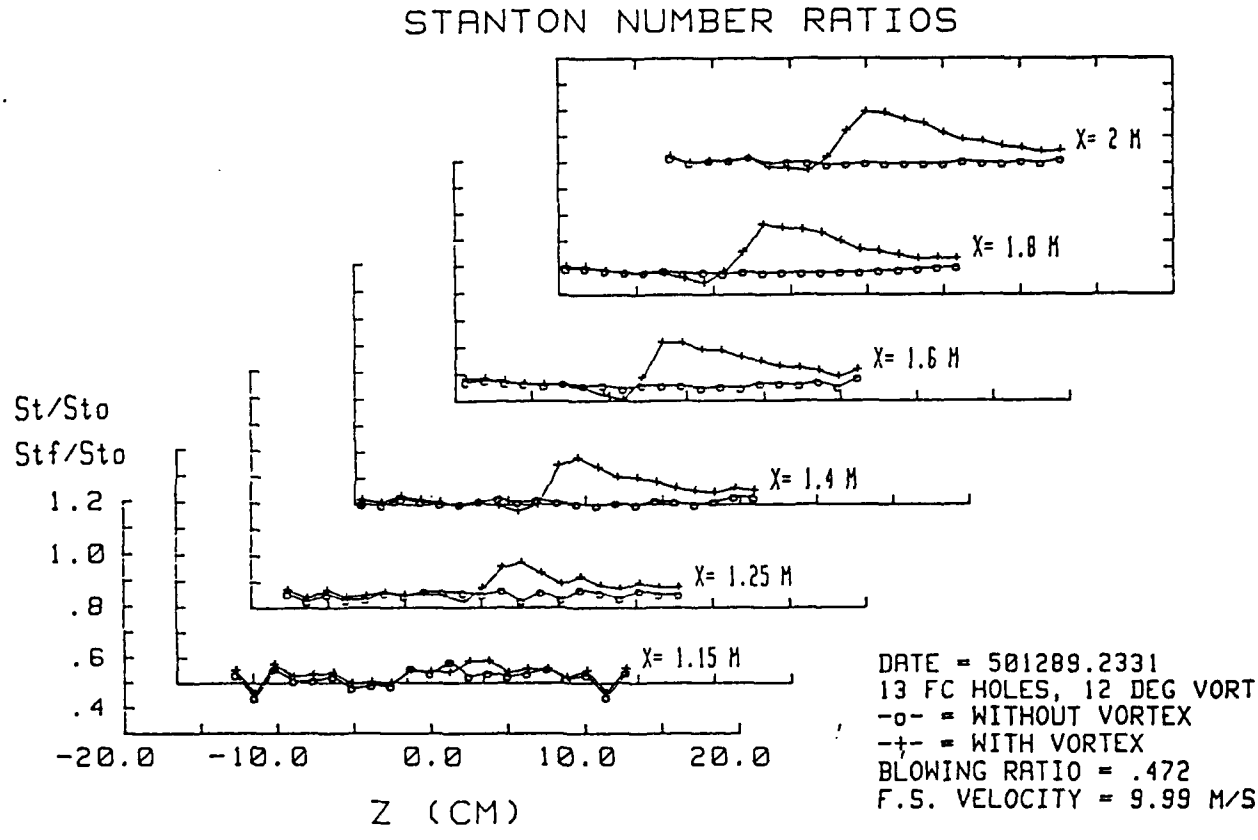

Figure 115 Local Stanton Number Ratios in Boundary Layers with Film-Cooling, with and without an embedded Vortex, 13 Injection Holes, m = 0.472, Vortex x

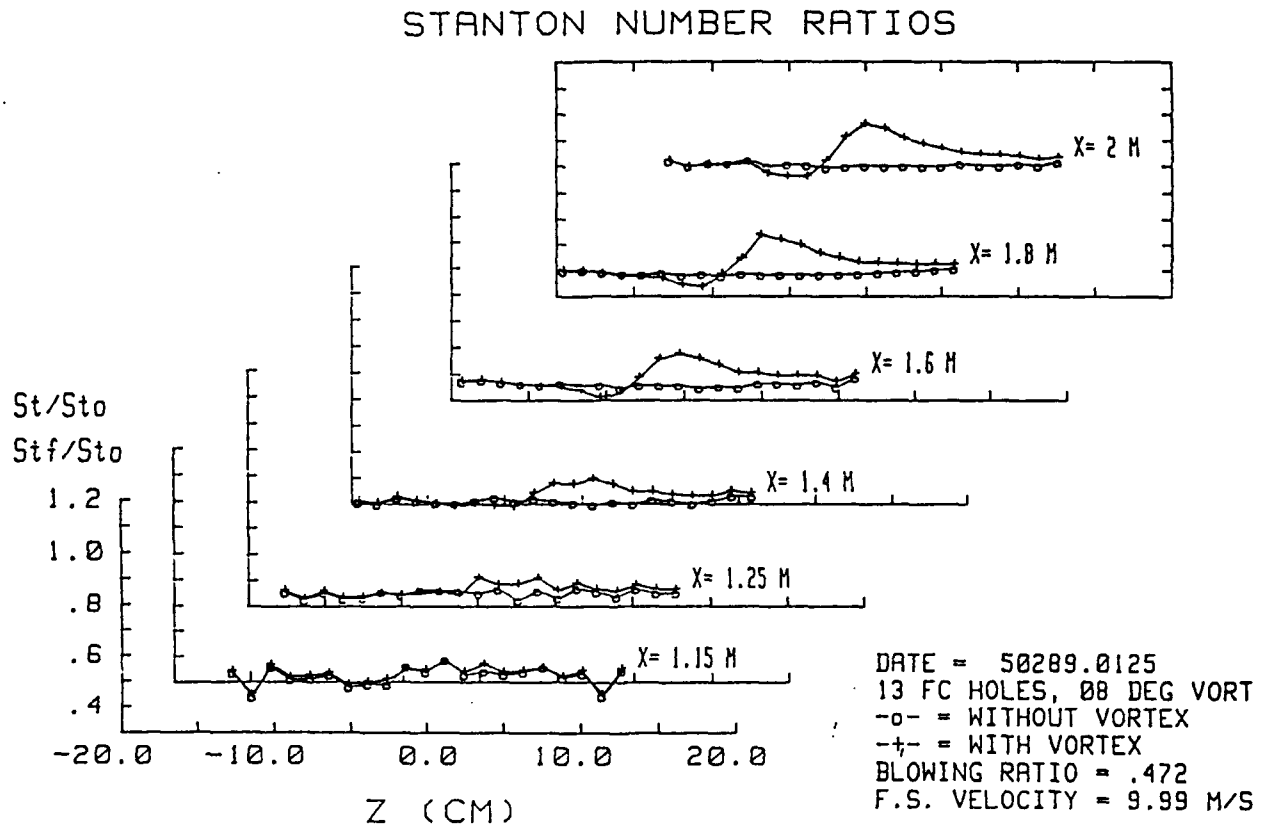

Figure 116 Local Stanton Number Ratios in Boundary Layers with Film-Cooling, with and without an embedded Vortex, 13 Injection Holes, m = 0.472, Vortex y

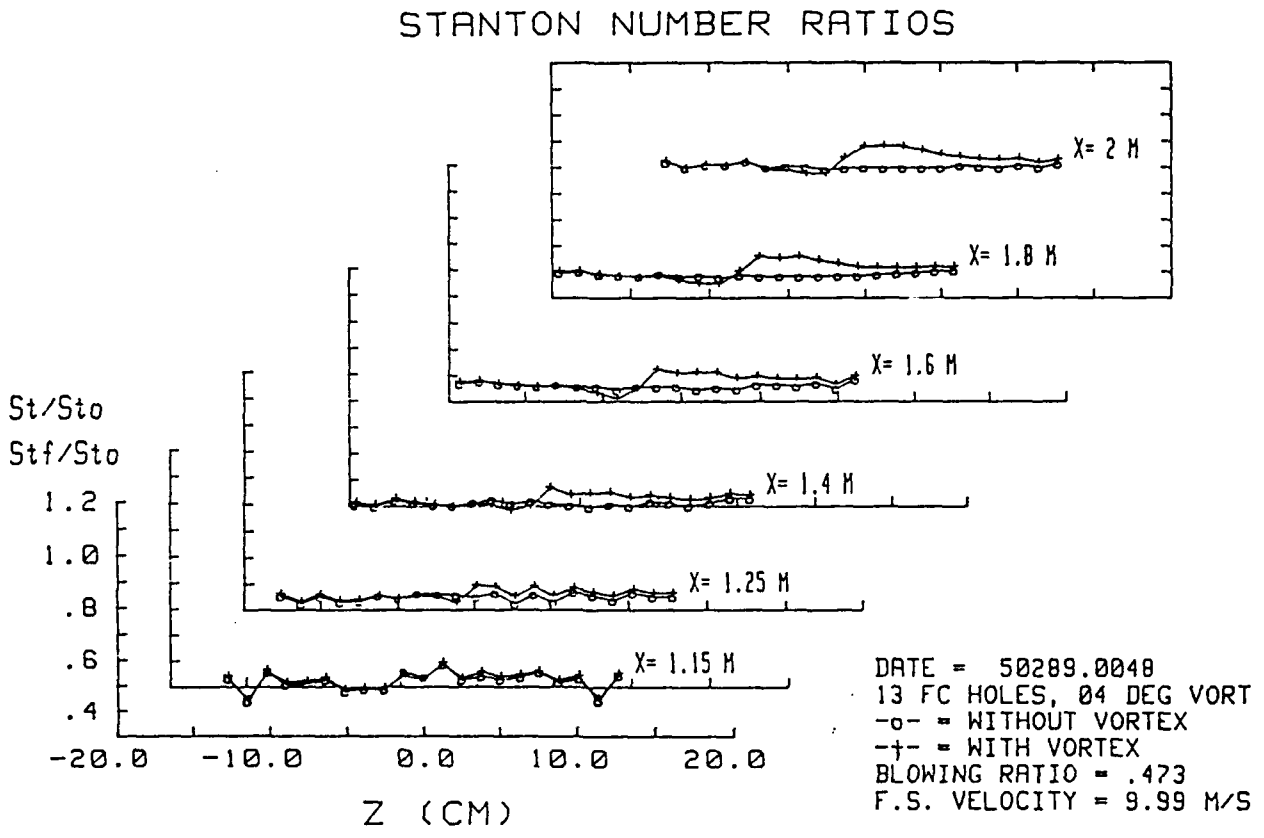

Figure 117 Local Stanton Number Ratios in Boundary Layers with Film-Cooling, with and without an embedded Vortex, 13 Injection Holes, m = 0.472, Vortex z

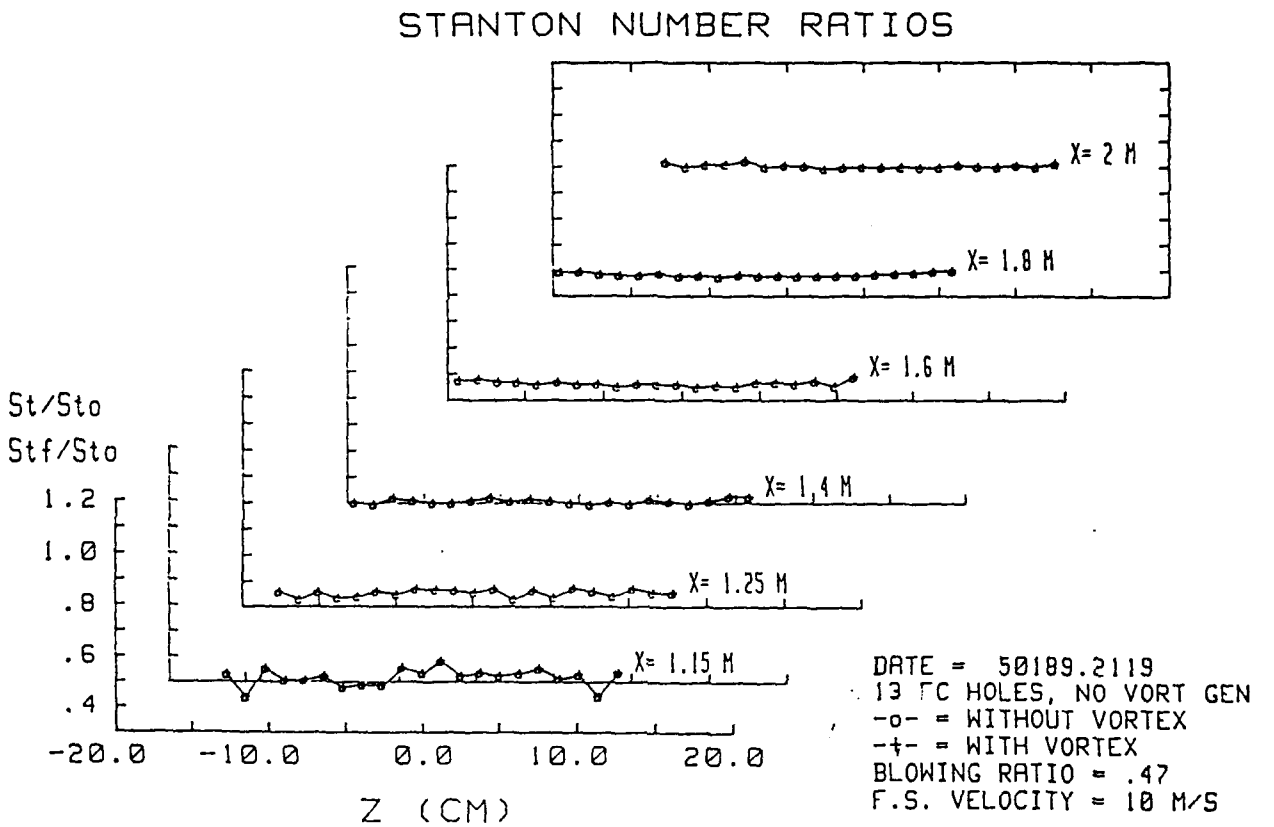

Figure 118 Local Stanton Number Ratios in Boundary Layers with Film-Cooling, with and without an embedded Vortex, 13 Injection Holes, m = 0.473, No Vortex Generator

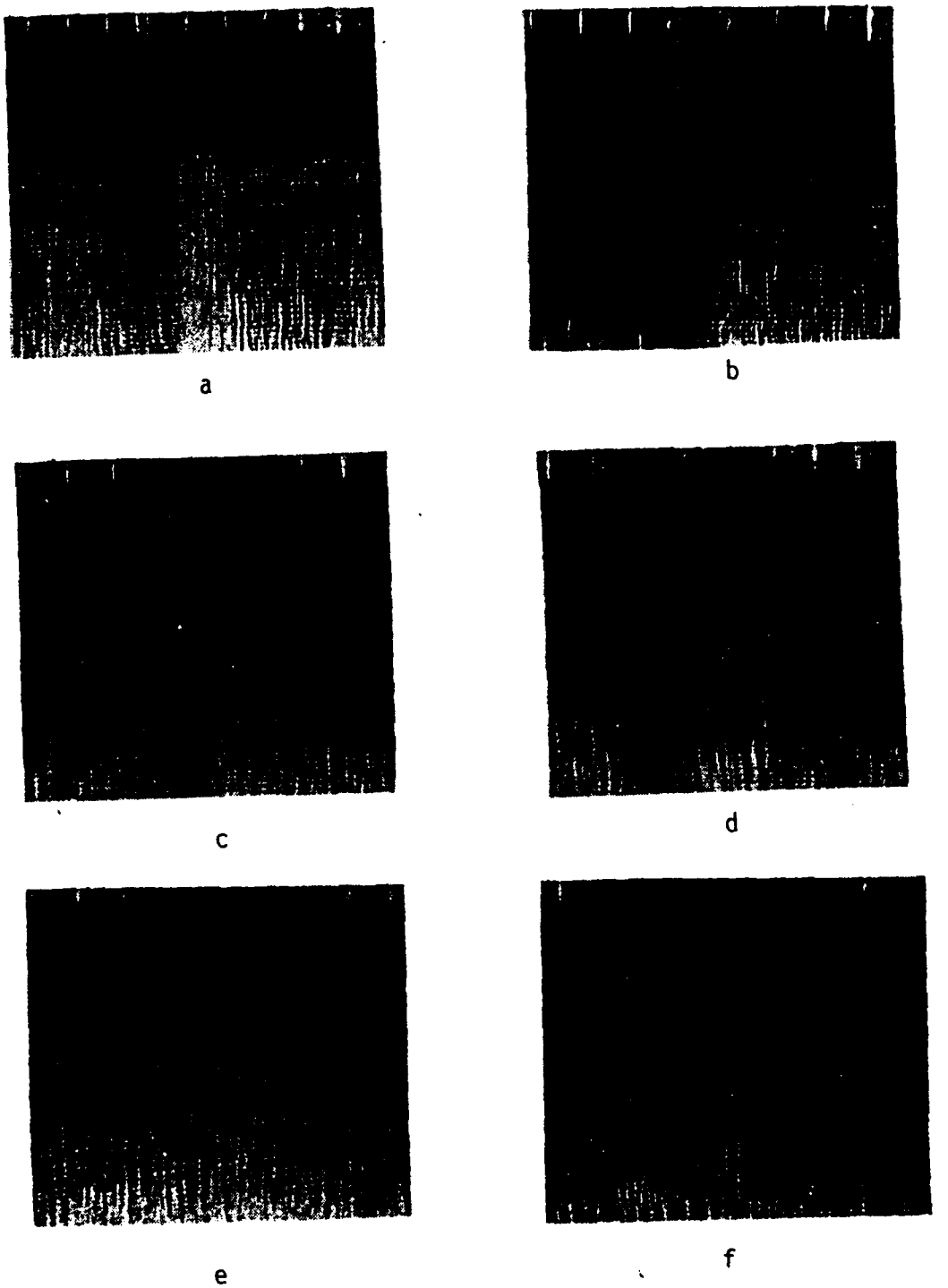

Figure 119 Surface Flow Visualization : A Single Injection Hole

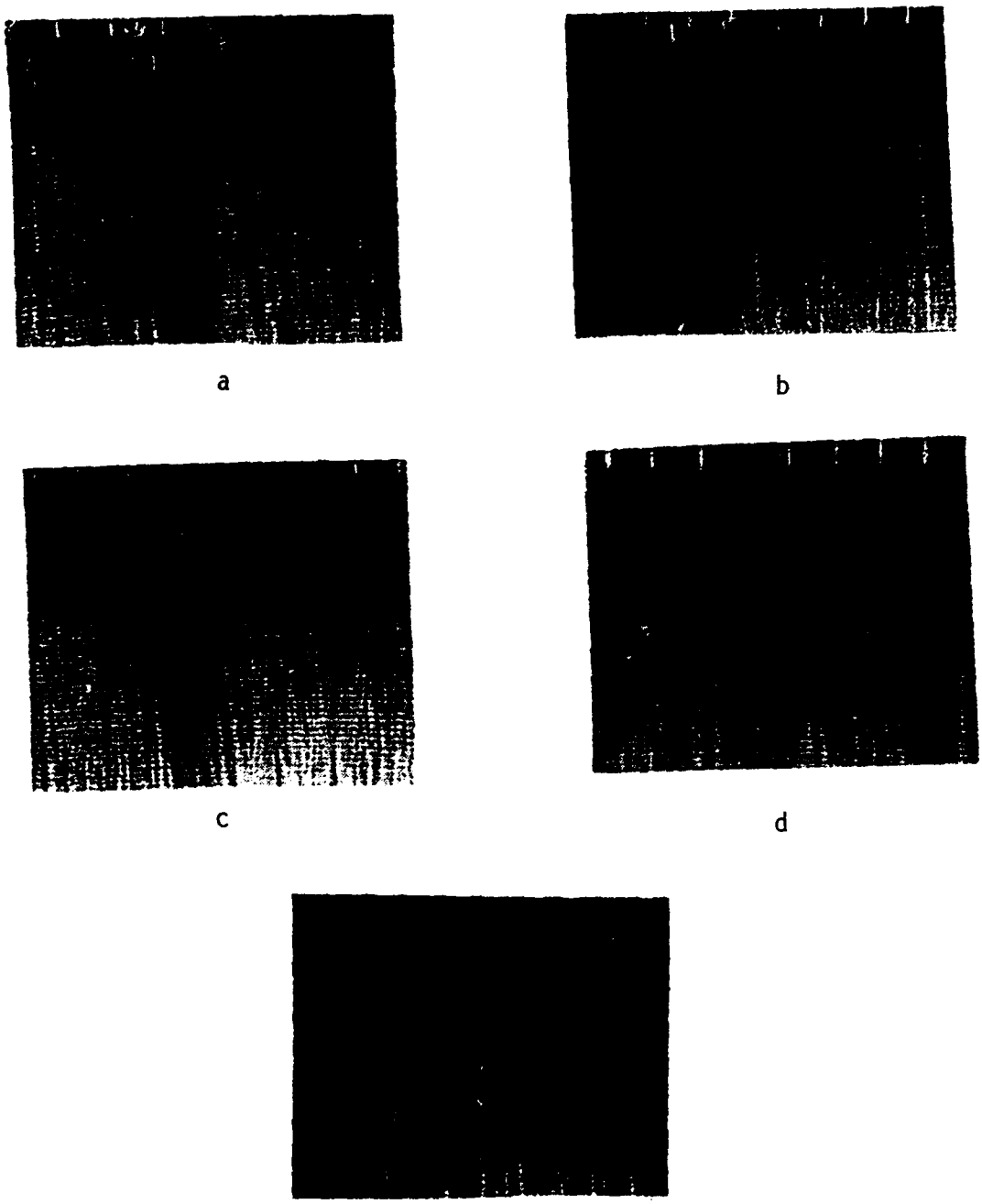

Figure 120 *Surface Flow Visualization : 13 Injection Holes*

APPENDIX B

SOFTWARE

The following program are listed :

ORIENT: This program is used for calculating calibration coefficients for each of the five pressure transducers associated with the five sensing ports of the five hole pressure probe. Additionally Orient is used to orientate the five hole probe so that at 0 yaw angle the pressures from the right and left ports are equal.

FIVEHOLE: This program acquires pressure data from each of the five transducers associated with the five hole probe.

PADJUST: This program accesses the FIVP data file created by FIVEHOLE and adjusts the pressures to account for special resolution problems. Pressure correction is performed using a curve fit to move the measurement location to the center sensing port location.

VELOCITY: This program accesses the data file created by PADJUST and computes the Ux, Uy and Uz velocity components.

UX2: This program accesses the data file created by VELOCITY and plots streamwise velocity contours of the Y-Z plane surveyed by the file hole pressure probe.

PTOT2: This program accesses the Velocity program data file and plots total pressure contours of the surveyed Y-Z plane.

VECTOR2: This program accesses the Velocity program output file and plots the secondary flow vectors in the surveyed Y-Z plane.

VORCIRC2: This program acquires the velocity component data file created by the Velocity program and plots streamwise vorticity contours of the surveyed Y-Z plane.

ROVER: This program acquires flow temperature data from the "roving" thermocouple mounted on the automatic traversing device.

PLTMP2: This program acquires the differential temperature data file created by Rover, and plots differential temperature contours of the surveyed Y-Z plane.

SETCOND: This program is used for set conditions for data run. It determines injection velocity, Reynolds number, and blowing ratio. It requires terminal input of freestream conditions, % on rotometer, and delta P Plenum. This program gets plenum temperature from thermocouple 148 and gets plate average temperature to calculate theta.

STANTON3: This program acquires multiple thermocouple data and creates a file to be read by STANTON4.

STANTON4: This program acquires multiple thermocouple data from STANTON3 and calculates heat transfer coefficients and Stanton number.

STAVRAT: This program accesses the HDATA files created by STANTON4 and creates an output file which consists of Stanton number ratios and X, Z coordinates for each of the thermocouple locations.

STANFC1: Heat transfer program to acquire thermocouple reading from DAS and Store information files on floppy disk.

STANFC2: This is a middle program that runs after STANFC1. This program calculates Stanton numbers for all flow conditions from input file data created by STANFC1.

NFCCOMBO: This program acquires the Stanton number ratios calculated by STAVRAT for various strength vortices and for no vortex. NFCCOMBO plots spanwise variations of St/Sto ratios for a user specified thermocouple row.

3DSTR3H: This program plots the spanwise variations of the St/Sto and Stf/Sto ratios for all six thermocouple row. 3DSTR3H is used only for a single injection hole film cooling data.

3DSTRAH: This program is used with 13 injection hole film cooling data.

3HCOMBO: This program accesses the Stanton number ratio file created by STANR1 for vortices r, w, x, y, z, and no embedded vortex. 3HCOMBO plots the Stf/Sto spanwise variations for a user specified thermocouple row, and then superimposes the St/Sto spanwise variations data for each of the vortices.

AHCOMBO: This program is the 13 injection hole version of 3HCOMBO, and is identical to 3HCOMBO with the exception of different upper and lower bounds on the plot axes.

VECTCOMBO & TEMPCOMBO: These are specifically adapted versions of VECTOR2 and PLTM2, which plot the differential mean temperature contours superimposed on top of the secondary flow vectors. VECTCOMBO is run first followed by TEMPCOMBO.

LIST OF REFERENCES

1. Eibeck, P. A. and Eaton, J. K.,"Heat Transfer Effects of a Longitudinal Vortex Embedded in Turbulent Boundary Layer," ASME Transactions-Journal of Heat Transfer, Vol. 109, pp. 16-23, February 1987.

2. Ligrani, P. M., Joseph, S. L., Ortiz, A. and Evans, D. L.,"Effects of Embedded Vortices on Film-Cooled Turbulent Boundary Layers," ASME Transactions-Journal of Turbomachinery, Vol. 111 No. 1, pp. 71-77, 1989.

3. Ligrani, P. M. and Williams, W., "Effects of an Embedded Vortex on Injectant from a Single Film-Cooling Hole in a Turbulent Boundary Layer," ASME Paper No. 89-GT-189, pp. 1-11, ASME Gas Turbine and Aeroengine Congress and Exposition, Toronto, Ontario, Canada, June, 1989, also to appear in ASME Transactions-Journal of Turbomachinery, January, 1990

4. Blair M. F., "An Experimental Study of Heat Transfer and Film Cooling on Large-Scale Turbine Endwalls," ASME Transactions-Journal of Heat Transfer, Vol. 96, pp. 524-529, 1974.

5. Goldstein, R. J. and Chen H. P., "Film-Cooling on a Gas Turbine Blade Near the Endwall," ASME Transactions-Journal of Engineering for Gas Turbines and Power, Vol. 107, pp. 117-122, January 1985.

6. Goldstein, R. J. and Chen H. P., "Film-Cooling of a Turbine Blade with Injection Through Two Rows of Holes in the Near-Endwall region," The American Society of Mechanical Engineers, Paper No. 87-GT-196, pp. 1-7, 1987.

7. Craig D. W., "Effects of Vortex Circulation on Injectant from a Single Film-Cooling Hole and a Row of Film-Cooling Holes in a Turbulent Boundary Layer, Part 1 : Injection Beneath Vortex Downwash,"M. S. Thesis, Department of Mechanical Engineering, Naval Postgraduate School, June 1989.

8. Ligrani P. M., Singer B. A. and Baun L. R., "Spatial Resolution and Downwash Velocity Correction for Multiple-Hole Pressure Probes in Complex Flows," Experiments in Fluids, Vol. 7, No. 6, pp. 424-426, 1989.

9. Ligrani P. M., Singer B. A. and Baun L. R., "Miniature Five-Hole Pressure Probe for Measurement of Mean Velocity Components in Low Speed Flows," Journal of Physics E-Scientific Instruments, in press, 1989.

10. Ortiz A. "The Thermal Behavior of Film Cooled Turbulent Boundary Layers as Affected by Longitudinal Vortices," M. E. Thesis, Department of Mechanical Engineering, Naval Postgraduate School, 1987.

11. Schwartz, G. E.,"Studies of the Interactions Between Vortices and Shear Layers," M. S. Thesis, Department of Mechanical Engineering, Naval Postgraduate School, September 1988.

12. Kline S. J. and McClintock F. A., "Describing Uncertainties in Single-Sample Experiments," Mechanical Engineering, 1953.

13. Moffat R. J., "Contibutions to the Theory of Single-Sample Uncertainty Analysis," ASME Transactions-Journal of Fluids Engineering, Vol. 104, pp.250-260, 1982.

14. Kays W. M and Crawford M. E., Convective Heat and Mass Transfer, Second Edition, McGraw-Hill Book Company, New York, 1980.

15. Williams, W., "Effects of an Embedded Vortex on a SIngle Film-Cooling Jet in a Turbulent Boundary Layer," M. S. Thesis, Department of Mechanical Engineering, Naval Postgraduate School, 1988.

16. Ligrani, P. M. and Camci, C., "Adiabatic Film Cooling Effectiveness form Transfer Measurements in Compressible Variable-property Flow," Journal of Heat Transfer, Vol. 107, pp. 313-320, May 1985.

17. Joseph, S. L.,"The Effects of an Embedded Vortex on a Film-Cooled Turbulent Boundary Layer," M. E. Thesis, Department of Mechanical Engineering, Naval Postgraduate School, December, 1986.

18. Evans, D. L.,"Study of Vortices Embedded in Boundary Layers with Film-Cooling," M. S. Thesis, Department of Mechanical Engineering, Naval Postgraduate School, March, 1987.

19. Ligrani P. M., Josept S. L., and Evans D. L., "Heat Transfer in Film-Cooled Turbulent Boundary Layers at Different Blowing Ratios as Affected by Longitudinal Vortices," Experimental Thermal and Fluid Science, Vol. 31, No. 12, pp. 347-362, 1988.

INITIAL DISTRIBUTION LIST

		No. Copies
1.	Defense Technical Information Center Cameron Station Alexandria, Virginia 22304-6145	2
2.	Library, Code 0142 Naval Postgraduate School Monterey, California 93943-5000	2
3.	Department Chairman, Code 69 Department of Mechanical Engineering Naval Postgraduate School Monterey, California 93943-5000	1
4.	Naval Engineering Curricular Office, Code 34 Department of Mechanical Engineering Naval Postgraduate School Monterey, California 93943-5000	1
5.	Professor Phillip M. Ligrani, Code 69Li Department of Mechanical Engineering Naval Postgraduate School Monterey, California 93943-5000	6
6.	Professor C. S. Subramanian, Code 69Su Department of Mechanical Engineering Naval Postgraduate School Monterey, California 93943-5000	2
7.	Dr. Dick Rivir Components Branch Turbine Engine Division Aero Propulsion Laboratory Department of the Air Force Air Force Wright Aeronautical Laboratories Wright-Patterson Air Force Base, Ohio, 45433	10

8. Commanding Officer
David Taylor R&D Center
Carderrock Laboratory
Bethesda, Maryland 20084 1

9. LCDR Pisut Kaisuwan
89/6 Charoensuknivet 4
Soi. Senanikom 1, Bangkapi
Bangkok 10230, THAILAND 3